

Titre: Use for specular hematite concentrate and fritmag for the
Title: production of iron ore sinters

Auteur: Anil Kumar Choudhury
Author:

Date: 1991

Type: Mémoire ou thèse / Dissertation or Thesis

Référence: Choudhury, A. K. (1991). Use for specular hematite concentrate and fritmag for
Citation: the production of iron ore sinters [Thèse de doctorat, Polytechnique Montréal].
PolyPublie. <https://publications.polymtl.ca/57964/>

 **Document en libre accès dans PolyPublie**
Open Access document in PolyPublie

URL de PolyPublie: <https://publications.polymtl.ca/57964/>
PolyPublie URL:

**Directeurs de
recherche:**
Advisors:

Programme: Non spécifié
Program:

UNIVERSITE DE MONTREAL

USE OF SPECULAR HEMATITE CONCENTRATE AND FRITMAG
FOR THE PRODUCTION OF IRON ORE SINTERS

par

ANIL KUMAR CHOUDHURY
DEPARTEMENT DE GENIE METALLURGIQUE
ECOLE POLYTECHNIQUE

THESE PRESENTE EN VUE DE L'OBTENTION
DU GRADE DE PHILOSOPHIAE DOCTOR (Ph. D.)
(GENIE METALLURGIQUE)

MAI 1991

© Anil Kumar Choudhury 1991

National Library
of Canada

Bibliothèque nationale
du Canada

Canadian Theses Service Service des thèses canadiennes

Ottawa, Canada
K1A 0N4

The author has granted an irrevocable non-exclusive licence allowing the National Library of Canada to reproduce, loan, distribute or sell copies of his/her thesis by any means and in any form or format, making this thesis available to interested persons.

The author retains ownership of the copyright in his/her thesis. Neither the thesis nor substantial extracts from it may be printed or otherwise reproduced without his/her permission.

L'auteur a accordé une licence irrévocable et non exclusive permettant à la Bibliothèque nationale du Canada de reproduire, prêter, distribuer ou vendre des copies de sa thèse de quelque manière et sous quelque forme que ce soit pour mettre des exemplaires de cette thèse à la disposition des personnes intéressées.

L'auteur conserve la propriété du droit d'auteur qui protège sa thèse. Ni la thèse ni des extraits substantiels de celle-ci ne doivent être imprimés ou autrement reproduits sans son autorisation.

ISBN 0-315-69643-5

Canada

UNIVERSITE DE MONTREAL

ECOLE POLYTECHNIQUE

Cette thèse intitulée:

USE OF SPECULAR HEMATITE CONCENTRATE AND FRITMAG
FOR THE PRODUCTION OF IRON ORE SINTERS

présentée par Anil Kumar CHOUDHURY

en vue de l'obtention du grade de: Philosophiae Doctor (Ph. D.)

a été dûment acceptée par le jury d'examen constitué de:

M. Frank Ajersch, Ph.D. président

M. Michel Rigaud, D.Sc. A.

M. Ivan Malinsky, Ph.D.

M. Jorgan Elbrond, M. Sc.

SUMMARY

The present work was undertaken to contribute to the solution of the problem encountered while using high quantity (>15%) of specularite concentrate in a sinter mix. The main problem is the significant decrease in the production rate. This is due to the drop in the bed permeability during sintering. There is also a deterioration of the sinter quality.

The work was then pursued with three specific objectives viz. i) to find suitable means to incorporate high amount (>15%) of specular hematite concentrate in a sinter mix, without dropping the production rate below 40 tonnes per day per square meter of the grate area (tpd/m²), ii) to improve the quality of these sinters to meet the industrial requirements and iii) to explore the possibility of using a new material, Fritmag as a source of MgO in sintering and to compare the quality of these sinters with that of the commonly used dolomite- or olivine-added sinters.

Effort was made to increase the bed permeability by improving the size-distribution of the green mix. This was achieved by enhancing the formation of micro-pellets during mixing with the help of a suitable mixing/micro-pelletizing device(s) and/or using a binder/additive. Three different mixing devices namely, roll compactor, turbulator and disc pelletizer and four binders (e.g. quick-lime, bentonite, peridur and peat moss) was tested. The effect of specularite concentrate was studied by adding it in three levels, e.g. 25%, 40% or 100%. Besides the specularite concentrate, the other raw materials used in the sinter mix were pellet fines, sinter fines, mill scale, iron fines, limestone, dolomite and flue dust (or coke breeze). The degree of micro-pelletization in the green mix was studied by size analysis of the green mix and by determining the pre-ignition (cold) permeability of the sinter bed.

A series of pot-grate tests (more than 200) was conducted in this work. All the sinters were produced at a constant basicity of 2.5 and MgO content 3.0%. Sintors were produced with and without using the additives viz. quick-lime, bentonite, peridur or peat moss. A combination of turbulator and disc or only a disc was used separately for mixing the raw materials.

Few pot-grate tests were carried out to study the effect of modified fuel addition (i.e. adding fuel in two stages during mixing). A series of pot-tests were also conducted on an industrial strand to compare the quality of the laboratory sinters under the industrial conditions.

The effect of Fritmag was studied by producing sinters at a basicity 2.0 by the laboratory pot-grate tests. The MgO content of the sinters was maintained 3.0% using Fritmag, dolomite or olivine as the source of MgO in the sinter mix. Then the quality of these sinters was evaluated following the standard methods.

From this study, the combination of turbulator and disc pelletizer or only a disc pelletizer was found to be quite suitable for the micro-pelletization process. The roll compactor did not show any encouraging effect. Among the additives, quick-lime and bentonite have enhanced the formation of micro-pellets by acting as binders in the sinter mix. Peridur or peat moss did not have any marked effect on micro-pelletization.

It was seen that up to 40% specularite in the sinter mix, the production rate was more than 40 tpd/m² (which was the limit set in the objectives). For any particular amount of specularite, it increased significantly with quick-lime

addition. Bentonite also to some extent, favorably affected the production rate. The other additives e.g. peridur or peat moss or turbulator did not have any visible effect on it. A decrease in the production rate with the increase in the specularite content of the sinter mix was observed.

The effect of modified fuel addition on production rate was found to be quite interesting. For any particular condition of the sinter mix, it (production rate) increased up to 20% by adding the fuel in two stages.

From the mineralogical study, it has been observed that the sinters were marked with high amount of calcium ferrite and secondary magnetite (about 35% vol. each), with (15-20%) of slag phase and (10-15%) of hematite phase. The ferrite and hematite content of the sinter increased with the increase in the specularite content and with lime addition, mainly replacing the magnetite phase and the slag phase.

The quality of the sinter containing up to 40% specularite in the sinter was better than that outlined in the objectives. The reducibility of these sinters were quite high (> 1.27) and increased with the increase in the specularite content of the sinter. Although the strength and RDI of the sinter decreased with the increase in amount of specular concentrate in the

sinter, they were within the limits required by the industries (e.g. T-index > 60 and RDI > 80 respectively).

Sinters produced with 100% specularite had high reducibility (>1.60). However, because of their low strength and RDI, the quality of these sinters was considered to be inferior than that required in the industrial practice.

The properties of the sinters produced on the industrial strand were found to be fairly comparable with those of the corresponding sinters produced in the pot-grate. These findings have confirmed the validity of the pot-grate test results under industrial conditions.

It was seen that Fritmag can be assimilated well into the sinter structure. The quality of these sinters have been found to be similar to that of the dolomite- or olivine-added sinters.

The objectives of the work have been met. Up to 40% specularite concentrate can be used in the sinter mix without dropping the production rate below 40 tpd/m². However, a disc pelletizer has to be used as the mixing device. Addition of quick-lime to the sinter mix is necessary to increase the production rate and to improve the sinter quality. Fritmag can be used as a source of MgO in the sinter mix.

SOMMAIRE

La présente étude a été amorcée en vue de contribuer à la solution du problème rencontré lors de l'utilisation d'une grande quantité de concentré d'hématite spéculaire (>15%) lors de la production d'agglomérés. Le principal problème c'est la diminution notable du taux de production. Ceci est causé par la chute de la perméabilité du lit de cuisson. Cette chute s'accompagne d'une détérioration de la qualité des agglomérés.

La présente étude a donc été entreprise avec les 3 objectifs précis suivant; i) trouver un moyen adéquat pour utiliser un haut pourcentage (>15%) de concentré d'hématite spéculaire lors de cuisson d'agglomérés sans diminuer le taux de production en dessous de 40 tonnes pour jour par mètre carré (de surface de grille); ii) améliorer la qualité de ces agglomérés pour satisfaire les besoins industriels et iii) explorer la possibilité d'utiliser un nouvel additif comme source de MgO dans le procédé de sintérisation et de comparer la qualité de ces agglomérés avec celle des agglomérés utilisant comme additif de la dolomie ou de l'olivine.

Des efforts ont été effectués pour augmenter la perméabilité du lit de cuisson et ceci en améliorant la distribution en taille des mélanges en cru. Ceci a été réalisé en favorisant la formation de micro-boulettes durant le mélange grâce à un équipement approprié et/ou en utilisant un additif/liant adéquat. Trois matériels ont été utilisés, un compacteur à rouleaux, un mélangeur à vis et un disque à bouletter ainsi que quatre additifs tels que la chaux, la bentonite, le "peridur" et la tourbe. Les additions d'hématite spéculaire ont été effectuées à trois niveaux en pourcentage: 25%, 40% et 100%. Pour chaque mélange, on a aussi utilisé des fines de boulettes, des fines d'agglomérés, de la calamine, des fines de minerais, de la pierre calcaire et/ou dolomitique et enfin des poussières de coke. Le degré de micro-boulettage dans le mélange cru a été mesuré en déterminant la taille des agrégats dans le mélange en cru et la mesure de la perméabilité à froid du lit d'agglomération avant cuisson.

Plus de 200 essais au simulateur de cuisson ont été effectués lors de ce travail. Tous les agglomérés ont été produits avec une basicité de 2.5 et un contenu en MgO de 3.0%. Les agglomérés ont été produits avec et sans les additifs. Lors de ces essais, le mélange des matériaux à l'état brut a été effectué soit à l'aide d'un mélangeur à vis et du disque soit du disque à bouletter seulement.

Quelques essais ont été effectués pour étudier le mode d'incorporation du combustible (c'est à dire une incorporation du combustible en deux étapes). D'autres essais de cuisson ont été aussi effectués sur une ligne d'agglomération en usine pour comparer la qualité des agglomérés produits en laboratoire et dans des conditions industrielles.

Le rôle du "Fritmag" a été étudié en produisant des agglomérés d'une basicité de 2, avec un contenu en MgO de 3.0%, en comparant le "Fritmag" avec la dolomie ou l'olivine comme source de MgO dans les mélanges. La qualité de ces agglomérés a été déterminée selon les méthodes standards.

A partir de cette étude, on a constaté que la combinaison mélangeur à vis et disque à bouletter ou l'utilisation d'un disque seulement est adéquate pour le micro-boulettage du mélange. Le compacteur à rouleaux n'offre aucun avantage quant à son utilisation. Parmi les additifs, la chaux et la bentonite ont favorisé la formation de micro-boulettes. Le Peridur et la tourbe n'ont pas d'influence notable sur le micro-boulettage.

On a réussi à faire en sorte que le taux de production puisse dépasser 40 tonnes par jour par mètre carré (tonne/jour.m²) avec un pourcentage en concentré d'hématite spéculaire atteignant 40% (productivité fixée dans les objectifs). L'addition de chaux augmente de beaucoup le taux

de production des agglomérés pour chaque niveau en pourcentage de concentré d'hématite spéculaire. La bentonite a aussi un effet favorable sur le taux de production. Ni le mélangeur à vis, ni les autres additifs ("peridur" et tourbe) n'ont d'effets notables sur le taux de production, mais le taux de production diminue lorsqu'on augmente le niveau d'hématite spéculaire dans le mélange.

L'effet sur le taux de production de l'addition en deux temps du combustible s'est révélé très intéressant. Indépendamment du type d'aggloméré produit, ce mode d'addition en deux étapes s'est traduit par une augmentation de production de l'ordre de 20%.

L'étude de la minéralogie des produits a révélé que les agglomérés contenaient une grande quantité de ferrite de calcium et de magnetite (environ 35% en vol. chaque phase), un pourcentage de 15 à 20% de scorie et de 10 à 15% d'hématite. Le contenu de ferrite augmente en proportion avec le contenu de concentré d'hématite spéculaire et avec l'addition de chaux dans le mélange.

La qualité des agglomérés contenant jusqu'à 40% de concentré d'hématite spéculaire était supérieure à celle fixée dans nos objectifs. La réductibilité de ces agglomérés était élevée (>1.27), croissant avec le pourcentage de concentré

d'hématite spéculaire dans l'aggloméré. Toutefois la résistance mécanique et la résistance à la dégradation lors de la réduction variaient dans le sens d'une diminution en fonction du pourcentage croissant de concentré d'hématite spéculaire tout en demeurant en deçà des limites admises dans l'industrie (indice de résistance > 60 et indice de résistance à la dégradation lors de la réduction > 80).

Les agglomérés produits avec 100% de concentré d'hématite spéculaire avaient une haute réductibilité (>1.60). Cependant, à cause de leur trop faibles résistance mécanique et résistance à la dégradation lors de la réduction ces agglomérés ne peuvent pas satisfaire aux exigences de l'industrie.

Les propriétés mesurées des agglomérés produits sur la ligne d'agglomération dans des conditions industrielles ont permis de constater qu'elles étaient semblables à celles des agglomérés produits dans le simulateur de cuisson en laboratoire. Ceci est venu confirmer la validité des résultats obtenus lors des essais dans le simulateur de cuisson.

Dans cette partie de l'étude, nous avons observé que le "Fritmag" s'assimile à la structure des agglomérés. Nous en avons conclu que la qualité de ces agglomérés est similaire à celle des agglomérés contenant des additions de dolomie ou d'olivine.

Tous les objectifs de cette étude ont donc été atteints. On a démontré que 40% de concentré d'hématite spéculaire peuvent être utilisés lors de production d'agglomérés, sans diminuer le taux de production à moins de 40 tonnes/jour.m². Afin de faire cela, il faut utiliser un disque à bouletter. La chaux est nécessaire pour augmenter le taux de production à plus de 45 tonnes/jour.m² mais également pour améliorer la qualité des agglomérés. Le mode d'addition du combustible dans le mélange peut aussi contribuer à augmenter notablement le taux de production. Le "Fritmag" peut être utilisé comme une source de MgO lors de la production d'agglomérés. La qualité de ces agglomérés sera similaire à celle des agglomérés avec addition de dolomie ou d'olivine.

ACKNOWLEDGEMENT

First, I would like to extend my sincere thanks and gratitude to my director, Professor Michel Rigaud for his continuous guidance and constructive criticism throughout this work. I very much appreciate his support during my stay at École Polytechnique.

I wish to thank Dr. S.C. Panigrahy for his help while carrying out the tests and the valuable discussions during the course of my research.

I thankfully acknowledge the help of Dr. H.O. Lien, Mr. Gerry Loxton and the personnel at Algoma Ore Division, Wawa, Ont. while conducting the pot-grate tests.

The financial assistance from Québec Cartier Mines, Algoma Steel Corporation, CERAM-SNA and École Polytechnique is thankfully acknowledged.

I am very much thankful to the faculty members and the technicians of the Metallurgical Department. The assistance of Mario Caron in the X-ray mapping is acknowledged.

Thanks are also due to the secretaries of the department, especially to Miss Julie Chamberlain, who was always ready to help me in the preparation of my thesis.

It is difficult to include the names of all my friends and colleagues who helped and encouraged me during this work. However, I do like extend my appreciation to Bertrand, Marin, Khaled, Frédéric, Pierre, Xiangmin, Changzun, Pascal, Denise, Stéphane, Denis, Birendra, José, Francis, Bin, Sundar and Tamal.

Lastly, I wish to express my sincere gratitude to my parents and family for their support and encouragement.

Table of Contents

	<u>Page</u>
Summary.....	iv
Sommaire.....	ix
Acknowledgement.....	xv
Table of Contents.....	xvii
List of Tables	xxii
List of Figures.....	xxiv
CHAPTER I: INTRODUCTION.....	1
1. The Problem.....	2
2. The Objectives.....	4
3. Sintering Process.....	5
3.1 Sintering Process and Types of Sinter.....	5
3.2 Industrial Sintering Practice.....	7
3.3 Laboratory Method for the Production of Sinter.....	10
3.4 Ignition.....	14
3.5 Recycling of Fines (Circulating Load).....	15
3.6 Waste Gas Analysis.....	16
3.7 Sintering Time.....	17
3.8 Production Rate.....	17
3.9 Carbon Rate.....	18
4. Quality of the Sinter.....	18
5. Scope of the Work.....	19

	<u>Page</u>
CHAPTER II - REVIEW ON SINTERING PROCESS.....	22
1. Production Rate.....	22
2. Permeability of the Sinter Bed.....	23
3. Micro-pelletization.....	29
3.1 Water Content.....	32
3.2 The Shape and Size Distribution of the Materials...35	
4. Sintering Reactions and Mineralogy of Sinters.....	38
4.1 Effects of MgO.....	50
5. Quality of Sinter.....	54
5.1 Properties of the Sinter.....	55
CHAPTER III - OPTIMISATION OF THE SINTERING CONDITIONS.....	70
1. Raw Materials.....	70
2. Equipments and Procedures.....	78
2.1 Description of the Mixing/Micro-pelletizing Equipments.....	78
2.2 Assessment of the Micro-pelletization Equipments...82	
2.3 Pot-Grate Tests.....	84
2.3.1 Sinter Mix Compositions.....	87
2.3.2 Mixing.....	89
2.3.3 Charging of the Green Mix.....	89
2.3.4 Sintering.....	90
2.3.5 Stabilization of the Sinter Cake and Recycling of Fines.....	91

Page

2.4	Pot-Grate Tests with Modified Fuel addition.....	92
2.5	Production of Sinters on the Industrial Strand.....	92
3.	Micro-pelletization Study.....	95
3.1	Size analysis of the Green Mix.....	95
3.2	Pre-ignition (or Cold) Permeability.....	101
4.	Production of Sinters.....	104
4.1	Bed Permeability during Sintering.....	104
4.2	Sintering Time.....	105
4.3	Production Rate.....	108
4.4	Carbon Rate.....	110
CHAPTER IV - CHARACTERIZATION OF THE SINTERS.....		112
1.	Mineralogical Study	114
1.1	Sample Preparation.....	114
1.2	Mineralogical Observation in the Optical Microscope.....	115
1.3	Semi-Quantitative Measurements of the Mineral Phases	132
1.4	Micro-analysis and X-ray Mapping.....	132
1.5	Discussion.....	134
2.	Chemical Analysis of the Sinters.....	141
3.	Evaluation of the Sinter Quality.....	143
3.1	Porosity.....	144
3.1.1	Test Procedure.....	144
3.1.2	Results and Discussion.....	147

	<u>Page</u>
3.2 Strength.....	152
3.2.1 Test Procedure.....	152
3.2.2 Results and Discussion.....	153
3.3 Reduction Degradation (or Low-Temperature Degradation).....	159
3.3.1 Test Procedure.....	160
3.3.2 Results and Discussion.....	160
3.4 Reducibility.....	164
3.4.1 Test Procedure.....	165
3.4.2 Results and Discussion.....	166
3.5 Softening/Melting.....	172
3.5.1 Test Procedure.....	172
3.5.2 Results and Discussion.....	174
 CHAPTER V - EFFECTS OF FRITMAG ADDITION.....	 176
1. Introduction.....	176
2. Production of Sinters.....	177
2.1 Raw Materials.....	177
2.2 Composition of the Sinter Mix.....	179
3. Thermal Analysis (DTA and TGA).....	181
4. Mineralogical Study.....	184
4.1 Mineralogical Observations.....	184
4.2 Micro-analysis X-ray Mapping.....	199
4.3 Discussion.....	207

Page

5. Quality of the Sinters.....	212
5.1 Methods Followed to Determine the Sinter Properties	212
5.1.2. Modified Conditions for the Reduction Degradation Test.....	212
5.1.1 Modified Conditions for the Reducibility Test..	213
5.2 Results and Discussions.....	213
 CHAPTER VI - SYNTHESIS, CONCLUSIONS AND RECOMMENDATIONS....	219
1. Synthesis.....	219
1.1 Micro-pelletization of the Green Mix and Production Rate.....	219
1.2 Characterization of Sinters.....	227
1.3 Effect of the Fritmag Addition.....	228
2. Summary and Conclusions.....	230
2.1 Summary.....	230
2.2 Conclusions.....	231
3. Recommendations.....	233
References.....	235
Annex 1 -Important Phase Diagrams.....	247
Annex 2 - Kinetics of Iron Ore Reduction.....	252
Annex 3 - Calculations for the Reducibility Index.....	277

LIST OF TABLES

<u>Table</u>	<u>Page</u>
2.1 Classification of raw particles by sizes.....	36
2.2 Analysis of different calcium ferrites	46
3.1 Chemical analysis (wt. %) of the raw materials	72
3.2 Size distribution of the raw materials (wt. % retained on stated size).....	73
3.3 Experimental sintering conditions	86
3.4 Amount of different iron-bearing materials in the base mix.....	88
3.5 Composition of the sinter mixes.....	88
3.6 Raw material conditions for the strand tests	93
3.7 Size analysis (cum. wt. per cent) of the green mix ...	96
3.8 Permeability of the sinter bed (in BPU)	102
3.9 Production rates of the sinters using only disc	106
3.10 Production rates of the sinters using turbulator and disc	106
4.1 Semi-quantitative measurement of the mineral phases in different sinters	133
4.2 Composition of the mineral phases	139
4.3 Composition of different types of calcium ferrites ..	139
4.4 Chemical analysis (wt. %) of the sinter produced	142
4.5 Porosity of the sinters	148
4.6 Tumbler strength of the sinters	154
4.7 Reduction degradation index (RDI) of the sinters	161

<u>Table</u>	<u>Page</u>
4.8 Reducibility of the sinters	168
4.9 Conditions for the softening tests	173
4.10 Results of the softening tests	174
5.1 Chemical analysis (wt. %) of the MgO-bearing materials.....	178
5.2 Size analysis (% wt. retained on stated size) of the MgO-bearing materials.....	178
5.3 The composition of the sinter mix for the first test.	180
5.4 Different types of the sinters produced.....	180
5.5 Semi-quantitative measurement of the mineral phases..	186
5.6 Composition of different mineral phases.....	200
5.7 MgO content of the magnetite phase in different sinters	200
5.8 Composition of different types of hematite.....	210
5.9 Composition of different types of calcium ferrites...	211
5.10 Properties of the sinters.....	213
6.1 Parameters used to assess the degree of micro- pelletization of the green feed Vs. sinter production rate.....	222
6.2 Degree of micro-pelletization of the green feed Vs. cold permeability of the sinter bed.....	224
A2.1 Oxygen dissociation pressure (P_{O_2}) in atmosphere of iron oxides.....	252

LIST OF FIGURES

<u>Figure</u>	<u>Page</u>
1.1 Schematic diagram of Dwight-Lloyd sintering machine ...	8
1.2 Zone structure developed on Dwight Lloyd strand	9
1.3 Laboratory sintering process	12
1.4 Temperature profile and the zone existing in the sinter bed at a particular time during sintering	12
2.1 Variation of permeability of the sinter bed with time, as sintering proceeds	24
2.2 Basic concept of sinter mix preparation	30
2.3 Typical relationship between permeability and moisture content	34
2.4 General changes of mineralogical phases during sintering	39
2.5 Variation of sinter mineralogy as its basicity changes	42
2.6 Change in the amount of calcium ferrites of sinter with its basicity	44
2.7 Phases in CaO-FeO-Fe ₂ O ₃ system	46
2.8 Effect of total hematite content on low-temperature breakdown index	61
2.9 The reduction curves of different mineral phases ...	63
3.1 The frequency histogram of the size-distribution of the iron-bearing materials	74
3.2 Schematic diagram of a disc pelletizer	79

<u>Figure</u>	<u>Page</u>
3.3 Turbulator	81
3.4 Roll compactor	83
3.5 Schematic arrangement of the experimental pot-grate test facilities	85
3.6 Effect of various conditions on micropelletization of the sinter mix	97
4.1 Tests conducted on sinters	113
4.2 Photomicrographs showing the typical microstructure of sinter containing no specularite or additive	119
4.3 Photomicrographs showing the typical microstructure of sinter containing 25% specularite, no additive ...	120
4.4 Photomicrographs showing the typical microstructure of sinters containing 40% specularite, but no additive	122
4.5 Photomicrographs showing the typical microstructure of sinters containing 25% specularite and 2% quick-lime	124
4.6 Photomicrographs showing the typical microstructure of sinters containing 25% specularite and 5% quick-lime	125
4.7 Photomicrographs showing the typical microstructure of sinters containing 25% specularite and .25% bentonite	127

<u>Figure</u>	<u>Page</u>
4.8 Photomicrographs showing the typical microstructure of sinters containing 40% specularite and 2% quick-lime	128
4.9 Photomicrographs showing the typical microstructure of sinters containing 40% specularite and 5% quick-lime	130
4.10 Photomicrographs showing the typical microstructure of sinters containing 40% specularite and .25% bentonite	131
4.11 Scheme of a Beckman air pycnometer	145
4.12 Variation in sinter porosity with the specularite content of the sinter mix	149
4.13 Variation of the mineralogical structure of the sinter produced with specularite	151
4.14 Change of T-index with specularite addition	155
4.15 Effect of sinter porosity on its strength	157
4.16 Effect of specularite addition on the RDI of the sinter	163
4.17 The reducibility curve obtained for the sinter with 40% specularite	167
4.18 Effect of specularite addition on the reducibility of the sinter	170
4.19 Variation of sinter reducibility with its porosity ..	171

FigurePage

5.1	Weight loss of the MgO-bearing materials and specularite concentrate as a function of time and temperature	182
5.2	DTA curves of specular hematite concentrate and the MgO-bearing materials	183
5.3	Photomicrographs showing similarity in the mineralogical structure of the sinters with different MgO-source	185
5.4	Mineralogical structure of the sinter with 45% specularite and Fritmag (3% MgO)	188
5.5	Mineralogical structure of the sinter with 45% specularite and dolomite (3% MgO)	191
5.6	Mineralogical structure of the sinter with 45% specularite and olivine (3% MgO)	194
5.7	Mineralogical structure of the sinter with 45% specularite and Fritmag (2.5% MgO)	197
5.8	Mineralogical structure of the sinter with 25% specularite and Fritmag (3% MgO)	198
5.9	X-ray mapping (at 50X) showing the distribution of MgO in the mineral phase of the sinter.....	202
5.10	X-ray mapping (at 100X) showing the distribution of MgO in the mineral phase of the sinter.....	203
5.11	X-ray mapping (at 500X) showing the distribution of MgO in the mineral phase of the sinter.....	204

<u>Figure</u>	<u>Page</u>
5.12 X-ray mapping (at 1000X) showing the distribution of MgO in the mineral phase of the sinter	205
5.13 X-ray mapping showing segregation of Fritmag	206
6.1 Effect of the amount of +1.7 mm size fraction in the green feed on sinter production rate.....	221
6.2 Effect of the amount of +0.8 mm size fraction in the green feed on sinter production rate.....	221
6.3 Effect of cold permeability of the sinter bed on sinter production rate.....	222
6.4 Effect of the amount of +1.7 mm size fraction in the green feed on cold permeability of the sinter bed...	223
6.5 Effect of the amount of +0.8 mm size fraction in the the green feed on cold permeability of sinter bed...	225
A1.1 System FeO-SiO ₂	247
A1.2 System CaO-SiO ₂	248
A1.3 System CaO-Fe ₂ O ₃	248
A1.4 System FeO.Fe ₂ O ₃ -MgO-SiO ₂	249
A1.5 System MgO-Fe ₂ O ₃	250
A1.6 System FeO-MgO	251
A2.1 Schematic representation of gaseous reduction of iron oxides above 575°C	253

Figure

A2.2	Plot of $r_0 d_0 [1-(1-F)^{1/3}]$ against t for natural single crystals of hematite reduced at 700°C to $F=0.9$, showing typical breakaway behavior in support of two stage reduction mechanism	257
A2.3	Reduction with CO at 1000°C	257
A2.4	Concentration profile of reacting gaseous species along a sectioned spherical particle.....	262
A2.5	Reducibility curve for the sinter without any specularite concentrate.....	269
A2.6	Reducibility curve for the sinter with 25% specularite concentrate.....	270
A2.7	Reducibility curve for the sinter with 40% specularite concentrate.....	271
A2.8	Reducibility curve for the sinter with 100% specularite concentrate.....	272
A3.1	A schematic representation of relationship between reduction at 40% degree of reduction and 60% degree of oxidation levels	278
A3.2	Reducibility index $(dR/dt)_{40}$ vs. $\frac{1}{\text{harmonic mean size, mm}}$	282
A3.3	Effect of the amount of sinter sample on the reproducibility of the reducibility test	283

Figure**Page**

A3.4	Difference in the reduction rate of a spherical hematite pellet reduced at first to 60% at 600°C and remainder at 1000°C and that of a pellet reduced fully at 1000°C	285
A3.5	Differences in the reduction rates of iron oxides with pure CO and H ₂ and their mixtures	287
A3.6	Variations of reduction rate with linear velocity of hydrogen	287

CHAPTER I

INTRODUCTION

In many parts of the world, presently, iron ore sinter (which is produced by agglomerating the ore fines) constitutes the major proportion of the blast furnace burden. Due to the depletion of the rich ore, it has become more and more important to use ore-fines and/or concentrates which are generated while up-grading the lean ores. Problems which may arise while sintering these fines and the quality of the sinters produced depend on several factors such as the physical nature and the chemical composition of the fines. In this work Mount-Wright ore concentrate has been used.

Mount-Wright iron ore is found in the North Shore of Quebec and is one of the largest ore reserves in Canada. Iron in this deposit is in the form of hard dense specular hematite with very low amounts of magnetite and goethite (about 1.0 percent and 0.5 percent respectively). The principal gangue material is mono-crystalline quartz with very low amounts of mica and amphiboles. However, this ore is of low grade and it needs a substantial up-grading.

During the process of grinding and beneficiation of this iron ore, a huge amount of concentrate (up to 18,400,000 MT per year) is generated. About 50% of the total concentrate is presently shipped to Europe. About 90% of the rest (i.e. 8,000,000 MT) is used in the pelletizing plant of Quebec Cartier Mines (Q.C.M.) while the remaining concentrate is consumed in various North American iron and steel industries for sintering and/or pelletization.

1. The Problem

Despite the fact that the Mount-Wright ore concentrate has excellent chemical properties in terms of uniformity and quality (about 65% iron), it is not extensively used in the sinter plants. The amount of this concentrate presently used in Canadian sinter mixes is low (e.g. in Algoma Steel Corporation, it is only about 15%). It seems that the problem encountered while using higher quantity (> 15%) of specularite concentrate in the sinter mix is the significant drop in the permeability of the sinter bed - resulting in a very low productivity of the sinter plant. Moreover, low permeability (which governs the temperature profile by determining the gas flow rate through the bed) also deteriorates the quality of the sinter bed.

The drop in bed permeability due to the specularite addition is mainly attributed to its unfavorable size distribution. Its high mid-size fraction (e.g. about 56% of 0.2-0.5 mm size fraction) is said to prevent the formation of micro-pellets in the green mix and subsequently reduce the permeability of the sinter bed. In order to explain the behavior of the particle size with regard to the micro-pelletization, some Japanese authors^(1,2) have classified the ore-fines into three size ranges and quoted that "The fewer intermediate size particles, the more desirable for the formation of the quasi-particles". The intermediate size particles here belong to the size fraction 0.2-0.7 mm (the detailed classification is given in Chapter II, Sec. 3.2). These particles neither form the seeds for the formation of the micro-pellets nor do they provide a coating on the seeds.

Beside the remarks made by these authors, no other research work in this area has been reported. It has been therefore decided to undertake the present work.

2. The Objectives

The first objective of this work was to produce sinter using more than 15% specularite concentrate in the sinter mix. The aim was to maintain a production rate* of more than 40 tonnes per day per unit grate area (tpd/m²). Since the decrease in production rate of sinters containing high specularite is mainly attributed to the loss in the bed permeability, it was aimed to improve the permeability by developing a suitable micro-pelletization process which would enable to use higher than 15% specularite hematite and still maintain good permeability (so as to obtain the required production rate).

The second objective was to produce sinters of acceptable quality i.e. with a reducibility value*, $(dR/dt)_{40} > 1.20$, strength represented by tumbler index* > 60 and RDI* > 80 . These values are for sinters produced in the pot-grate, tests being conducted following the standard test methods. The values have been set conforming the normal practice.

Lastly, it was aimed to explore the possibility of using a new material, FRITMAG, in the sinter mix as a source of MgO

* These terms will be discussed later in this chapter.

and compare the quality of the sinters produced with that of dolomite-or olivine-added sinters. Fritmag is an asbestos-derived "synthetic olivine" containing about 47% of MgO (and 47% of SiO₂).

3. Sintering Process

A brief outline on the sintering process and the definition of the terms often used in sintering will be given in the following sections.

3.1 Sintering Process and Types of Sinter

Sintering is a process of roasting in which heat (generated by the combustion of carbon) is spread in a layer of ore and fuel by air current sucked down through the mass. The objective here is to form a strong and reducible agglomerate, to incorporate flux into the blast furnace burden and to remove the volatile materials from the burden. The raw materials used are:

1. The iron bearing materials such as iron ore fines, iron fines, mill scales etc. normally -12 mm.
2. Fuel, normally coke breeze (-3 mm) or blast furnace flue dust.
3. Flux, usually -3 mm limestone and/or dolomite.

Depending on whether any flux is incorporated in the raw mix, sinters are broadly divided into two classes e.g. acid sinters (no flux is added to the sinter mix) and fluxed sinters.

For practical purposes, composition of sinter is expressed by its basicity which is the weight ratio of its basic constituents to its acid constituents [i.e. $B = (\text{CaO} + \text{MgO})/(\text{SiO}_2 + \text{Al}_2\text{O}_3)$]. Sometimes, it is calculated by the weight ratio of CaO to SiO_2 (B') or CaO and MgO to SiO_2 (B'') for convenience. Further classification of sinter (depending on its basicity) are:

- (a) Self-fluxing sinters: Those where sufficient flux is added to have the same basicity as the blast furnace slag. However, an extra amount of flux has to be added to consider the acidic gangue of the lump ore, pellets and coke. The basicity of this type of sinter is usually 1-1.5.
- (b) Super-fluxed sinters: In this case, flux materials are incorporated to the mix in excess such that there is no need to charge any more flux into the blast furnace. The basicity here, is >1.5 .

3.2 Industrial Sintering Practice

Dwight-Lloyd continuous travelling grate sintering machine is used in most of the sinter plants. A schematic diagram of such a sintering machine is given in Fig. 1.1⁽³⁾. Here, the raw materials are properly mixed in a suitable mixer (such as mixing trommel or pug-mill) and laid uniformly across the width of the sinter strand using a feeder. Before the mix is charged, a layer (4-5 cm thick) of sinter (size 8-10 mm) known as hearth layer is spread on the grate. This is to prevent any leakage of the mix and to avoid any sticking problem due to the melt produced during sintering.

As the strand moves, the mix is levelled off by a cut-off plate. Fuel in the top layer of the sinter bed is ignited by a gas or oil burner while the bed passes under the ignition hood. Air is continuously sucked down through the charge from under the grate with the help of suction fan. The cold air which gets pre-heated in the upper layers of the sinter bed sustains combustion of the fuel inside. It is then cooled by the water evaporating from the layers immediately below the combustion zone. The waste gas leaving the bed passes to the fan. Thus, the flame front gradually moves downward and sintering proceeds. Several physical and chemical changes can occur during sintering. Various zones existing during the process are shown in Fig. 1.2⁽⁴⁾.

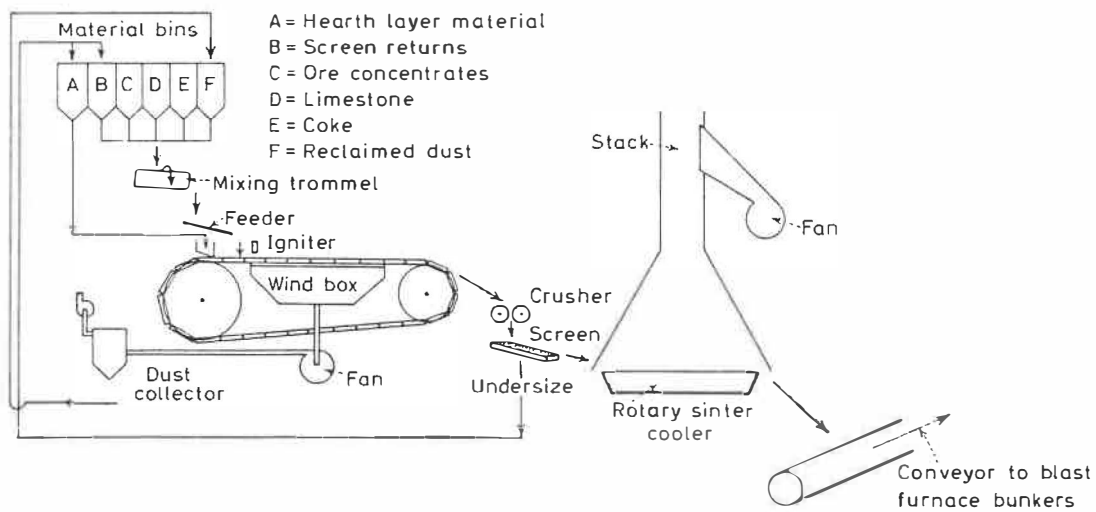


**Fig. 1.1 Schematic diagram of Dwight-Lloyd sintering machine
 (Ref. 3).**

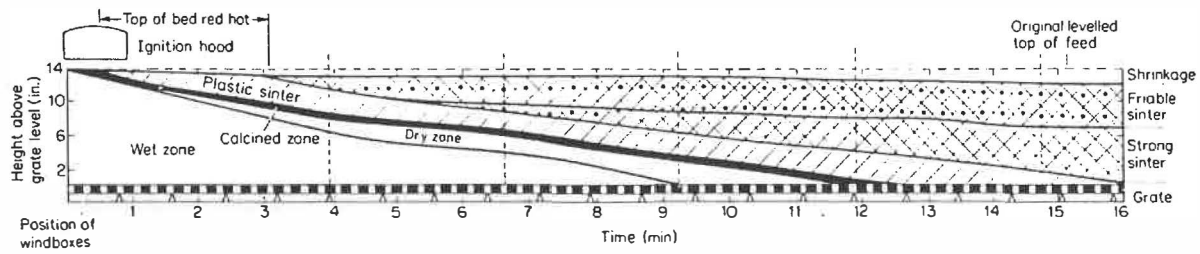


Fig. 1.2 Zone structure developed on Dwight-Lloyd strand (Ref. 4).

Sintering is complete when all the fuel in the bed is consumed. In practice, the end of sintering is marked when the temperature of the waste gas reaches its maximum. The sinter cake is then tipped off at the discharge end, crushed and screened. The oversize sinter is cooled down and conveyed to the blast furnace while the undersize is recycled as return fines (details will be given in Sec. 3.5).

The grate area of the sinter strand and the bed height vary with different practices. The typical values of the grate area and bed height are 400-500 m² and 50-60 cm respectively.

3.3 Laboratory Method for the Production of Sinter

Generally, fundamental studies on sintering are not carried out on the industrial strand as they may interfere in the regular plant operation and decrease its productivity. They are instead studied in the laboratory using a batch process. Tests are simulated to represent the actual plant practice conditions and information gathered from these tests can be used to improve the plant operation and to produce sinter of better quality. Unlike the industrial sintering process, this sinter bed is static and the flame front is made to move vertically by sucking air down through the bed. The schematic diagram of a typical pot-grate test apparatus is shown in Fig. 1.3⁽⁵⁾.

A cylindrical- or square-shaped stainless steel sinter pot is generally used for the test. The green mix is first prepared by mixing the raw materials properly in a suitable mixer and charged into the sinter pot. Before charging the green mix, the hearth layer is spread on the grate. The bed temperatures and the pressure-drops across the bed during the sintering process are measured by the thermocouples and the pressure probes in the bed (see Fig. 1.3).

Ignition of the sinter bed is achieved by using a gas or oil fired burner. In order to have proper ignition, a layer of coke is usually spread on the top of the bed. A constant suction is maintained until the process is completed. During the sintering period, the temperatures and pressure-drops of the bed at different positions, waste-gas temperature and composition are continuously recorded. A vertical section of a static sinter bed is shown in Fig. 1.4⁽⁵⁾. Different zones and the temperature profile of the sinter bed at a particular time during sintering can be seen in this figure. The end of the sintering period occurs when the maximum temperature of the waste-gas is reached. No further experimental measurements are normally made beyond this point.

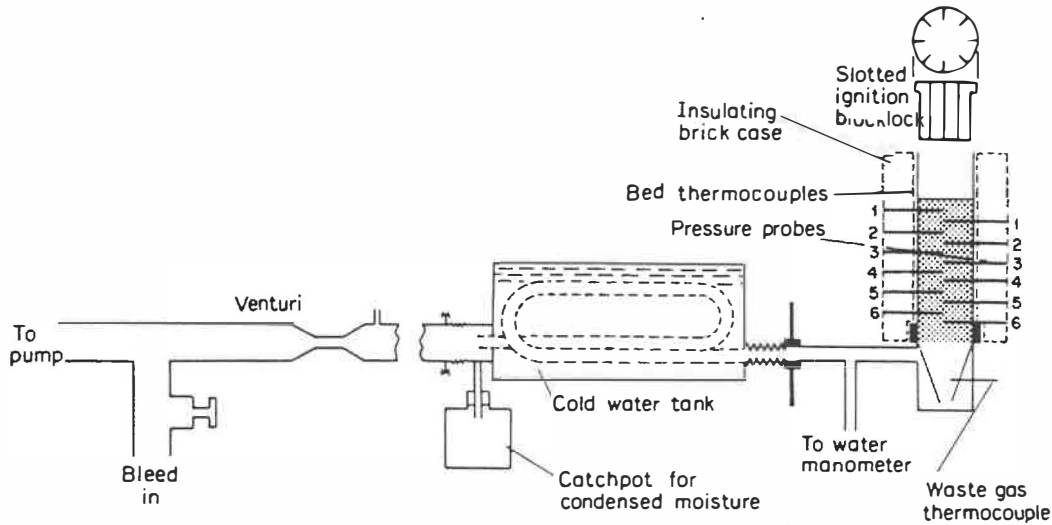


Fig. 1.3 Laboratory sintering apparatus (Ref. 5).

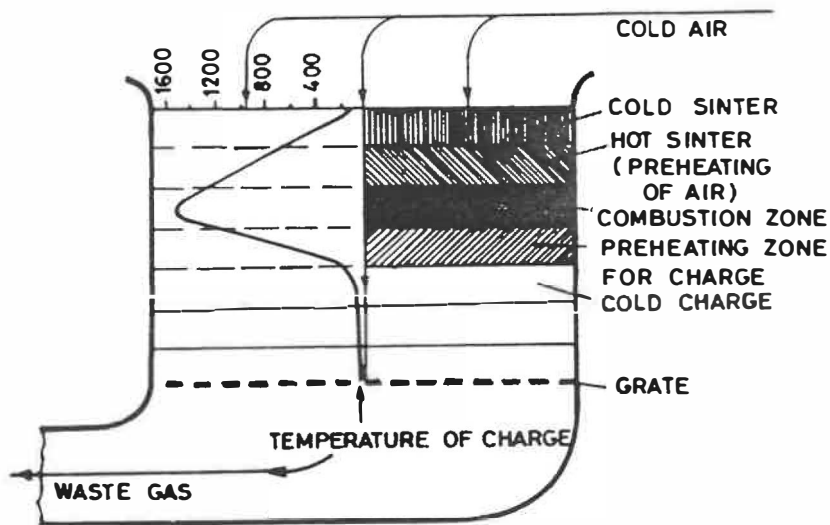


Fig. 1.4 Temperature profile and the zones existing in the sinter bed at a particular time during sintering (Ref. 5).

The sinter cake is then removed from the pot, stabilized (by dropping it from a height of 2 m (or 6 ft.) on a steel plate) and screened. The oversize (+6.36 mm or $+\frac{1}{4}$ ") is used to characterize the sinters while the undersize is recycled. For an optimum sintering condition, the weight ratio of the return fines generated in the process to the amount added to the mix should be close to 1 (see recycling of fines in Sec. 3.5).

The major problem encountered in this process is the "wall effect". Depending on the pot size and the type of raw materials used, some amount of unsintered materials are generated at the walls. This is because of the shrinkage of the raw mix - leading to air-leakage at the walls and also due to the heat loss around the walls. It can be overcome by using a larger size sinter pot. However, some handling problems may arise due to this. A smaller size pot can be successfully used by excluding large pieces and the materials which can cause excessive shrinkage from the sinter mix.

With proper laboratory method, some important process parameters such as permeability of the bed, temperature profile, sintering rate, amount of return fines generated, coke rate and moisture content of the mix for optimum bed-permeability can be investigated. In addition, utilization of fuel can be studied from the waste gas analysis. Sintors can also be characterized to evaluate its quality.

3.4 Ignition

At the onset of sintering process, a good ignition of the top layer of the bed is very essential. Improper ignition may lead to non-uniform movement of the flame front which would eventually generate sinter of inferior quality.

The ignition condition for sintering has been studied by several authors⁽⁶⁻⁸⁾ by using static bed with different kinds of ore mix. They have noted that use of a few percent of excess air, (5-10 % depending on the composition of the mix) over the stoichiometric amount that is required for the coke-burning, is the best condition to obtain sinter strength. Lower amount of air causes loss in heat due to carbon solution reaction ($C + CO_2 = 2CO$), while higher amount reduces the flame temperature resulting in weaker sinter. Amount of air depends on the size and the composition of the raw materials.

Different techniques such as pre-heating the air or addition of higher amount of fuel in the top layers are sometimes used to ensure proper ignition.

3.5 Recycling of Fines (or Circulating Load)

Due to the size requirement of the blast furnace burden, return fines can not be charged to the blast furnace. They are therefore recycled in the sintering process. The upper limit of these fines normally varies between 5-10 mm.

Considerable amounts of sinter fines (about 20-40%) are generated in the sintering process. It is mainly due to the unsintered or poorly sintered materials and because of the breakage during handling of the sinters. A lot of unsintered/poorly sintered materials is produced in the top part of the sinter bed. This is due to the low sintering temperature attained in that part because of cold air passing through it. Wall effects or insufficient amount of fuel or high amount of moisture in the mix can also generate poorly sintered material.

Return-fines are to some extent, useful for the sintering process. They serve as nuclei for the formation of quasi-spheres (micro-pellets) during mixing and increase the permeability of the sinter bed. Due to their lower fusion temperature than the raw mix, they also serve as seeds for initiation of the sintering process. However, an excess of these fines decreases the productivity and the process becomes uneconomical. The amount of fines recycled depends on various industrial practices (usually varies from 20-30%). Hence,

conditions are chosen (mainly by changing the amount of water and/or fuel) to have an optimum amount of return fines.

The optimum sintering condition refers to a condition for which the return fine balance is approximately equal to 1, i.e.

$$F_B = F_o/F_i \text{ is as close as possible to 1.}$$

where, F_B = Fine sinter balance

F_o = Fine sinter output

F_i = Fine sinter input

In order to achieve this condition, for any particular mix, usually few tests are carried out by changing the amount of water or fuel or both.

3.6 Waste Gas Analysis

It is important to know the analysis (the CO, CO₂ and O₂ content) of the waste-gas. This provides the information regarding the combustion efficiency of the sintering process. Though an excess amount of O₂ is always present in the sintering atmosphere, combustion is never complete in sintering and there is always some amount of CO in the waste-gas. A typical range of analyses of waste-gas⁽⁹⁾ would be 5-16 % CO₂, 1-3 % CO and 8-15 % O₂. High ratio of CO/(CO₂ + CO) indicates high suction pressure and/or high reactivity of the fuel. High CO/(CO₂ + CO)

ratio in the waste gas lowers the total heat generated in the sintering process and decrease the fuel efficiency. This can be overcome by decreasing the suction pressure (thus, reducing the volume of air drawn) and/or increasing the size of the fuel (thus, decreasing its reactivity).

3.7 Sinter Time

Sintering time is the duration between the start of the ignition and the time when the temperature of the waste-gas reaches its peak. It depends on the rate of movement of the flame front which in turn depends on the bed permeability and the reactivity of the fuel.

3.8 Production Rate

The production rate of the sinter is an important parameter as it largely affects the economics of the process. It is calculated on the basis of the amount of usable sinters (which depend on the plant practice, usually +6.36 or +9.5 mm) produced and it is expressed in terms of tons of sinter produced per day per unit grate area (tpd/m²).

Production rate can be increased by increasing the amount of usable sinters produced or decreasing the sintering time.

3.9 Carbon Rate

The carbon rate of the sinter is calculated from the amount of fuel used and the weight of the usable sinter produced. This is expressed as kilograms of carbon (knowing the carbon content of the fuel) required to produce a ton of sinter (i.e. kg/t).

4. Quality of Sinter

The quality of iron ore sinter is evaluated from its behavior during its handling and during its reduction in the blast furnace. It should have a minimum strength to avoid breakage while being transported from the sinter plant to the furnace. It should not generate lot of fines during its reduction in the furnace. It should have a high reduction rate. The details of the various properties of the sinter and the factors affecting will be discussed in the next chapter.

The strength of sinter and its degradation during reduction are represented by two indices viz. Tumbler index (or T-index) and Reduction Degradation Index (RDI) respectively. The rate of reduction or reducibility of sinter is expressed by $(dR/dt)_{40}$. The details of the methods followed to determine these values will be described in Chapter IV.

5. Scope of the Work

More than 200 pot-grate tests were carried out to produce sinters using different percentage (e.g. 0%, 25%, 40% and 100%) of specular hematite concentrate. The mixing conditions were optimised by following various techniques such as using different mixing/micropelletizing devices and additives/binders so as to achieve maximum degree of pelletization. This has consequently increased the permeability of the sinter bed and increased the production rate. Three different devices, namely roll compactor, disc pelletizer and turbulator and four additives/binders e.g. quick-lime, bentonite, peridur and peat moss were used for this purpose.

The quality of these sinters was evaluated by determining the properties following the standard testing methods. For few selected mix conditions pot-grate tests were carried out in the actual industrial sinter strand. The properties of these sinters were compared with those of the corresponding sinters produced in the laboratory pot-grate. A few tests were also carried out by adding the fuel in two stages to the sinter mix. Effect of such a modification on the production rate and sinter quality were studied.

Finally, some pot-grate tests were also carried out by adding Fritmag in two levels (aiming to have 2.5 and 3.0 % MgO in the sinter) to study its effect. Sinters were also produced with dolomite or olivine as the source of MgO. The quality of these sinters were then evaluated.

The thesis consists of five chapters. As it has been noticed, the first chapter deals with the problem and the objectives of this work, followed by a brief description on the sintering process. The chapter concludes with the summary and scope of the present work.

In the second chapter, the details of the theoretical aspects involving the productivity of the sintering process, bed permeability and the micro-pelletization process are given. Reactions occurring in the sintering process, mineralogy of sinter, effect of MgO, and the properties of sinter are also discussed in this chapter.

In the first section of Chapter III, the description of the raw materials used for this work are given. The equipment used and the procedure for the micro-pelletization study as well as for sinter production are also discussed in the second section. The results and the discussions of the micro-pelletization study are dealt in the third section and in the last section we will discuss the production of the sinters in the laboratory

pot-grate and on the industrial strand. In Chapter IV, we will discuss about the mineralogy and the quality of the sinters.

Chapter V deals with the effects of Fritmag addition on sintering. A comparison have been made among the properties of these sinters with those produced with dolomite and natural olivine.

In the final chapter, Chapter VI, the synthesis of the important results obtained in this investigation is presented. The thesis ends with our conclusions and recommendations.

CHAPTER II

REVIEW ON SINTERING PROCESS

This chapter is divided into three sections. In the first section, a detailed discussion on the production rate of sintering process, factors affecting it and the ways to optimise them (to get maximum production rate) are given. The second section deals with the sintering reactions, mineralogy of the sinter and the effects of MgO. The properties of sinter and how they are affected by the nature and amount of mineralogical phases are described in the third section.

1. Production Rate

Having discussed the sintering process, we can now realize that production rate of the sintering process can be increased by decreasing the circulating load (i.e. the amount of return fines recycled in the process), increasing the amount of sinter produced and/or decreasing sintering time. Return fines are mainly generated in the top part of the sinter bed and around the walls. Although the amount of the fines can be reduced by using pre-heated air or by drying the uppermost layers of the sinter bed, its control is difficult.

Another way is to increase the sinter output or reduce the sintering time. We know that in order to sinter a given weight of raw mix, a specific volume of air is required. Hence, for high sinter outputs, a large volume of air must flow through the bed. This can be achieved by using high suction or having a mix of high permeability. Since very high suction can not be used (due to practical and economical reasons) it makes the permeability of the sinter mix vitally important in determining sintering time and the strand output.

2. Permeability of the Sinter Bed

The rate at which air is drawn through the sinter bed has a profound effect on the movement of the flame front inside the bed and thus, it significantly controls the sintering time. The permeability of the sinter bed changes with time during the sintering process. As shown in the typical "permeability - sintering time" curve (Fig. 2.1), the bed permeability first decreases, reaches a minimum and then increases, initially at a slow rate gradually becoming faster.

The initial bed permeability is relatively high because of the voids created by the green mix. After ignition, the temperature of the bed rises. The bed permeability decreases due to the physical changes (such as melt formation) occurring in the process. After reaching the minimum value it again

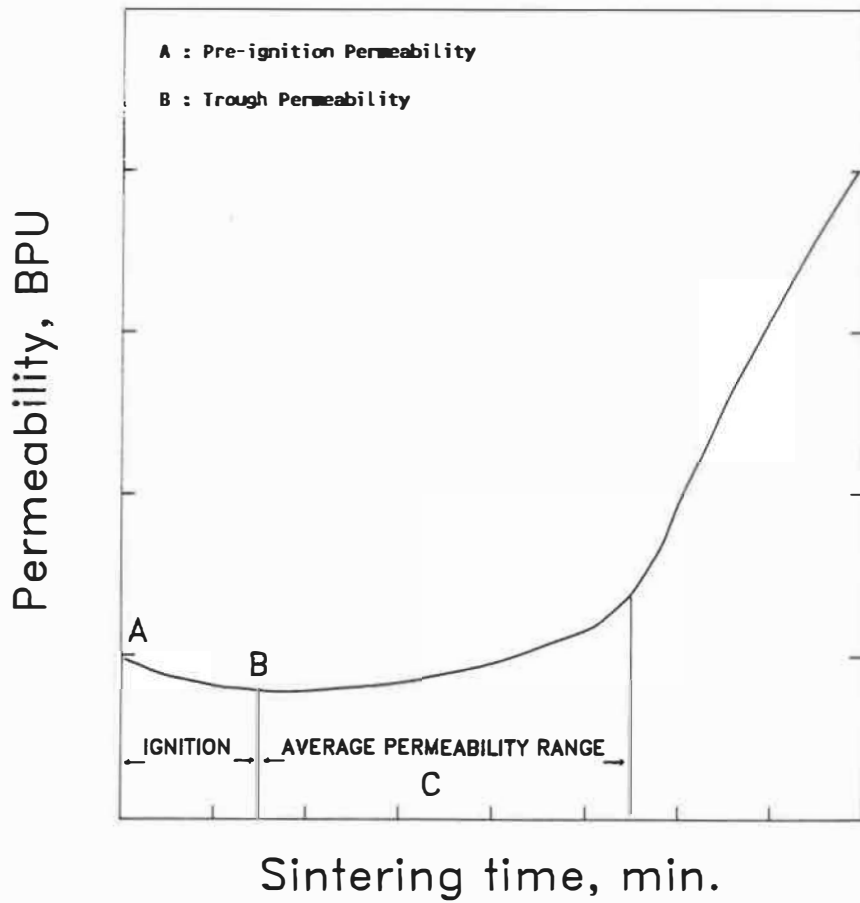


Fig. 2.1 Variation of permeability of the sinter bed with time, as sintering proceeds.

increases due to the porous sinter produced on the top part of the bed. When sintering is complete, permeability reaches its maximum because of large amount of pore formation.

Usually, three values of permeability are considered in the regular plant practice. These are:

- a) the pre-ignition permeability (i.e. permeability before ignition, point A in Fig. 2.1);
- b) the trough permeability (i.e. the minimum permeability after the ignition, point B);
- c) the average permeability (i.e. the average of the permeability values measured during sintering, the range C in Fig. 2.1).

The gas flow per unit area, F/A is a function of the bed height, h and suction, s . This can be expressed as:

$$F/A = f(s^n/h^m) \quad \dots(2.1)$$

where, n and m are constants.

In case where $n = m$, we have:
$$F/A = P (s/h)^n \quad \dots(2.2)$$

where P is a constant, known as permeability and it represents the air flow per unit area under conditions of unit suction and unit bed height.

By re-arranging Eq. (2.2), we have: $P = (F/A)(h/s)^n$ (2.3)

Considering the fundamental factors governing the air flow through the packed bed of granular and fine materials, Carman⁽¹⁰⁾ has developed two equations:

$$\text{for laminar flow} \quad \frac{g\epsilon^3}{5S^2} = \frac{F}{A} \left(\frac{h}{s}\right)^{1.0} \quad (2.4)$$

and for turbulent flow

$$0.62\eta^{0.053} \frac{g^{0.526} \epsilon^{1.58}}{S^{0.579} \rho^{0.474}} = \frac{F}{A} \left(\frac{h}{s}\right)^{0.526} \quad (2.5)$$

where g = acceleration due to gravity

ϵ = voidage

ρ = density of fluid

S = total surface area

η = absolute viscosity of fluid

It has been seen that the flow is likely to be in the transitional range between laminar and turbulent flow. Calculation involving these considerations is quite complex as substantial changes in gas density, bed temperature and surface area takes place during sintering. A remarkable agreement between theory and practice is observed by considering these factors⁽¹¹⁾. However, it is quite complicated and in normal practice the simple expression given by Eq. (2.2) is used to calculate the bed permeability.

The value of n also depends on many factors such as raw mix, moisture content and bed height and it changes from 0.55 to 0.65) during sintering^(12,13). For regular plant use, permeability is calculated by assuming $n = 0.6$ (which has been empirically determined by Voice et al⁽¹²⁾) in Eq. (2.2);

$$\text{i.e.} \quad P = (F/A) (h/s)^{0.6} \quad \dots(2.6)$$

Permeability is expressed in British Permeability Units (BPU) when air flow F is in normal ft^3/min , the cross-sectional area of the bed A is in ft^2 , the bed height h is in inches and suction s is in inches of water gauge.

As we have already discussed, an increase in permeability increases the strand output. Moreover, since it controls the heat transfer characteristics in the bed, it has also a significant influence on the quality of sinter. If it is too high, the rapid air-flow down the bed will carry the CO produced at the surface of the fuel into the cold zone so fast that combustion will never be complete and there will be a loss in fuel efficiency. Also, due to high rate of air flow, the transfer of heat between gas and solid will become less efficient. This will eventually cause non-uniform sintering and produce sinter of inferior quality. Hence, it is desirable to attain the maximum value of permeability without deteriorating the fuel efficiency and the quality of sinter.

It is clear that the amount and distribution of the fuel both influence the bed permeability by determining the width of the combustion zone and the amount of the melt formed during sintering.

Resistance to air flow is offered by the combustion zone, drying (or pre-heating) zone and the unsintered material (or cold charge). These zones have been shown in Fig. 1.4. The sintered materials do not offer any significant resistance because of their porous structure. The resistance in different zones changes during sintering. Hence, the bed permeability is not only affected by the initial condition of the sinter mix, but also by the physical changes occurring during sintering. However, little can be done to control the bed permeability during sintering.

Permeability of the sinter mix is largely controlled by the size distribution of the raw materials. The effects of raw material size on the bed permeability have been studied by Voice et al.⁽¹²⁾, Wild et al.⁽¹³⁾ and more recently by others^(14,15). They have seen that the bed permeability can be improved by using coarser size materials or by increasing the degree of micro-pelletization during mixing.

3. Micro-pelletization

The necessity to use higher amount of finer materials has encouraged some researchers^(14,15) to study different means to increase the bed permeability of a mix containing large amount of fines. Efforts have been made to improve the size distribution (i.e. increase the amount of the coarser fractions) of such a mix by pre-granulating it before sintering. The micro-pellets formed in the process should have sufficient strength to avoid any breakage during their handling. This process of forming strong micro-pellets is known as micro-pelletization. By following a suitable micro-pelletization process, the bed permeability can be improved. Besides, it will also lead to desirable coke burning and thereby, improve the sinter quality.

Water is commonly used to help forming the micro-pellets in sinter mix. Several other techniques are also followed to prepare the mix so as to enhance the degree of micro-pelletization. A schematic diagram showing the basic concept of preparing the sinter mix is given in Fig. 2.2. As we can see in this figure, the amount and the strength of the micro-pellets can be improved by improving the size-distribution pattern of the raw materials, the mixer application technique and using binder. Before discussing the influence of these techniques, we will briefly see the theory of the formation of the micro-pellets (or theory of the balling process).

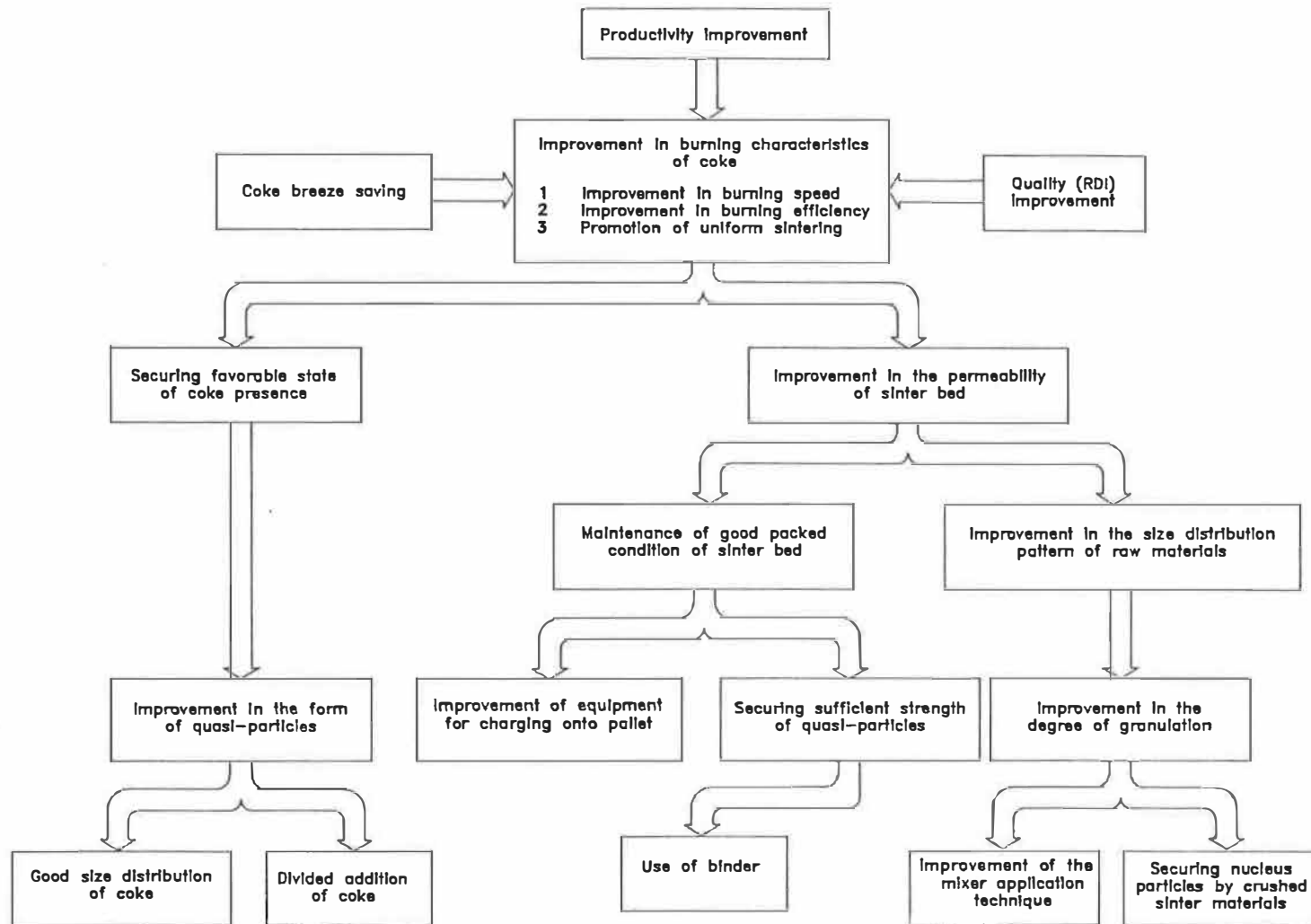


Fig. 2.2 Basic concept of sinter mix preparation.

The theory of the balling process and the mechanism of the ball formation with regard to the pelletization process have been explained by many authors⁽¹⁶⁻²⁰⁾. Unlike in the pelletization process, while preparing the sinter mix, the aim is not to produce well developed and strong pellets, but to form strong micro-pellets to improve the size-distribution of the green mix (for high permeability).

Both, physical and mechanical factors can influence the formation of the pellets. The physical factors involved are the forces of attraction between the particle (such as Van der Waals, magnetic and electrostatic forces), size distribution and shape of particles, material wettability and its absorption capability, interfacial and capillary forces due to the presence of a liquid phase.

In order that these physical forces can act efficiently for the development and growth of the green pellets, it is necessary to bring the individual wetted particles into contact with one another⁽¹⁸⁾. This can be attained by using a suitable mixer.

3.1 Water Content

When water is added to the raw mix, the capillary forces developed between the particles due to water-air interfacial tension holds the particle together. To achieve maximum ball formation, the water content is critical and it largely depends on the type of material used. This can be explained with regard to the capillary forces. Insufficient water reduces the capillary effect by air inclusion within the ball. On the contrary, excess water forms a coherent film of water around the ball and thus, neutralizes the capillary effect.

The measurement of porosity of the materials can serve as an indicator of the optimum water content. Porosity is given by:

$$\epsilon = \frac{\text{specific volume} - \text{weight/true density}}{\text{specific volume}} \quad \dots(2.7)$$

Knowing the true density of the material and determining its specific volume, porosity can be calculated. The specific volume is defined as the volume occupied by a specific weight of material which has been vibrated until the minimum volume is attained. The above equation can now be written as:

$$\epsilon = \frac{\text{vol. of voids}}{\text{specific vol.}} \quad \dots(2.8)$$

The quantity of water just sufficient to fill up the voids can be calculated. It is to be noted that this method does not take the absorption capability of the material into account. The sinter mix consists of many different kinds of materials and hence, it is quite complicated to calculate the optimum moisture content theoretically.

In normal practice, the optimum water content is determined empirically, by measuring the bed permeability for different amount of water. The change in the permeability of the mix is plotted against the water content. A typical shape of such a curve can be seen in Fig. 2.3. As shown here, the permeability of the mix first increases with the water content, reaches a maximum and then decreases. The optimum amount of water corresponds to the maximum value of the permeability. Up to this level, the development of the agglomerates takes place and beyond this level, the agglomerates collapse. Usually, the amount of water is expressed as per cent of dry mix. It should be noted that in practice, sometimes, the optimum water content is slightly changed to adjust for the return fine balance (see Sec. 3.5, page 15).

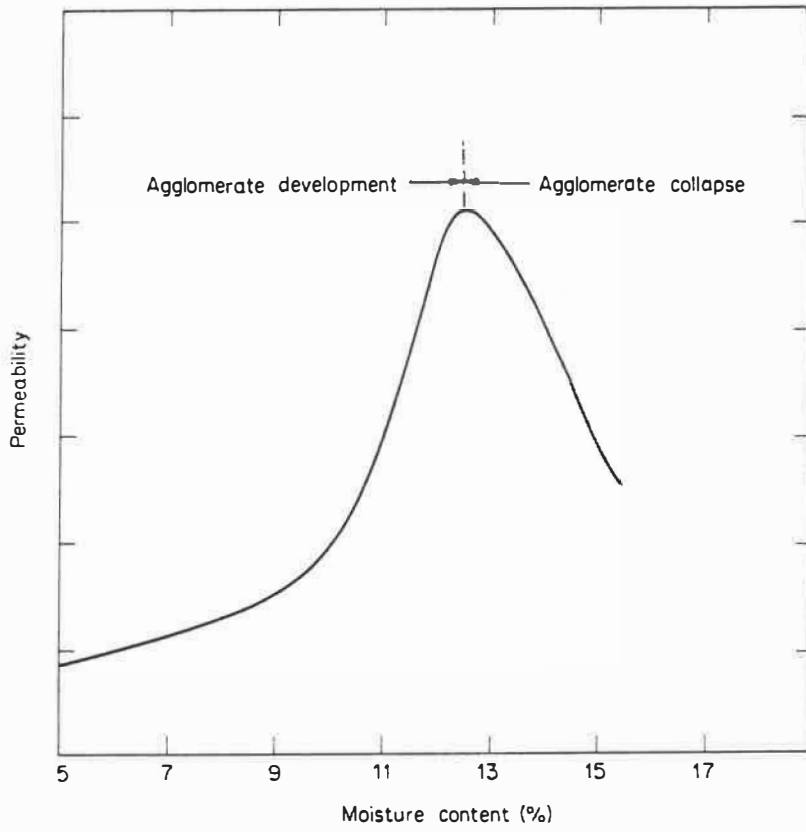


Fig. 2.3 Typical relationship between permeability and moisture content (Ref. 4).

3.2 The Shape and Size Distribution of the Materials

The shape of the iron-ore particles largely depends on their mineralogical structure. It plays a significant role in the balling process. In case of specular hematite (where the particles are plate-shaped), when the grains are stacked parallelly, they yield a low voidage. On the contrary, there is high voidage when they are charged at random. These materials are relatively difficult to micro-pelletize.

The size of the iron ore particles also has a major bearing on micro-pelletization. It determines the total surface available, the porosity and the optimum water content. In order to explain the effect of the particle size on micro-pelletization, some Japanese authors^(1,2) have classified the ore-fines by their size. It is given in Table 2.1. They have suggested that +0.7 mm (1 to 3 mm) particles serve as nuclei particles for pre-granulation and -0.2 mm size particles form adhering layers on the nuclei. These two size fractions are beneficial for the formation of quasi-particles and should be present in the mix in good proportion. On the other hand, the intermediate size fraction (i.e. 0.2-0.7 mm) does not serve any of the above purposes and is detrimental to the micro-pelletization process.

Table 2.1: Classification of raw material particles by sizes

Nucleus particle	Particle forming a nucleus of quasi-particle (N)	+ 0.7 mm (1 - 3 mm) is particularly good
Adhering particle	Particle which adheres to quasi-particle and forms an adhering layer (F)	- 0.2 mm
Intermediate particle	Particle which hardly forms nucleus or hardly adheres to an adhering layer (M)	0.2 - 0.7 mm

From this, it is clear that micro-pelletization of the specularite hematite, which is plate-shaped and has more than 50% of intermediate size particles (see Table 3.2, Chap. 3) is difficult to achieve. One way to overcome this problem is by crushing this concentrate so as to overcome the problem of its shape and size. This would, however necessitate the change in the grinding system and would incur high cost.

Another alternate is to find a suitable mixing/micro-pelletizing device(s) and/or using proper additive/binder(s). The equipment commonly used to mix the materials for sintering are: pug mill, mixing trommel or drum mixer⁽¹⁴⁾. These units efficiently mix the commonly used materials with high coarse size fraction. They are not so useful for micro-pelletizing the mix containing large quantity of fine materials. Being designed as mixing devices, they would rather break up the micro-pellets to achieve better mixing. It is therefore necessary to test some other devices.

The first alternate is to mix in a disc pelletizer which is normally used for the pelletization process. There are two other devices namely, turbulator and roll compactor which may be of some help in this regard. These equipments are presently used for the pharmaceutical and agro-industries for mixing/granulating. The details of these equipments will be described in the next chapter.

With regard to the use of binders, quick-lime may be considered because of its hygroscopic nature. Some other materials which have also been tested are bentonite, peridur and peat moss. These materials have been found useful as binder in pelletization process^(21,22). The details of these binders will be discussed in the next chapter.

4. Sintering Reaction and Mineralogy of the Sinters

Sintering of iron ore is a very crude process because of the wide size-range of the materials used, non-uniform temperature profile of the sinter bed and above all, the inadequate time factor (for the completion of the reactions). Local heating (or slow burning) may also occur depending on the size distribution of the coke particles. Some compounds which are unexpected from the composition of the sinter mix are often found in the final sinter structure. This is due to the segregation of some reaction components, thus changing the local sinter chemistry. A schematic diagram showing the general changes in the mineralogical phases taking place during the sintering process is shown in Fig. 2.4. From this figure it can be seen that the sinter structure is essentially marked with three types of constituents, viz.:

1. the unaltered or relict mineral constituents which have not undergone any change;
2. the mineral phases which have undergone structural changes by recrystallization in solid state;
3. Secondary constituents recrystallized or consolidated as glassy phase from the liquid solution formed during sintering; the crystals could be dendrites, skeletal or fully developed. This results in the formation of calcium ferrites, dicalcium silicates, spinel etc.

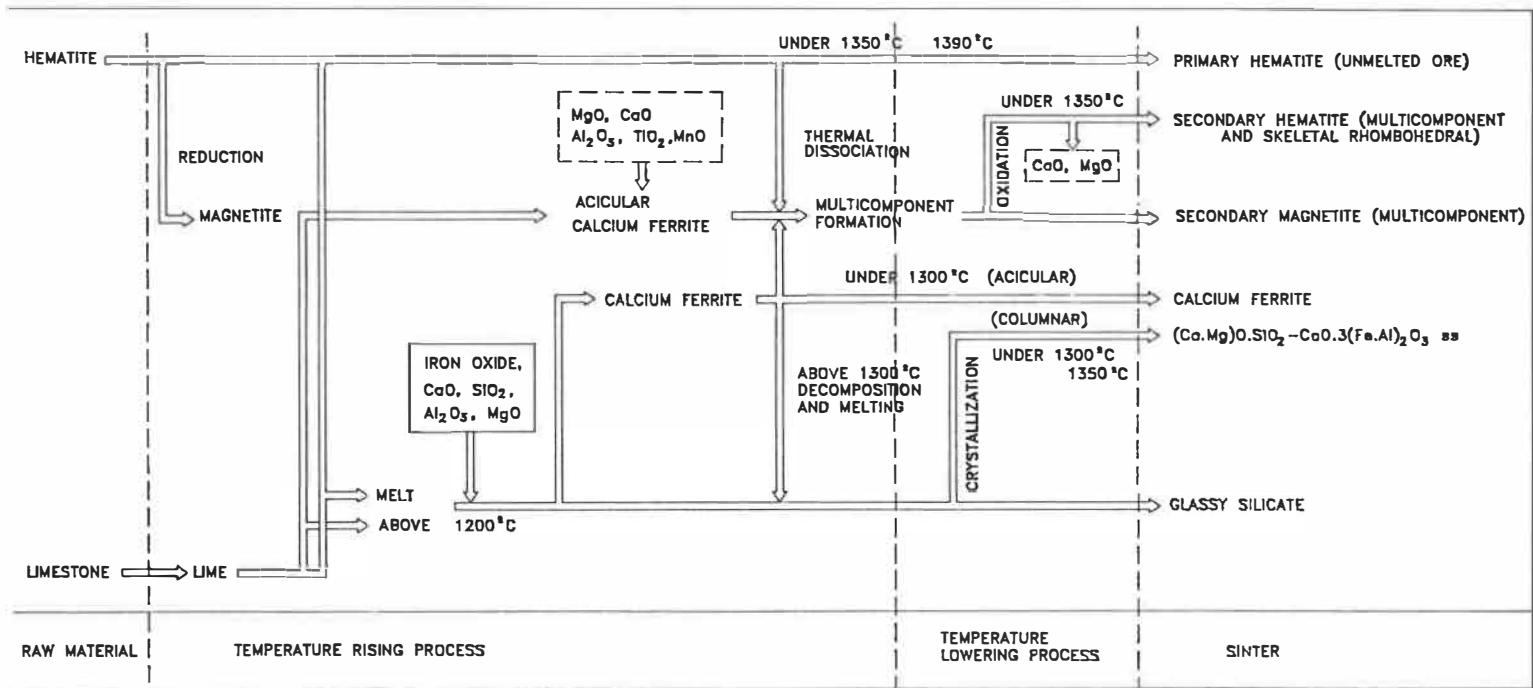
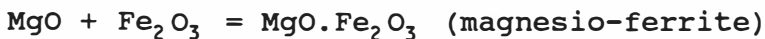
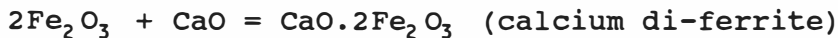
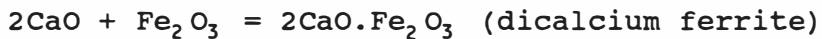
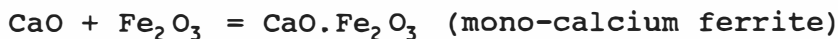
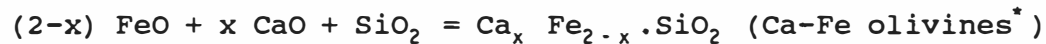
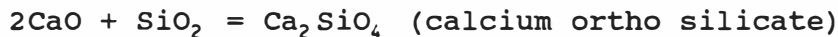
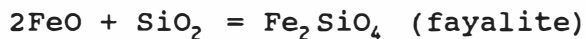


Fig. 2.4 General changes of mineralogical phases during sintering.

Besides the iron oxides, the other principal constituents involved in the sintering reactions are CaO, SiO₂, MgO, Al₂O₃ and in much smaller amount MnO, TiO₂, Na₂O and K₂O. The reactions are further complicated by the divalent and trivalent states of iron. Some of the reactions that can occur during sintering are:



Reaction equilibrium is difficult to attain in sintering. The higher the temperature and duration, the closer will be the approach to equilibrium. However, the equilibrium phase diagrams are useful to understand the formation of certain phase and hence, some important diagrams are given in Annex 1.

* Olivines consist of a group of minerals. It is an ortho-silicate of ferrous iron (e.g. fayalite), in which several other basic oxides such as CaO, to some extent MgO and MnO may substitute for FeO.

The mineralogy of sinters is of great interest and it has been extensively studied by many authors⁽²³⁻²⁶⁾. It is seen that the type and the amount of mineral phases largely control the properties and the quality of the final sinter (details will be discussed later). The type and the amount of different mineral phases present are believed to depend mainly on the chemical constituents of the ore and flux and the fuel rate. Change in sinter mineralogy with its basicity is shown in Fig. 2.5⁽²⁵⁾.

In the above figure, the basicity is expressed as the weight ratio of only CaO and SiO₂ (the MgO and Al₂O₃ contents are low). As evident from this figure, at low basicity (B<0.5), the major phases are magnetite, hematite and fayalite while at higher basicity (B>2.0), the predominant phase is calcium ferrite with some magnetite and hematite. In the following paragraphs we will discuss the changes in the mineral phases with the changes in the composition of the sinter.

The acid sinters (in the absence of lime and alumina) are almost entirely made up of magnetite, hematite and fayalite. Some amount of higher iron oxides are invariably reduced to FeO because of the reducing atmosphere which prevailed in sintering due to coke burning. FeO combines with SiO₂ to form fayalite, 2FeO.SiO₂. Fayalite which has a melting point of 1210°C (as shown in Fig. A1.1, Annex 1), can form low melting liquid phase

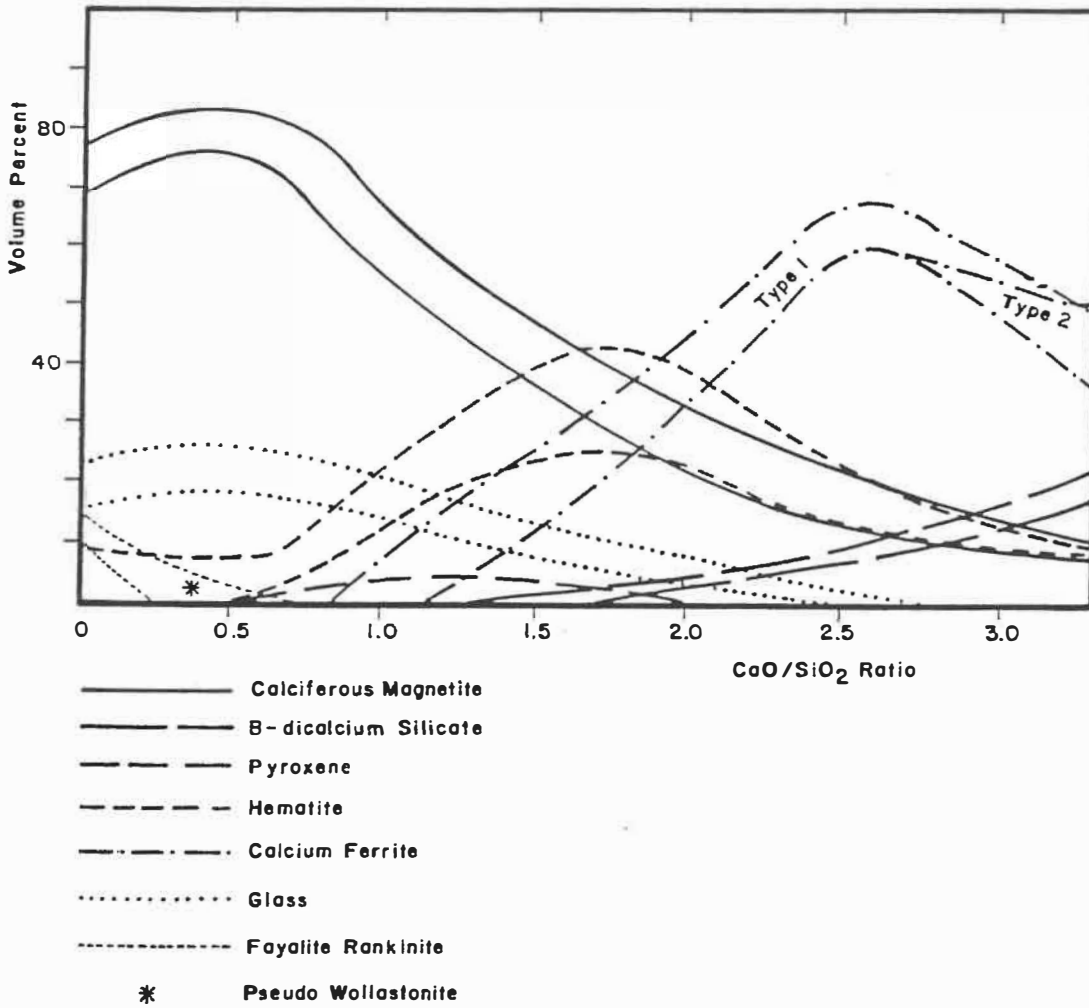


Fig. 2.5 Variation of sinter mineralogy as its basicity changes (Ref. 25).

in presence of SiO_2 , FeO and Fe_3O_4 . Viscosity of the liquid phase increases with silica and alumina content leading to the formation of the glassy phases while cooling. The fayalite⁽²³⁾ content of the sinter increases with the amount of fuel.

With the increase in the sinter basicity, the volume of the slag phase increases. The viscosity of the liquid decreases due to lime addition. The glassy phase of the sinter is gradually replaced by crystalline calcium silicates. CaO can form several silicates e.g CaO.SiO_2 , $3\text{CaO}.2\text{SiO}_2$, 2CaO.SiO_2 and 3CaO.SiO_2 (see CaO-SiO_2 phase diagram in Fig. A1.2, Annex 1). Fayalite dissolves in dicalcium silicate (2CaO.SiO_2). Knepper et al⁽²⁴⁾ have observed that the maximum solubility of fayalite in dicalcium silicate is 10% at 1230°C . While cooling, the phases that can form are: 2FeO.SiO_2 ; CaO.FeO.SiO_2 (olivines of general composition $\text{Ca}_x.\text{Fe}_{2-x}.\text{SiO}_4$, $x>2$); and calcium silicates⁽²⁴⁾.

The mineralogy of the self-fluxing sinters ($B = 1.0-1.5$) consists of mainly hematite, magnetite, calcium olivines and calcium ferrites⁽²⁵⁾. Kissin et al.⁽²⁶⁾ have noticed some dendrites of hedenbergite (CaO.FeO.SiO_2) in this type of sinter. Increase in FeO decreases the ferrite contents and favors the formation of calcium olivines; decrease in the amount of calcium orthosilicates is marked⁽²⁷⁾.

At basicity around 1.2, small needle and plate shaped monocalcium ferrites ($\text{CaO}\cdot\text{Fe}_2\text{O}_3$), calcium diferrites ($\text{CaO}\cdot 2\text{Fe}_2\text{O}_3$) and ternary ferrites ($\text{CaO}\cdot\text{FeO}\cdot\text{Fe}_2\text{O}_3$) start forming in a slag matrix⁽²⁷⁾. Formation of ternary ferrites is possible due to the reducing atmosphere of the sintering process. As the basicity increases beyond 1.2, the amounts of calcium ferrites increase. The effect of basicity on the ferrite formation is shown in Fig. 2.6⁽²⁷⁾. With the addition of lime, the melt formation temperature and the viscosity of the liquid phase decrease. It has been observed^(28,29) that the formation of ferrites is very much facilitated in this slag.

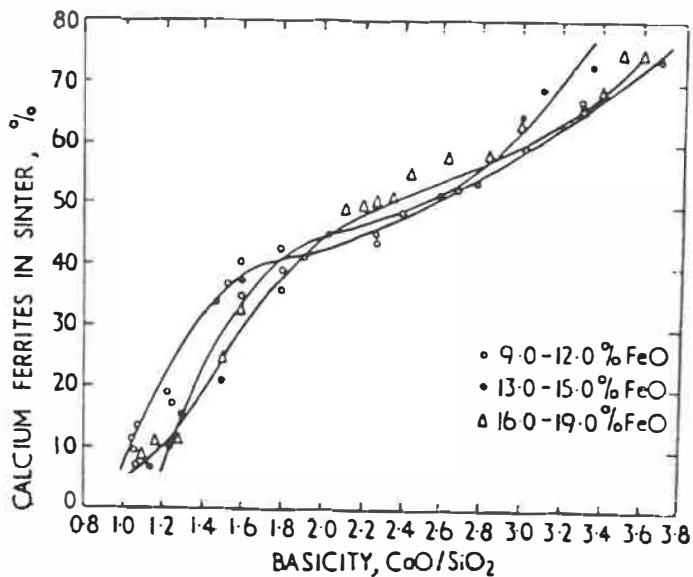


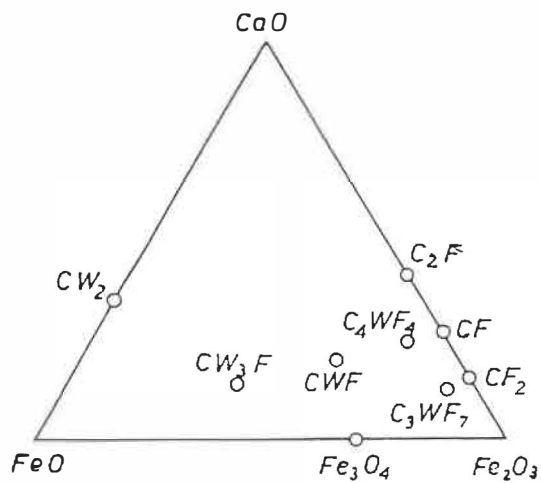
Fig. 2.6 Change in the amount of calcium ferrites of sinter with its basicity (Ref. 27).

In fluxed sinters calcium ferrites are the major phases. As shown in the CaO-Fe₂O₃ phase diagram in Fig. A1.3, Annex 1, the ferrites that can form are dicalcium ferrite, Ca₂Fe₂O₅ (2CaO.Fe₂O₃), monocalcium ferrite, CaFe₂O₄ (CaO.Fe₂O₃), calcium diferrite, CaFe₄O₇ (CaO.2Fe₂O₃). Some ternary ferrites containing FeO are also formed. Chemical analysis of the ferrites and their position in the ternary diagram CaO-FeO-Fe₂O₃ as reported by Nyquist⁽³⁰⁾ are given in Table 2.2 and Fig. 2.7 respectively.

Ferrites can form both by the reaction in the solid state as well as by the reaction of the components in molten state. According to Hass et al.⁽³¹⁾ by solid state reaction between CaO and Fe₂O₃ in air at 1185-1195°C, all the three binary ferrites (dicalcium ferrite, monocalcium ferrite and calcium diferrite) are formed and in reducing atmosphere only ternary ferrite (CaO.FeO.Fe₂O₃) is formed by the reaction between CaO and Fe₃O₄. These reactions are presumably controlled by diffusion in the layers initially formed and hence, the overall rate of formation of these ferrites are slow. The diffusion coefficient of CaO.2Fe₂O₃ appears to be the highest and that of CaO.Fe₂O₃ is the lowest. Because of the low formation rate of these ferrites by this process, it is believed that in sintering process ferrites are mainly formed by the reaction of the components in molten state.

Table 2.2 : Analysis of different calcium ferrites

		Fe (%)	Ca (%)	O (%)	Notation
CaFe_5O_7	$\text{CaO} \cdot 3\text{FeO} \cdot \text{Fe}_2\text{O}_3$	64.74	9.29	26.07	CW_3F
$\text{Ca}_3\text{Fe}_{15}\text{O}_{25}$	$3\text{CaO} \cdot \text{FeO} \cdot 7\text{Fe}_2\text{O}_3$	61.70	8.85	29.45	C_3WF_7
CaFe_4O_7	$\text{CaO} \cdot 2\text{Fe}_2\text{O}_3$	59.49	10.68	29.83	CF_2
CaFe_3O_5	$\text{CaO} \cdot \text{FeO} \cdot \text{Fe}_2\text{O}_3$	58.26	13.93	27.81	CWF
$\text{Ca}_4\text{Fe}_9\text{O}_{17}$	$4\text{CaO} \cdot \text{FeO} \cdot 4\text{Fe}_2\text{O}_3$	53.76	17.15	29.09	C_4WF_4
CaFe_2O_4	$\text{CaO} \cdot \text{Fe}_2\text{O}_3$	51.76	18.58	29.66	CF
$\text{Ca}_2\text{Fe}_2\text{O}_5$	$2\text{CaO} \cdot 7\text{Fe}_2\text{O}_3$	41.00	30.00	29.00	C_2F

Fig. 2.7 Phases in $\text{CaO-FeO-Fe}_2\text{O}_3$ system (Ref. 30).

In the basicity range of 1.5 to 2.0, a decrease in the olivine content and increase in the quantity of calcium ortho-silicates e.g. γ - $2\text{CaO}\cdot\text{SiO}_2$ and β - $2\text{CaO}\cdot\text{SiO}_2$ have been observed by Mazanek and Jasienska⁽²⁷⁾. An increased amount of dicalcium ferrite was also noted. Higher amount of FeO, in this basicity range seems to lower the dicalcium ferrite content. Thick needle shaped crystals of $\text{CaO}\cdot\text{FeO}\cdot\text{Fe}_2\text{O}_3$ are formed beside it around the magnetite grains.

Further increase in basicity (beyond 2) results in more change in the sinter structure. The amount of Ca-ferrites increases significantly, while the iron oxides content (both hematite and magnetite) decreases. Besides the iron oxides, the other chief mineral constituents of super fluxed sinter ($B > 2$) are Ca-ferrites and calcium silicates (γ - $2\text{CaO}\cdot\text{SiO}_2$ and $3\text{CaO}\cdot\text{SiO}_2$)⁽²⁷⁾. Relatively low amount of irregular skeletal magnetite crystals in a background of Ca-ferrites is observed. The ferrites, in the super fluxed sinters are mostly calcium diferrites. Although calcium diferrite is not stable at room temperature (it only exists in a narrow temperature range, e.g. 1155 - 1205°C as evident from the binary $\text{CaO}\text{-}\text{Fe}_2\text{O}_3$ phase diagram shown in Fig. A1.3, Annex 1), its presence in sinter is caused probably due to rapid cooling after sintering and also due to its sluggish decomposition below 1000°C ⁽³²⁾.

The commonly used term calcium ferrite in the fluxed sinters has been lately found to be a solid solution with a wide range of composition⁽³³⁻³⁸⁾. Besides calcium and iron oxides, these ferrite crystals also contain variable amounts of oxides of aluminium and silicon. Hence, a more general term SFCA (silico-ferrite of calcium and aluminium) is used for these ferrites. The complex ferrites identified are:

in $\text{CaO-Al}_2\text{O}_3\text{-Fe}_2\text{O}_3$ ternary system;

brownmillerite ($\text{Ca}_4\text{Al}_2\text{Fe}_2\text{O}_{10}$) and calcium alumino-ferrite $\text{CaO}_2(\text{Fe,Al})_2\text{O}_3$ and

in $\text{CaO-Al}_2\text{O}_3\text{-SiO}_2\text{-Fe}_2\text{O}_3$ quaternary system;

silico ferrite of calcium and aluminium (SFCA).

Presence of Al_2O_3 can also influence the mineral phase formation in sinter. According to the earlier findings of Karner⁽³³⁾, Al_2O_3 normally goes to the slag phase and it does not have any noticeable effect on the sinter structure. However, this has been contradicted by several authors⁽³⁴⁻³⁸⁾. From more recent study by Mazanek and Jasienska⁽³⁴⁾, it is evident that Al_2O_3 promotes the formation of Ca-ferrites in the fluxed sinters. They have also observed a visible amount of an undesirable phase (for its low reducibility), brownmillerite ($4\text{CaO}\cdot\text{Al}_2\text{O}_3\cdot\text{Fe}_2\text{O}_3$) in samples with 7% Al_2O_3 . Presence of two other ferrites viz. $3\text{CaO}\cdot\text{FeO}\cdot 0.7\text{Fe}_2\text{O}_3$ and $\text{CaO}\cdot\text{Al}_2\text{O}_3\cdot 0.2\text{Fe}_2\text{O}_3$ was observed in sinter with 12% Al_2O_3 .

Ahsan et al.⁽³⁵⁾ have also confirmed that Al_2O_3 facilitates the formation of Ca-ferrites. They have found a significant amount (up to 12% by wt.) of Al_2O_3 in the SFCA. From the similarity in the crystal structures of SFCA and magnetite, they have come to the conclusion that SFCA is a superlattice of magnetite. Presence of some eutectic phases such as eutectics of magnetite and slag, Ca-ferrites and slag as well as Ca-ferrites and magnetite has also been reported by the same authors⁽³⁵⁾. They have also reported that SFCA can exist in different morphological structures such as lath/block and needle/acicular.

Calcium ferrites, particularly acicular ferrites are quite desirable phases in the sinter. High amount of these ferrite can greatly improve the sinter quality. The effects of calcium ferrites will be discussed in detail while discussing the properties of the sinter.

The composition of the ferrite changes with its morphology. A range of composition has been noticed for each particular ferrite-structure. Hancart et al.⁽³⁶⁾ have suggested the composition of SFCA to be: $X\text{Fe}_2\text{O}_3 \cdot Y\text{SiO}_2 \cdot Z\text{Al}_2\text{O}_3 \cdot 5\text{CaO}$, where $X + Y + Z = 12$. According to Inoue and Ikeda⁽³⁷⁾, SFCA is a solid solution of $\text{CaO} \cdot \text{SiO}_2$ and $\text{CaO} \cdot 3(\text{Fe,Al})_2\text{O}_3$ and the solubility limit of SiO_2 in ferrite is 12.5 (mole%) at 1250°C . Dawson et

al.⁽³⁸⁾ have reported that SFCA is a calcium diferrite with a part of Fe_2O_3 replaced by SiO_2 and Al_2O_3 .

4.1 Effects of MgO

In the sintering practice, magnesia (MgO) is considered to be quite desirable as it improves some of the properties of the sinter such as reduction degradation behavior (to be discussed later). In some cases, it is externally added to the sinter mix in various forms (e.g. dolomite, olivine, magnesite or dunite) to maintain a MgO level of as high as 9 to 10% in sinter. Magnesia is known to increase the liquid formation temperature and also the viscosity of the melt.

Magnesian-ferrite ($\text{MgO-Fe}_2\text{O}_3$) spinel is a common phase in the magnesia-fluxed sinters. It is the primary phase in a large region of $\text{MgO-FeO-Fe}_2\text{O}_3\text{-SiO}_2$ system (phase diagram in Fig. A1.4, Annex 1). The SiO_2 solubility in magnesian-ferrite is almost zero. As reported by Rait⁽³⁹⁾, no ternary compound is formed by CaO , MgO and Fe_2O_3 . The first liquid is formed for a composition of 60% Ca_2SiO_4 and 40% spinel at 1370°C .

Since the reaction between Fe_2O_3 and MgO in molten state can take place only around 1600°C (ref. $\text{MgO-Fe}_2\text{O}_3$ phase diagram in Fig. A1.5, Annex-1) which is hardly reached in the sintering process, formation of magnesian-spinel $(\text{Mg,Fe})\text{O-Fe}_2\text{O}_3$ occurs in

solid state. This is possible because of the similarity in the ionic radii of Mg^{2+} and Fe^{2+} (viz. 0.66 Å and 0.74 Å respectively). Similar to magnetite structure $[Fe^{3+}(Fe^{2+}.Fe^{2+})O_4]$, magnesio-ferrite $[Fe^{3+}(Mg^{2+}.Fe^{2+})O_4]$ also has an inverse spinel structure and it possesses magnetic properties⁽⁴⁰⁾. Its close optical resemblance with magnetite makes it difficult to distinguish in the sinter mineralogy. It has a range of composition and the maximum solubility of MgO in Fe_2O_3 (conforming to the stoichiometric composition of $MgO.Fe_2O_3$) is 20% by weight.

At higher temperature magnesio-wustite can co-exist with the spinel. It is formed in solid state as well as in liquid state (see MgO-FeO system, in Fig. A1.6, Annex 1). Higher temperature increases the solubility of MgO in FeO and enhances the magnesio-wustite formation.

Mazanek and Jasienska⁽²⁵⁾ have reported that as MgO in the self-fluxing sinter increases, the formation of Ca-ferrites is suppressed and dicalcium silicates and glassy phases are more easily formed in certain slag pools. They have noticed the presence of MgO in the slag phase forming complex olivines and pyroxenes. It may be noted here that their work is not quite thorough and the conclusions are based on observations made on sinters containing only 0-6% MgO.

Zudin et al⁽⁴¹⁾, have suggested that addition of MgO causes a reduction of FeO content in the slag. Mg²⁺ can easily replace Fe²⁺ cations in Ferromontecellite (CaO.FeO.SiO₂) during the sintering process. Fe²⁺ cations so liberated forms oxide (magnetite) while cooling.

More recent and thorough studies on the effects of MgO on sinter- and pellet-mineralogy have been made by Panigrahy⁽⁴²⁾ and Hegde⁽⁴³⁾ respectively. From his observations, Panigrahy has reported that increase in MgO in the sinter in general increases the formation of secondary magnetite and decreases the Ca-ferrite contents. Magnetite which has a spinel structure (FeO.Fe₂O₃), is gradually replaced by a mixed spinel of the type (Fe.Mg)O.Fe₂O₃ and the Mg content of the spinel increases, with the total MgO content of the sinter. Formation of glassy phase is favored with the increase in the amount of MgO. For certain condition, the glass phase was found devitrified, often to olivines. Formation of magnetite dendrites is also favored by MgO addition.

Hegde⁽⁴³⁾ has noted that the main effect of MgO addition to pellets was the formation of the solid solution, magnesio-ferrite during the induration of the pellets. The amount of magnesia-ferrite in the pellet was found to be greatly affected by the peak induration temperature and the oxygen partial pressure of the induration atmosphere.

It has been widely believed that in self-fluxing sinters MgO mainly goes to the magnetite phase - resulting in the formation of magnesio-ferrite spinel. The amount of MgO detected in the slag phase has been quite low ($< 2\%$)⁽⁴⁴⁻⁴⁸⁾. In sinters containing high amount of iron, presence of magnesio-wustite has been mentioned by some authors⁽⁴⁹⁾.

The exact amount of MgO in Fe_3O_4 depends on the sintering condition such as temperature and of course the MgO content of the sinter mix. Friel and Erickson⁽⁴⁷⁾ have studied the distribution of MgO in the dolomite added pellets (from magnetite concentrate). They observed that the MgO content in the spinel structure varied from 1.6% to 13.8% (by weight). Bentell and Mathisson⁽⁴⁶⁾ have reported 14.3 wt.% of MgO in the spinel structure.

By studying the dolomite and magnesite added pellets, Ball et al.⁽⁵³⁾ have reported the formation of magnesio-ferrite at temperature as low as 700°C .

The formation of the mineral phases may change noticeably with the particle size and the source of magnesia⁽⁵⁰⁻⁵³⁾. The main reason as cited by these authors is the difference in the extent of assimilation of MgO present in these materials into the sinter structure.

5. The Quality of Sinter

The characteristics of the final sinter is of great importance with regard to the blast furnace performance. For good quality sinter, reduction reaction in the blast furnace should proceed without any hindrance i.e. it should ensure the following requirements.

- 1) High permeability and uniform gas distribution inside the blast furnace.
- 2) High gas efficiency inside the blast furnace.

In order to meet these requirements in the blast furnace, sinter should have:

- a) a close size range with minimum amount of fines (-5 mm);
- b) sufficient strength to resist the stresses encountered during its transportation from the sinter plant to the blast furnace;
- c) good low-temperature break down properties so as to generate minimum amount of fines during reduction at low temperature;
- d) as high reducibility as possible;
- e) high softening/melting temperature.

The cost of production of the sinters also plays an important role while evaluating the sinter quality.

The quality of the sinter can be evaluated by determining its individual properties. These properties are largely influenced by the nature and amount of different mineral phases present in the sinter⁽⁵⁴⁾. As we will see later in this section, factors which can improve a certain property, may have negative effect on another property. Hence, in practice, always a compromise among the properties is made. Generally, improvement in the quality of sinter can be achieved by increasing its reduction rate (reducibility) without lowering any other property below the acceptable value.

5.1 Properties of Sinter

The properties of sinter which are normally considered to evaluate its quality are:

I. Porosity

The amount of pores in the iron ore sinters can vary between 15 to 30 % (volume). These pores may consist of micro and/or macro pores and they are mostly open in nature. The size, amount and distribution of pores have a significant influence on the strength and reducibility of the sinter^(25,55). Higher porosity may increase the reducibility by providing more surface exposed to the reaction. This, however, may reduce the

sinter strength. Hence, usually a compromise is made between the two properties.

The formation of pores is affected by the several factors (such as physical and chemical nature of different raw materials) which control the amount and type of melt formed during sintering⁽⁵⁴⁾. Increase in the amount of fuel, generally increases the width of the combustion zone (or the melt zone), thereby lowers the porosity of sinter⁽⁵⁶⁾.

II. Strength

Since one of the principal purposes of sintering is to produce large and physically strong agglomerate, the strength of the final sinter is an important consideration for its quality evaluation. It is needed to sustain the stresses encountered during handling. The strength of the sinter is achieved by establishing bonding between the ore particles. Theoretically, two types of bonding are possible; viz diffusion bonding and slag bonding⁽¹⁶⁾.

A. Diffusion bonding: Diffusion bonding mainly occurs while sintering pure concentrates and it forms a porous agglomerates. This kind of bonding is desirable as it produces strong sinters with high reducibility (because of the porous structure). However, in practice, it is hardly

achieved, because of the presence of low melting constituents which forms liquid at lower temperature during sintering and enhances slag bonding.

B. Slag bonding: Slag bonding is produced by the liquid formed during the sintering process. During sintering, liquid which is first produced by the fusion of low-melting constituents can rise to a significant quantity. While cooling, slag bonding is produced. The gangue constituents (e.g. SiO_2), flux (e.g. CaO) and the sintering temperature play a major role in slag bonding by influencing the amount and viscosity of the slag formed. Large amount of low viscous slag can coat the solid particles providing good bonding in the sinter structure; as a result, sinter with excellent strength is produced.

The dependence of sinter strength on its mineralogy has been discussed by many authors^(44,57-60). In general, when there is no large cracks or pores present in the sinter, its strength is mainly governed by the nature of the matrix (which consists of hematite, magnetite, calcium ferrites and the silicates).

The high strength of acid sinters (basicity around 0.5) is due to the glassy phase which forms the main matrix. As the basicity increases, transition from glass to crystalline

materials in the sinter matrix takes place. The sinter strength decreases due to the reduction in the amount of glassy phase. The lowest value of the sinter strength is observed when the basicity is around 1.5⁽⁶¹⁾. At this basicity, the sinter matrix consists of partly complex crystalline silicates and partly glassy phase. They have different coefficients of thermal expansion. (For example, the volume expansion accompanying the phase transformation of β - to γ -dicalcium silicates can cause severe internal stresses and generate cracks during cooling.)

Raise in the sinter strength for basicity beyond 1.5⁽⁶²⁾ is mainly attributed to the presence of calcium ferrite phases which increasingly take over as the bonding phase as the basicity increases. The needle-shaped or acicular ferrites which are the predominant phases in the highly fluxed sinters (e.g. B \geq 2.5) form an interlocking structure and provide excellent strength to these sinters.

III. Reduction Degradation (or Low-temperature Degradation)

In the upper stack of the blast furnace sinters often breakup while undergoing reduction in the mild reducing conditions at a temperature of 400-600°C. This behavior of the sinter is known as reduction degradation or low-temperature degradation. Fines generated due to this have deleterious effects on furnace operation by hindering the air flow.

During the reduction process, structural transformation of different mineral phases of the sinter occurs and this is often associated with volume changes generating stresses within the structure⁽⁶³⁾. Transformation of rhombohedral α -hematite to cubic magnetite (which takes place at about 570°C) is particularly responsible for low-temperature degradation⁽⁶⁴⁾. The dissimilarity in the crystal structure gives rise to lattice distortion leading to deterioration of the physical integrity of the particles. The above transformation is also accompanied by a significant volume change (expansion of about 25%)^(63,65). Cracks are formed both within the hematite grain and at the grain boundaries due to the stress developed in this process, thereby embrittling the material. Sometimes, it is so extensive that the sinter structure gets disintegrated. Moreover, magnetite formed is highly porous and it severely weakens the bond between the iron oxides.

According to Grebe⁽⁶⁶⁾, micro-cracks formed in the surrounding matrix during the transformation process inevitably bring about the break down of sinters.

It is believed⁽⁶⁷⁾ that the anisotropic behavior of hematite crystals during reduction also plays an important part in this regard. The hexagonal hematite grains has a lower reduction velocity in the direction $\langle 0001 \rangle$ than in any other closed packed direction. Due to this the thickness of magnetite layers

formed during reduction are different at the individual interfaces which could lead to tension and breakdown in the grains.

Several types of hematite have been reported in the literature^(68,69). Among them a characteristically shaped hematite known as skeletal hematite⁽⁶⁸⁾ (also known as multicomponent hematite^(69,70)) has been found to be more detrimental as regard to the low-temperature degradation.

Based on the above observation, it can be said that the principal cause of low-temperature breakdown is the presence of hematite phase in the sinter. The effect of hematite content of sinter on its reduction degradation index (RDI) is shown in Fig. 2.8⁽⁷¹⁾. As seen in this figure the RDI of sinter varies inversely as the hematite content.

Wanatabe⁽⁵⁸⁾ and Edstrom⁽⁷²⁾ have determined the strength of the calcium ferrites after their reduction. They have seen that the strength of these compounds do not decrease and their structure remains compact during reduction. Hence, calcium ferrites have no effect on the reduction degradation behavior of sinter.

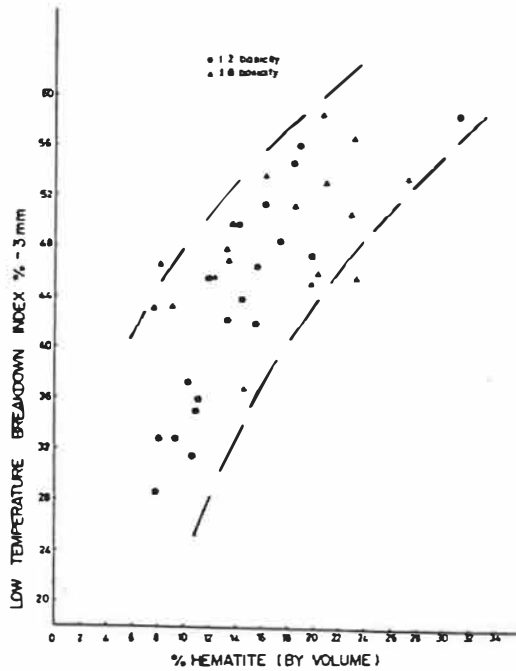


Fig. 2.8 Effect of total hematite content on low-temperature breakdown index.

In summary, the RDI or the generation and propagation of crack can be controlled by increasing the slag volume, and decreasing secondary hematite content⁽⁷³⁾. Increasing the amount magnetite phase (by MgO addition⁽⁷⁴⁻⁷⁶⁾), and calcium ferrite phases will also increase the RDI.

IV. Reducibility

Reducibility is an important property of the iron ore sinter as it has a significant influence on the efficiency of the blast furnace and the economics of this process. The principal factors which can affect the reducibility of sinter are the amount of different mineral phases and their morphology and the amount of pores (their sizes and distribution).

From the study on the reduction rate of various compounds synthesized from the pure components, the following order of reduction (in descending order) has been established⁽⁷⁷⁾:

Hematite (Fe_2O_3)

Calcium diferrite ($\text{CaO} \cdot 2\text{Fe}_2\text{O}_3$)

Monocalcium ferrite ($\text{CaO} \cdot \text{Fe}_2\text{O}_3$)

Dicalcium ferrite ($2\text{CaO} \cdot \text{Fe}_2\text{O}_3$)

Magnetite (Fe_3O_4)

Silicates (olivines, pyroxenes, etc.)

The above order of reduction rate can also be seen in the reduction curves⁽⁷⁸⁾ (Fig. 2.9) obtained for some of the minerals containing iron oxides and iron ore sinters. The high reduction rate of calcium diferrite is ascribed to its thermodynamical unstability^(45, 79). However, it should be noted that

measurements lack precision as the surface area and porosity of the specimen under investigation have not been precisely determined.

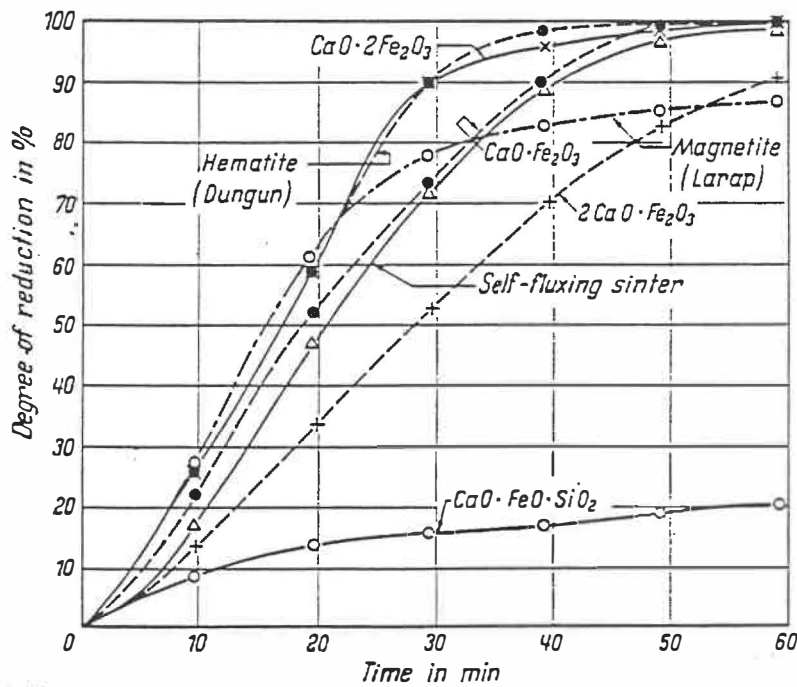


Fig. 2.9 The reduction curves for different mineral phases.

All these factors (e.g. basicity, type and amount of fuel, bed permeability, maximum temperature, T_{\max} reached during sintering which can affect the sinter mineralogy, can also influence the reducibility of the final sinter. It has been reported by many authors that the principal reason for the

increase in the sinter reducibility with the increase in the basicity is due to the formation of calcium ferrites. The instability of Ca-ferrites in the reducing atmosphere increases the reducibility of the sinters with a basicity above 1.3⁽²⁴⁾.

As mentioned earlier in this section, diffusion bonding can produce highly reducible sinter. Because of the porous structure of this sinter, the reducing gas can penetrate into it more easily and increase the reduction rate. However, diffusion bonding is not very common in the normal sintering practice.

The acid sinters contain a large amount of low reducible fayalite. Besides, the impervious nature of the glassy matrix impairs the reducibility of such sinter by making it inaccessible to the reducing gas.

As the basicity increases (in the lower range of basicity i.e. $B < 1.2$), the viscosity of the slag reduces due to lime addition. The less viscous slag needs lower temperature and hence, less quantity of fuel. Thus, there is increasing degree of oxidation and hematite content (both primary and secondary). This leads to high reducibility.

Increase or decrease of the reducibility of sinters with basicity between 1.2 - 1.5 depends on the amount and morphology

of the complex crystalline silicates and the glassy phase. For basicity beyond 1.5, the reducibility of sinter steadily increases with the increase in basicity. This is mainly due to the increase in the calcium ferrite content of these sinters.

The high reducibility of the super fluxed sinters (basicity >2.0) is principally attributed to the high calcium ferrite content of these sinters. As discussed earlier (in Sec. 4), these ferrites are mainly complex calcium diferrites (or silico ferrites of calcium and aluminium, SFCA) which have high reduction rate. The morphology of the ferrites also has a major influence on the reduction rate. According to Dawson⁽⁸⁰⁾, since the reduction is a gas-solid reaction, the reducibility of the mineral phases, in general, is related to its accessibility of the reducing gas and it depends on their morphology. He has found that the reducibility of SFCA is significantly decreased if it is coated or surrounded by glass.

Influence of some common factors on the reducibility of sinter is discussed in the following paragraphs. When MgO is added to the sinter to improve its RDI and softening property, it decreases the reducibility. It is due to the increase in magnetite phase (MgO stabilizes the magnetite phase during sintering) which has a lower reducibility.

Alumina (Al_2O_3) decreases the reducibility of the sinter at low basicity ($B < 1.2$). This is because Al_2O_3 being a glass

former⁽³³⁾, increases the glass phase (at low basicity) which has negative effect on reducibility. However, at basicity ($B > 1.5$), Al_2O_3 increases the reducibility by enhancing the ferrite formation.

Increase in the amount of the fuel increases the quantity of melt formed during sintering. This may result in higher strength, but may decrease the reducibility.

The reduction rate of sinter is further influenced by the nature and amount of pores, sinter-size and temperature of reaction. The structural changes such as crack and/or pore formation also play an important role on the reduction rate of the sinter.

More details of the iron oxide reduction are given in Annex-2. Some studies on the reduction of the sinters produced in the present work are also discussed in this Annex.

In order to improve the performance of the blast furnace, it is necessary to optimise the reducibility of the sinters whilst other properties such as cold strength, reduction degradation, softening temperature and cost of production are maintained at an acceptable level.

V. Softening/melting

As the burden materials descends down the furnace stack, its temperature increases and it undergoes progressive reduction. With the increase in temperature, softening/melting of any particular material may occur, depending its chemical composition e.g. fusion may occur in the ores in a wide range of temperature, 700-1350°C. However, for sinter and pellets, this range is much narrower i.e. 1000-1350°C. In this range the materials start softening and melting and a sticky fusion zone (cohesive zone) is formed. A wide range of melting temperature is undesirable as it creates a large cohesive zone. This hinders the gas flow by lowering the permeability and causes a non-uniform gas distribution in the furnace. Thus, it is detrimental to smooth furnace operation. It is, hence, essential to discard the materials with abnormally low melting temperature (<1000°C) and maintain a narrow cohesive zone inside the furnace.

Investigations have shown that besides the melting temperature, other factors which could also affect the softening/melting behavior of the materials are the load, size of the material, heating rate and the degree of reduction⁽⁶²⁾.

The causes of softening/melting of the sinters can be explained by referring to its mineral phases and the changes it undergo during reduction. As we have already seen before, the sinter mineralogy mainly consists of iron oxides, calcium ferrites, slag and pores. As reduction proceeds inside the furnace, the higher iron oxides gradually reduces to wustite and metallic iron. By the time sinter reaches the lower stack, a significant amount of FeO is produced.

In general, liquid formation first begins in the slag which principally contains CaO, SiO₂, FeO, Al₂O₃ and MgO. Depending on the FeO content, fusion could start at as low as 1100°C^(81, 82). In presence of a small amount of Na₂O and K₂O, liquid formation could occur even earlier.

The principal effect of low softening/melting temperature is the loss in permeability and gas distribution inside the blast furnace due to a wider cohesive zone. Furthermore, as the temperature increases, more liquid is formed and the solubility of FeO in the liquid is also increased. This could deteriorate the oxide bonds and reduce its strength. Dissolution of FeO in the slag decreases its activity making it difficult for reduction.

The dissolved FeO can be reduced by solid carbon resulting in low fuel efficiency. Moreover, metallic iron produced by the direct reduction of FeO by carbon may form solid in the fusion zone. To summarize the effects of low softening/melting temperature of sinters - it is likely to form a larger viscous semi-fused zone and cause a pressure drop inside the furnace stack leading to non-uniform gas distribution and material descent, hanging and scab formation.

Softening/melting properties of sinter are commonly improved by adding MgO to the sinter mix. This raises the melt formation temperature during reduction.

CHAPTER III
OPTIMISATION OF THE SINTERING CONDITIONS

In this chapter, we will describe the raw materials used for the present investigation. The equipments used and the methods followed to study the micro-pelletization and the experimental procedure to produce the sinters will also be described. The results and discussions on micro-pelletization study will be presented in the end of the chapter.

1. Raw Materials

The iron-bearing materials used in this work were specular hematite concentrate, sinter fines, pellet fines, iron fines and mill scale. The flux consisted of limestone and dolomite. Flue dust was used as fuel for all the sinters except for the ones produced with 100% specularite concentrate* where coke breeze was used. The additives used were quick-lime, bentonite, peridur and peat moss. All the raw materials have been procured from the Algoma Steel Corporation.

* Throughout this text (unless specified) the percentage of specularite has been calculated on the basis of total iron-bearing materials.

The chemical composition and the size distribution of the raw materials are given in Tables 3.1 and 3.2 respectively. The iron in these materials is mainly present as oxides and the percentage of iron for any material in Table 3.1 represents the total amount of iron (both as FeO and Fe₂O₃) in it. As we can see in Table 3.2, there is a significant difference in the size distribution of the different raw material used.

The frequency histogram of size distribution of the iron-bearing materials are shown in Fig. 3.1. A large difference in the size distributions of these materials are clearly marked from this figure.

Specular Hematite Concentrate

The major iron-bearing constituent of the sinter mix in this study was specular hematite concentrate, "as received" from Quebec Cartier Mines. The total iron content of the concentrate is about 65% (Table 3.1) and it is mainly present as hematite (Fe₂O₃). As we can see in Table 3.2, the intermediate size i.e the 0.2-0.5 mm size-fraction (Table 2.1, Chap.II) of this concentrate is about 53%. It has got the finest size distribution of all the iron-bearing materials (Fig. 3.1).

Table 3.1 : Chemical analysis (% wt.) of the raw materials

Materials	Fe	SiO ₂	Al ₂ O ₃	CaO	MgO	TiO ₂	MnO	Na ₂ O+ K ₂ O	Loss or (gain) on ignition
Pellet fines	59.8	6.7	1.2	2.5	0.8	0.1	0.3	0.1	2.3
Sinter fines	47.5	7.6	1.1	10.9	7.9	0.2	3.2	0.0	0.7
Spec. Conc.	65.3	4.1	0.5	0.3	0.2	0.2	0.1	0.0	0.2
Iron fines	54.8	10.8	2.2	14.4	3.2	0.2	2.8	0.1	(14.0)
Mill scale	72.5	1.0	0.6	0.7	0.3	0.0	1.1	0.0	(8.9)
Limestone	0.3	0.7	0.1	54.1	0.7	---	---	---	43.3
Dolomite	0.2	1.0	0.1	30.3	20.8	---	---	---	46.7
Quick-lime	1.6	0.2	1.5	92.9	1.5	---	---	---	----
Bentonite	2.5	57.8	16.8	1.5	2.3	---	---	2.3	----
Flue dust	19.9	5.5	1.9	3.6	2.8	0.1	0.7	0.5	55.0
Coke breeze	1.1	3.9	2.2	0.5	0.2	0.1	0.1	0.2	89.1

Table 3.2 : Size distribution of the raw materials (% wt. retained on stated size)

Sieve size (mesh)	Sieve opening (mm)	Spec. conc.	Pellet fines	Sinter fines	Iron fines	Mill scale	Limestone	Dolomite	Flue dust	Coke breeze
3	6.730	---	1.4	15.8	14.7	5.2	0.4	----	----	----
6	3.360	---	31.3	53.6	16.9	19.4	8.2	----	----	----
10	1.680	0.6	36.6	19.9	18.0	20.9	35.3	18.1	0.6	22.2
20	0.840	8.1	13.2	6.3	15.2	20.3	28.9	29.9	7.5	23.2
28	0.595	10.5	2.5	1.3	5.7	7.5	6.5	10.2	9.7	7.9
35	0.420	17.0	2.0	0.9	6.0	7.2	5.4	8.3	15.6	15.2
65	0.210	36.2	2.6	1.0	10.5	10.6	6.6	9.8	34.3	9.9
100	0.149	11.9	0.8	0.2	3.5	3.0	1.6	2.9	11.5	6.7
150	0.105	8.5	0.8	0.2	2.6	2.4	1.1	3.1	8.1	4.8
200	0.074	4.5	0.7	0.1	1.8	1.4	0.7	3.0	4.4	3.0
270	0.053	1.7	0.6	0.1	1.4	0.8	0.6	3.2	2.0	1.6
325	0.044	0.6	0.6	0.1	0.9	0.5	0.4	3.3	2.0	1.7
-325	-0.044	0.4	6.9	0.5	2.8	0.8	4.3	8.2	4.3	3.8

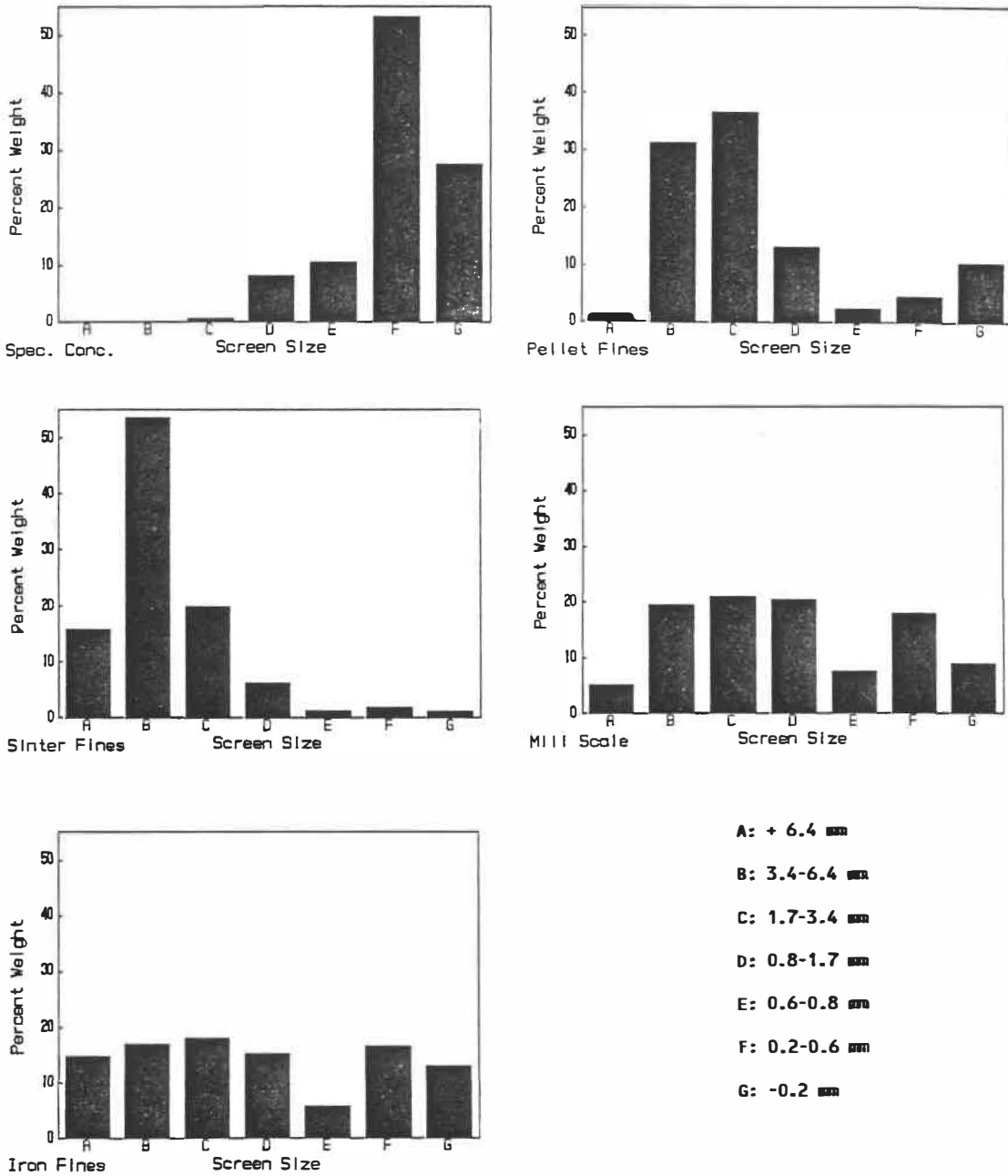


Fig. 3.1 The frequency histogram of the size distribution of the iron-bearing materials.

Pellet Fines

Pellet fines are generated by the breakdown of the pellets during their transportation. Because of the size-requirement of the burden materials in the blast furnace, these fines can not be charged into the furnace directly. They are therefore used as feed material for sintering. The pellet fines used for the tests had about 60% of iron (total). They had a coarse size distribution containing more than 80% of 20 mesh or +0.8 mm size-fraction.

Sinter Fines

Sinters fines are generated while transporting the sinters produced at Algoma Ore Division, Wawa, to the blast furnace at Sault Ste. Marie. They are normally recycled in the sintering process at Sault Ste Marie. The relatively low iron content and high MgO content (46% and 7.6% respectively) of the fines can be seen in Table 3.1. They contained about 96% of +0.8 mm size-fraction and had the coarsest size distribution of all the iron-bearing materials, as shown in Fig. 3.1.

Mill scales and iron fines are generated in the rolling mills and in various other sections respectively of Algoma Steel. They are also used in the sinter mix. The size distribution of the mill scales and iron fines used in this

work were intermediate between the specularite concentrate and sinter fines (or pellet fines).

Limestone and Dolomite

Limestone and/or dolomite have been used to control the sinter chemistry. Their amounts were adjusted so as to maintain the basicity* and the MgO content of the sinters constant.

Flue Dust and Coke Breeze

Flue dust is the dust collected from the blast furnace chimneys. It contains about 55% (by wt.) of fixed carbon. Flue dust was the principal fuel in the present work.

As mentioned earlier, coke breeze was used only for the sinters containing 100% specularite concentrate. Before using, it was dried and crushed to -3 mm size.

The amount of fuel and water has been selected from previous experience and by repeating the tests with different amount of fuel and water until the optimum condition for fuel and water was achieved (Sec. 2.3.4).

* Basicity, $B = \frac{\text{CaO} + \text{MgO}}{\text{SiO}_2 + \text{Al}_2\text{O}_3}$

Additives/Binders

Four different additives have been tried to improve the micro-pelletization process. They are:

Quick-lime: Quick-lime used in this investigation was of laboratory reagent grade containing 92.9% CaO. It was in powder form.

Bentonite: Bentonite is a clay material containing high amount of SiO₂ and Al₂O₃ (e.g. 57.8 and 16.8 respectively as given in Table 3.1). It is used as binder for the pelletization process.

Peridur: Peridur is a dry cellulose material which has been recently found useful as an organic binder in the pelletization process^(21, 22, 83).

Peat moss: Peat moss is a fibrous material, produced from the decomposed vegetation that have been deposited in a wet environment. Recent studies⁽⁸⁴⁻⁸⁵⁾ on this material with regard to its use as binder in the pelletization process has shown positive results. The proximate analysis of dry peat moss is as below:

% fixed carbon	: 29.2
% volatile	: 59.1
% ash	: 11.7
KJ/kg	: 20.580

2. Equipments and Procedures

Before conducting the actual pot-grate tests, first the suitable mixing/micro-pelletizing equipment(s) was selected by some preliminary studies.

2.1 Description of the Mixing/Micro-pelletizing Equipments

As mentioned earlier, in order to select the proper equipment for micro-pelletization of the sinter mix, three different mixing equipments e.g. disc pelletizer, turbulator and roll compactor have been used. Brief descriptions of these equipments are given below.

Disc pelletizer

A disc pelletizer mainly consists of a disc with peripheral wall. It usually rotates while being inclined to the horizontal. A scraper is fitted to the disc to prevent any build-up of material on the disc. By adjusting the position of this scraper, the flow pattern of the material on the disc can be controlled. A schematic diagram of the disc pelletizer is given in Fig. 3.2.

The material is charged and the disc is set to rotate. Water is added as the disc rotates. The growth of the balls is

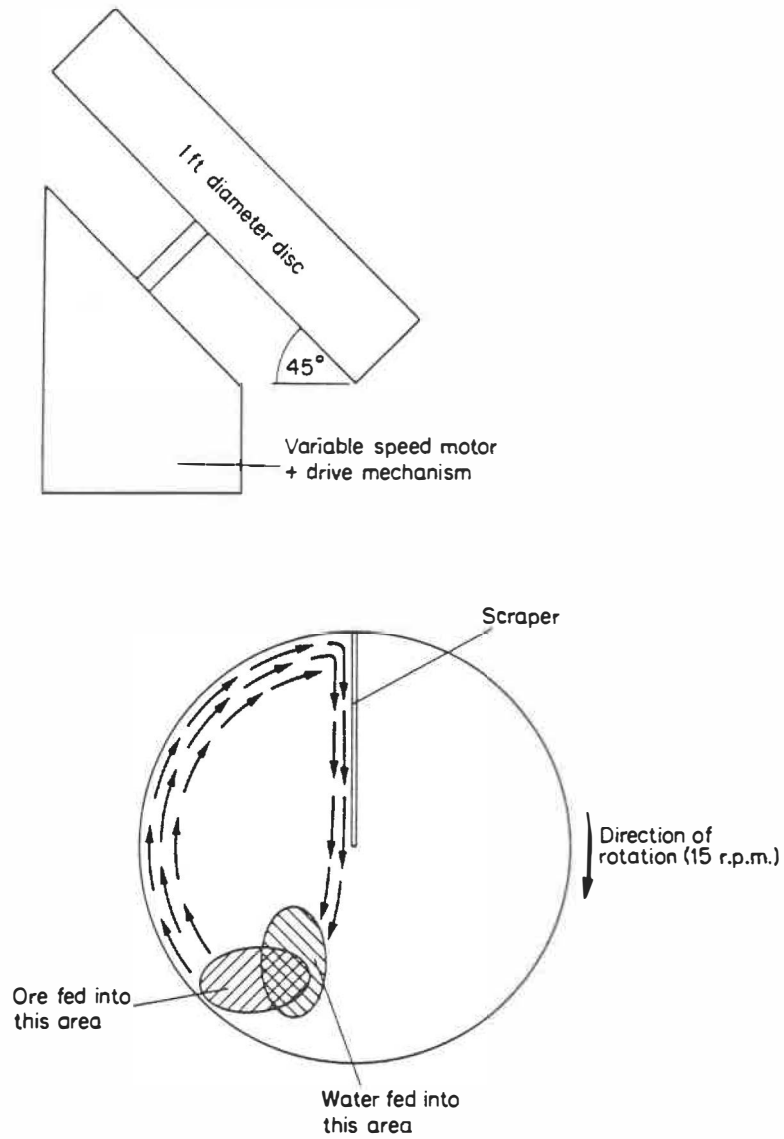


Fig. 3.2 Schematic diagram of a disc pelletizer.

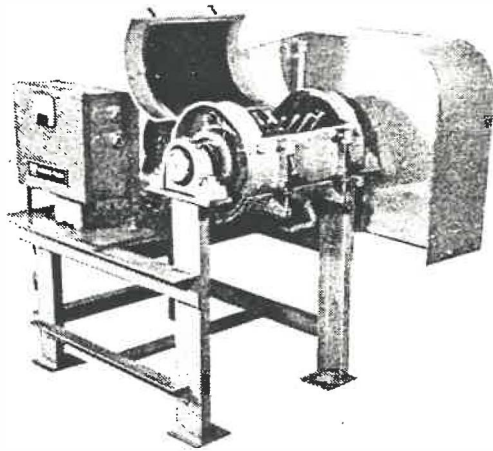
considered to take place in two stages viz. nucleation (in which nuclei or seeds are formed) and growth (in which the seeds grow by layering of other particles).

The major parameters affecting the performance of the disc are its diameter, angle of inclination, speed of rotation and the height of the peripheral wall.

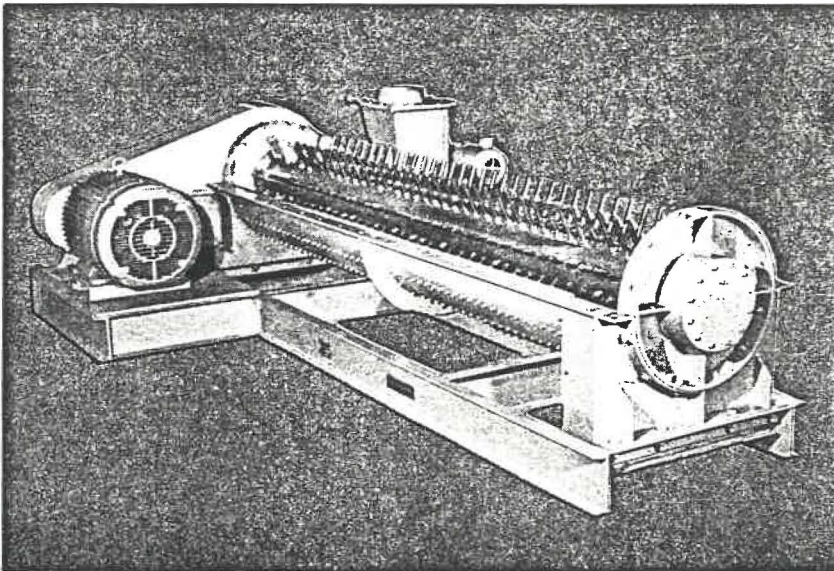
Turbulator

Turbulator is a solids-liquid mixer. The diagram of a batch type turbulator used for the present work is shown in Fig. 3.3. It consists of a horizontal stationary shell with a rotating shaft extending axially through its length. The shaft is fitted with a number of cylindrical rods or pins (as shown in Fig. 3.3). The material to be agglomerated is charged into it from the top and the pelletized mix is discharged from the bottom of the turbulator.

The design of the shaft (i.e. the arrangement and location of the pins) and its speed have a major role in the agglomeration process. Due to the vigorous agitation caused by the rotating shaft, the particles collide with great force. The liquid layers (on the solid particles) coalesce and capillary bonds are formed at the point of contact. Such a densifying action essentially eliminates air from between the



a)



b)

Fig. 3.3 Turbulator.

particles and strengthens their bonding. This equipment is useful for agglomerating different fine particles, particularly those which are difficult to wet such as specularite concentrate (due to the absence of clay material in it).

Roll Compactor/briquetter

Roll compactor consists of two rolls of equal diameter. The rims of the rolls are pocketed with matching pockets as shown in Fig. 3.4.

The material is forced into the rolls as they rotate in opposite direction at synchronous speed with a screw type feeder. The design of the pockets (shape and size) is the important factor and it largely controls the agglomeration process.

2.2 Assessment of the Micro-pelletizing Equipments

In order to assess the mixing/micro-pelletizing equipments a preliminary study was undertaken in the laboratory of an agglomerating equipments supplier industry, Ferro-Tech Inc. at Wyandotte, Michigan. Few typical mixes containing 40% and 100% specularite and with quick-lime and bentonite (as additive) were used for this study. The equipments were used independently as well as in combination with one another.

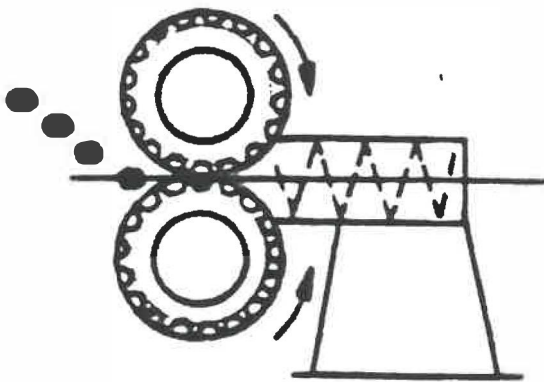
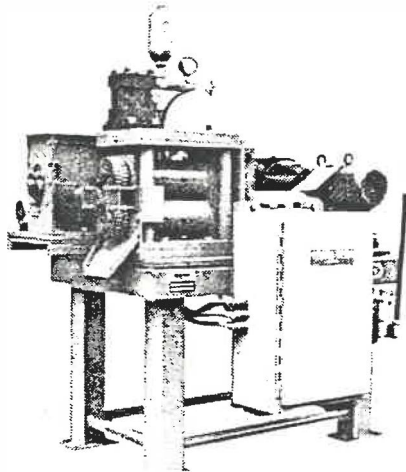


Fig. 3.4 Roll compactor/Briquetter.

The efficiency of the equipments were evaluated by visual observation, size analysis and measuring the cold permeability of the green mix (the details will be given later in section 3). The results obtained for the roll compactor were not quite encouraging. Out of different trials, the mix using disc pelletizer and the combination of turbulator and disc showed some interesting results. Hence, further tests using roll compactor was discarded and it was decided to study the effects of disc and turbulator more thoroughly.

2.3 Pot-grate Tests

More than 200 hundred sintering tests have been conducted to produce sinters with different conditions. The conditions will be mentioned later in this section.

Sintering tests were carried out using the pot-grate facility at Algoma Ore Division, Wawa, Ont.. The schematic arrangement of the pot-grate is shown in Fig. 3.5 and important sintering conditions given in Table 3.3.

A 6" diameter sinter pot was used for the pot-grate tests. The pot was covered on the sides with some insulating materials on the sides to minimize the heat loss. There were provisions to insert the thermocouples, T_1 to T_3 and the pressures probes P_1 to P_4 to measure the temperatures and the pressure drops at

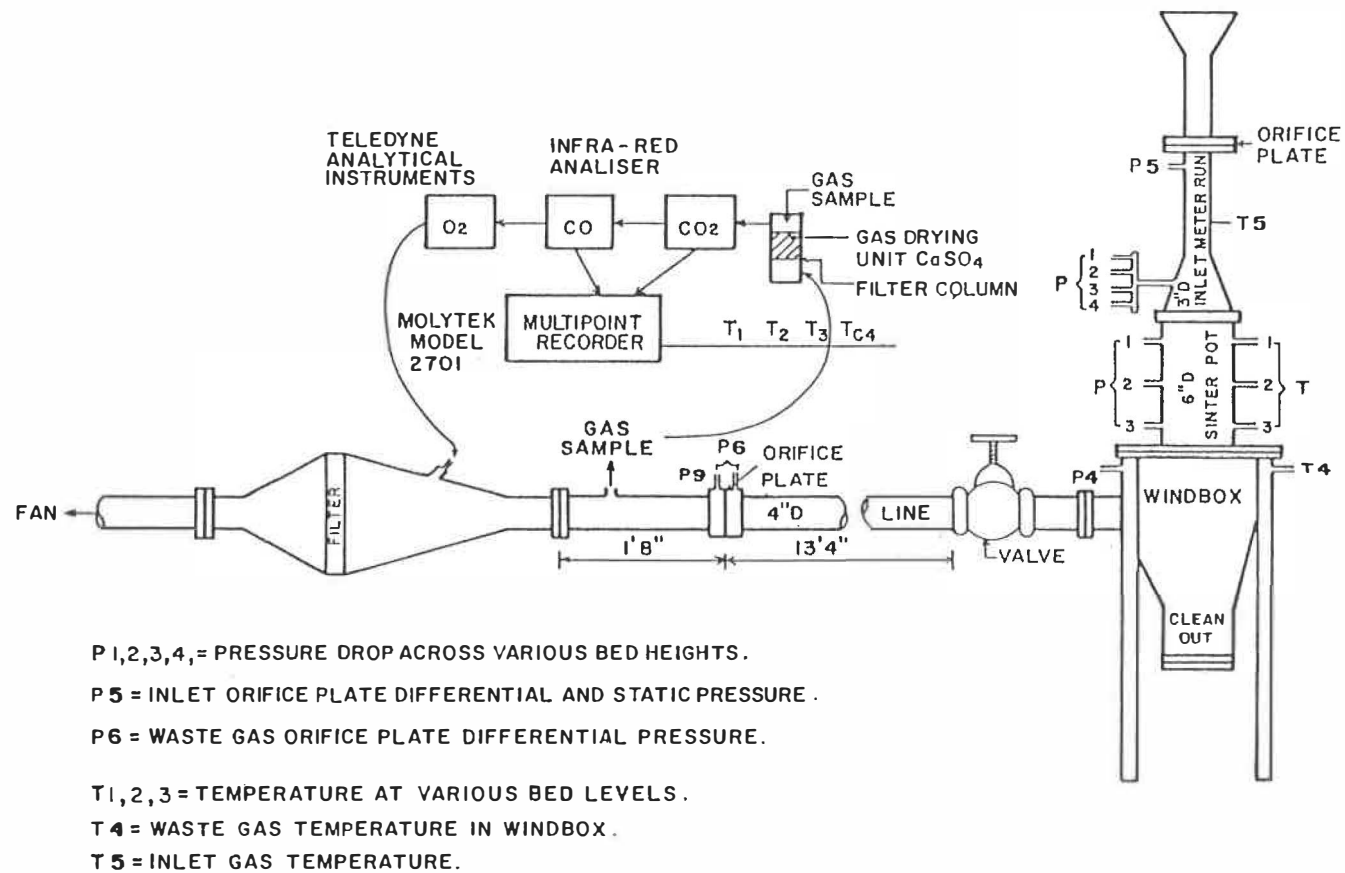


Fig. 3.5 Schematic arrangement of the experimental pot-grate test facilities.

Table 3.3 : Experimental sintering conditions

Mass of the hearth layer (10-12.5 mm)	0.5 Kg
Net bed height	380 mm
Mass of the charcoal (for ignition)	0.1 Kg
Ignition time	1 min.
Suction during sintering	760 mm water
Sinter feed throughput	13.5 - 15 kg
Return fines in the sinter mix	23 %
Return fine balance	0.9 - 1.1
Number of balance tests	3

different bed heights respectively (see the figure). The inlet air and the waste gas temperatures were also noted by the thermocouples placed in the inlet hood and the wind box respectively. The valve was adjusted to maintain a constant suction during the sintering process. The waste gas leaving from the sinter bed was allowed to pass through the wind box to the fan. A sample of this gas was made to pass through the infra-red CO-CO₂ analyser and Teledyne O₂ analyser. During sintering, the pressure drops were noted manually at an interval of 5 mins. while the temperatures and the percentages of CO, CO₂ and O₂ were continuously recorded by a multipoint recorder. The Pt-Pt, 10% Rh thermocouples were used to measure the temperature.

2.3.1 Sinter Mix Compositions

Various conditions of the sinter mix were first selected. The first test was carried out using the typical sinter mix used at Algoma Steel Corporation's Sault Ste. Marie Plant. Throughout this text, this mix has been referred as the base mix and the corresponding test as the base test. The base mix did not contain any specularite concentrate. The proportion of different iron-bearing feed materials in the base mix is given in Table 3.4.

The other conditions were selected by replacing the iron-bearing materials of the sinter mix (exclusive of return fines) by 25, 40 and 100% specularite concentrate, first without using any binder and later by using 2% and 5% quick-lime, 0.25% bentonite, 0.1% peridur and 1.0% peat moss separately. The different compositions of the sinter mixes prepared are given in Table 3.5.

The charge calculations were made aiming to have a basicity of 2.5 and a MgO content of 3.0% in the final sinter for all the conditions. While using quick-lime, its effect on sinter basicity has been considered. The effect of other binders (in this regard) has been neglected as the amount of these binders used were quite low (<1.0%).

Table 3.4 : Amount of different iron-bearing feed materials in the base mix*

Iron-bearing materials	Amount (%)
Pellet fines	20
Sinter fines	46
Mill scale	10
Iron fines	20
Flue dust	4

* Exclusive of return fines

Table 3.5 : Compositions of the sinter mixes

Specularite concentrate (%)	Additive/Binder	Mixing device(s)	Total number of conditions
0	NA	D, TD	2
25	NA, 2L, 5L, 0.25B, 0.1P, 1PM	D, TD	12
40	NA, 2L, 5L, 0.25B, 0.1P, 1PM	D, TD	12
100	NA, 2L, 5L, 0.25B	D, TD	8

NA : no additive; 2L : 2% quick-lime;
 5L : 5% quick-lime 0.25B: 0.25% bentonite;
 0.1P: 0.05% peridur; 1PM : 1% peat moss
 D : disc pelletizer; TD : turbulator and disc pelletizer

It should be noted that in order to produce one particular type of sinter, about two/three tests were carried out by changing the water and/or fuel content of the sinter mix before obtaining a balance test. Once a balance test was achieved, it was repeated twice (without changing any condition) to check the reproducibility and to produce sufficient amount of sinter for their subsequent characterization.

2.3.2 Mixing

The materials were weighed to the calculated amount and mixed in the disc pelletizer. The angle of inclination of the pelletizer was set at 45°. After 30 sec. of dry mixing, measured amount of water was sprinkled over the mix and it was further mixed for 2½ min. This practice was maintained for all the tests except when turbulator was used where the raw materials were first charged in the turbulator and mixed for 15 sec. in dry condition. Water was added and it was again mixed for 15 sec. and then mixed in the disc pelletizer for 2½ min.

2.3.3 Charging of the Green Mix

The hearth layer consisting of 500 g of sinter of size 10-15 mm (previously made) was spread on the grate of the sinter pot. The green mix was then charged uniformly into the sinter pot. While charging, care was taken to prevent any segregation.

The capacity of the sinter pot varied from 13.5 to 15 kg depending on the type and amount of different raw materials. After the sinter pot was filled up, it was levelled of using a cut-off plate ensuring desired height of the bed. The thermocouples were inserted in different positions of the bed and the pressure probes were connected properly (as shown in Fig. 3.5).

2.3.4 Sintering

In order to facilitate the ignition of the sinter bed, 100 g of crushed charcoal (-3 mm) was spread uniformly on the top of the sinter bed. Then a mixture of 40 g of saw dust and 60 ml of kerosene was spread on it. Suction was started and ignition was initiated with a match stick. The hood was placed on the pot and suction was gradually increased to 30" (760 mm) water column in 1 minute and maintained at that level throughout the sintering process.

All the sintering parameters such as pressure drops, temperatures at different heights of the bed, waste gas temperature and air inlet temperature were recorded. The volume of air flow was also measured. Sintering was stopped when the waste gas temperature reached 200°C. After taking out the thermocouples and disconnecting the pressure probes, the sinter cake was removed and stabilized.

2.3.5 Stabilization of the Sinter Cake and Recycling of Fines

After sintering was complete, the sinter cake was taken out and stabilized by dropping it from a height of 6 ft on a steel plate. It was then screened on 50.8 mm (2"), 38.1 mm (1½"), 25.4 mm (1"), 15.9 mm (5/8"), 12.7 mm (½"), 9.5 mm (3/8") and 6.36 mm (¼") sieves. The +9.5 mm size fraction of the sinter was used for further characterization. The +6.36 mm size fraction was considered to calculate the production rate while the undersize fraction (i.e. -6.36 mm) was recycled as returned fines. The amount of latter fraction was used for calculating the return fine balance.

Sintering condition was considered to be optimum when the fine sinter balance, F_g (see Sec. 3.5, Chap. 1) was within 0.9 to 1.1. The amount of sinter fines recycled in the process was 23%. This was in line with the practice at Algoma. For any particular condition, at least 2 or 3 tests were usually carried out by changing the amount of water and/or fuel to obtain the optimum condition i.e. to obtain a ratio of fine sinter output to fine sinter input close to 1 (0.9 - 1.1). After this condition was reached, the test was repeated twice to accumulate sufficient sinter for subsequent testing to evaluate the properties. All the results reported in this text are, therefore, the averages of three tests representing the optimum condition, for a particular sinter mix.

2.4 Pot-Grate Tests with Modified Fuel Addition

Few tests were conducted to study the effects of the modified fuel addition (i.e. fuel added to the sinter mix in two steps) on the production rate and the properties of sinter. Three mix conditions containing 40% specularite with no additive, 2% and 5% quick-lime were selected for these tests.

The raw materials were mixed only with the disc pelletizer. The experimental procedure and all the sintering parameters remained the same as the previous set of tests except that half of the fuel was added in the beginning (before mixing). The other half was added after two minutes of mixing and it was again mixed for one more minute.

2.5 Production of Sinters on the Industrial Strand

In order to compare the quality of the sinters produced in the laboratory pot-grate with the corresponding sinters produced in the industrial strand, five sinter mix conditions were chosen (with 40% and 100% specularite concentrate) for the strand tests. These conditions are given in Table 3.6. Only a disc pelletizer has been used for mixing/micro-pelletizing the sinter mix.

Table 3.6 : Raw material conditions for the strand tests

Specularite Concentrate (%)	Additive/Binder	Total number of conditions
40	NA, 2L, 5L	3
100	2L, 5L	2

The sinter mix was prepared in the laboratory. For each condition, the raw materials were first weighed out and mixed in the disc pelletizer. The mixing practice was same as the previous set of tests (i.e. $\frac{1}{2}$ min of dry mixing and $2\frac{1}{2}$ min. wet mixing). The green mix was then taken to the plant to charge into the pot.

The diameter of the sinter pot used was 6". Some steel rods were welded to the bottom of the sinter pot in parallel making a grid with an opening of 6 mm. The grate layer was spread on the bottom of the sinter pot.

The green mix was charged uniformly into the pot. After it was filled up, a cone-like structure was made with some extra sinter mix. This was to avoid charging of the plant sinter mix while the pot passed under the charging bins.

The sinter pot was placed on the strand at the feed-end (just before the charging-bins). As the strand moved, the pot passed under the cut-off plate and the ignition hood. The conical structure of the pot was levelled off by the cut-off plate. Ignition was started as the pot passed under the ignition hood. Sintering proceeded from top layer to the bottom in the sinter pot as it moved to the discharge end. The pot was retrieved there using an overhead crane. The test was repeated once more without changing any condition to produce sufficient material to evaluate their properties.

The use of sinter pot facilitated the sintering of an experimental sinter mix on the strand without interfering in the regular plant operation.

3.0 Micro-pelletization Study

It is quite difficult to measure the extent of micro-pelletization of the sinter mix because of a variety of materials with a wide size range used in it. Moreover, there is hardly any precise control to monitor the size of these materials. In the present work, it has therefore been assessed indirectly, by performing the size analysis of the green mix and by measuring the pre-ignition (or cold) permeability of the sinter bed.

3.1 Size Analysis of the Green Mix

For each condition of the sinter mix, 500 g of green mix (after the mixing was over) was collected to perform size analysis. In order to avoid any breakage of the weak micro-pellets during screening, the green mix was frozen with liquid nitrogen and then it was screened. The cumulative weight percentage of +1.7 mm (10 mesh) and +0.8 mm (20 mesh) size fractions have been calculated to compare the extent of micro-pelletization for different mixes. These values for disc (D) and the combination of turbulator and disc (TD) are reported in Table 3.7. The effect of various conditions on the amount of the above size fractions are also shown in Fig. 3.6.

Table 3.7 : Size analysis (cum. wt. per cent) of the green mix

Specularite concentrate (%)	Additive/Binder	+ 1.7 mm (10 mesh)		+ 0.8 mm (20 mesh)	
		D	TD	D	TD
0	NA	87.6	79.0	97.5	94.2
25	NA	60.7	72.3	86.6	94.5
	2L	73.0	78.9	91.7	92.0
	5L	74.1	73.5	88.3	90.0
	.25B	69.8	65.8	87.0	86.0
40	NA	56.5	65.8	82.4	65.8
	2L	64.9	71.9	86.5	71.9
	5L	64.3	72.8	78.9	72.8
	.25B	57.1	65.4	80.2	65.4
100	2L	43.9	----	74.6	----
	5L	39.8	----	62.2	----

D : Only disc ; TD : Turbulator and disc

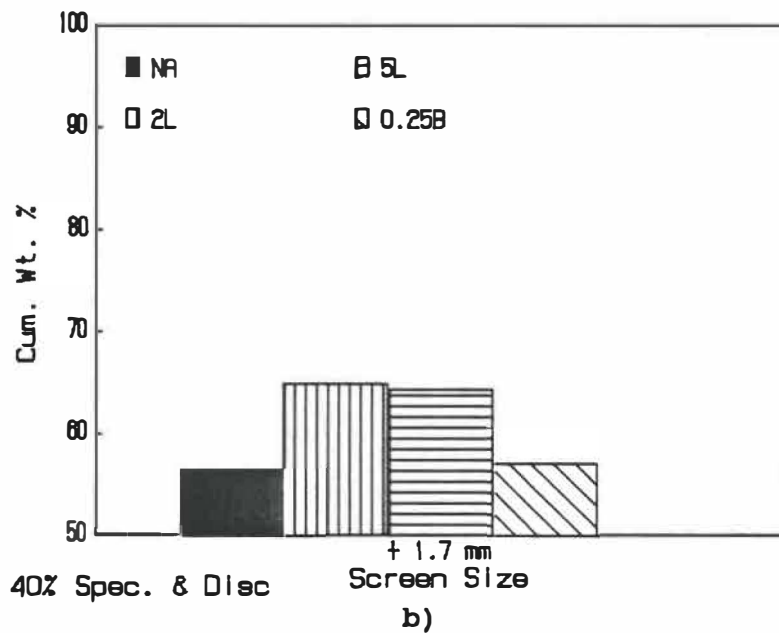
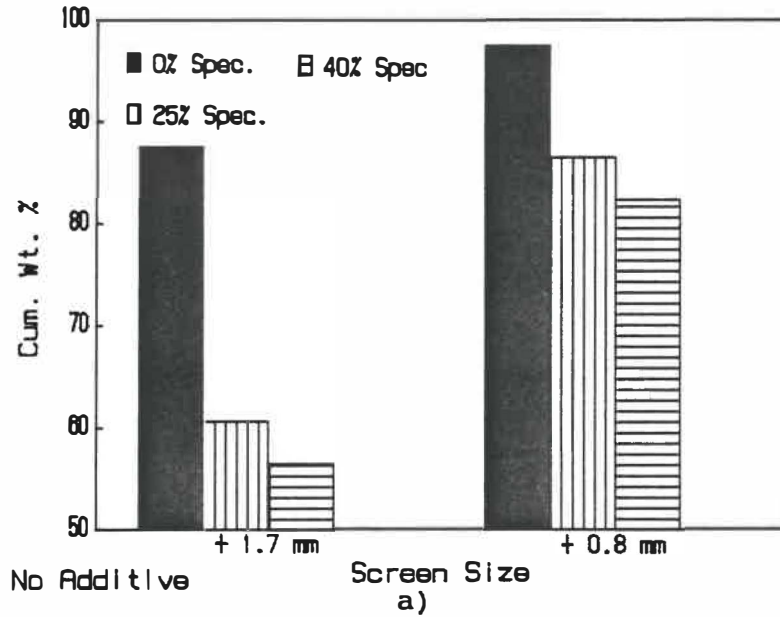
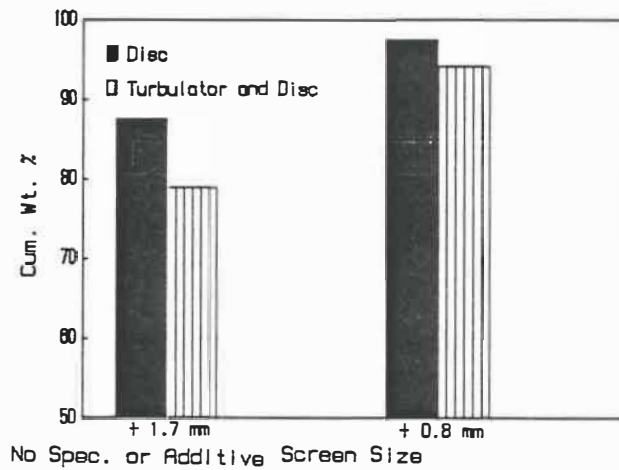


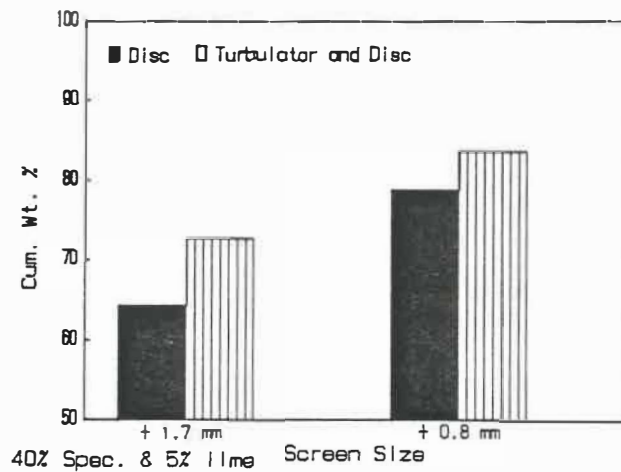
Fig. 3.6 Effect of various conditions on the micro-pelletization of the sinter mix

a) Effect of specularite addition and

b) Effect of quack-lime and bentonite



c)



d)

Fig. 3.6 Effect of various conditions on the micro-pelletization of the sinter mix

c) Effect of turbulator on the base mix (no specularite or additive)

d) Effect of turbulator on a mix containing 40% specularite and 5% quick-lime.

It can be seen from Table 3.7 that the amount of +1.7 and +0.8 mm size fractions was maximum for the base mix (see Table 3.4) e.g. 87.6% and 97.5% respectively for the disc and 79% and 94.2% respectively for turbulator and disc. However, it is to be noted here that this mix did not contain any concentrate; on the contrary, the iron-bearing materials e.g. sinter fines, pellet fines, mill scale etc. contained high amount of +1.7 and +0.8 mm size fractions to start with. The coarse particles also served as nucleus for micro pelletization, enhancing (to some extent) the formation of the micro-pellets.

When specularite concentrate was added to the sinter mix, the amount of +1.7 and +0.8 mm fractions in the green mix decreased. As shown in Table 3.7, (for the mix prepared in the disc pelletizer) the cumulative weight percent +1.7 mm size fraction in the green mix dropped from 87.6% to 60.7% when the amount of specularite concentrate was increased from 0 to 25%. This was obvious as the coarse iron-bearing materials were replaced by the fine ones. The decrease in the above size fraction due to the addition of specularite concentrate is clear from Fig. 3.6a.

It was observed that for any particular level of concentrate in the mix and for any mixing condition (i.e. disc or combination of turbulator and disc), the amount of +1.7 mm and +0.8 mm size fractions increased with the addition of

quick-lime. Although quick-lime was added in powder form and it replaced about double its amount of much coarser limestone (% of CaO being half that of quick-lime), it can be seen that the +1.7 and +0.8 mm fractions of the green mix containing lime were more than those of the green mix with limestone. In the mix containing 40% specularite concentrate (using disc) the +1.7 mm of the green mix with quick-lime was 64.3% while that in the mix without any additive (with limestone) was 56.5%. From this it was evident that quick-lime has acted as a binder and enhanced the formation of micro-pellets.

Bentonite, peridur or peat moss did not have any significant effect with regard to the micro-pelletization process. The effect of quick-lime (2% and 5%) and bentonite on the +1.7 and +0.8 mm size fractions of a mix containing 40% specularite can be seen in Fig. 3.6b.

Comparing the amounts of +1.7 and +0.8 mm size fractions for same raw materials but mixed in a disc pelletizer or disc pelletizer with turbulator, it was noticed that in general, the above fractions were higher in the latter case (although, the values are slightly lower for the base mix. For example, with 40% specularite (no additive), when turbulator and disc were used, the amounts of +1.7 and +0.8 mm size fractions were 65.8 and 90.6 per cent respectively compared to 56.5 and 82.4 per cent respectively, when only the disc was used.

The effect of turbulator on micro-pelletization was not encouraging when a large amount of coarse materials were used in the mix (e.g. base mix). However, as the amount of fines in the mix increased, particularly with additives/binders, it became more efficient. This is clear from the Fig. 3.6c and 3.6d. In Fig. 3.6c, the +1.7 mm size fractions of the base mix (no additive) using disc and turbulator with disc have been compared. Similar comparisons have been made for a mix containing 40% specularite and 5% quick-lime in Fig. 3.6d.

3.2 Pre-ignition (or Cold) Permeability

As expected, the pre-ignition (or cold) permeability was found to be maximum for the base mix, 83.8 and 89.7 BPU for disc and turbulator with disc respectively (see Table 3.8). Increase in the amount of concentrate in the mix significantly reduced the cold permeability value. For example, when the specularite content was increased from 0 to 40%, for disc pelletizer, it dropped from about 84 to 48 BPU.

The cold permeability has been improved to some extent by using the turbulator. For the mix containing 40% specularite and 2% lime, when only disc pelletizer was used, the cold permeability was about 49 BPU. It increased to about 60 BPU by using a turbulator and disc. Quick-lime and bentonite had similar effects. As reported in Table 3.8, for 40% specularite

Table 3.8 : Permeability of the sinter bed (in BPU)

Specularite concentrate (%)	Additive/Binder	Cold Permeability		Trough permeability		Average permeability	
		D	TD	D	TD	D	TD
0	NA	83.8	89.7	61.9	60.7	92.8	102.2
25	NA	57.3	62.8	44.3	48.4	68.1	74.1
	2L	65.4	83.3	53.2	57.0	77.3	93.7
	5L	71.1	86.2	56.4	59.3	84.1	89.0
	.25B	58.6	65.4	48.1	47.5	80.1	82.7
40	NA	47.9	50.0	38.7	43.5	63.8	65.1
	2L	49.3	60.7	43.2	48.2	66.7	74.6
	5L	66.4	74.1	57.9	46.8	73.2	75.9
	.25B	46.4	56.7	40.3	42.4	63.2	66.0
100	2L	45.7	----	34.9	----	74.3	----
	5L	39.7	----	32.9	----	80.9	----

D: only disc; TD: turbulator and disc

and disc with turbulator, the cold permeability which was about 50 BPU increased to about 74 and 56 BPU for quick-lime and bentonite addition respectively. Peridur and peat moss did not have any visible effect in this regard.

The improvement in the permeability values in all the above cases were mainly due to micro-pelletization of the green mix. These mixing conditions promoted the formation of strong micro-pellets which can sustain the stresses during their handling and subsequently increased the permeability of the sinter mix.

From the visual observations, size-analysis and cold permeability values, turbulator was found to be an efficient mixer for the mix containing higher amount of fines and additive. It helped coating the particle with additive. The formation of micro-pellets was thus promoted during the later stage of mixing in the disc.

Disc pelletizer has been found to be a good micro-pelletizing device. For any amount of specularite concentrate in the mix, the maximum degree of micro-pelletization was observed when a combination of turbulator and disc was used for mixing and when lime or bentonite was used as additive.

4.0 Production of Sinters

In this section, we will discuss about the change of sintering parameters (such as bed permeability, sintering time and the production rate) for different conditions of the mix.

4.1 Bed Permeability during Sintering

Pre-ignition permeability, trough (minimum) permeability and average permeability for the important sintering conditions have been calculated and reported in Table 3.8. Since, for all the practical purposes permeability during sintering usually refers to the average permeability, we will also discuss the bed permeability with respect to this value.

As we can see in Table 3.8, when there was no specularite (i.e. in the base test) and only disc pelletizer was used for mixing, the average permeability of the sinter bed was found to be about 93 BPU. It dropped to 64 BPU by adding 40% of specularite concentrate. However, it slightly improved (to 65 BPU) when turbulator was used along with the disc pelletizer. By adding quick-lime and bentonite the permeability increased to about 76 and 66 BPU respectively.

In Chapter II we have seen that the cold-permeability value mainly depends on the size distribution of the green mix while the average permeability value is influenced by both the size distribution of the green mix as well as the physical changes occurring during sintering. However, here, both these values (in general) have shown a similar trend. The combination of turbulator and disc pelletizer, quick-lime and to some extent bentonite have increased the bed permeability mainly by enhancing the micro-pelletization process.

4.2 Sintering Time

The sintering times for different sintering conditions are given in Tables 3.9 and 3.10. As expected, a general relationship has been found between the average bed permeability and sintering time. It was observed that sintering time decreased with the increase in bed permeability. The base test (no specularite) with disc pelletizer had an average permeability of 92.8 BPU corresponding to 12.7 min. of sintering time (Table 3.9). By adding 25% specularite, the bed permeability dropped to 68.1 BPU, increasing the sintering time to 15.5 min. Permeability was increased to 84.1 BPU by lime addition, resulting in a lower sintering time, 13.8 min.

Table 3.9 : Production rates of the sinters using only disc

Specularite Additive	0 %	25%				40%				100%	
	NA	NA	2%L	5%L	.25%B	NA	2%L	5%L	.25%B	2%L	5%L
Sintering time in min	12.7	15.5	14.8	13.8	14.5	16.0* 14.0	16.5* 13.0	14.3* 12.0	17.0	14.3	15.2
Prod. rate (sinter) TPD/M ²	55.2	44.1	52.0	54.5	45.5	41.3* 49.5	42.5* 51.4	49.2* 57.9	41.2	43.1	45.5
Prod. rate (total iron) TPD/M ²	26.4	22.1	26.1	27.5	22.3	21.4	22.0	25.4	21.0	25.3	26.4
Carbon rate (Kg/t)	16.0	23.3	22.4	21.5	23.8	28.5	24.4	19.8	27.3	52.2	47.8

* : Production rate of the sinters with modified fuel addtion

Table 3.10 : Production rates of the sinters using turbulator
and disc

Specularite Additive	0%	25%				40%			
	NA	NA	2%L	5%L	.25%B	NA	2%L	5%L	.25%B
Sintering time in min	13.0	16.1	14.5	14.9	14.9	17.5	18.5	17.6	16.4
Prod. rate (sinter) TPD/M ²	50.6	46.6	49.3	43.9	43.9	41.7	40.8	43.9	42.8
Prod. rate (total iron) TPD/M ²	24.2	23.4	24.9	22.0	22.0	21.6	21.2	22.9	21.8
Carbon rate (Kg/t)	20.5	22.8	----	23.7	25.7	28.2	23.8	19.2	24.5

We have already mentioned that the average permeability of sinter bed was higher when turbulator and disc were used than that when only disc pelletizer was used. No such behavior was noticed with respect to the sintering time. On the contrary, in most cases, sintering time was found to increase with the use of turbulator. Sintering time for 40% specularite and 5% lime (with disc) was 14.3 min which was increased to 17.6 min by using turbulator (Table 3.10).

The reason for this is not quite clear. It was most probably due to the heating characteristics of the flue dust and the amount of liquid formed during sintering. When turbulator was used there was a better mixing and the flue dust were distributed causing more efficient burning. This has lead to more liquid formation and thus, higher sintering time.

From Table 3.9, it can be seen that the sintering time increased with the increase in the specularite concentrate in the mix. It was reduced to some extent due to the addition of lime or bentonite. Peridur and peat moss did not have any beneficial effect on the sintering time.

4.3 Production Rate

Production rates for different sinters have been calculated using +6.36 mm (+ $\frac{1}{4}$ ") size fractions following the stabilization test. These values are given in Tables 3.9 and 3.10. As we can see here, depending on the type of micro-pelletizing device(s) and additive used and the amount of specularite concentrate, production rates varied from 41-55 tonnes per day per square meter of the grate area. These figures compare favourably with that obtained in the Algoma Steel's Sault Ste Marie works.

The increase or decrease in the production rate for any sinter condition was mainly attributed to its sintering time. The mixing conditions had similar effects on production rate as they had on sintering time. As we will see later, in Chapter IV, the sinter strength has also played a role by affecting the amount of usable sinters produced.

The maximum production rate was obtained for the base test. As the amount of specularite concentrate in the mix increased, the sintering time increased and production rate decreased. Quick-lime addition had salutary effect on the production rate. It not only decreased the sintering time, but also increased the sinter strength (we will discuss it later in Chapter IV), and thereby, increased the amount of usable sinter produced.

Production rate of the base test (no specularite) with disc was about 55 tpd/m². By adding 40% specularite, it dropped to 41 tpd/m². It increased to 49 tpd/m² by adding 5% lime to the mix. No significant change in the production rate was noticed with bentonite addition for any particular level of specularite.

Production rates obtained for the sinters with peridur or peat moss were not reported as they were too low (<40 tpd/m²). It was due to both high sintering time and low sinter strength (which produced less quantity of usable sinters). The lower production rate of the sinters using turbulator and disc are mainly attributed to their higher sintering time.

Although the production rate in terms of sinter output decreased with specularite addition, when it was calculated on the basis of Fe output (i.e. tonnes of Fe per day per square meter of the grate area) the difference was reduced (as shown in Table 3.9). For example, when the amount of specularite was increased from 0 to 40% (and 5% quick-lime) the sinter output dropped from 55.2 to 49.2 tpd/m². However, in terms of Fe output the values were close, 26.4 and 25.4 tpd/m² respectively. With 25% specularite and the production rate in terms of Fe output was higher than that of the base test (e.g. 27.5 and 26.4 tpd/m² respectively). This can be considered as an advantage with regard to the use of specularite concentrate.

The results obtained for the sinters with modified fuel addition (in terms of production rate) were quite interesting. In this case, the production rate was about 20% higher than that of the corresponding sinter with regular fuel addition. For example, (as given in Table 3.9) the production rate of sinter with 40% specularite and 5% quick-lime has increased from about 49 tpd/m² to about 58 tpd/m² by adding flue in two stages.

It is believed that by adding half of the fuel towards the end of the mixing, it coats the quasi-particles formed during the initial stages of mixing. Since, the fuel is available on the external surface of the micro-pellets, it has better heating characteristics. The sintering time decreases (see Table 3.9), thereby increasing the production rate

4.4 Carbon Rate

The carbon rates (given in Table 3.9) follows the similar trend as the production rates. It should be noted that unlike the production rate, here, the sintering time does not play any direct role. The lowest carbon rate (16 kg/t) was found to be for the base test when only disc pelletizer was used. It was possible as the mix contained high amount of pre-sintered materials (e.g. pellet fines, sinter fines). It increased with the increase in the amount of specularite concentrate in the

mix indicating that more fuel was needed to sinter the concentrates than the pre-sintered materials.

The highest carbon rate (52.2 kg/t) was noted for sinters with 100% specularite. These sinters did not contain any pre-sintered material. Moreover, some extra fuel was required, to calcine dolomite added to maintain the MgO level (3%) in the final sinter.

Relatively lower carbon rates have been observed for all the sinters with quick-lime addition. This was because little (or no) limestone required for the lime-added sinters and heat needed to calcine this limestone was low. Other conditions such as using turbulator or adding bentonite, peridur or peat moss did not have any significant effect on the sinter carbon rate.

CHAPTER IV

CHARACTERIZATION OF THE SINTERS

This chapter consists of three sections. In the first section, we will discuss the mineralogy of sinters. The chemical analysis of different sinters will be given in the following section. In the last section, we will deal with each of the sinter properties e.g. porosity, strength, reduction degradation, reducibility and softening/melting temperature. The test methods will be described first, followed by the results and discussions.

The various tests conducted to characterize the sinters and the size fractions used are shown in Fig. 4.1. As we can see in this figure, the +9.5 mm (3/8") fraction (following the stabilization of the sinter cake) was used for the tests. It is to be noted here that since no encouraging result with regard to micro-pelletization and other sintering parameters was observed with peridur and peat moss addition, characterization of these sinters have not been carried out.

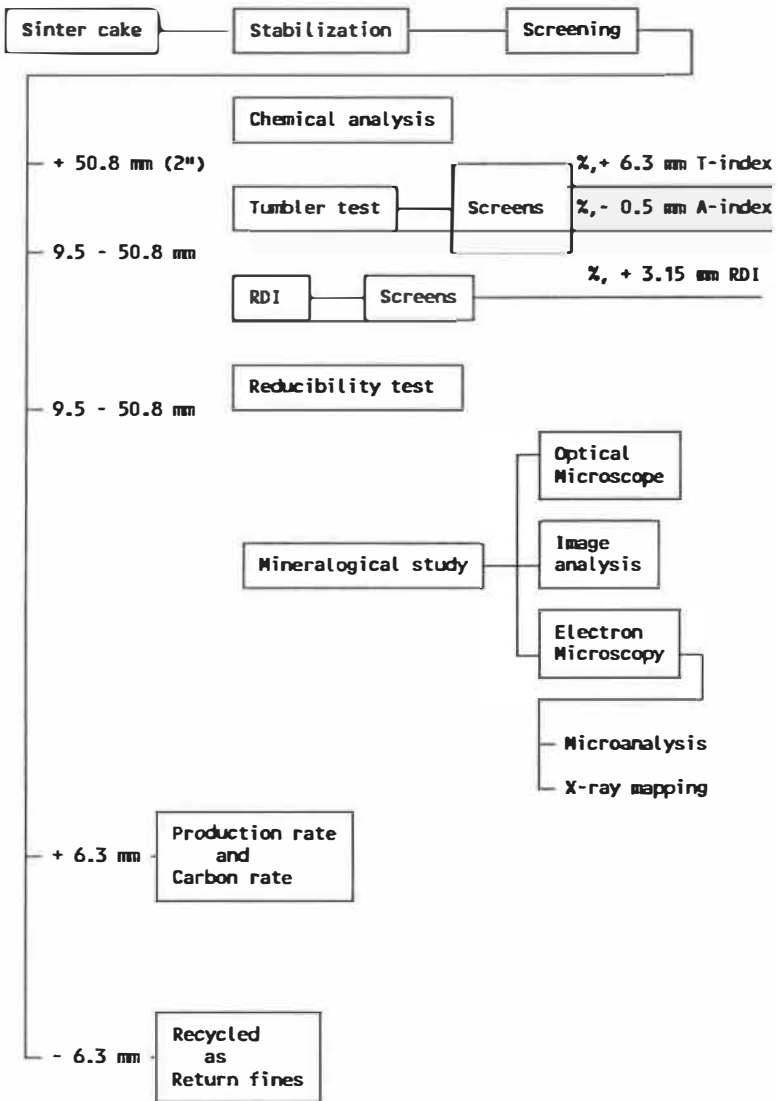


Fig. 4.1 Tests conducted on sinters.

1. Mineralogical Study

The mineralogical structures of the sinters have been studied by using optical microscope, image analyser and scanning electron microscope attached with a LINK EDS Analytical system. The mineralogy of sinters with 100% specularite concentrate was not studied as the quality of these sinters were found to be inferior to the acceptable limit mainly because of its low strength (will be discussed later in this chapter).

1.1 Sample Preparation

For each condition, a minimum of five samples were prepared for the mineralogical study. The sinter pieces (size 10-15 mm) were randomly chosen. These samples were sectioned and mounted in a piece of brass tube using epoxy. They were polished using the standard polishing method. The final polishing was done using 1 μm diamond paste. The specimens were then cleaned properly with carbon tetrachloride in an ultrasonic cleaning bath and dried. The same specimens were used for all the mineralogical study.

1.2 Mineralogical Observations in the Optical Microscope

Specimens were thoroughly observed under the reflected light optical microscope. Hematite phase appeared white. Magnetite also appeared white, but slightly less than hematite. Calcium ferrite was marked as grey crystal while the silicates appeared dark. In some cases, it was difficult to distinguish one phase from another (for example, some small magnetite crystals from calcium ferrite crystals). However, after studying carefully, the mineralogical phases can be summarized as below:

- In the sinter produced from the base mix (no specularite or additive), the major phases are secondary magnetite and calcium ferrite. Few tertiary hematites (re-oxidized from magnetite crystals) are present. The amount of slag phase was relatively high.
- It is observed that the mineralogy of sinters changes significantly with the increase in specular hematite concentrate and by using additives. In general, with the increase in specularite concentrate;
 - a) the calcium ferrite content of the sinter increases;
 - b) the secondary magnetite content decreases;
 - c) the hematite content (all three types e.g H_1 , H_2 and H_3) increases;
 - d) the slag phase decreases.

- For any particular amount of specularite concentrate (25 or 40 or 100 %), quick-lime or bentonite enhances the formation of Ca-ferrite in the sinter.
- Turbulator, peridur or peat moss does not have any marked effect on the sinter mineralogy.

The details of the observations are given in the following pages.

Notations used for Mineralogical Study

- H₁ : Primary hematite - the original relict hematite which has remained unchanged during the sintering process.
- H₂ : Secondary hematite - hematite phase that has been solidified from the liquid phase.
- H₃ : Tertiary hematite - it is formed due to the reoxidation of the magnetite phase during cooling and often it is found around the pores.
- M₁ : Primary magnetite - the original relict magnetite which has not dissolved or changed during sintering.
- M₂ : Secondary magnetite - the magnetite phase recrystallised from the melt.
- CF : Calcium ferrite phase - it includes all types of ferrite phases e.g. monocalcium ferrite, dicalcium ferrite etc..
- S : Slag phase which includes both crystalline silicates as well as glassy phase.

Notations used to specify different sintering conditions

- NA : no additive; 2L : 2% quick-lime; 5L: 5% quick-lime;
 .25B: 0.25% bentonite; .1P: 0.1% peridur; 1PM: 1% peat moss;
 D : only disc; T&D: turbulator and disc

Note: All the photomicrographs presented in this section (unless specified) are at 200X.

Condition
a b c

Mineralogical observations 118

#1) 0 NA D Secondary magnetite is the major phase in this
(Base test) sinter followed by high amount of columnar slag
Fig. 4.2 phase. The Ca-ferrite content of the sinter is
low. It is mainly present in needle-like
structure. At times, a thin layer of ferrite is
seen overlapping the M_2 crystals (Fig. 4.2a).

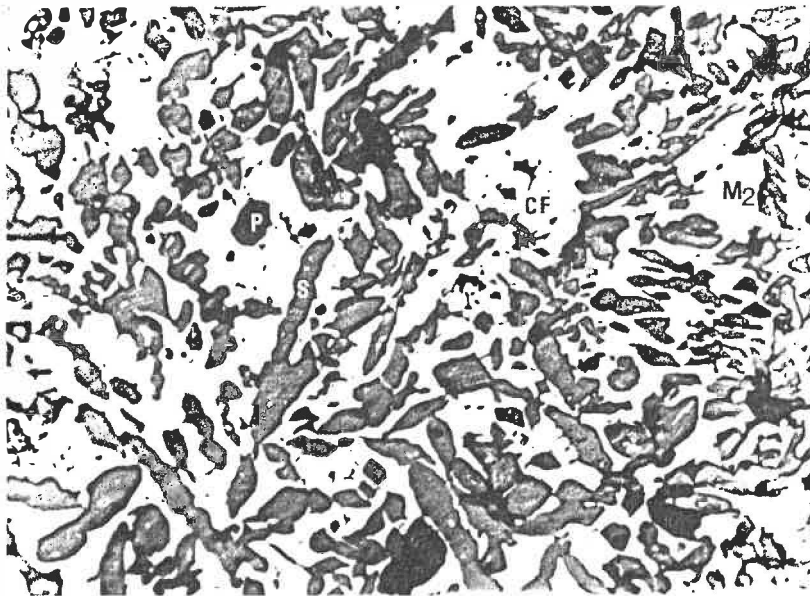
Almost no hematite (except few tertiary
hematites, re-oxidized from M_2) is marked. Slag
phase seems to be the main bonding phase in the
sinter. Precipitation of M_2 in the slag phase and
eutectic of M_2 and slag are also often seen in
the sinter structure as shown in Fig. 4.2b.

Summarizing the phases: secondary magnetite (M_2):
45-50 %; calcium ferrite (CF): 15-20 %; hematite
(H): < 5 %; and slag (S): 25-30 %.

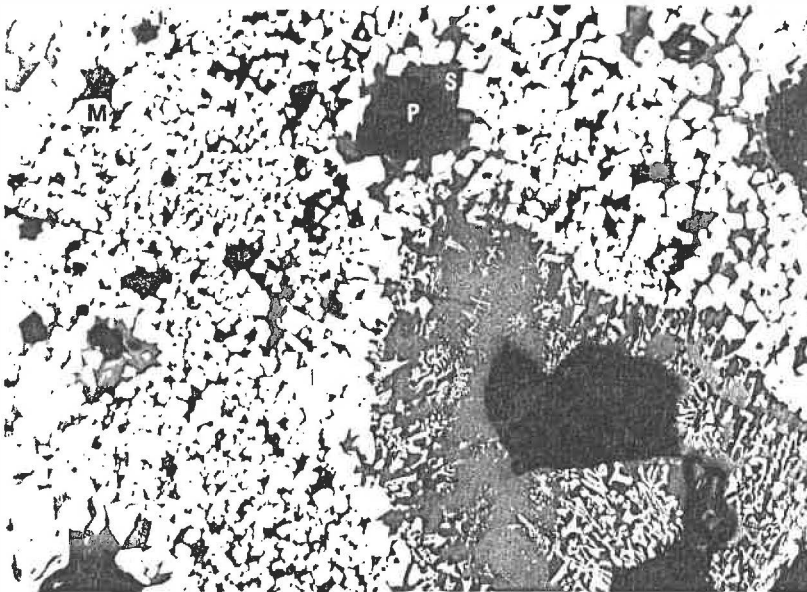
#2) 25 NA D The major phase is M_2 , but the amount has
Fig. 4.3 decreased. The crystals are irregularly shaped.
Like the previous one, precipitations of some M_2
crystals in the slag phase are also marked.

Note: The amount of phases are in vol. % and has been
determined by Image analyser (to be discussed later).

a: % of specularite: b: type of additive, c: type of device



a)

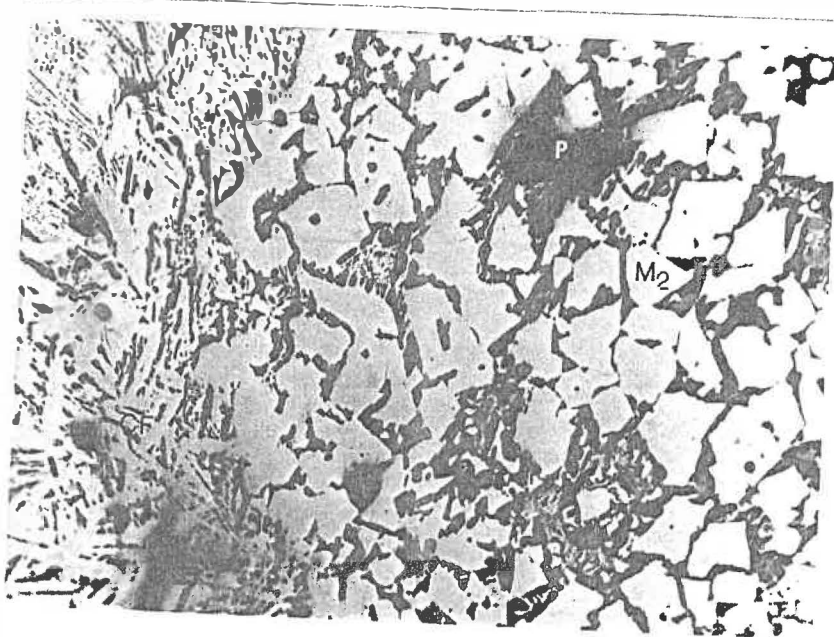


b)

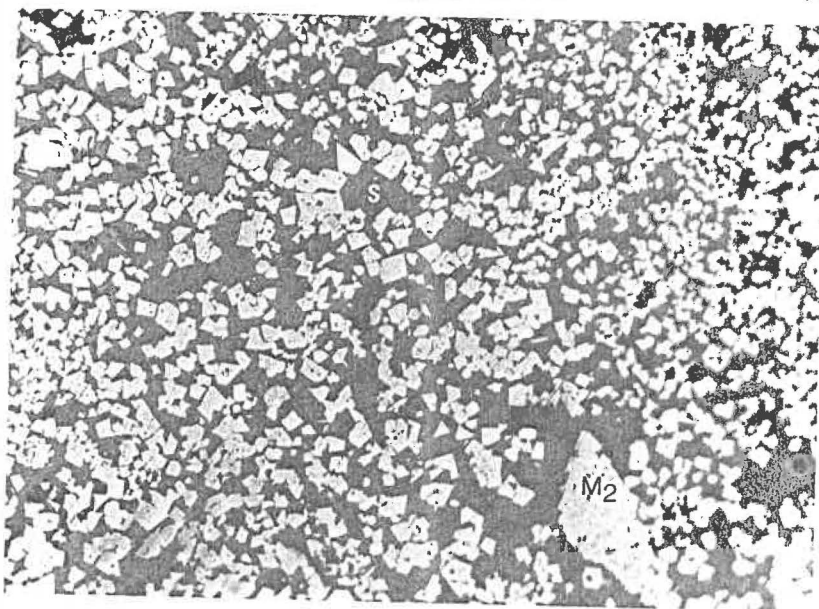
Fig. 4.2 Photomicrographs showing the typical microstructure of sinter containing no specularite or additive

a) Ca-ferrites overlapping M_2 crystals and columnar slag

b) M_2 crystals and precipitates of M_2 in slag phase



a)



b)

Fig. 4.3 Photomicrographs showing the typical microstructure of sinter containing 25% specularite, no additive

- a) Ca-ferrite needles and M_2
- b) small M_2 crystals in a slag phase

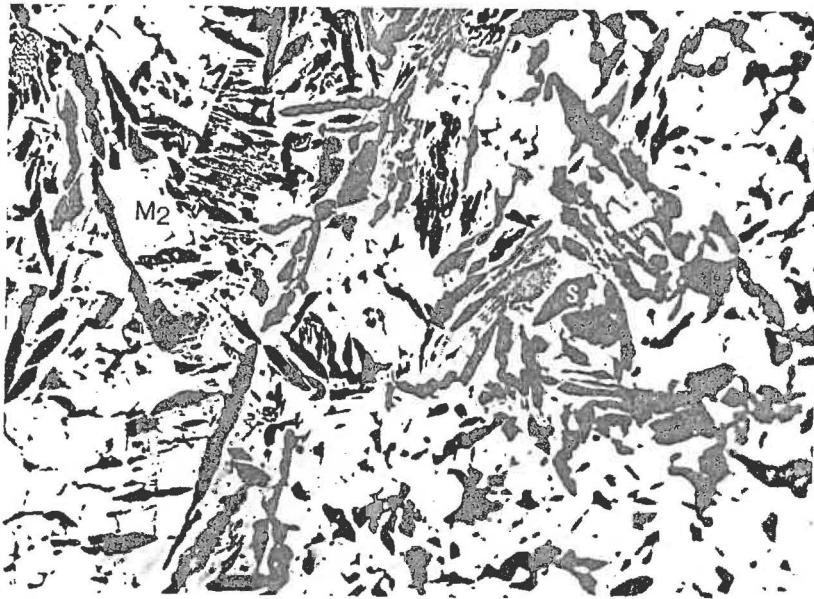
(cont'd) to the base case, but still remains low. The morphology of the ferrites is similar to the previous condition.

Few primary or relict hematite grains are noticed. Some magnetite crystals are partly reoxidized (mainly around the pores) tertiary hematite. The amount of slag phase is still high.

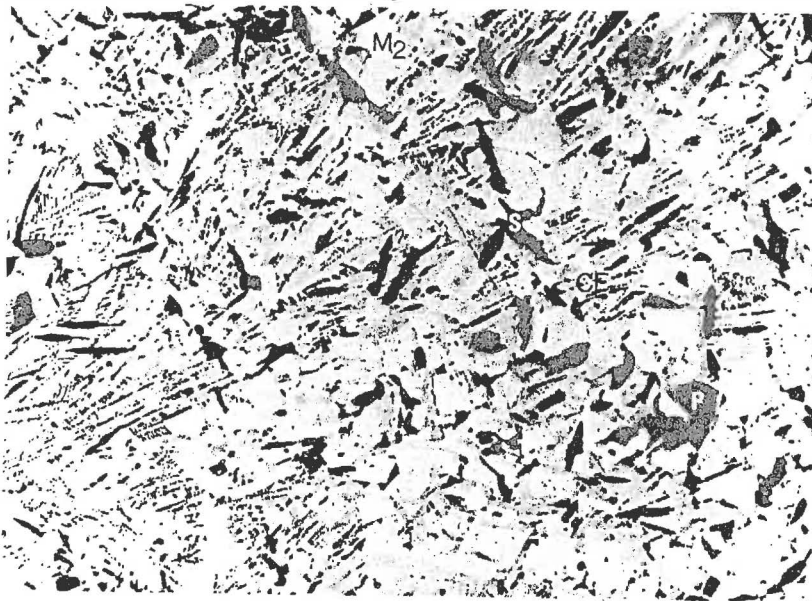
M_2 : 40-45 %; CF: 20-25 %; H: 5-10 %; and S: 20-25 %.

#3) 40 NA D Magnetite is still the major phase, followed by
Fig. 4.4 Ca-ferrite. M_2 crystals are small and sometimes covered with a thin layer of Ca-ferrite (Fig. 4.4a). Acicular (or needle-shaped) as well as blocks of ferrite are also often marked. The hematite content of the sinter has increased. Tertiary hematite, H_3 are seen around the pores. Slag phase is present mainly in columnar shape. Eutectic phases of slag and M_2 are occasionally seen.

M_2 : 35-40 %; CF: 25 %; H: 5-10 %; and S: 15-20 %.



a)



b)

Fig. 4.4 Photomicrographs showing the typical microstructure of sinter containing 40% specularite, but no additive

a) M_2 crystals and columnar slag

b) Acicular CF and M_2 crystals overlapped with CF

Condition
a b c

Mineralogical observations 123

#4) 25 2L D
Fig. 4.5

The amount of Ca-ferrite has increased significantly compared to the base test. In this sinter, magnetite and Ca-ferrite are present almost in equal amount. Ca-ferrite is present in blocks, as needles and also as a thin layer on the M_2 grains. Near the pores (the periphery of the specimen), it is often found to be the main matrix as seen in Fig. 4.5 a.

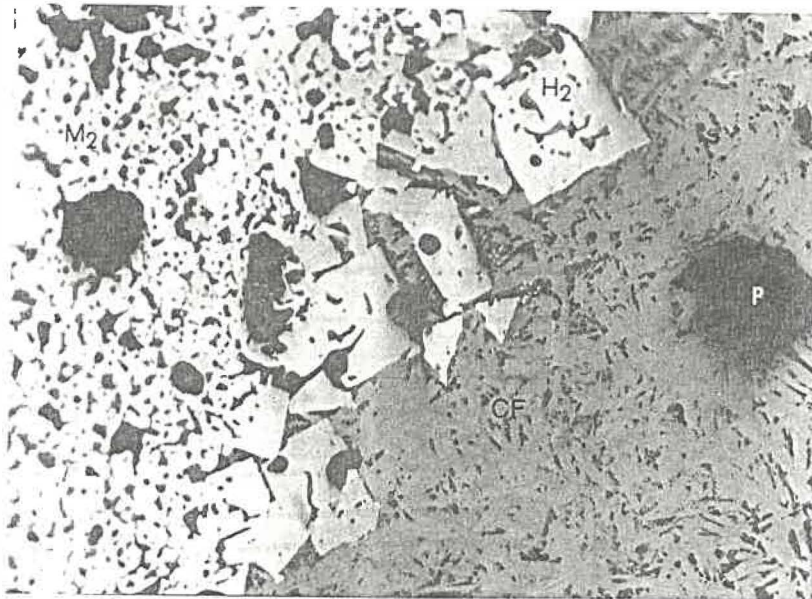
All the three type of hematite (i.e. H_1 , H_2 and H_3) are present. Columnar slag phase is often observed. Eutectic of M_2 and slag is also seen.

M_2 : 30-35 %; CF: 30-35 %; H: 5-10 % and S: 20%

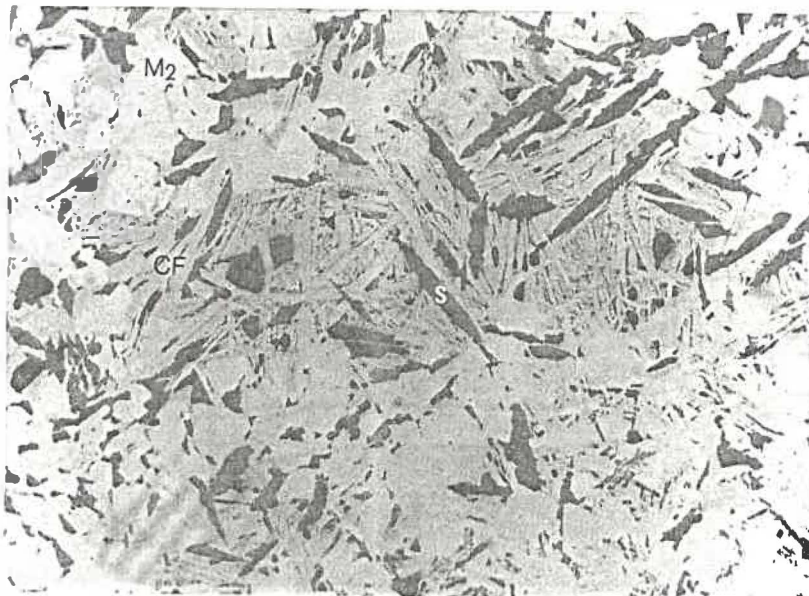
#5) 25 5L D
Fig. 4.6

The mineralogy of this sinter is almost similar to the previous specimen. However, the magnetite content is slightly higher and it is distributed all over the structure. Unlike the previous specimens, the amount of columnar slag is quite low. It is often present as the matrix, binding the small M_2 crystals together (Fig. 4.6b).

M_2 : 35%; CF: 30-35 %; H:5-10 %; and S: 20%.



a)



b)

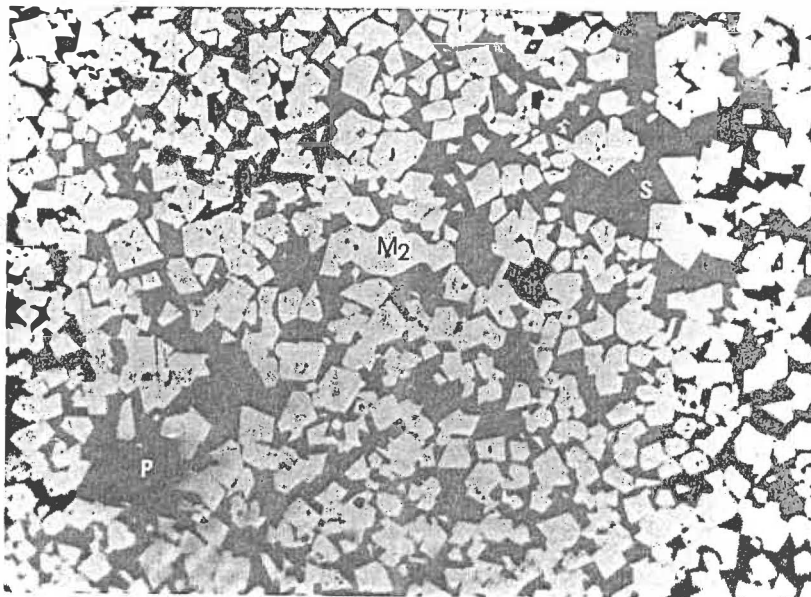
Fig. 4.5 Photomicrographs showing the typical microstructure of sinter containing 25% specularite and 2% quick-lime

a) Ca-ferrite, M_2 and H_2

b) Ca-ferrite, M_2 and columnar slag



a)



b)

Fig. 4.6 Photomicrographs showing the typical microstructure of sinter containing 25% specularite and 5% quick-lime
a) ferrite structure and M₂
b) Small M₂ crystals in slag phase

Condition
a b c

Mineralogical observations 126

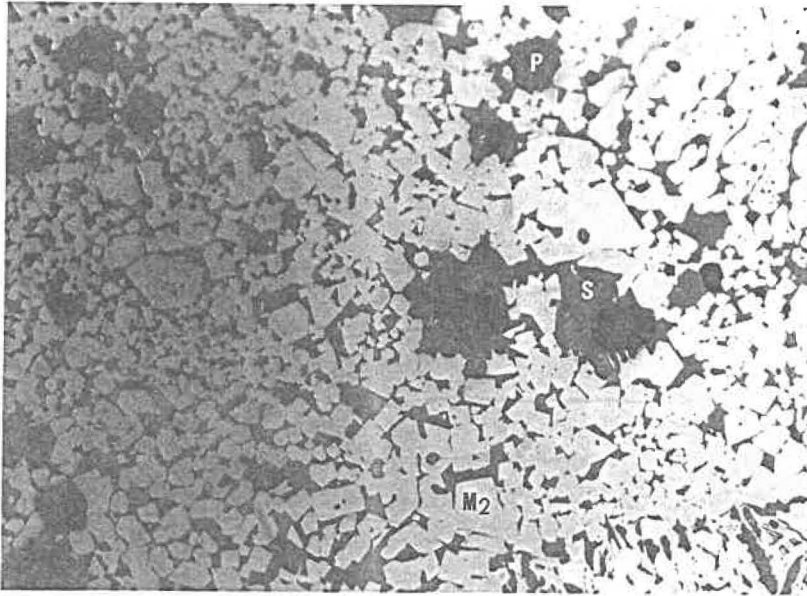
#6) 25 .25B D The structure of this sinter is similar to that
Fig. 4.7 of #5 (25 5L D), except that in this case, the
amount of the eutectic phases is higher.

#7) 25 .1P D The microstructure of this sinter is quite
similar to that of specimen #2 (i.e. 25 NA D).

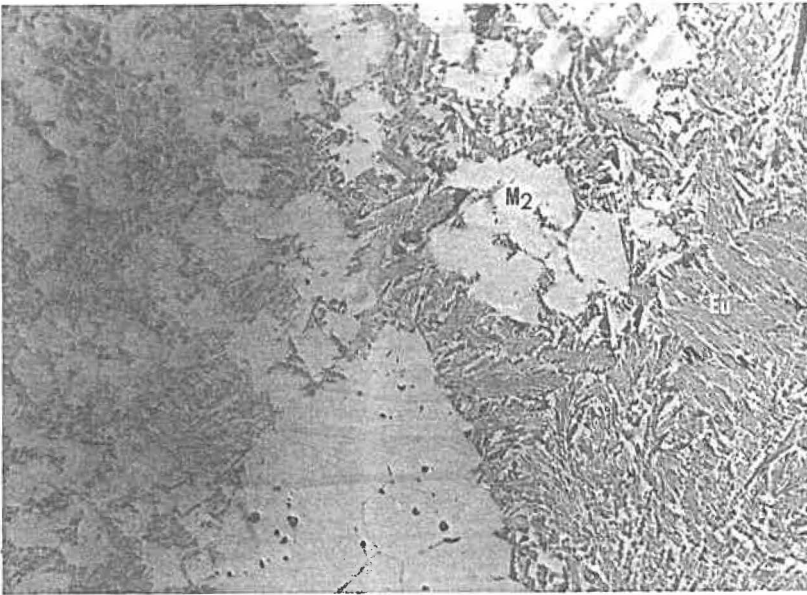
#9) 40 2L D Calcium ferrite is the predominant phase in this
Fig. 4.8 sinter. The morphology of the ferrite phase
varies from fine needles (network-like structure)
to columnar (or lath shaped) to blocks. Magnetite
is present in small crystals, at times, partly
or completely re-oxidized to the hematite (H_3).
Sometimes, it is also found to covered with a
thin layer of Ca-ferrite.

Large primary (relict) hematite (H_1) crystals are
seen in the sinter mineralogy. The slag content
of the sinter is relatively low. Precipitations
of M_2 in the slag phase and eutectic structures
are also noticed.

M_2 :30%; CF: 40-45 %; H: 10-15 %; and S: 15%.



a)

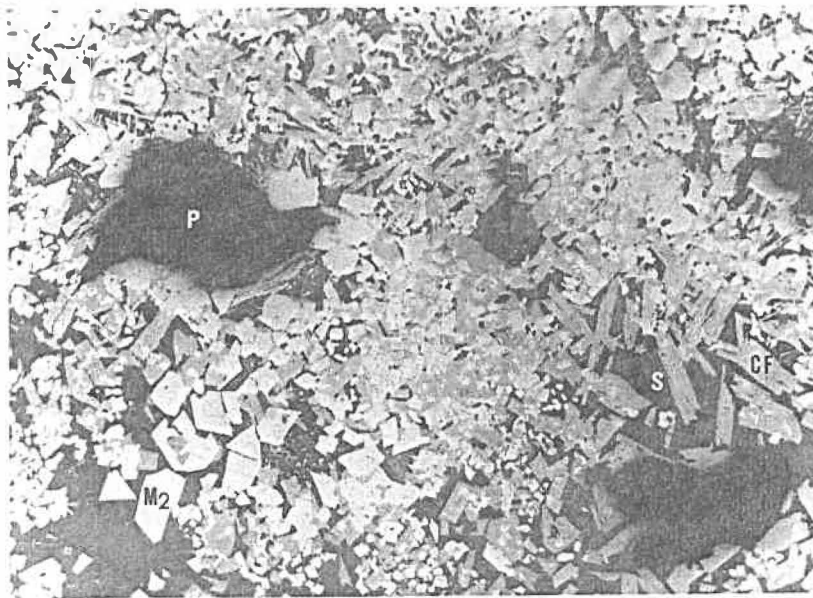


b)

Fig. 4.7 Photomicrographs showing the typical microstructure of sinter containing 25% specularite and .25% bentonite

a) M_2 crystals in slag matrix

b) M_2 and eutectic of M_2 and Ca-ferrite



a)



b)

Fig. 4.8 Photomicrographs showing the typical microstructure of sinter containing 40% specularite and 2% quick-lime
a) lath shaped and blocky Ca-ferrite
b) acicular Ca-ferrite

Condition
a b c

Mineralogical observations

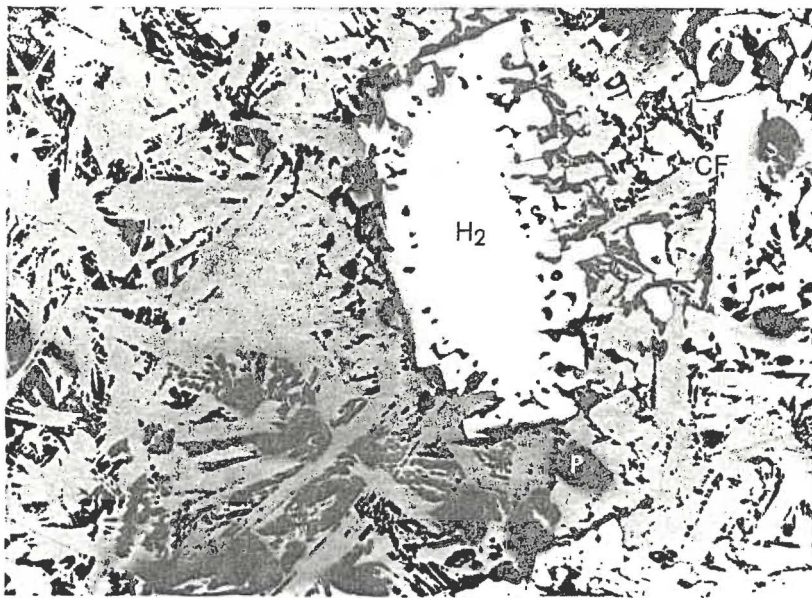
129

#10) 40 5L D The calcium ferrite content of this sinter is the highest of all the cases studied in the present investigation. Similar to the previous condition, it is present in a wide range of morphology e.g. from needle-like structure to big well-defined crystals. Small M_2 crystals (often covered with a thin layer of Ca-ferrite) are noticed.

Hematite is found as large crystals of primary hematite (H_1), secondary hematite (H_2) and tertiary hematite (H_3). The slag phase is present mainly in columnar shape. Precipitations of M_2 in the slag phase and eutectic phases are also observed in the sinter.

#11) 40 .25B D The structure is almost similar to that of the specimen #9 (40 2L D) with high calcium ferrite followed by magnetite. Large primary hematite crystals are observed in the sinter. The slag phase is mostly long columnar in shape.

#12) 40 .1P D Almost same as #3 (i.e. 40 NA D)



a)

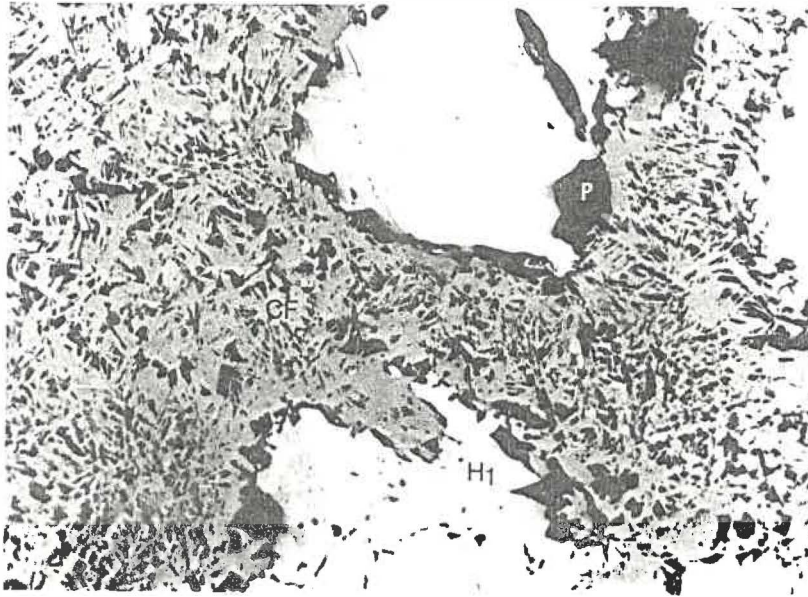


b)

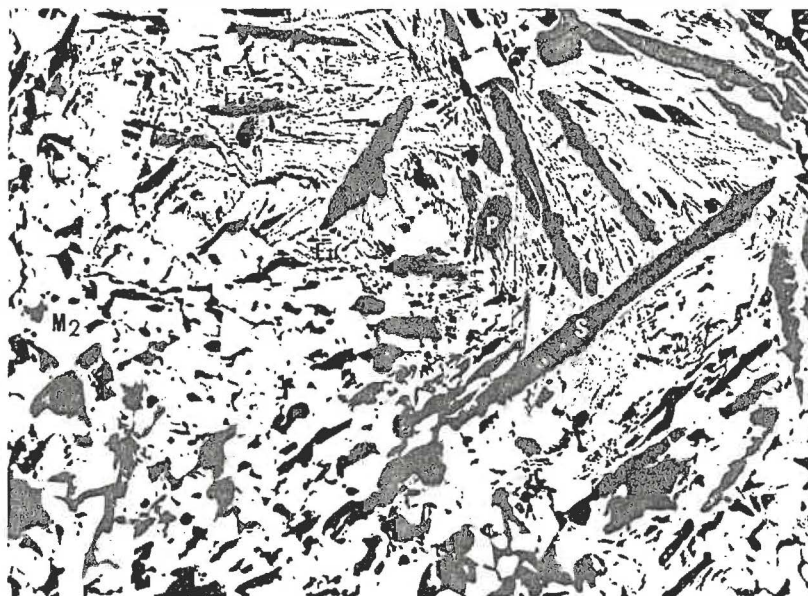
Fig. 4.9 Photomicrographs showing the typical microstructure of sinter containing 40% specularite and 5% quick-lime

a) H_2 in Ca-ferrite structure

b) CF structure and M_2 crystal partly reoxidized to H_3



a)



b)

Fig. 4.10 Photomicrographs showing the typical microstructure of sinter containing 40% specularite and .25% bentonite

a) H_1 in Ca-ferrite matrix

b) Columnar slag, eutectic of Ca-ferrite and slag

1.3 Semi-Quantitative Measurement of the Mineral Phases

The area of different phases has been measured semi-quantitatively by an IBAS interactive image analyser system. The specimen was placed under the microscope and the image was transferred to the image processing unit by a video camera. The area of each phase was determined by discriminating the grey labels. For each sinter condition, the phase areas have been measured at least in 20 different fields and the average of these values have been reported in Table 4.1. It should be noted that due to the close resemblance (i.e. little difference in their grey levels) and overlapping of the phases, the reported values do not represent the exact volume of the phases present in the sinter. They, however, give a good indication about the trend of phase changes taking place due to the changes in the sinter mix compositions.

1.4 Micro-analysis and X-ray Mapping

Specimens have been studied in a Jeol JSM-840 scanning electron microscope. The epoxy surface of the specimen was coated with graphite paint to make it conducting. Micro-analysis of the mineral phases were carried out at different spots using LINK (EDS) ANALYTICAL SYSTEM attached to the above microscope. The spots were carefully chosen so as to keep the influence of the surrounding phase-compositions on the analysis

Table 4.1 : Semi-quantive measurement of the mineral phases in different sinters (using only disc)

Specularite Concentrate (%)	Additive	Volume of mineral phase (%)			
		H	M	CF	S
0	NA	5	50	15	30
25	NA	5	45	25	25
	2%L	10	35	35	20
	5%L	10	35	35	20
	0.25%B	Similar to 25% Spec., 2% lime			
40	NA	10	35	35	20
	2%L	15	30	45	15
	5%L	Similar to the previous condition			
	0.25%B	Similar to 40% spec. & 2% lime			

H: Hematite; M: Magnetite; CF: Calcium ferrite; S: Slag phase

minimum. Analysis at any spot was done by accumulating the X-ray spectrum for 60 seconds. For any particular specimen, at least, 50 point-analyses have been made. Some X-ray mappings have been performed to study the distribution of different elements (e.g. Fe, Ca, Si, Al and Mg)

The conditions for the micro-analysis have been chosen from experience and from the literature. These conditions were:

voltage : 20 kv
 probe current : 3×10^{-8}
 working distance : 39 cm

1.5 Discussion

We have seen that calcium ferrite is the predominant phase in most of the sinters. This can be mainly attributed to the high basicity ($B = 2.5$) of the sinters. As discussed earlier (in Chap. II), due to increase in the lime content of the sinter mix the amount of liquid increases and its viscosity decreases. There is a strong tendency for the formation of calcium ferrites in this melt^(28,29).

Ferrites and silicates react in molten state. At this stage calcium diferrite is formed. However, on cooling it decomposes into monocalcium ferrite and hematite. The latter is then re-crystallized as secondary hematite or secondary magnetite depending on the sintering atmosphere.

The high temperature and the reducing conditions during sintering facilitates the formation of Fe^{2+} ions in the melt. While cooling, they crystallize out as magnetite. The oxygen is supplied by the melt. The absorption of oxygen in the melt is facilitated by the turbulence created in low viscous liquid formed in this high basicity sinters. Thus, there is a significant amount of magnetite found in the sinter structure. Some magnetite crystals (particularly those around the pores) often get partly or completely re-oxidized to tertiary hematite during cooling.

In the presence of large amount of pre-sintered materials (as in the base mix), the temperature attained during sintering is high (as the heat necessary to sinter these materials is relatively less). When these materials are replaced by increasing amount of specularite in the mix, the sintering temperature drops and the reduction of Fe^{3+} to Fe^{2+} in the melt is retarded (this reduction reaction is strongly endothermic). Besides, due to the crystallization of magnetite in the beginning, there is an enrichment of Ca^{2+} ions in the melt and it facilitates the oxidation of some Fe^{2+} to Fe^{3+} . Hematite is crystallized from the melt, leaving behind a Ca^{2+} enriched slag.

The concentration of Ca^{2+} in the melt gradually increases and finally, it becomes so high that it also precipitates as calcium ferrites and often associated with silicates and other phases. As described before, calcium ferrites are also produced by direct reaction with iron oxides. Since calcium ferrite have low viscosity (e.g. viscosity of monocalcium ferrite, $\text{CaO} \cdot \text{Fe}_2\text{O}_3$ at 1300°C is 0.15 poise)⁽⁸⁶⁾ and since it is formed at a later stage, it is often found overlapping the magnetite crystals.

The last phase to be formed from the melt in such highly basic sinter is slag containing CaO and SiO_2 . Because of high CaO content, usually dicalcium and tricalcium silicates are formed. The slag phase is also found eutectically associated with other phases (e.g. magnetite and calcium ferrites).

Hematite can easily react with lime at temperature above 950°C forming calcium ferrite. By increasing the specularite content in the mix, there is a better contact between the hematite particles and the lime particles. The reactions between the iron oxides and CaO are accelerated and there is an increase in the amount of calcium ferrites content of the sinter. The hematite content (original or primary, secondary and tertiary) also increases due to higher state of oxidation of the raw mix and relatively lower temperature attained in the sintering. The amounts of magnetite and slag decrease.

Replacement of limestone by quick-lime also has similar kind of effect (with regard to ferrite formation). Besides, the fine quick-lime has higher reactivity than limestone. It accelerates the reaction between CaO and Fe_2O_3 and enhances the formation of different ferrites.

The reason for the increase in the ferrite content with bentonite addition is not quite clear. By enhancing pre-agglomeration in sinter mix, it probably establishes better contact between hematite and lime leading to more ferrite formation. Pre-agglomeration also helps maintaining uniform gas flow and improves the heating characteristics of the sinter bed. Thus, it influences the mineral phase formation.

As mentioned earlier (in Chap. II), the reactions occurring during the sintering process are of quite complex nature and some phases whose formation is not evident from the average composition of the sinter are often noticed in the final sinter structure. Hence, the microstructure of sinters vary at different spots.

Numerous analyses have been made to investigate the composition of different phases. Each mineralogical phase has a range of composition as shown in Table 4.1. The elements shown in this table are present as oxides in the sinter.

In these sinters, up to 4.9% CaO is present in the secondary magnetite phase. This contradicts the findings of some authors (e.g. Matsuno⁽⁸⁷⁾) who have reported that the maximum amount of CaO which could dissolve in M_2 is 2.5%. However, this is in agreement with result obtained by Ahsan et al.⁽³⁵⁾.

The magnetite phase contains a large amount of MgO, up to 4.6% (with 3.5% as an average). As discussed in the Chapter II, due to the similarity in the structure of MgO and magnetite, magnetite can dissolve up to 20% of MgO forming magnesio-spinel. In actual sintering practice, the stoichiometric magnesio-ferrite which contains 20% (by wt.) of MgO is hardly found and usually, the amount of MgO varies from

8-15%⁽⁴²⁾. These magnesio-spinels appear as a grey phase^(43,88). However, these spinels, in the present investigation, contains relatively lower MgO and optically they are found to be almost the same as magnetite (with very low MgO (<0.5%).

Calcium ferrites have a wide range of composition (e.g. Fe content varies from 20.7 - 60.7 %) as seen in Table 4.2. Three principal forms of ferrites are observed in the present sinters. They are lath-shaped or block, acicular or needle-like and eutectic ferrites or precipitates of ferrites in the slag phase. From their microanalysis, it is observed that each type (morphologically) of ferrite corresponds to a particular range of the composition. The morphology of ferrites and the corresponding composition are given in Table 4.3. The thin layers of ferrites on M_2 grains have almost same composition as lath or block ferrite crystals. The composition of eutectic ferrites or the ferrites associated with the silicates corresponds (more or less) to monocalcium ferrite ($CaO \cdot Fe_2O_3$) or dicalcium ferrite ($2CaO \cdot Fe_2O_3$) while the composition of the other ferrites are close to that of calcium diferrite ($CaO \cdot 2Fe_2O_3$). All these calcium ferrites contain different amount of Si and Al (0.4-12.3 % and 0.3-1.2 % respectively. Hence, they are usually referred as silico ferrites of calcium and aluminium (SFCA) in the literature.

Table 4.2 : Composition of the mineral phases

Phase	Fe	Ca	Si	Mg	Al	Mn
H ₁	69.1-70.2	0.0-0.1	1.2-3.2	0.0	0.1	0.1
H ₂	68.7-69.7	0.2-0.6	0.1-0.3	0.0-0.4	0.1-0.2	0.5-0.9
M ₂	60.7-65.6	1.2-4.9	0.1-0.5	0.5-4.6	0.3-0.5	1.2-3.6
CF	20.7-60.7	8.0-32.9	0.4-12.3	0.0-0.7	0.3-1.2	0.3-1.1
G	1.6-10.5	40.3-51.5	11.5-12.9	0.0-0.3	0.0-0.6	0.0-0.3

Note: The elements are present as oxides.

Table 4.3 : Composition of different types of calcium ferrites

Morphology	Fe	Ca	Si	Mg	Al	Mn
Lath/block	57.9-60.7	9.0	0.4-1.1	0.3-0.7	0.3-0.6	0.4-0.8
Acicular/needle	48.2-52.3	12.4-13.3	1.5-4.3	0-0.5	0.9-1.2	0.9-1.2
Eutectic*	20.7-29.9	21.8-32.9	10.8-12.3	0-0.4	0.3-0.5	0.3-0.5

* The compositions of the eutectic ferrites might have been affected by the surrounding phases.

The composition of the slag phase also varies within a wide range (e.g. Fe: 1.6-10.5 % and Ca: 40.3-51.5 %, refer Table 4.3). The average composition of the columnar slag phase mainly corresponds to that of tricalcium silicate.

The composition of the primary hematite is distinguished from that of the secondary and tertiary by its high Si content. It contains slightly higher amount of Si (up to 3.2 %), but no Ca, Al and Mg. Secondary hematite which is re-crystallized from the liquid phase contains relatively more Ca, Al and Mg (see Table 4.2). The tertiary hematite has almost same composition as the secondary magnetite from which it is re-oxidized.

From the X-ray mapping, it is seen that Si is present mainly in the slag phase and in Ca-ferrites. As expected, during sintering, Mg preferentially dissolves in the magnetite phase. However, it is also found in other phases, but only to a limited amount. The alumina content of these sinters is very low (about 1%, as given in Table 3.3, in the next section). It is mainly associated with Ca-ferrites.

2. Chemical Analysis of the Sinters

The chemical composition of the sinters are given in Table 4.4. Besides the oxides mentioned in this table, the sinters also contain some other oxides such as TiO_2 and MnO in small amounts. These oxides do not have any significant influence on the properties of sinter. The compositions of sinters using turbulator and disc or only disc were the same because the same raw materials have been used.

Although effort was made to produce sinters with a constant basicity of 2.5 and MgO content 3.0% while calculating the charge for the sinter mix, it was hardly achieved. The sinter basicity varied from 2.36 to 2.76. Similarly the MgO content ranged from 2.33 to 3.47%. This shows the crudeness of the process. It was difficult to control the final sinter composition using a variety of raw materials with a wide range of composition. In fact, this is what happens in the regular industrial sintering practice. For example, in the base test, the proportions of different raw materials used were same as the sinter plant in the Algoma Steel Corporation where the aim is to have sinter with 3.0% MgO . However, the MgO content of the sinter produced in this work is 4.44% (see Table 4.4)

Table 4.4 : Chemical Analysis (wt. %) of the Sinters
Produced

Spec. Conc. (%)	Additive	Fe _t	FeO	SiO ₂	Al ₂ O ₃	CaO	MgO	B
0	NA	47.90	7.7	7.21	1.26	17.40	4.44	2.58
25	NA	50.05	10.3	6.11	1.02	16.20	3.47	2.76
	2%L	50.20	9.4	6.27	1.18	16.14	3.43	2.63
	5%L	50.05	8.8	6.21	1.18	15.41	3.60	2.57
	.25%B	49.0	10.0	6.67	1.17	17.46	3.34	2.65
40	NA	51.80	8.20	5.90	1.01	14.92	3.19	2.62
	2%L	51.73	7.20	5.94	0.98	15.46	2.94	2.66
	5%L	51.68	7.7	6.13	1.01	15.47	3.04	2.59
	.25%B	40.93	7.4	6.20	1.04	15.63	3.01	2.57
100	NA	59.4	10.9	4.44	0.61	8.83	3.20	2.38
	2%L	58.7	10.6	4.41	0.73	9.17	2.98	2.36
	5%L	58.2	10.0	4.76	0.69	9.97	2.33	2.27

Fe_t: Total Fe content

B : Basicity = (CaO + MgO)/(SiO₂ + Al₂O₃)

With the increase in the amount specularite concentrate in the mix, the total Fe content (Fe_t) of the sinter increased and the amount of the gangue constituents decreased. As shown in Table 4.4, the iron content has increased from 48 to 58 % when the specularite content was increased from 0 to 100%.

The FeO content of the sinter mainly represents the amount of its magnetite phase and slag phase. Although FeO improves the reduction degradation index (RDI) of sinter, it is usually considered undesirable in the sinters principally because of its adverse effects on reducibility. As given in Table 4.4, the FeO content of these sinters are below (except in few conditions) the maximum amount of FeO allowed in the industrial sinter (which is usually 10%).

3. Evaluation of the Sinter Quality

The quality of the sinter is evaluated by determining its properties by different laboratory test methods developed from the industrial experience. While developing these methods, particular attention has been given to simulate (as much as possible) the test conditions to those in the actual practice. Some of the methods have been standardized by different standardizing organisations. A summary of different test methods is given in Ref. 89 and 90. Efforts have been made to correlate the results (obtained by different methods) with the blast furnace operation.

3.1 Porosity

The porosity of sinter has a marked effect on other properties (e.g. reducibility and strength, as discussed in Chap. II) and knowledge of it can provide useful informations.

Sinter porosity can be determined by measuring its volume by various means. Accuracy of the results depends mainly on the precision of the volume measurement. In the present work, a Beckman Air Pycnometer has been used. A schematic diagram of the pycnometer is shown in Fig. 4.11. The test method will be briefly described in the following paragraphs. The detail experimental procedure can be found in Ref.55.

3.2 Test Procedure

The sample consists of 50 sinter pieces (size 9.5-15.9 mm) chosen at random. It is then divided into five batches and weighed. The volume of each batch is measured using the pycnometer. It is kept in a perforated steel basket and dipped in molten wax. The temperature of wax is maintained at 60°C, about 5°C above its melting temperature. It is important to maintain this temperature in order to obtain a thin coating of wax on the sinter for better reproducibility of the results.

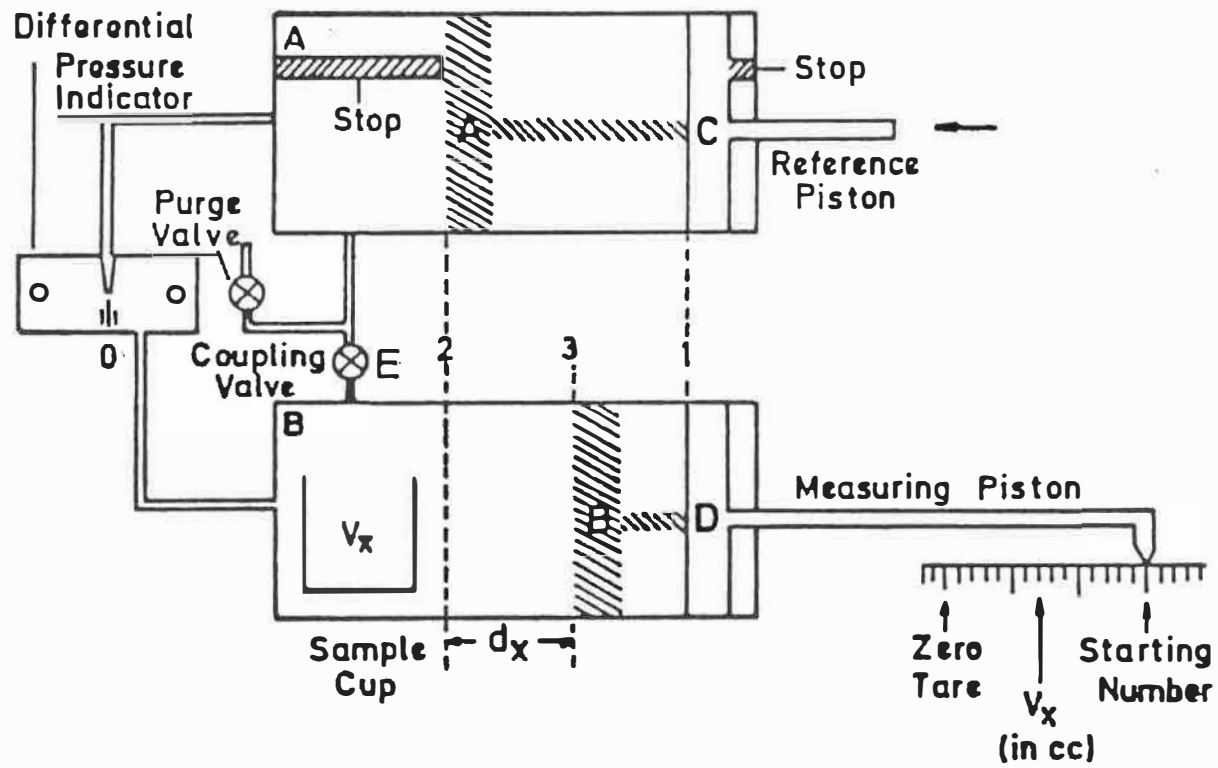


Fig. 4.11 Scheme of a Beckman air pycnometer.

As soon as the sinter pieces are dipped in the molten wax, air bubbles come out. The amount of bubbles gradually reduces and they cease to appear after 5/6 minutes. They are then taken out and the excess wax is drained. They are rolled over a blotting paper to wipe out any remaining wax and cooled down to room temperature. Volume of each batch of wax-coated sinters is again measured and it is weighed.

About 200 g of a fresh batch of the sinter in the granulometric fraction at +9.5 mm is ground to -200 mesh size and its volume is measured. The densities d_a , d_t and d_m are calculated from the corresponding weights and volumes of uncoated, wax-coated and ground samples respectively. The porosity is calculated by the following equations:

$$\% \text{ open porosity } (P_o) = \left(1 - \frac{d_t}{d_a}\right) \times 100$$

$$\% \text{ closed porosity } (P_c) = \left(\frac{1}{d_a} - \frac{1}{d_m}\right) d_t \times 100$$

$$\% \text{ total porosity } (P_t) = \left(1 - \frac{d_t}{d_m}\right) \times 100$$

3.1.2 Results and Discussion

The porosity values (which include open and close porosity) obtained from these tests are given in Table 4.5. As we can see in this table, sinter porosity increases with the increase in specularite content of the sinter mix. By increasing the specularite content from 0 to 40%, it has increased from 13 to 20% (volume). Plot between the porosity values and the specularite content (Fig. 4.12) shows a linear relationship (within a variation of 2σ).

From Table 4.5 it is also evident that for any level of specularite concentrate in the mix, sinter porosity is found to be maximum when no additive is used. It decreases with the addition of quick-lime. With 40% specularite concentrate, porosity of sinter has decreased from 19.8 to 17.5 % by adding 5% quick-lime in the sinter mix.

The use of turbulator or bentonite does not have any detectable effect on the porosity of sinter. The porosity values of the sinters produced in the industrial strand or with modified fuel addition are lower (except for the sinters with 100% specularite) than that of the corresponding sinters by the regular pot-grate tests. As given in Table 4.5, for 40% specularite and 2% quick-lime in the sinter mix, the porosity

Table 4.5 : Porosity of the sinters

Spec. Conc. (%)	Additive	Porosity (in % Vol.)	
		Disc	Turbulator & Disc
0	NA	12.9	18.1
25	NA	14.9	17.1
	2%L	14.3	17.5
	5%L	12.6	16.7
	0.25%B	17.1	17.9
40	NA	19.8 (15.7) 19.0*	18.9
	2%L	19.2 (13.8) 16.3*	15.4
	5%L	17.5 (15.0) 15.5*	18.1
	0.25%B	18.5	18.6
100	NA	----	----
	2%L	19.9 (19.8)	----
	5%L	18.3 (20.3)	----

() : Values for the sinters produced in the industrial strand

* : Values for the sinters with modified fuel addition

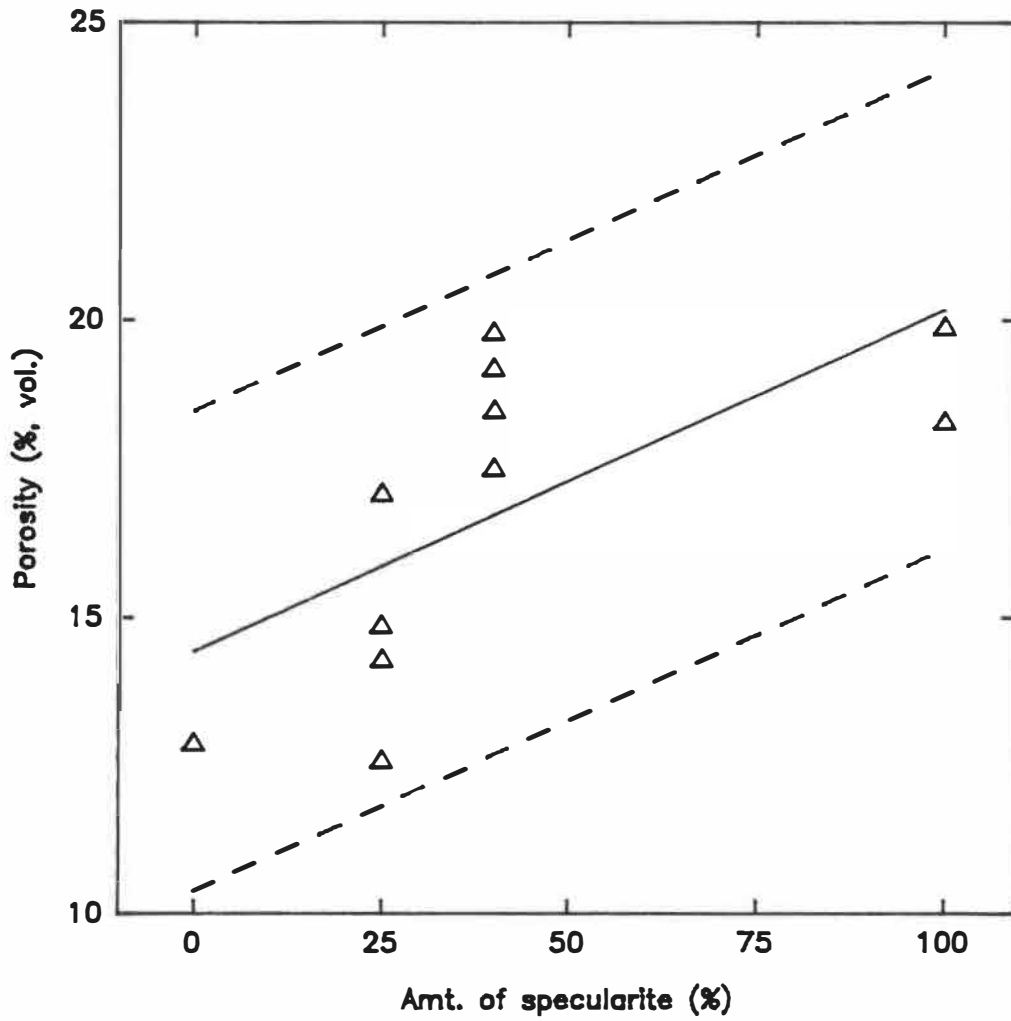
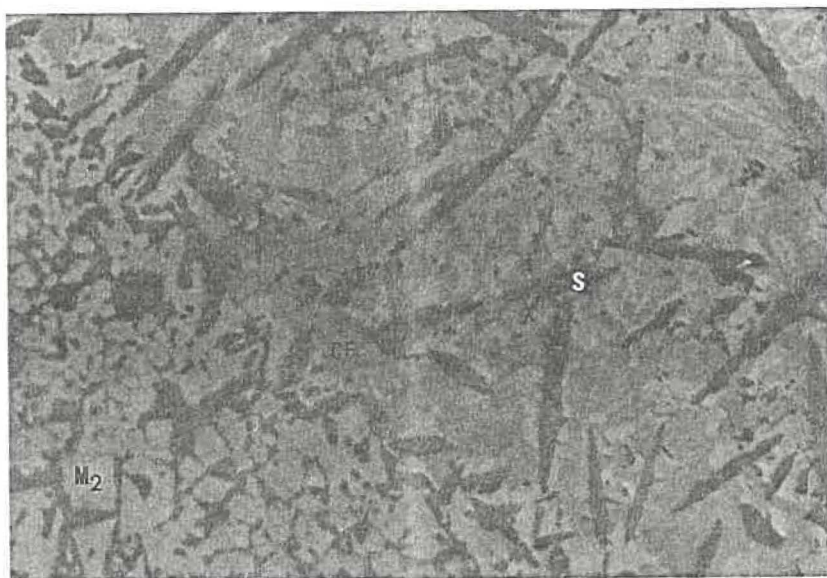


Fig. 4.12 Variation in sinter porosity with the specularite content of the sinter mix.

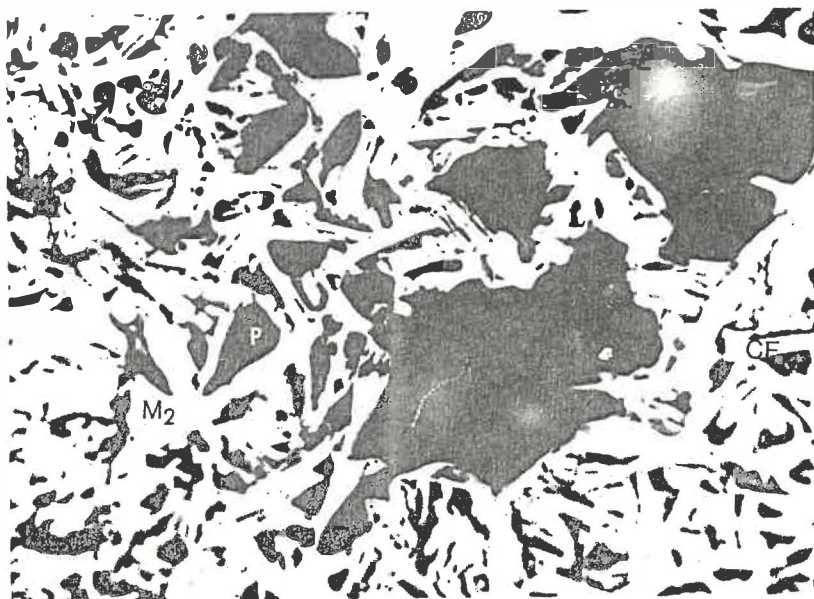
has reduced from 19.2% to 13.8% and 16.3% for industrial strand and modified fuel addition respectively.

As discussed in Chapter II, the porosity of the sinter is largely affected by the nature and amount of melt formed during sintering which in turn is controlled by the physical and chemical nature of the raw materials and the heating characteristics of the fuel. In the previous section, we have seen that, sintering temperature decreases with the increase in the amount of specularite in the mix and the melt formation temperature increases (due to less pre-sintered materials). Hence, there is a lower amount of liquid formation during sintering. This causes more porous structure. The change in the sinter structure due to the variation in specularite content of the sinter mix can be seen in Fig. 4.13. The structure of sinter with 40% specularite (Fig. 4.13b) is more heterogeneous and marked with many large pores compared to that of the sinter with no specularite (Fig. 4.13a).

The bed temperature and the amount of melt formed during sintering increases with the addition of quick-lime. It also reduces the viscosity of the slag formed. Besides, increase in the bed permeability leads to more uniform flame-front movement and better heat distribution in the bed. As a result, the amount of melt formed during sintering increased and strength of the sinter was improved.



a)



b)

Fig. 4.13 Variation of the mineralogical structure of the sinter produced with its specularite content
a) 0% specularite; b) 40% specularite.

The amount of bentonite was probably too low to have any detectable effect on the sinter porosity. Decrease in the heat loss in the industrial strand and improved heating characteristics with the modified fuel addition have lowered the amount of pores formed during sintering.

3.2 Strength

Breakdown of the sinters is inevitable during their transportation from the sinter plant to the blast furnace. In order to avoid excessive breakage, they should have sufficient strength. A prior knowledge of the magnitude of the breakdown is essential for quality control purpose.

The strength (impact and abrasion resistance) of sinter was determined following the ASTM Tumbler test method⁽⁹¹⁾. In this method the impact resistance, represented by the Tumbler index (or T-index) and the abrasion resistance represented by the Abrasion index (or A-index) are determined. The T-index value is usually referred as the cold strength of the sinter.

3.2.1 Test Procedure

The procedure consists of subjecting 11.3 kg (25 lb) \pm 0.15 kg of sinter in the size range of 9.5 - 50.8 mm (3/8 - 2") to 200 revolutions at 25 \pm 1 rpm in a standard steel drum. The

diameter and length of this drum are 915 mm (38") and 458 mm (18") respectively.

The sample is then taken out and screened. The +6.3 mm and -0.5 mm portions of the sinter (expressed in %) are designated as tumbler index (T-index) and abrasion index (A-index) respectively.

3.2.2 Results and Discussion

The results of the tumbler test are given in Table 4.6.

Tumbler Index

As we can see in Table 4.6, up to 40% specularite in the sinter mix, the strength of the sinter (the T-indices varying between 63-68) is above the limit accepted for the industrial practice. In general, strength of the sinter decreases as the amount of specularite concentrate in the sinter mix increases. The tumbler index has dropped from 67.8 to 63.7 by adding 40% specularite in the sinter mix. The decrease in the T-index due to specularite addition is clear from Fig. 4.14.

For any amount of specularite content in the sinter mix, quick-lime increases the strength. Turbulator or bentonite does not have much influence on it. Similarly, no marked difference

Table 4.6: Tumbler strength of the sinters

Specularite Concentrate (%)	Additive	Disc		Turbulator & Disc	
		T-Index	A-Index	T-Index	A-Index
0	NA	67.8	3.8	----	---
25	NA	64.6	4.3	67.6	4.3
	2%L	67.5	4.0	66.2	4.6
	5%L	67.6	3.6	68.5	4.2
	0.25%B	67.7	4.0	63.6	4.5
40	NA	63.7 (62.7) 59.5	4.2 (5.2) 5.1	63.3	5.0
	2%L	64.8 (63.3) 61.6	4.6 (5.6) 4.6	68.5	2.3
	5%L	62.5 (63.7) 62.1	4.5 (5.2) 4.9	65.7	4.8
	0.25%B	64.1	4.0	65.0	2.2
100	NA	----	---	----	---
	2%L	44.7	5.7	----	---
	5%L	55.0	6.0	----	---

() : Values for the sinters produced in the industrial strand

* : Values for the sinters with modified fuel addition

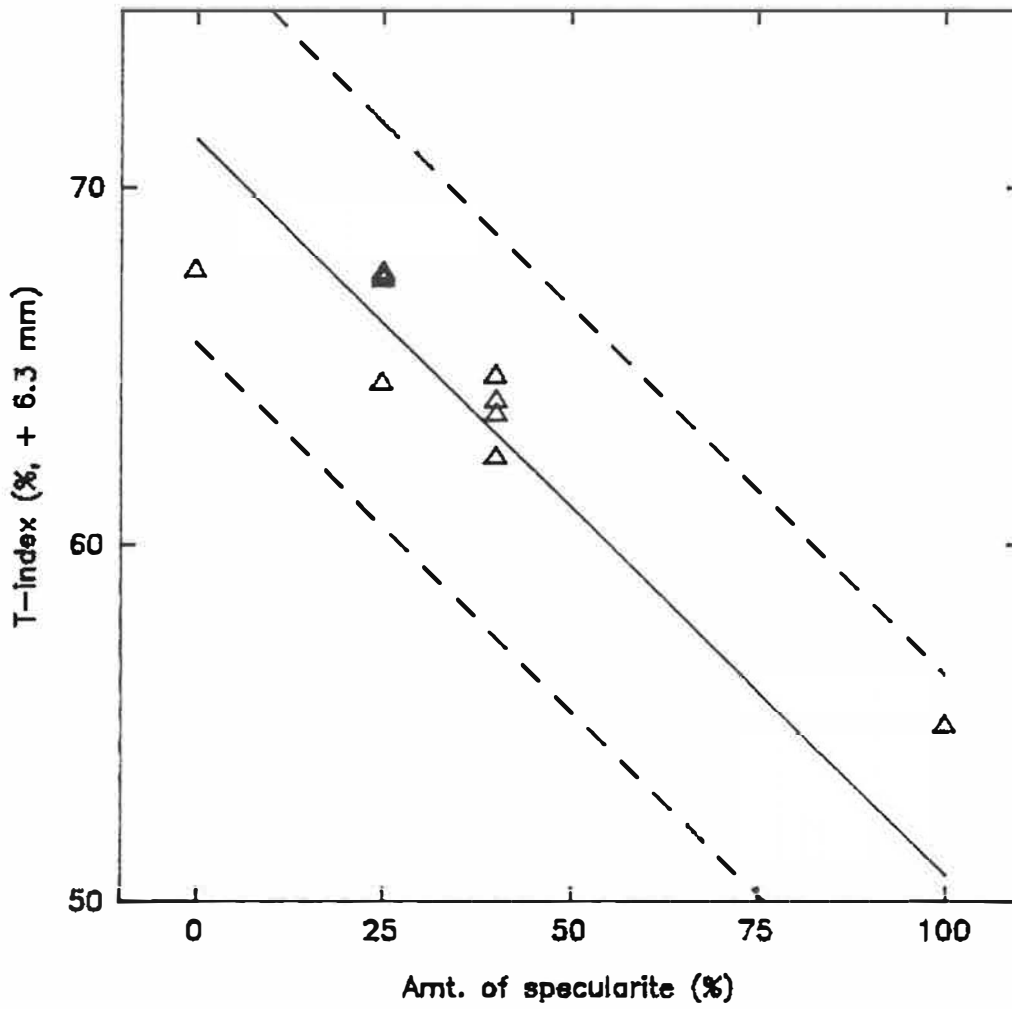


Fig. 4.14 Change in T-index with specularite addition.

is noticed between the T-indices of the sinters produced in the industrial strand or with modified fuel addition and the corresponding sinters produced in regular pot-grate tests.

We have seen in Chapter II that the strength of sinter depends on its final matrix (i.e the amount of iron oxides, calcium ferrites and slag phases, both crystalline and glassy). The amount of pores and cracks also play an important role in this regard. All these factors are affected by the nature and quantity of liquid formed and the reactions taking place during sintering, which in turn are mainly controlled by the physical and chemical nature of the raw materials and the heating characteristics of the fuel.

In case of the base mix, the gangue content of sinter is higher and the high slag phase (about 30%) formed in this sinter provides a good bonding medium. As we discussed earlier, increase in the amount of specularite concentrate in the sinter mix decreases the slag phase (with 40% specularite, it is about 15%) and sinter becomes more porous (see Fig. 4.13).

As expected, increase in the porosity values has a negative effect on sinter strength (as seen in Fig. 4.15). Although, calcium ferrites (which is beneficial for sinter strength, see Chap II) increase with the specularite content of the sinter

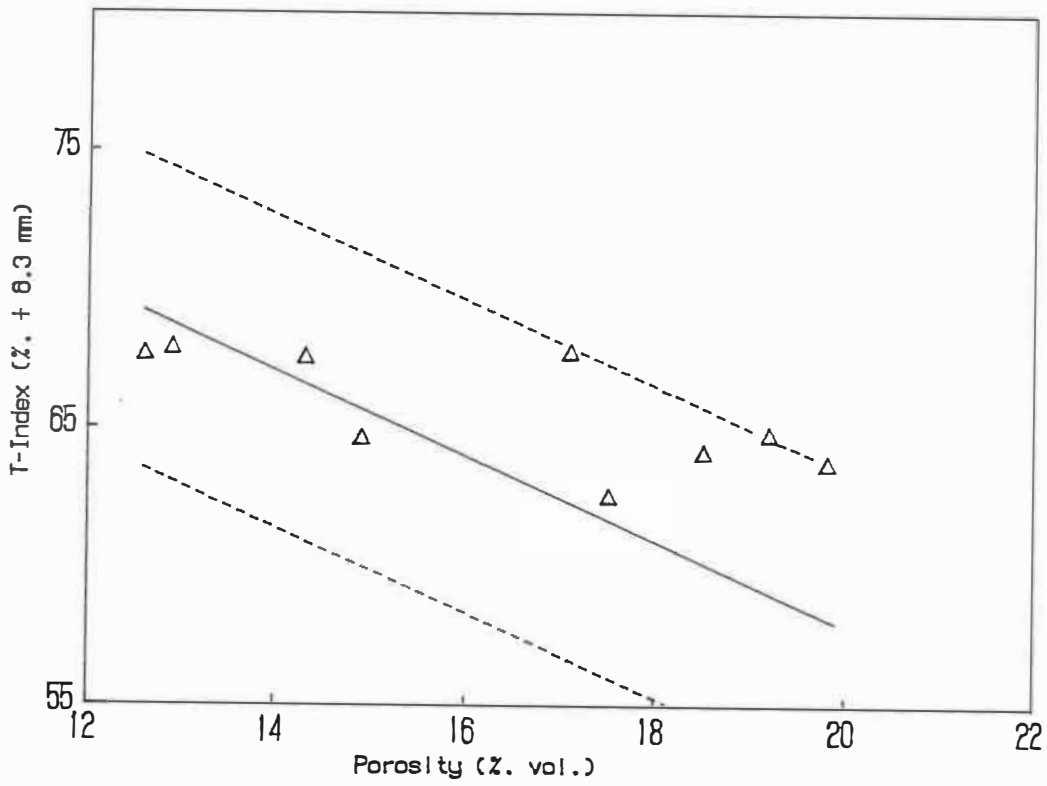


Fig. 4.15 Effect of sinter porosity on its strength.

mix, its salutary effect is largely superseded by the deleterious influence caused by the presence of large pores.

Replacement of coarser iron-bearing materials by fine concentrates has adverse effects on the bed permeability and on the heating characteristics. Thus, there is a deterioration in sinter strength.

Increase in strength due to quick-lime addition is mainly attributed to higher amount of liquid formation during sintering. Besides, it increases the amount of calcium ferrites (which increases the sinter strength by providing a good bonding phase⁽⁶⁰⁾) in sinter. Improve in bed permeability due to lime addition also have positive effects on sinter strength.

The amount of bentonite used is very low (0.25%) and it does not have much influence on sinter mineralogy (we have seen before). Similarly, it does not have any marked effect on sinter strength. The marginal difference in T-indices of sinters using bentonite or turbulator is mainly ascribed to the change in micro-pelletization of the sinter mix.

Abrasion Index (A-Index)

The abrasion index (% , - 0.5 μm) of all sinters (up to 40% specularite) is lower than 5 (the usual acceptable value),

indicating these sinters have adequate abrasion resistance. The decrease in A-index due to increase in specularite is mainly due to the production of heterogeneous and brittle sinter structure. No significant difference is marked in sinters using turbulator and/or additives.

The strength of the sinter produced from 100% specularite concentrate is quite low (T-index < 60). The sinter structure is very brittle and open. This is due to low permeability (causing non-uniform air-flow and flame-front movement) and insufficient liquid formation during sintering. The amount of slag phase is also low because of low gangue content of sinter. Due to their low strength, these sinters are not considered as of acceptable quality.

3.3 Reduction Degradation (or Low-temperature Degradation)

The reduction degradation behaviour of sinter is determined by simulating the test method to the conditions (thermal and atmospheric) in the upper stack of the blast furnace. The result is expressed by an index known as Reduction Degradation Index (RDI).

In this investigation, the reduction degradation index was determined by the ISO test method for the low temperature disintegration test⁽⁹²⁾.

3.3.1 Test Procedure

The method consists of subjecting the sample to static reduction followed by tumbling. The equipment for reduction of the sinter used for this test is same as that of the reducibility test. The sample consisting of 500 g of sinter (10 - 12.5 mm size) is heated in a furnace to $500 \pm 10^\circ\text{C}$ in about an hour in a N_2 atmosphere. The sample is then isothermally reduced for one hour in a mild reducing atmosphere by passing the gas mixture (consisting of 20% CO , 20% CO_2 and 2% H_2 (by vol.) and balance N_2) at a flow rate of 20 l/min. It is cooled down to room temperature in a nitrogen atmosphere.

The sample is taken out and tumbled in a stainless steel drum (internal dia. = 130 mm and length = 200 mm) for 10 min. at 30 rpm. The sample is then screened. The percentage of +3.15 mm portion of the sinter is reported as reduction degradation index or RDI.

3.3.2 Results and Discussion

The reduction degradation indices of the sinters are given in Table 4.7. Up to 40% specularite in the sinter mix, the reduction degradation indices are quite high (> 86 %). They decrease with the increase in specularite concentrate. As seen in the above table, the RDI of base sinters (without any

Table 4.7: Reduction Degradation Index (RDI) of the sinters

Specularite Concentrate (%)	Additive	RDI (% , + 3.15 mm)	
		Disc	Turbulator & Disc
0	NA	93.7	96.1
25	NA	92.0	94.0
	2%L	93.0	95.3
	5%L	93.0	95.2
	0.25B	92.4	93.5
40	NA	87.9 (88.0) _* 87.9 _*	89.9
	2%L	86.3 (88.3) _* 89.3 _*	89.0
	5%L	86.8 (90.2) _* 90.6 _*	88.0
	0.25B	89.2	87.8
100	NA	73.3	----
	2%L	78.2 (75.6)	----
	5%L	78.2 (80.5)	----

() : Values for the sinters produced in the industrial strand

* : Values for the sinters with modified fuel addition

specularite or additive in the mix) is 94 while that of sinter with 40% specularite is about 88%. The decrease in RDI due to specularite addition is shown in Fig. 4.16. The RDI values do not change much with the use of turbulator or additives (quick-lime and bentonite).

We know that the principal reason for the low temperature breakdown is the transformation of hematite to magnetite. As observed from the mineralogical study of these sinters, by increasing the specularite concentrate in the sinter mix, the amount of hematite increases (e.g. it has increased from < 5% to about 10% with 40% specularite). The RDI of the sinter decreases due to increase in the hematite content (Fig. 2.8, Chap. II). Moreover, as we have discussed before, the sinter structure becomes more and more heterogeneous and brittle due to specularite addition. The non-uniform heating pattern caused by lower permeability of the mix (with high specularite) adversely affect the RDI⁽²⁾. The beneficial effects of increased calcium ferrite content due to specularite content is overcome by other deleterious effects of the sinter.

Slight change in RDI value due to turbulator or quick-lime or bentonite is probably due to the change in bed permeability while sintering these mixes. Only a marginal difference in the RDI values of the sinters produced in the industrial strand or with modified fuel addition is noticed.

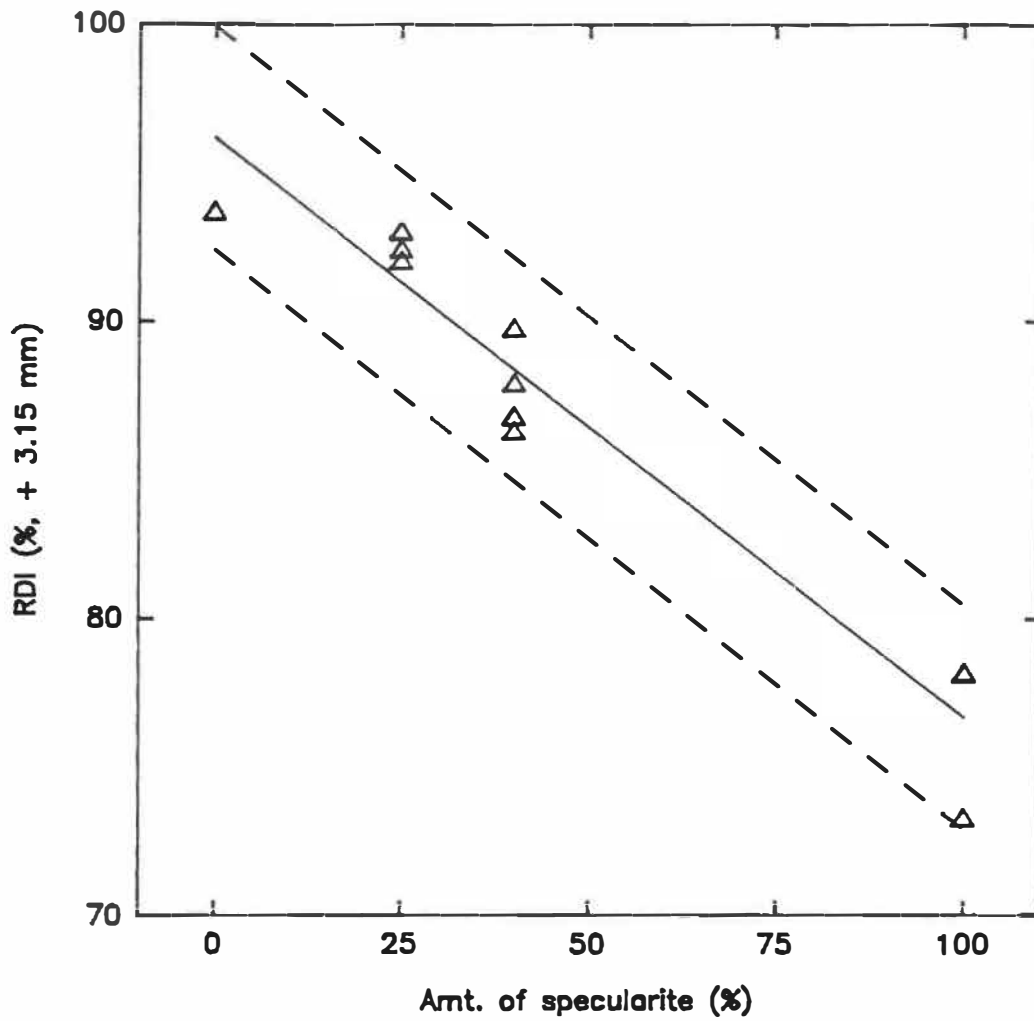


Fig. 4.16 Effect of specularite addition on the RDI of the sinter.

The sinters produced with 100% specularite have lower RDI values (< 80%) than required in the industries. This is mainly due to high specularite content and brittle structure of these sinters. Due to their low RDI, these sinters are considered to be of inferior quality.

3.4 Reducibility

Reducibility data are used as an aid to the operational management. They provide an indication about some important furnace-operation parameters such as the fuel rate and the optimum size of the sinters required in the blast furnace. Ideally, these (reducibility) values should be determined by following a method which simulates the conditions inside the blast furnace i.e. using the same size fractions of the sinters, gas compositions, flow rates, and the variation of temperature as in the blast furnace. However, this is quite complicated and practically very difficult to achieve.

Several test methods have been devised to determine the reducibility of the sinters^(93,94). The selection of the test method depends on the subsequent use of the test results. In the present work, a method proposed by the International Standards Organisation (ISO) has been followed. The detail test method is given in Ref. 95. However, an outline of this method will be described below.

3.4.1 Test Procedure

In this method, about 500 g of sinter of size 10-12.5 mm is charged into a stainless steel reduction tube. The gas is made to flow from the bottom of the tube. In order to preheat the gas and to have a uniform gas-flow, two layers of ceramic pellets (10-12.5 mm) is placed between the perforated bottom and the sample. The tube is closed and inserted into a furnace.

The sample is heated up to $950 \pm 10^\circ\text{C}$ in a nitrogen atmosphere and then reduced isothermally by passing a gas mixture of $40 \pm 0.5\%$ (V/V) CO and $60 \pm 0.5\%$ (V/V) N_2 at a flow rate of 50 ± 0.5 l/min. This temperature is chosen to reflect the importance of the reduction of wustite in the range of $900\text{-}1000^\circ\text{C}$ as the rate-determining process (see Annex 1) in the blast furnace.

The weight loss of the sample due to reduction is noted at every 5 min. interval from the balance. Test is continued until reduction in excess of 60% is affected. This is calculated by knowing the weight loss and the chemical composition (the % of total Fe and FeO) of the sinters. The sample is then cooled down to room temperature. In order to prevent any re-oxidation N_2 gas is passed while cooling up to 200°C .

Knowing the total oxygen content of the sample (from chemical analysis), the percent reduction is calculated and plotted against the reduction time. The time required for 30 percent and 60 percent reduction is determined from this reducibility curve. A typical reducibility curve for a sinter containing 40% specularite is shown in Fig. 4.17.

The reducibility, $(dR/dt)_{40}$ is expressed as the rate of oxygen removal (percent/min) at a reduction state of 40%. It is calculated from the following expression:

$$(dR/dt)_{40} = 33.6 / (t_{60} - t_{30})$$

where, t_{60} and t_{30} are the time (minutes) required for 60 percent and 30 percent reduction respectively and 33.6 is a constant calculated from the reducible oxygen at 40 percent reduction state of the sinter. The details of the calculation are given in Annex 3.

3.4.2 Results and Discussion

The results of the reducibility tests are given in Table 4.8. As seen in this table, the reducibility of the sinter increases with the amount of specularite concentrate. It has increased from 1.27 for the base sinter (no specularite) to 1.51 for 40% specularite. Increase in the sinter reducibility

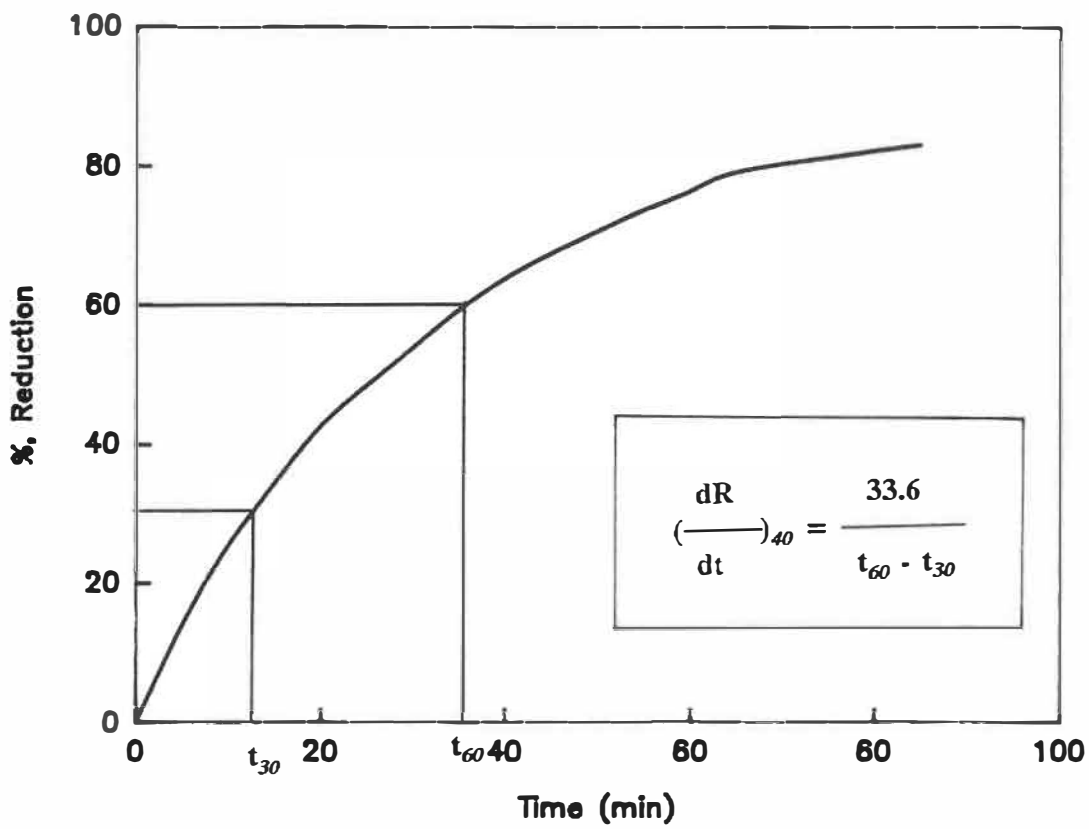


Fig. 4.17 The reducibility curve obtained for the sinter with 40% specularite.

Table 4.8 : Reducibility of the sinters

Specularite concentrate (%)	Additive	Reducibility, (dR/dt) ₄₀	
		Disc	Turbulator & Disc
0	NA	1.27	1.31
25	NA	1.32	1.37
	2%L	1.38	1.37
	5%L	1.32	1.40
	0.25B	1.33	1.42
40	NA	1.51 (1.46) ₍₎ 1.62 _*	1.42
	2%L	1.61 (1.65) ₍₎ 1.62 _*	1.43
	5%L	1.57 (1.48) _* 1.54 _*	1.47
	0.25B	1.54	1.57
100	NA	1.72	----
	2%L	1.66 (1.82)	----
	5%L	1.62 (1.71)	----

() : Values for the sinters produced in the industrial strand

* : Values for the sinters with modified fuel addition

due to specularite addition is also clear from Fig. 4.18. Turbulator or the additive (quick-lime or bentonite) has only a marginal effect on it. Similarly, no marked difference in reducibility of the sinters produced in the industrial strand or with modified fuel addition is observed.

As we have discussed in Chapter II, the change in sinter reducibility is mainly due to the type and the amount different mineral phases and pores in the sinter⁽⁹⁶⁾.

With the increase in specularite concentrate in the sinter mix the hematite and calcium ferrites contents of the sinter increase and the magnetite and slag phase decrease (as discussed in Sec. 1). All these factors have a salutary effect on sinter reducibility. Moreover, the sinter porosity also increases providing more surface exposed for the reduction. The linear relationship between the porosity and reducibility of sinter can be seen in Fig. 4.19.

Though the amount of calcium ferrites increase with quick-lime addition, its beneficial effects are suppressed by decrease in the porosity of these sinters. The marginal change in reducibility due to turbulator or additive is due to several factors such as the nature and amount of the melt formed influencing the sinter mineralogy.

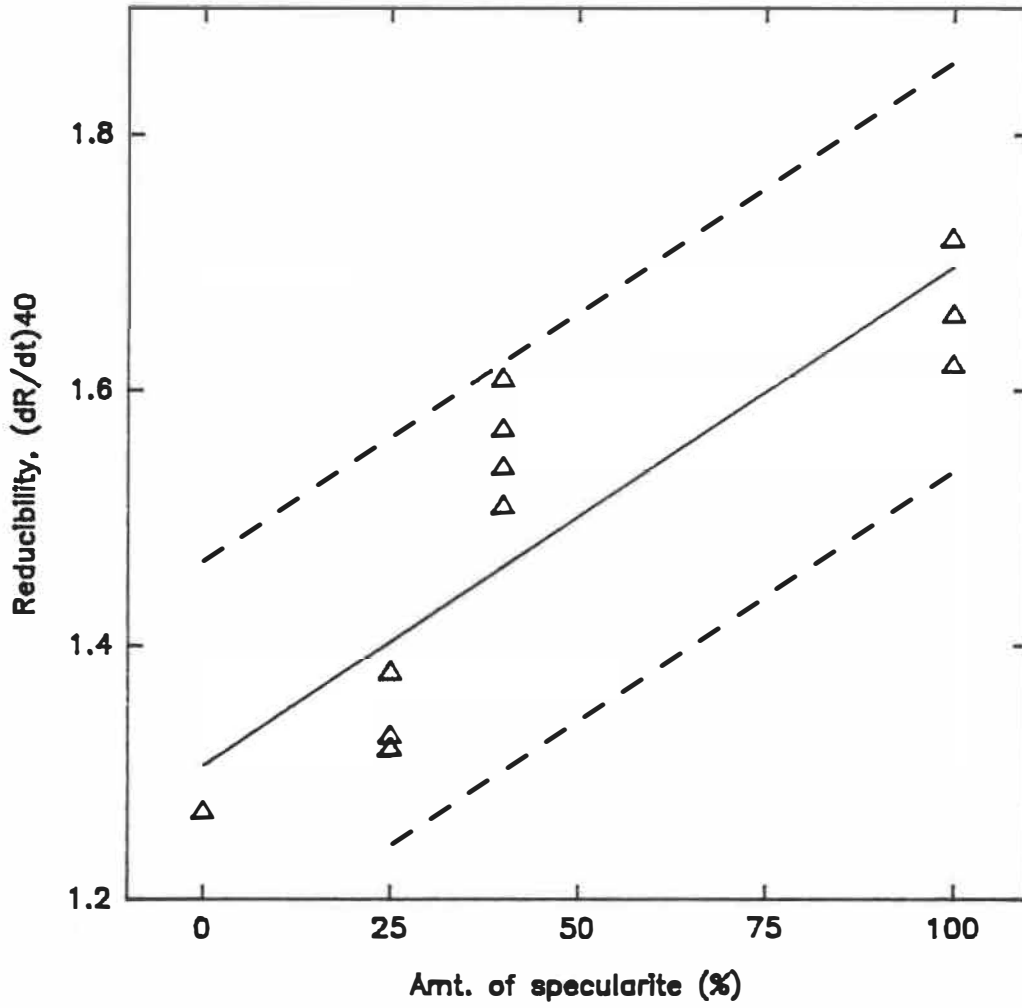


Fig. 4.18 Effect of specularite addition on the reducibility of the sinter.

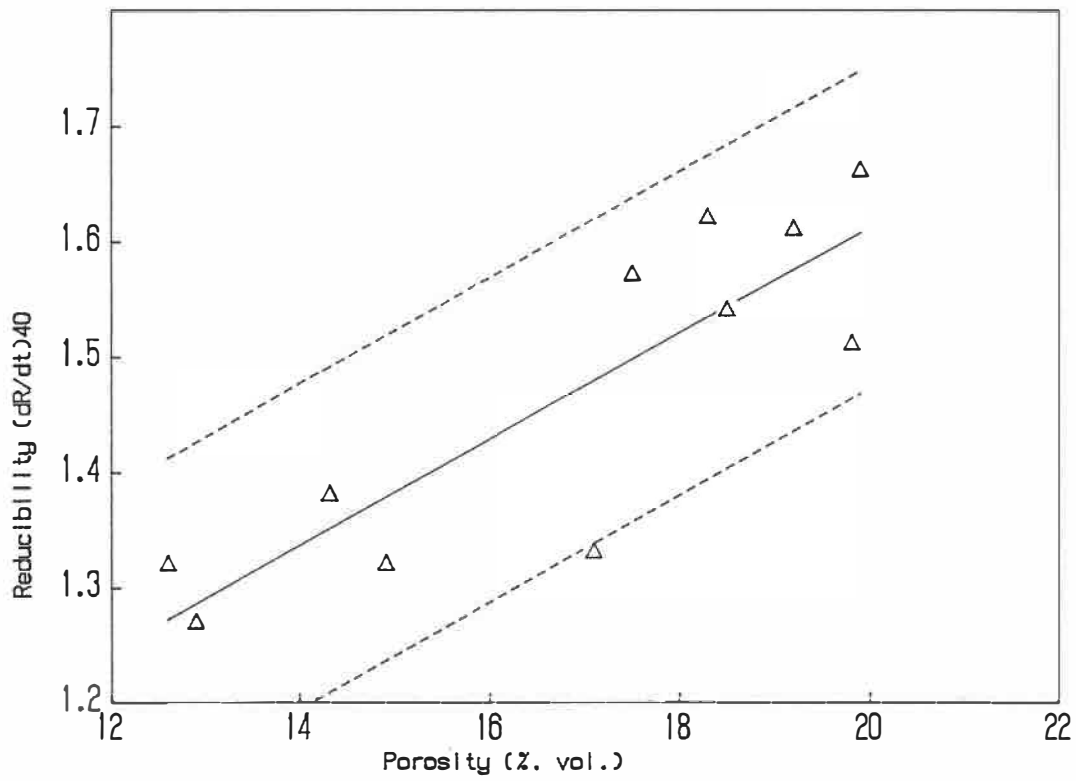


Fig. 4.19 Variation of the sinter reducibility with its porosity.

3.5 Softening/Melting

Like the other properties, several test methods have been developed to determine the softening properties of sinters⁽⁸³⁾. The principle of these processes is to reduce the sinter sample under a load by raising the temperature gradually. The temperature at which melting starts is conveniently noted.

3.5.1 Test Procedure

In the present work, the softening temperatures of sinters under load have been determined at Centre de Recherches Minérales (CRM), Ste-Foy, Quebec. The method consists of continuously reducing the sample in a temperature range of 400-1300°C under a constant load of 0.8 kg/cm². The composition of the gas is changed in order to simulate the conditions in the blast furnace condition. The contraction (shrinkage) of the sample as a function of temperature and the final degree of reduction are noted to evaluate this property of the sinter. Various other important test conditions are given in Table 4.9.

Table 4.9 : Conditions for the softening test

Parameter	Condition		
Dimension of the sample	Dia. 42 mm and height 65 mm		
Size of the sinter	10 - 12 mm		
Top layer	No coke		
Bottom layer	26 g of coke (6.3 - 9.5 mm)		
Heating rate	6.7°C/ min		
Gas flow rate	9 l/min		
Gas composition at different temperatures (°C):	CO (%)	CO ₂ (%)	N ₂ (%)
25 - 400	--	--	100
400 - 600	18	22	60
600 - 800	24	16	60
800 - 1000	28	12	60
1000 - 1400	40	--	60

3.5.2 Results and Discussions

The results of the softening and melting tests are given in Table 4.10.

Table 4.10 : Results of the softening tests

Specularite concentrate (%)	Additive	Softening temp. (°C)	Wt. loss (%)	Reduction (%)
0	NA	1352	14.7	49.5
25	NA	1340	16.8	52.3
	2%L	1330	16.4	52.1
40	NA	1342	16.9	52.0
	5%L	1340	17.5	52.6
100	5%L	1330	19.9	54.5
	0.25%B	1340	17.8	55.4

The causes and the effects of this type of high temperature degradation has been already discussed earlier. When the reduction of the sinters takes place at high temperature (above 1000°C), the degradation begins with light sintering of partially metallized agglomerates⁽⁹⁷⁾. Towards the end molten material trickle down through the burden materials. This mainly results in the loss of permeability in the furnace stack. It is necessary to keep the cohesive zone in the stack as narrow as possible.

As we can see from Table 4.10, the softening temperatures (under load of the sinters produced for the present investigation are quite high ($>1330^{\circ}\text{C}$). This can be probably attributed to the high basicity and high MgO content of the sinter. Increase in the basicity decreases (or even completely eliminates depending on the basicity) the formation of fayalite which is detrimental to the softening properties (brings down the softening temperature). On the contrary, MgO in the sinter increases its softening temperature. These effects have already been discussed in detail in Chap. 2.

The softening temperatures of the sinters do not seem to change much with the variation of the specularite content. However, the percentage of reduction before the start of softening increases with the specularite content. This is because of higher reducibility of sinter with more specularite. Addition of quick-lime seems to cause softening at a slightly lower temperature.

CHAPTER V

EFFECTS OF FRITMAG ADDITION

1. Introduction

The beneficial effects of MgO on various sinter properties (such as reduction degradation and softening/melting) have been discussed earlier in Chapter II. Different materials containing MgO are often added to the sinter mix.

At present, the commonly used MgO-containing materials in the iron ore sinters are dolomite (or burnt dolomite), magnesite, natural olivine, to some extent serpentine and fosterite. In certain cases (as in Wawa Iron Ore Mines of Algoma Steel Corporation), the ore itself contains high amount of MgO (up to 8%). Since, the use of other sources of MgO such as natural olivine are not quite economical, at present dolomite is the only cost-effective MgO source. It is hence required to find some other alternative MgO-source. Fritmag with its high MgO content could effectively serve the purpose.

FRITMAG is a "synthetic olivine", recently developed by the asbestos industry. It contains 47% MgO (see Table 5.1). Evaluation of FRITMAG as source of MgO for sintering would not

only provide the sintering plants with a new MgO source, but also could create a potential market for Fritmag.

2. Production of Sinters

Sinters were produced on laboratory scale at a constant basicity, ($B=2.0$), but at different levels of MgO (e.g. 1.5, 2 and 3%) by adding Fritmag, dolomite or olivine in the sinter mix. The quality of the Fritmag-added sinters was then compared with that of the dolomite or olivine-added sinters.

2.1 Raw Materials

Raw materials used for the tests were specular hematite concentrate, sinter fines, pellet fines and iron fines, limestone, flue dust (fuel), Fritmag, dolomite and olivine. All these materials have been procured from the Algoma Steel Corporation. The chemical composition and the size distribution of the iron-bearing materials, limestone and flue dust have been already given in Chapter III while those of MgO-bearing materials (e.g. Fritmag, dolomite and olivine) are given in Tables 5.1 and 5.2. Fritmag is a fibrous material containing higher amount of MgO than dolomite (e.g. 47% compared to 20% of dolomite).

Table 5.1 : Chemical analysis (wt. %) of the MgO containing materials

Material	MgO	SiO ₂	Fe ₂ O ₃	Al ₂ O ₃	CaO	Na ₂ O +K ₂ O	Loss on Ignition
Fritmag*	47.0	47.0	3.0	1.0	1.0	1.0	1.0
Olivine	46.0	41.0	7.0	0.6	---	---	---
Dolomite	20.8	1.0	0.2**	0.1	30.3	---	46.7

** The chemical formula of Fritmag is Mg₂SiO₄

*: Fe is mainly present as FeO.

Table 5.2 : Size analysis (% wt. retained on stated size) of the MgO-bearing materials

Mesh size	Sieve opening (mm)	Olivine	Dolomite
10	1.7	--	18.1
20	0.8	--	29.9
28	0.6	--	10.2
35	0.4	--	8.3
65	0.2	--	9.8
100	0.15	38	2.9
150	0.11	37	3.1
200	0.07	21	3.0
270	0.05	3	3.2
325	0.04	1	3.3
-325	-0.04	--	8.2

Note: Because of the fibrous nature of Fritmag, its size distribution is represented by the surface area. It is 14-18 m²/g for the Fritmag used in this work.

2.2 Composition of the Sinter Mix

The first sinter mix condition was chosen with 45% specularite concentrate and Fritmag. The amount of Fritmag was calculated aiming to obtain 3.0% MgO in the final sinter. The typical composition of this mix is given in Table 5.3. The other conditions were set by replacing Fritmag by dolomite or natural olivine and/or reducing the MgO level from 3.0% to 2.5%. The amount of specularite in the mix was also changed to 40% and 25%. In total, seven different sinter mix conditions (as shown in Table 5.4) have been chosen.

The amounts of flue dust (fuel) and water were determined in such a way to obtain optimum sintering condition (with regard to the return fine balance).

2.3 Pot-Grate Test

All the pot-grate tests were carried out at Algoma Ore Division, Wawa, Ontario. The equipments, experimental method and the sintering conditions for these tests were same as those discussed in Chapter III. However, it is to be noted that only disc pelletizer has been used as the mixing device and no turbulator has been used for this study.

Table 5.3 : The composition of the sinter mix for the first test

Material	Weight per cent
Specularite concentrate	24.5
Pellet fines	13.7
Mill scale	8.8
Iron fines	7.6
Return fines	30.0
Fritmag	1.5
Limestone	8.9
Flue dust	5.0

Table 5.4 : Different types of the sinter produced

Number	Spec. Conc. (%)	Source of MgO	MgO Content (%)	Notation
1	45	Fritmag	3.0	45 3.0 F
2	45	Dolomite	3.0	45 3.0 D
3	45	Olivine	3.0	45 3.0 O
4	45	Fritmag	2.5	45 2.5 F
5	45	Dolomite	2.5	45 2.5 D
6	40	Fritmag	3.0	40 3.0 F
7	25	Fritmag	3.0	25 3.0 F

3. Thermal Analysis (DTA and TGA) of the Materials

Thermo-Gravimetry Analysis (TGA)

Thermogravimetry analysis of specular hematite concentrate, Fritmag, dolomite and olivine has been carried out in air up to 1200°C. The weight loss as a function of time and temperature is shown Fig. 5.1. As seen in this figure, specularite, Fritmag and olivine virtually do not undergo any weight loss up to a temperature of 1200°C. The weight loss associated with dolomite is due to the dissociation of the carbonates e.g.



Differential Thermal Analysis (DTA)

Differential thermal analysis of the above materials has also been carried out. The DTA curves in the temperature range of 600 to 1200°C are shown in Fig. 5.2. As we can see here, no peak is observed for any of the materials (except dolomite). The single peak observed in dolomite (in the range of 650 to 800°C) is due to the dissociation of the carbonates which is endo-thermic. It is evident from the curves that no melt is formed below 1200°C in these materials when heated separately.

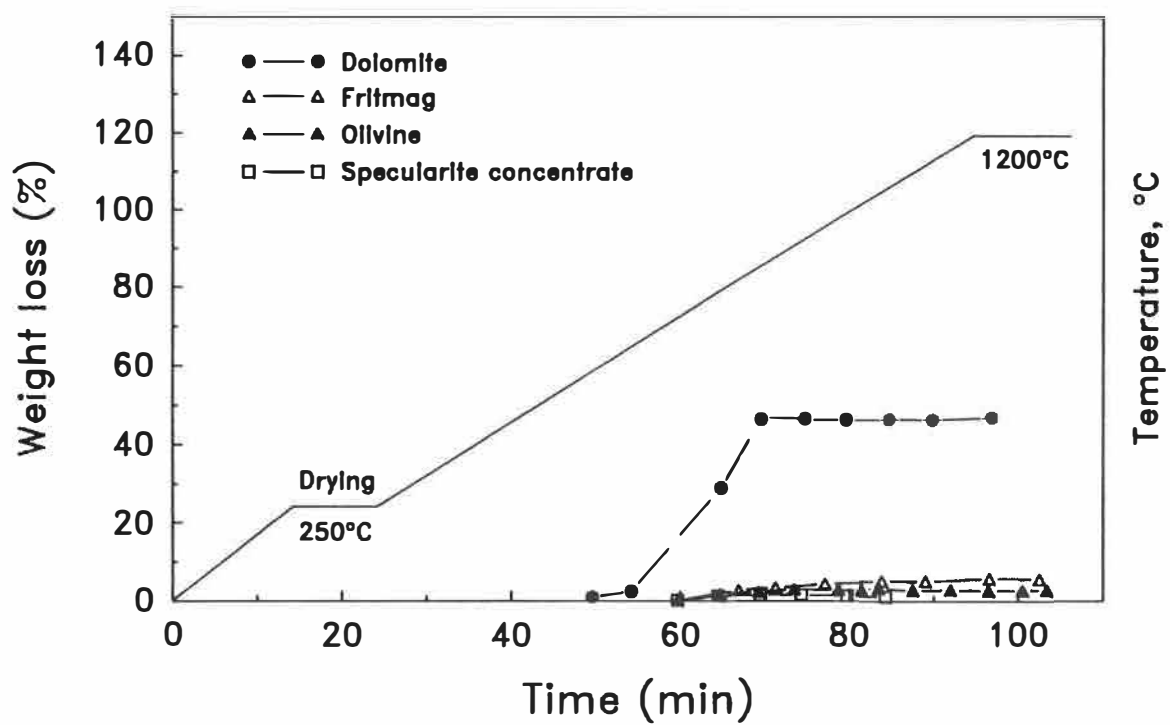


Fig. 5.1 Weight loss of the MgO-bearing materials and specularite concentrate as a function of time and temperature.

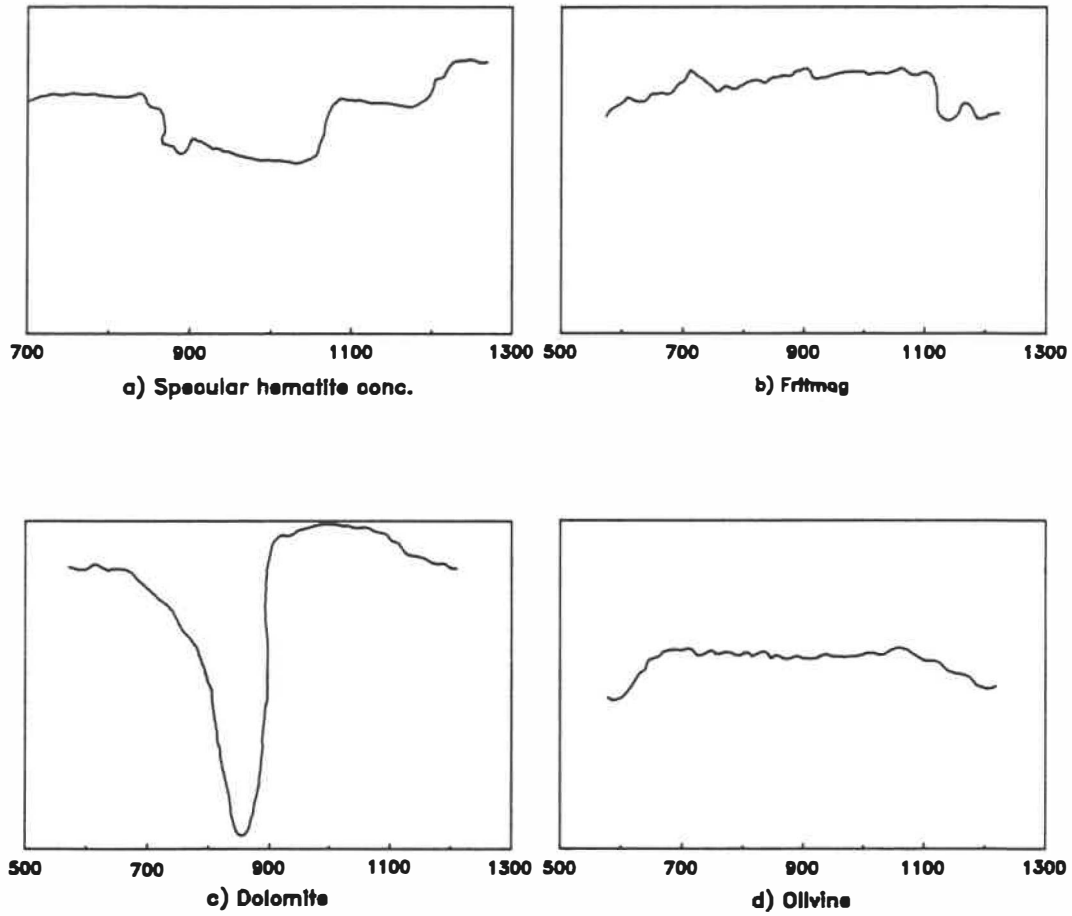


Fig. 5.2 DTA curves of specular hematite concentrate and the MgO-bearing materials.

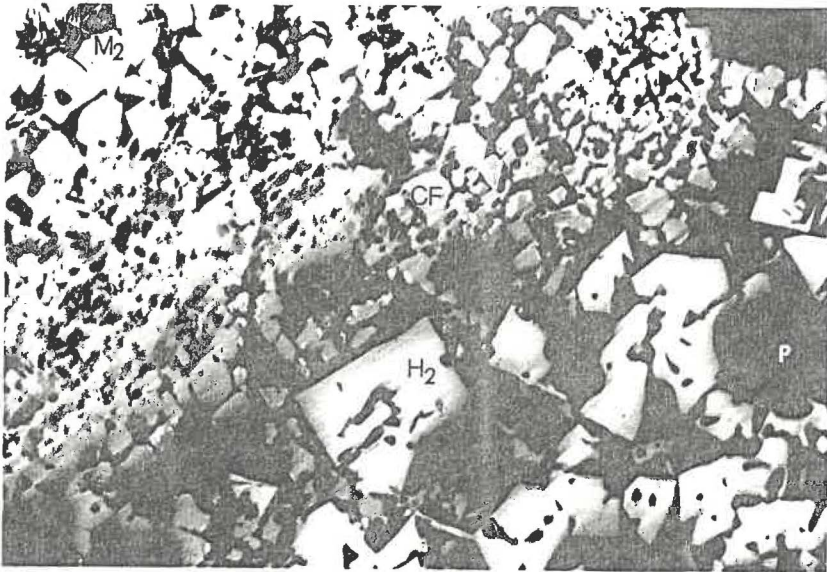
4. Mineralogical Study

The preparation of the sample and the mineralogical study of the sinters have been carried out in the same way as explained in Chapter IV.

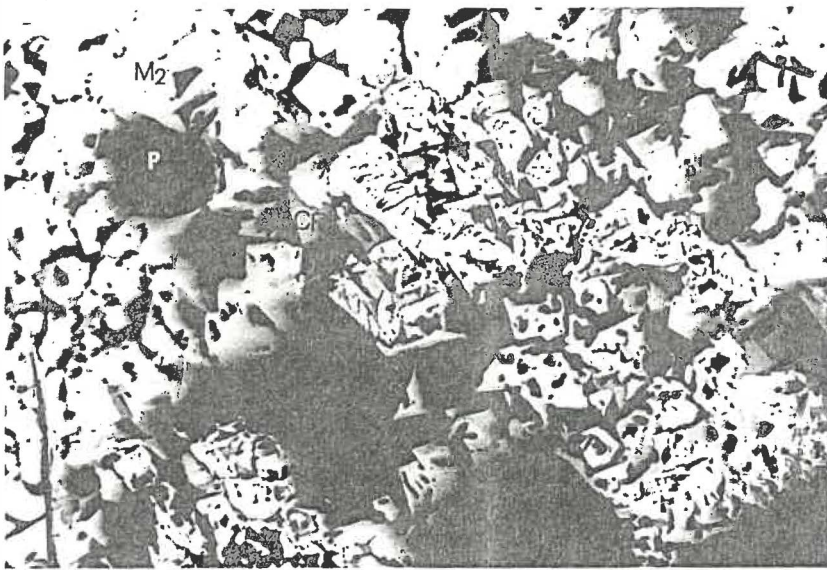
4.1 Mineralogical Observations

The mineralogical structure observed in each type of sinter by optical microscope and image analyser is described below. The amounts of different phases mentioned here are in volume percent and they have been determined by excluding the pores. The notations used for the mineral phases are same as in the previous Chapter II.

Careful study on the mineralogy of these sinters reveals that there is no significant difference among their mineralogical structure. The similarity in the mineral structure of these sinters (with 45% specularite and 3.0% MgO) can be seen in Fig. 5.3. In general, as given in Table 5.5, all these sinters contain high amount of calcium ferrite and magnetite (about 40% each) followed by the slag phase (15%) and hematite (10-15 %).

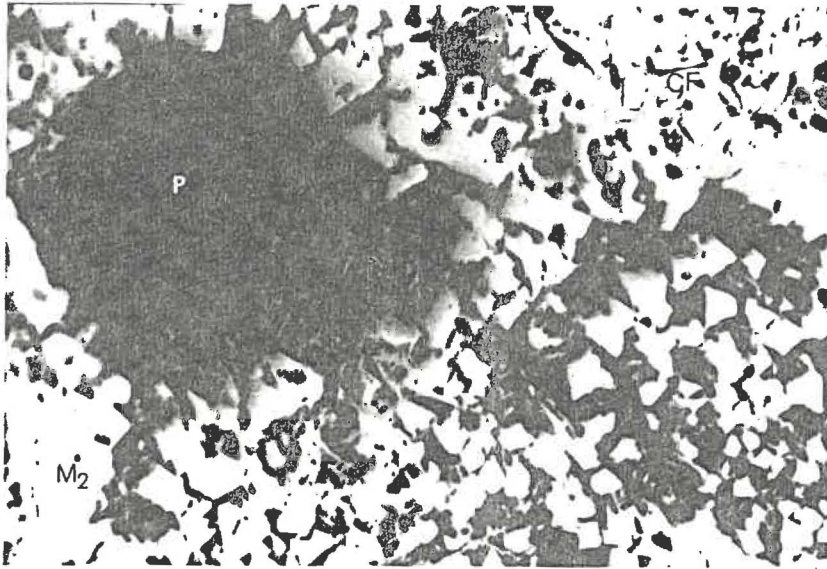


a) Fritmag



b) Dolomite

Fig. 5.3 Photomicrographs (200X) showing similarity in the mineralogical structure of sinters with different MgO-source.



c) Olivine

Fig. 5.3 Photomicrographs (200X) showing similarity in the mineralogical structure of sinters with different MgO-source.

Table 5.5 : Semi-quantitative measurement of the mineral phases

Spec. Conc. (%)	MgO Source	%, MgO	Volume of the Mineral Phases (%)			
			H	M	CF	S
45	Fritmag	3.0	15	35	35	15
45	Dolomite	3.0	10	45	30	15
45	Olivine	3.0	15	35	35	15

The details of the mineralogical observations are given in the following pages.

a b c

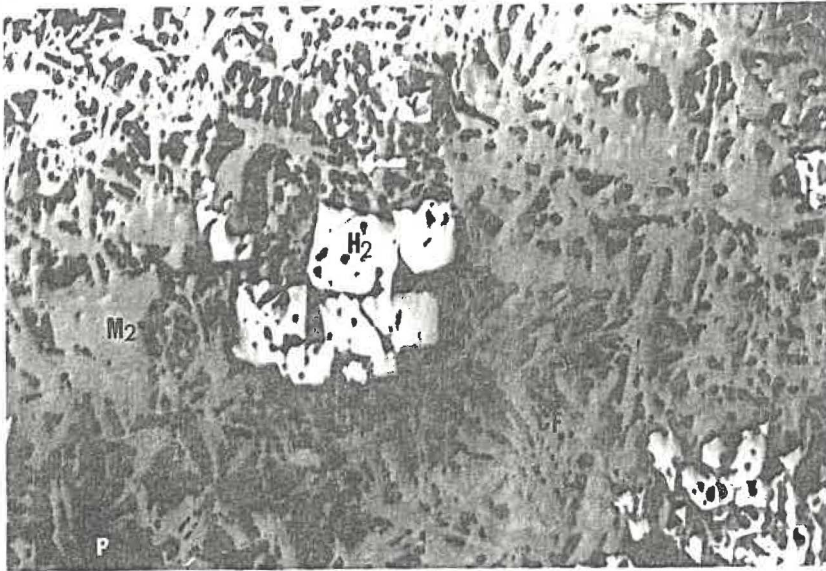
45 3 Fritmag Calcium ferrite and secondary magnetite are present in almost equal amount (30-35 % each). Ferrites are mainly acicular, although some lath-shaped crystals (Fig. 5.4a) and eutectic of ferrite and slag phase (Fig. 5.4b) are also noticed.

Magnetite phase is distributed all over the sinter structure. It varies from eutectic of M_2 and slag (or precipitates of M_2 in slag phase) to small M_2 crystals (Fig. 5.4b). Sometimes, a typical dark phase is marked in the magnetite grains (shown in Fig. 5.4b).

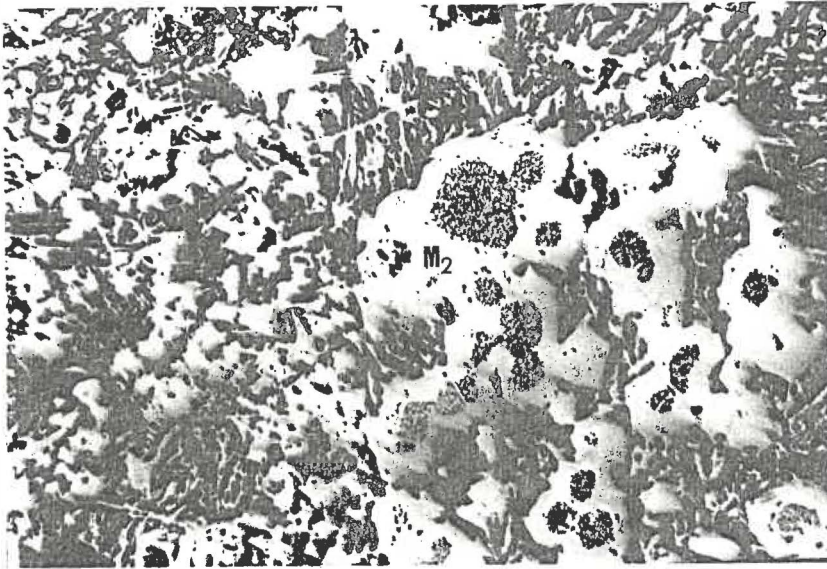
Hematite is present in three forms e.g. primary (H_1), secondary (H_2) and tertiary (H_3) as shown in Fig. 5.4. The lamellar shaped re-oxidised hematite (H_3) on the M_2 grains (Fig. 5.4c) are generally known as martite. The total hematite content of the sinter is about 10-15%.

The total slag content of the sinter is about 10-15% and it is present throughout the sinter.

a: Amt. of specularite (%); b: Amt. of MgO (%); c: MgO source

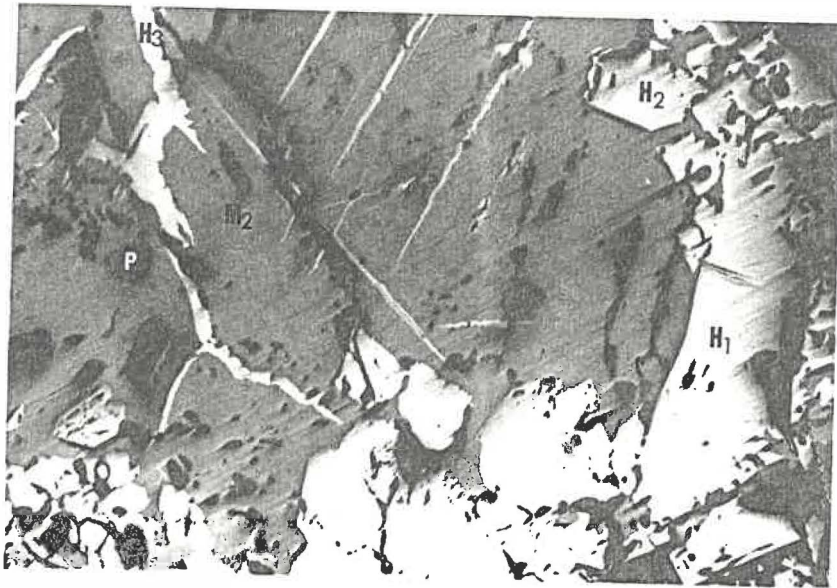


a)

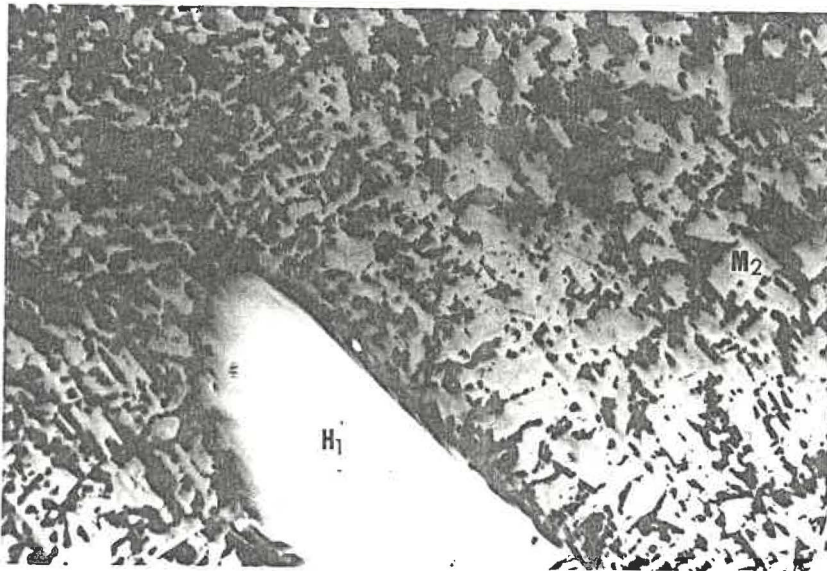


b)

Fig. 5.4 Mineralogical structure (at 200X) of the sinter with 45% specularite and Fritmag (3% MgO).



c)



d)

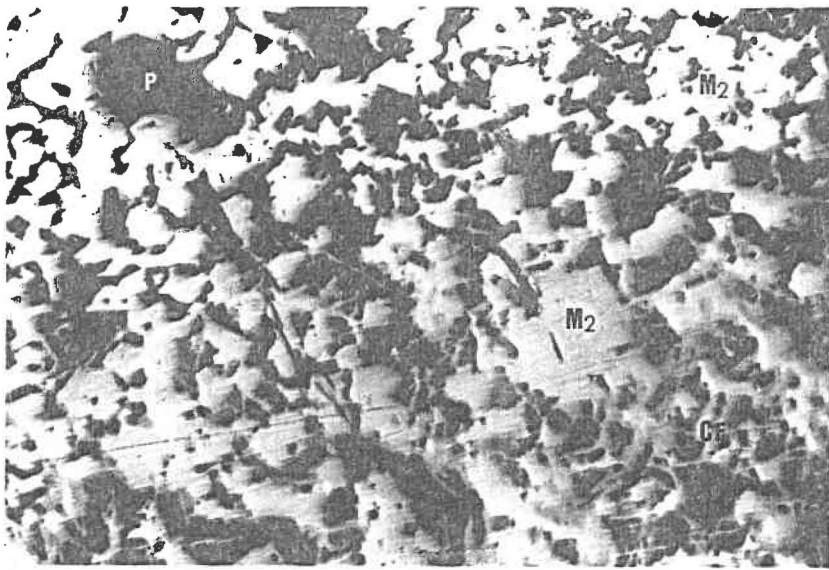
Fig. 5.4 Mineralogical structure (at 200X) of the sinter with 45% specularite and Fritmag (3% MgO).

a b c

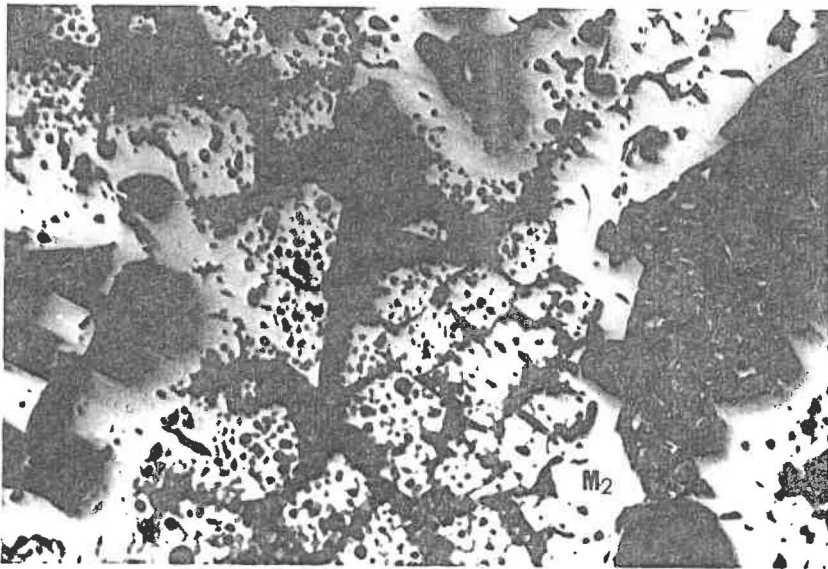
45 3 Dolomite The secondary magnetite content of these sinters
Fig. 5.5 is higher than the previous one (about 40%). The
small M_2 crystals are distributed almost
uniformly throughout the sinter structure (Fig.
5.5a). Some darker spots inside the magnetite
grains (Fig. 5.5b) are occasionally observed.

Calcium ferrite is the second major phase. It
amounts up to 30% of the total sinter volume
(excluding the pores). The ferrites are mainly
acicular and often found around the pores in a
slag matrix (Fig. 5.5c). Larger crystals (lath)
are also marked often associated with the M_2
phase (Figures 5.5a and 5.5d).

The hematite content of sinter has been slightly
decreased (e.g. about 10%). The slag phase is
about 10-15 % of the total volume. In general,
the slag phase is well-developed, devitrified
from the liquid phase. Sometimes, eutectics of
Ca-ferrite or magnetite with the slag phase (as
in Fig. 5.5b) are also marked.



a)



b)

Fig. 5.5 Mineralogical structure (at 200X) of the sinter with 45% specularite and dolomite (3% MgO).

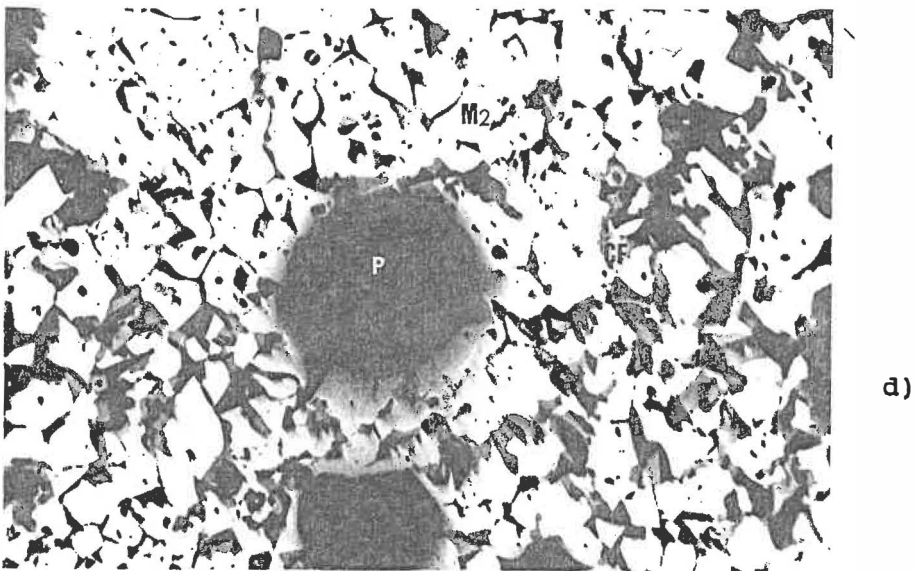
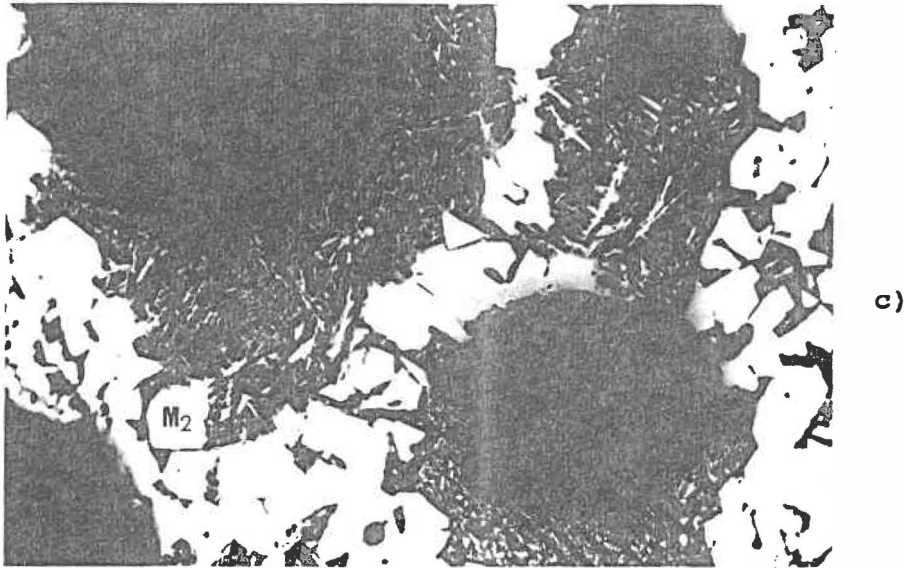


Fig. 5.5 Mineralogical structure (at 200X) of the sinter with 45% specularite and dolomite (3% MgO).

a b c

45 3 Olivine

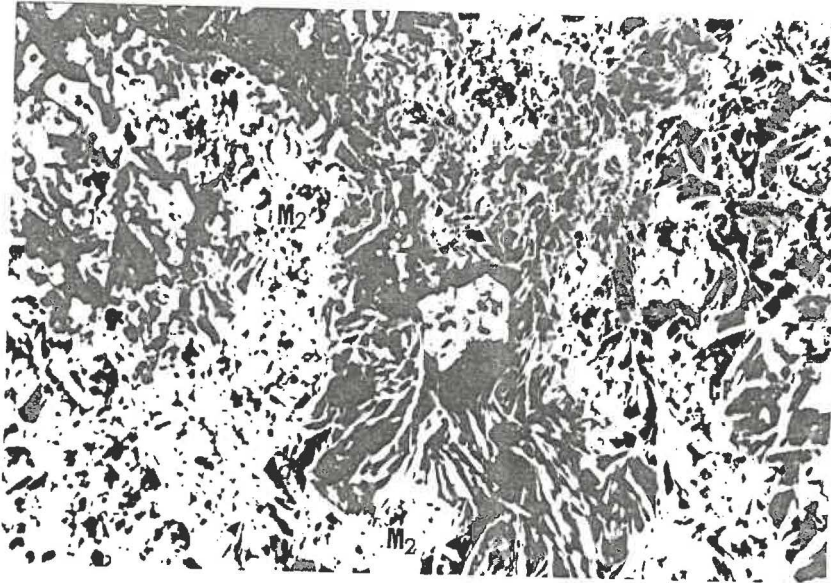
Fig. 5.6

Similar to the Fritmag-added sinters, in this sinter the amounts of calcium ferrites and secondary magnetite are almost equal (about 35-40 %). Ferrites are present in acicular form (Fig. 5.6a) and in lath-shape (Fig. 5.6b). Ferrite crystals are often found to be bridging the M_2 grains (as seen in Fig. 5.6c).

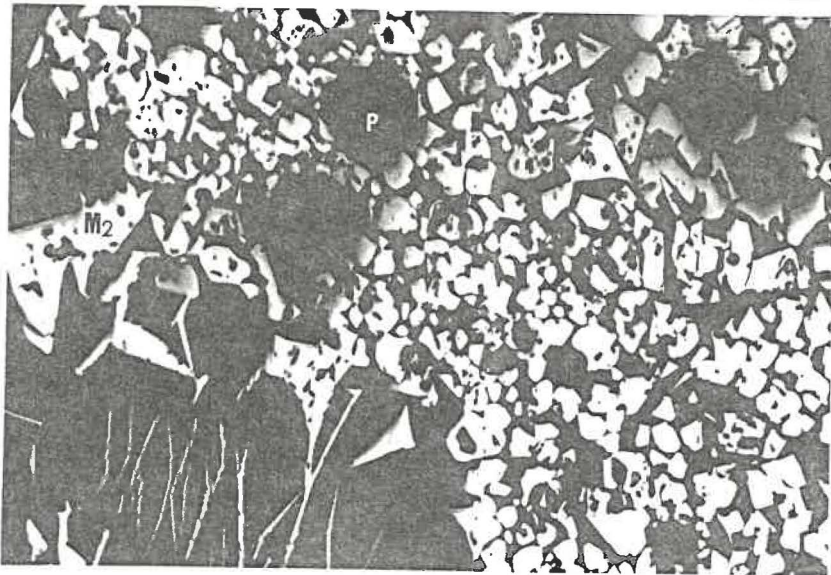
Magnetite crystals are small, but well-defined and uniformly distributed over the sinter structure (Figures 5.6b and 5.6c).

Hematite consists of 10-15 % of the total volume. Although some primary hematite are seen, it is mainly present as secondary hematite (Fig. 5.6a). Tertiary hematite is observed occasionally.

Slag phase is similar to that of the fritmag or dolomite added sinters. Eutectics of slag and M_2 /Ca-ferrite are also observed (Fig. 5.6d).

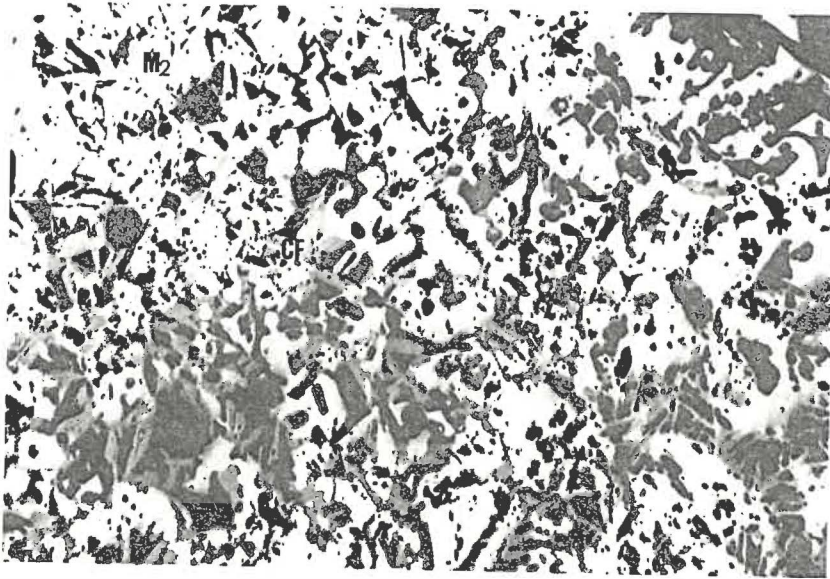


a)

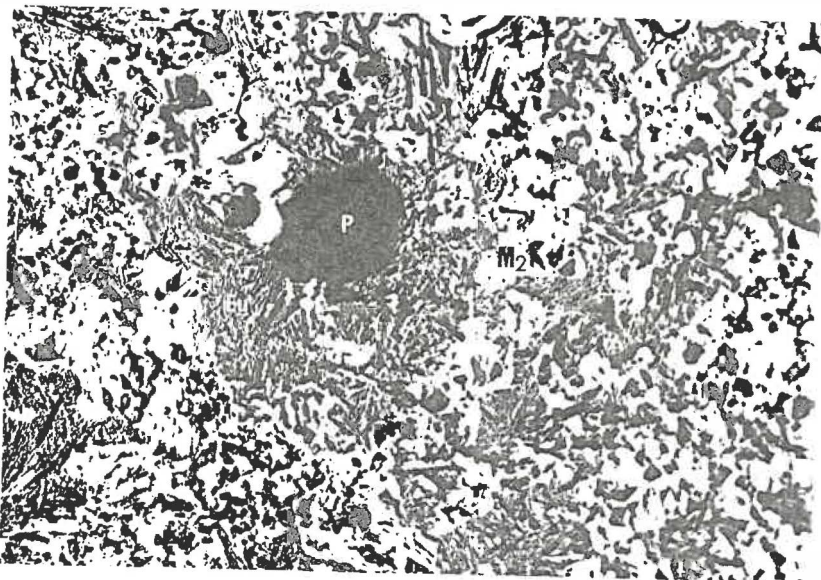


b)

Fig. 5.6 Mineralogical structure (at 200X) of the sinter with 45% specularite and olivine (3% MgO).



c)



d)

Fig. 5.6 Mineralogical structure (at 200X) of the sinter with 45% specularite and olivine (3% MgO).

a b c

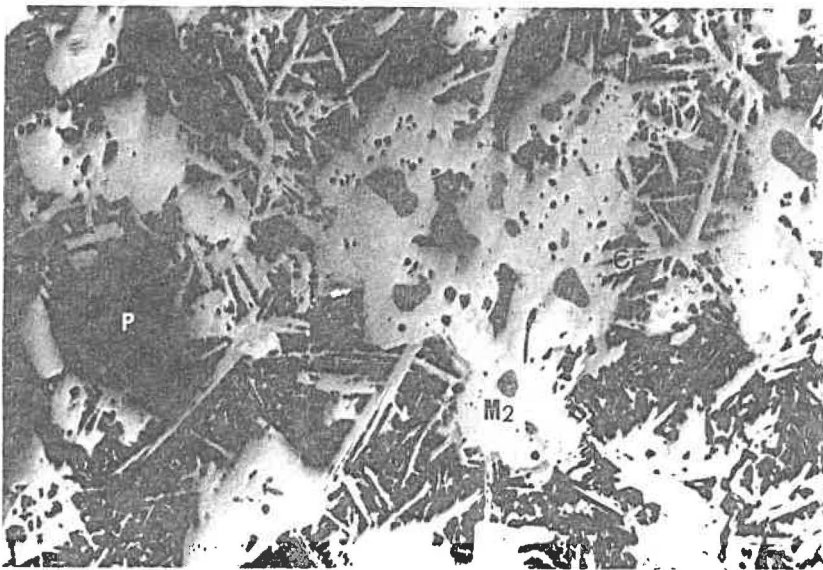
45 2.5 Fritmag The mineralogical structure of this sinter is almost similar to that of the first one (i.e. 45 3 Fritmag). Calcium ferrite and magnetite are present in almost equal amounts. A dark phase inside the magnetite grains are also observed sometimes. The typical structure of this sinter is shown in Fig. 5.7.

25 3 Fritmag Almost similar mineral structure except significantly low amount of hematite phase (about 5%) is observed. Precipitations of magnetite and calcium ferrite in the slag phase are often marked. The typical structure of this sinter is shown in Fig. 5.8.

No marked difference in the microstructure of sinter types (40 3 Fritmag) and (45 2.5 Dolomite) is observed and they almost resemble the structure of (45 3 Fritmag) and (45 3 Dolomite) respectively.

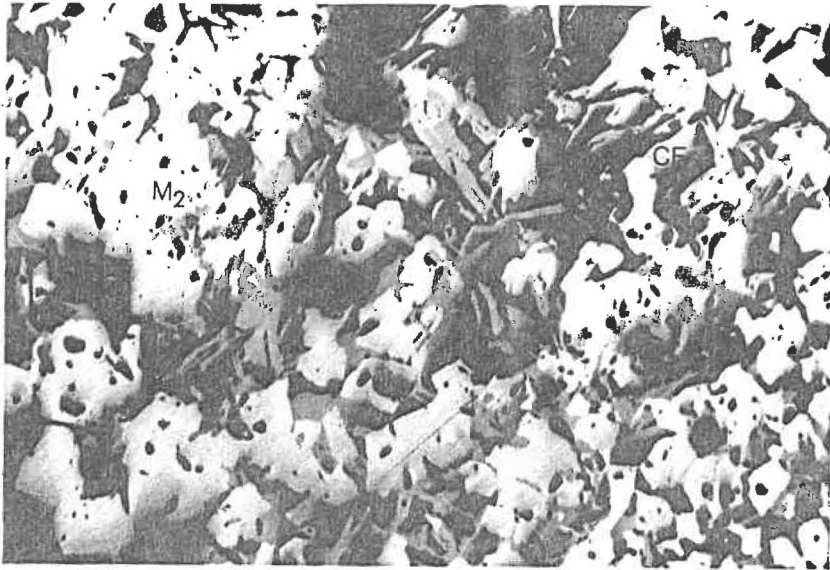


a)



b)

Fig. 5.7 Mineralogical structure (at 200X) of the sinter with 45% specularite and Fritmag (2.5% MgO).



a)



b)

Fig. 5.8 Mineralogical structure (200X) of the sinter with 25% specularite and Fritmag (3% MgO)

4.2 Micro-analysis and X-ray Mapping

Micro-analysis and X-ray mapping of the sinters have been carried out to analyse the composition of different mineral phases and to observe the distribution of Mg in different phases. The range of composition associated with each of the phases are given in Table 5.6.

The range of composition given in the table for hematite phase includes all, the primary, secondary and tertiary hematite phases. It contains up to 98.7% iron oxide. The amount of other oxides are relatively low. As seen in Table 5.6, magnetite phase contains high amount of MgO (up to 5.1%). The MgO contents of the magnetite phase in different types of sinters are given in Table 5.7. In the Fritmag-added sinters it has a narrow range (e.g. 2.5-3.0 %), while a wide range of MgO is observed for the olivine-added sinters (e.g. 2.5-5.1 %). The magnetite phase also contains up to 2.7% CaO and 2.0% SiO₂ (see Table 5.6).

As seen in Table 5.6, there is a significant variation in the composition of calcium ferrite. Iron oxide and calcium oxide of this phase vary from 73.1% to 84.7% and 11.2% to 15.7%

Table 5.6 : Composition of the different mineral phases

Phase	Fe ₂ O ₃ *	CaO	SiO ₂	Al ₂ O ₃	MgO
Hematite	94.6-98.7	0.1-2.5	0.1-4.5	0.1-0.5	0.1-1.1
Magnetite	92.5-94.9	1.7-2.7	0.2-2.0	0.3-0.9	1.7-5.1
Ca-ferrite**	73.1-84.7	11.2-15.7	0.6-6.5	0.1-1.6	0.2-0.6
Slag	26.5-37.2	49.7-55.1	6.0-27.1	0.5-1.7	0.1-0.4

* : For the magnetite and slag phase iron oxide has been calculated for Fe₃O₄ and FeO respectively.

** : The composition of the eutectic ferrite has not been considered.

Table 5.7 : MgO content of the magnetite phase in different sinters

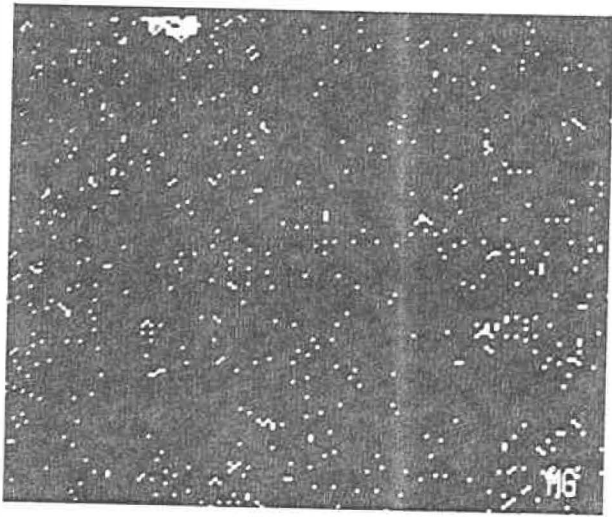
Type of MgO-source	MgO (%)
Fritmag	2.5 - 3.0
Dolomite	1.7 - 3.2
Olivine	2.5 - 5.1

respectively. Besides, it also contains up to 5.5% of SiO_2 and 1.6% Al_2O_3 . The MgO content in this phase is quite low (<0.6).

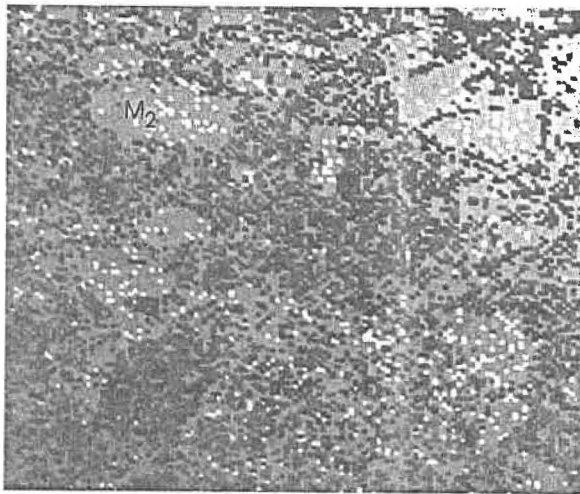
The slag phase consists of mainly CaO, FeO and SiO_2 with very low quantity of Al_2O_3 e.g. 0.4%. Only a marginal amount of MgO is found in this phase.

X-ray mapping of the sinter (45% spec., 3% MgO with dolomite) at various magnification are shown in Figs. 5.9 to 5.12. At low magnification (i.e 50x and 100x) it is observed that Mg is distributed almost uniformly all over the sinter (Figs. 5.9 and 5.10). With the increase in magnification, Mg is found to separate out and at 1000x it is only limited to the magnetite phase as shown in Fig. 5.12.

It is also revealed from the X-ray mapping that the dark phase inside the magnetite grain of the Fritmag-added sinters (shown in Fig. 5.4b) is due to segregation of Mg. This can be seen in Fig. 5.13.

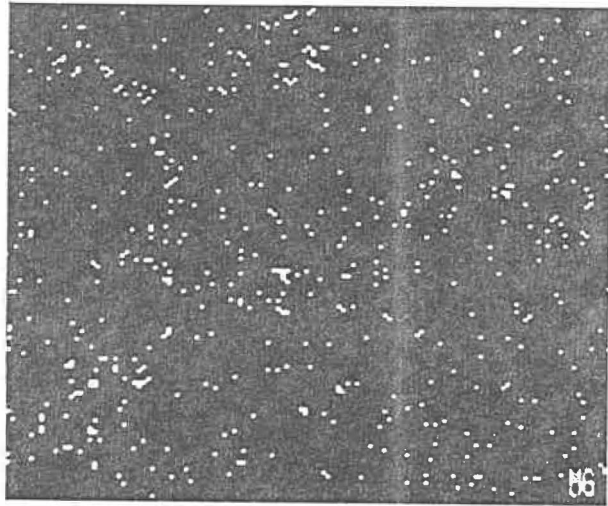


a) X-ray mapping
Mg-K_α

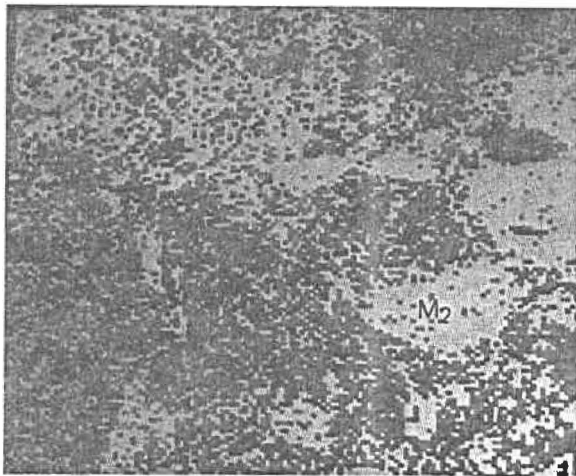


b) Back-scattered
image

Fig. 5.9 X-ray mapping (50X) showing the distribution of MgO in the mineral phases of the sinter.

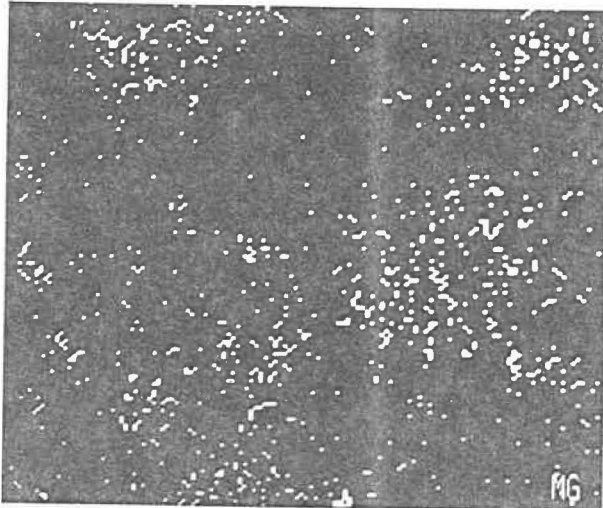


a) X-ray mapping
Mg-K α

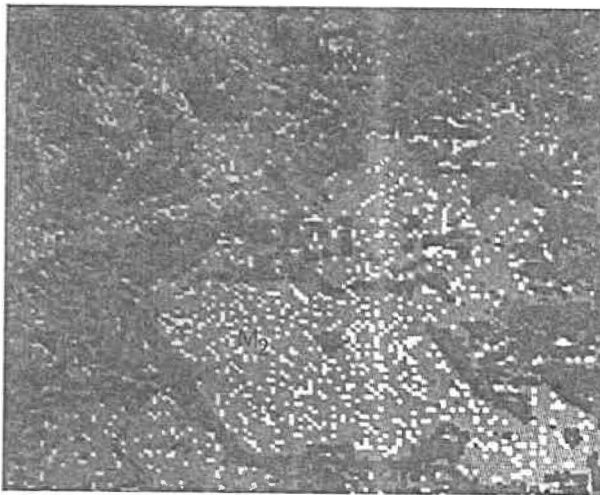


b) Back-scattered
image

Fig. 5.10 X-ray mapping (100X) showing the distribution of MgO
in the mineral phases of the sinter.

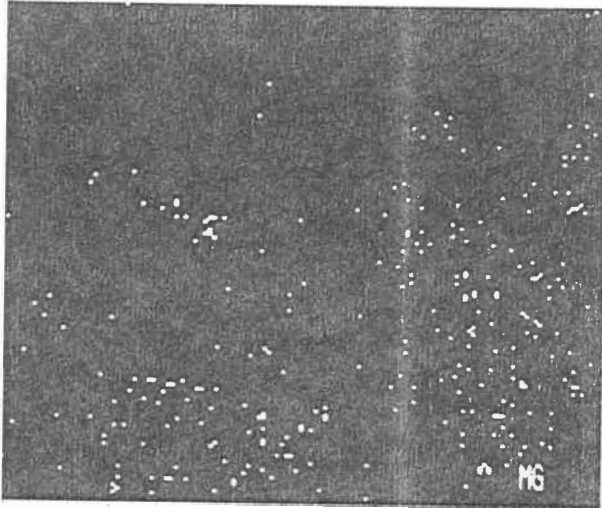


a) X-ray mapping
Mg-K_α

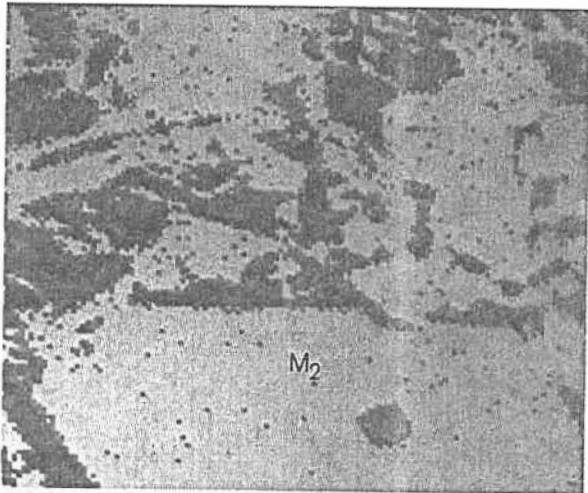


b) Back-scattered
image

Fig. 5.11 X-ray mapping (500X) showing the distribution of MgO in the mineral phases of the sinter.

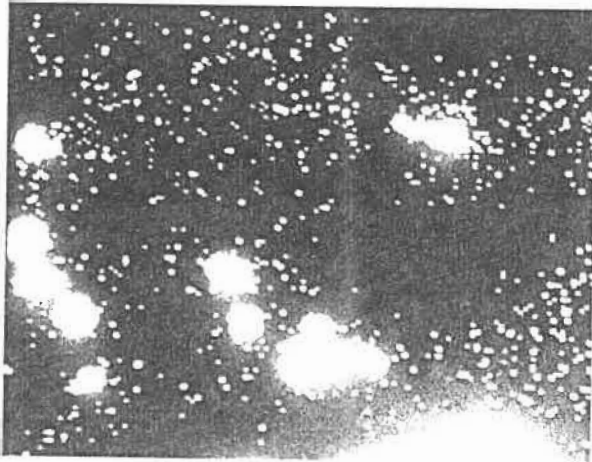


a) X-ray mapping
Mg-K α



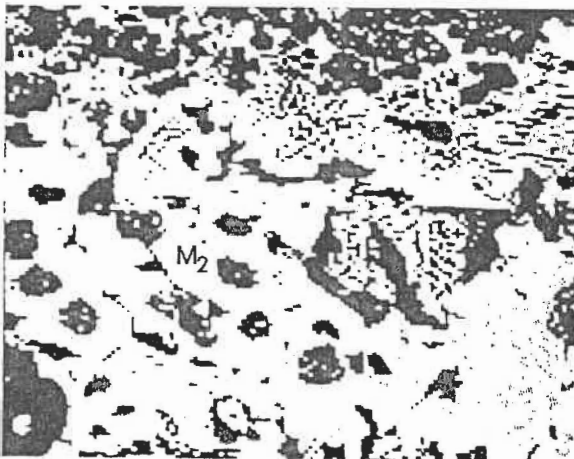
b) Back-scattered
image

Fig. 5.12 X-ray mapping (1000X) showing the distribution of MgO in the mineral phases of the sinter.



X-ray mapping

Mg-K_α



Back-scattered

image

Fig. 5.13 X-ray mapping (500X) showing segregation of Fritmag in the sinter mineralogy.

4.3 Discussion

Based on the literature review on the mineralogy of super fluxed sinters, calcium ferrite was expected to be the predominant phase in all the sinters (since the basicity of these sinters, $B=2$). Instead, almost equal amount of Ca-ferrite and secondary magnetite is observed in all the sinters except that with dolomite where the amount of M_2 is slightly higher. With addition of MgO to the sinter, its CaO content has to be decreased in order to maintain constant basicity. Thus, CaO available for Ca-ferrite formation is less, causing lower amount of ferrites in the sinter. Decrease in the amount of liquid formed and increase in its viscosity due to MgO addition also has a negative effect on the formation of Ca-ferrites. Moreover, the Mg^{2+} substitutes Fe^{2+} in the magnetite lattice stabilizing M_2 during oxidation.

The presence of the dark phase inside the magnetite grain of the Fritmag-added sinters (Fig. 5.4b) and association of high Mg with it indicates the segregation of Fritmag in the sinter. Because of its fibrous nature, Fritmag which has a tendency to cluster together and there is always a chance of segregation in the sinter mix. The segregated Fritmag particles need more time to be dissolved into the sinter and during the

rapid sintering process they are only partially assimilated. This is evident from Fig. 5.4b which shows the Fritmag in the slag phase surrounded by M_2 crystal.

The amount of MgO present in M_2 phase in this type of sinter is minimum (<3.0 as seen in Table 5.7). This is again due to the segregation of Fritmag, thereby limiting the reaction between MgO and iron oxide. Segregation of MgO can be avoided by changing the mixing process (probably by dry-mixing for about a minute) and/or replacing the mixing device with a suitable one.

Dolomite and olivine has dissolved into the sinter structure almost completely and no segregation of Mg is noticed. The dark spots occasionally observed in the magnetite grains of the dolomite-added sinters (as shown in Fig. 5.5b) are due to high concentration (about 3%) of MgO. This is because of some (relatively) larger dolomite particles present in the sinter mix. The CaO present in these dolomite dissolves faster than MgO in the slag. During the resolidification of magnetite from the liquid phase, there are still some MgO particles undissolved and magnetite grains are formed around these particles.

We have seen that the magnetite phase contains a variable amount of MgO (up to about 5%). These are magnesio-ferrites. As discussed in Chapter II, it is often seen that the amount of MgO can vary within a wide range (although the stoichiometric $\text{MgO} \cdot \text{Fe}_2\text{O}_3$ contains 20% MgO). The magnesio-ferrites usually look slightly darker than the magnetite phase. However, in the present case it is not distinguishable (under the optical microscope) from the magnetite phase. This is because of its low MgO content.

Different types of hematite have been observed in the sinter specimens. As shown in Table 5.8, there are noticeable differences in the composition of these phases. The composition of the primary hematite is high SiO_2 (4.4% by wt.). The other oxides (e.g. CaO, Al_2O_3 and MgO) present in this phase are marginally low (0.1%). The secondary hematite contains the highest amount of iron oxide (about 98%). All other oxides (except CaO) present in this phase are quite low (<0.2). It dissolve up to 1.0% CaO. It is seen that the composition of tertiary hematite is close to that of the magnetite phase from which it is formed. It contains relatively high amount of MgO (1.1%).

Calcium ferrite is present mainly in three different morphological forms e.g. lath-shaped (or block), acicular (or

Table 5.8 : Composition of different types of hematite

Type of hematite	Fe ₂ O ₃	CaO	SiO ₂	Al ₂ O ₃	MgO
Primary (H ₁)	95.3	0.1	4.4	0.1	0.1
Secondary (H ₂)	98.5	1.0	0.2	0.1	0.2
Tertiary (H ₃)	94.8	2.2	1.5	0.4	1.1

needle-shaped) and eutectic of ferrite and slag. After sorting and arranging their composition ranges, it is found that a particular range of composition corresponds to a specific morphology of the ferrite phase. The morphologies and the corresponding compositions are given in Table 5.9. In general, the lath-shaped ferrite is high in Fe and Ca (and low in Si and Al. The acicular ferrite has relatively lower Fe and Ca. The amount of Si and Al of these ferrites are higher. These ferrites are often referred to as silico ferrite of calcium and aluminium (SFCA) in the literature. The composition of the eutectic ferrite phase could be ambiguous as the surrounding slag could have affected the analysis. This phase contains low amount of Fe and high amount of Ca. The Si and Al content is also high (up to about 29% and 15% respectively).

The ferrite are often found to be associated with the magnetite phase. This is due to the structural similarities between these two phases as observed by Ahsan and

Table 5.9 : Composition of different types calcium ferrites

Morphology	Fe ₂ O ₃	CaO	SiO ₂	Al ₂ O ₃	MgO
Lath-shaped	79.6-84.7	12.3-15.7	0.6	0.1	0.2
Acicular	73.1-78.6	11.2-14.1	3.0-6.0	1.6	0.6
Eutectic	54.1-69.1	15.7-29.2	7.0-15.0	1.1	0.5

5. Quality of the Sinters

5.1 Methods Followed to Determine the Sinter Properties

After the sinters were produced in the pot-grate, they were stabilized and characterized as discussed in Chapter III. The test methods used for determining the sinter properties e.g. tumbler strength and porosity were same as before. Although the test procedure have been the same, the conditions have been slightly modified in order to use the facilities available at Ecole Polytechnique.

5.1.1 Modified conditions for the Reduction Degradation Test

The experimental set-up and procedure were similar to those described in Chapter III. However, due to the smaller size of the reduction tube, required amount of sinter sample (500 g) of was reduced in two batches. All the test conditions such as temperature and gas composition were same. The flow rate of the gas has been reduced to from 20l/min to 7.5 l/min. The RDI of the sinter was then determined in the same way as before.

5.1.2 Modified conditions for the Reducibility Test

In this method instead of 500 g, 100 g of sinter sample has been used. The gas flow rate has also been changed to 12.5 l/min (instead of 50 l/min). All other test conditions were same as described in Chapter III.

5.2 Results and Discussions

The results of all the tests are given in the table below.

Table 5.10 : Properties of the sinters

Condition			Porosity (%, vol.)	Tumbler strength		RDI (%, +3.15 mm)	Reducibility (dR/dt) ₄₀
a	b	c		T-index	A-index		
45	3.0	F	24.9	50.2	5.2	83.0	1.33
45	3.0	D	28.6	37.3	6.7	84.8	1.20
45	3.0	O	25.4	47.5	6.4	85.2	1.25
45	2.5	F	25.0	54.4	6.1	81.2	1.29
45	2.5	D	25.8	45.6	6.9	86.1	1.32

a: Specularite (%); b: MgO (%); C: Source of MgO;

F: Fritmag; D: Dolomite; O: Olivine

I. Porosity

As we can see Table 5.10, porosity values of these sinters are relatively high (>25%). It is mainly ascribed to the high specularite content (about 45%) of the sinter. The reason for this has already been discussed in the previous chapter. It is because there is a loss in permeability of the sinter bed due to the increase in the amount of concentrate in the sinter mix which results in non-uniform air-flow and heat front movement. The high amount of specularite and MgO in the sinter mix reduces the amount of liquid formed during sintering. This results in higher amount of pores in the sinter.

Both the Fritmag- or olivine-added sinters have same porosity (25%). Dolomite-added sinter has the highest porosity (28.6%). As we will see later, these porosity values can be related to the strength (T-indices) of the corresponding sinters.

II. Tumbler Strength

Both indices e.g. T-index and A-index have been determined to evaluate the tumbler strength of these sinters. The T-indices of the sinters are lower than that required in the industry

(>60). However, it is seen that for any particular condition, the T-index of the sinters produced by the laboratory pot-grate test is lower than that produced in the industrial sinter strand. In other words, sinters if produced in the industrial strand from these mixes would have higher strength than the corresponding sinters from the pot-grate. This is due to the significant amount of heat loss from the sides of the sinter pot during sintering in the pot-grate tests.

It should be noted that the objective of this investigation was not to improve the T-index of the sinter, rather to compare the Fritmag-added sinters with respect to the traditionally used dolomite or olivine-added sinters. Hence, no special effort has been made to improve it. However, we believe that this can be improved by changing the amount of flue dust (fuel) or water or both in the sinter mix.

Similar to the porosity, the low strength of the sinters are largely attributed to their high specularite content. It should be noted here that the strength (T-index) of the dolomite-added sinters is very low (37.3, which corresponds to the highest porosity).

Addition of MgO in the sinter mix increases the temperature of liquid formation. The amount of liquid formed during sintering decreases as the MgO content of the sinter increases. This has a negative effect on the strength of the sinter which is quite evident from Table 5.10 where we can see that for both Fritmag or dolomite-added sinters as the MgO content of the sinters increases their T-indices decrease. Moreover, as discussed earlier, sinter strength is also adversely affected by the increase in the amount of specularite concentrated present in the sinter mix.

The change in the abrasion index or "A" index values with the amount of specularite concentrate or with the source of MgO was found to be only minor and no definite trend has been noticed. As seen from the Table 5.10, these values are within the acceptable limits as required in the industrial practice (>5).

III. Reduction Degradation Index (RDI)

As given in Table 5.10, the RDI of all the sinters are above 80% and it does not vary much. Because of high MgO, these sinters have relatively higher amount of magnetite phase which has contributed to their good RDI values.

Decreasing the MgO or specularite content of the sinter the RDI values decrease. When the MgO content of the sinter decreases by 0.5% (i.e. from 3.0 to 2.5) the RDI of the sinter increases from 83 to 85. This is because MgO decreases the hematite content of the sinter (by reducing the transformation of magnetite to hematite) which is responsible for the reduction degradation.

IV. Reducibility

All these sinters have high reducibility. These values vary between 1.25 to 1.33 (except for the dolomite-added with 3.0% MgO). The high reducibilities of the sinters are mainly due to their high calcium ferrite content and high porosity. The effect of Ca-ferrite and pores on the sinter reducibility have already been discussed in Chapter II.

The relatively low reducibility of the dolomite-added sinters is due to its higher magnetite content (higher than the other two). As we know magnetite has a lower reduction rate and by increasing its content the reducibility of the sinter decreases.

No significant difference (or definite trend in variation) of reducibility has been marked with change in the MgO-source of the sinter.

CHAPTER VI

SYNTHESIS, CONCLUSIONS AND RECOMMENDATIONS

1. Synthesis

1.1 Micro-pelletization of the Green Mix and Production Rate

As we know, in the sintering process two contradicting conditions have to be satisfied. It is necessary to have a good permeability of the sinter bed for the effecient burning of the fuel and also to increase the productivity of the process. At the same time, optimization of the inter-particle contact is also required as to obtain the maximum bonding strength. Both these conditions can be satisfied by enhancing the micro-pelletization process by means of appropriate raw material preparation.

In our results, we have demonstrated that use of disc pelletizer and quick-lime increases the production rate of the sintering process. This increase is mainly attributed to the high degree of micro-pelletization of these mixes as all the process parameters remain unchanged. It has been shown that use of suitable device and binder promote and stabilize the micro-

pellets of the feed mix by overcoming the inherently poor granulation of the specular hematite concentrate.

The strong interrelationship between productivity of the sintering process and degree of micro-pelletization of the green feed is clearly shown in Figs. 6.1 to 6.3. Since in this work, we have used +1.7 mm and +0.8 mm size fractions and the cold permeability of the green mix to assess the degree of micro-pelletization of the green feed, the production rate has been linearly regressed against the cumulative weight percentages of +1.7 mm and +0.8 mm size fractions present in the green mix and the cold permeability in Figs. 6.1 and 6.2 and 6.3 respectively. The equations for the linear regression can be expressed in the form of $y = ax + b$, where y represents the productivity of the sintering process and x represents the +1.7 mm or +0.8 mm size fractions or cold permeability of the green feed. The values of a , b and the regression coefficient, r are given in Table 6.1. These results were found to be statistically significant.

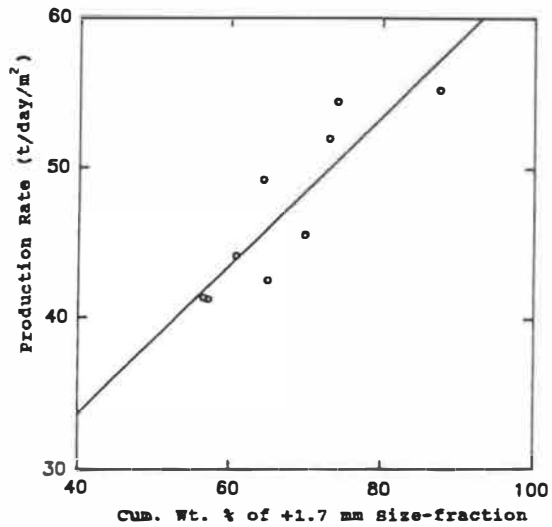


Fig. 6.1 Effect of the Amount of 1.7 mm Size-fraction in the Green Feed on Sinter Production Rate.

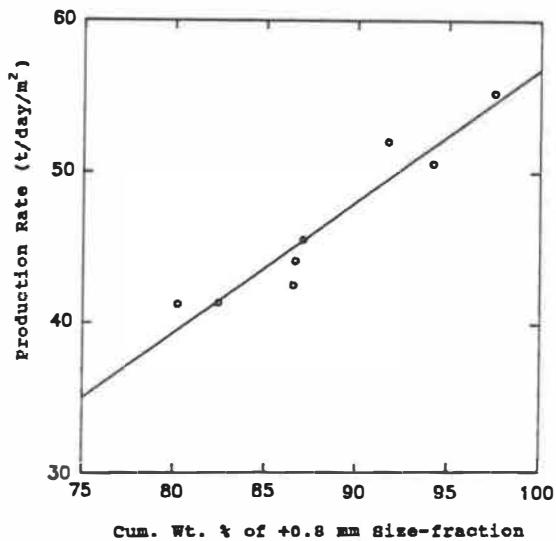


Fig. 6.2 Effect of the Amount of 0.8 mm Size-fraction in the Green Feed on Sinter Production Rate.

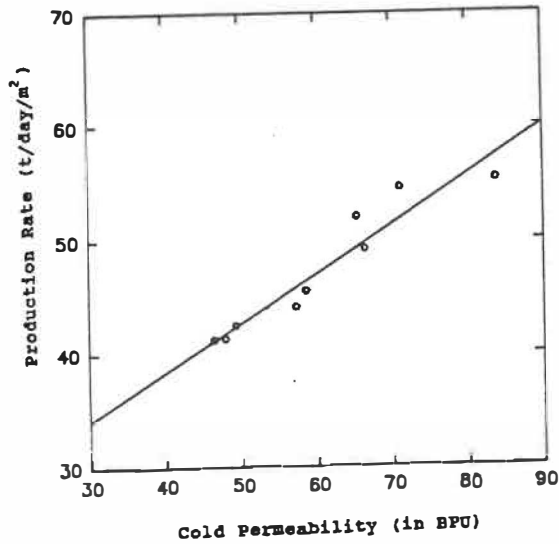


Fig. 6.3 Effect of Cold Permeability of the Sinter Bed on Sinter Production Rate.

Table 6.1 Parameters Used to Assess the Degree of Micro-pelletization of the Green Feed Vs. Sinter Production Rate ($y = ax + b$)

y	x	Parameters Used to Assess the Degree of Micro-pelletization		
		%, +1.7 mm	%, 0.8 mm	Cold Permeability (BPU)
<u>Production Rate</u>				
a		0.5	0.85	0.43
b		13.7	-27.67	21.02
r		0.77	0.7	0.91

r : Coefficient of the linear regression

Figs. 6.1 to 6.3 demonstrate conclusively that sinter productivity is highly dependent on size distribution of the green feed. This increase is attained mainly by the improvement in bed permeability. The linear relationship between the size distribution of the green feed and cold permeability can be seen in Figs. 6.4 and 6.5 where cold permeability has been linearly regressed against +1.7 mm size fraction in Fig. 6.4 and against +0.8 mm size fraction in Fig. 6.5. The regression coefficients and the equations for the straight lines shown in Figs. 6.4 and 6.5 are given in Table 6.2.

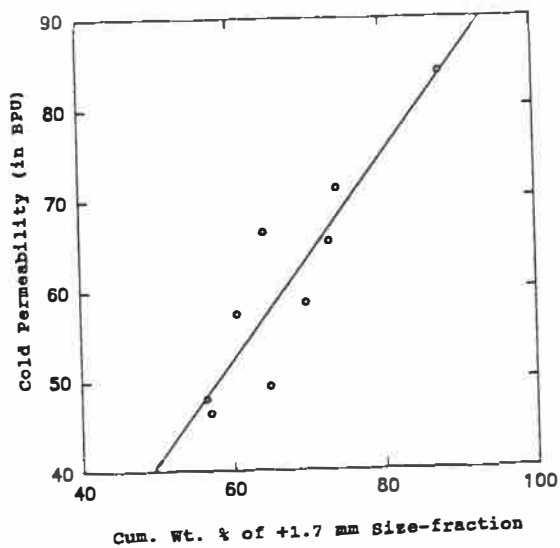


Fig. 6.4 Effect of the Amount of 1.7 mm Size-fraction in the Green Feed on Cold Permeability of the Sinter Bed.

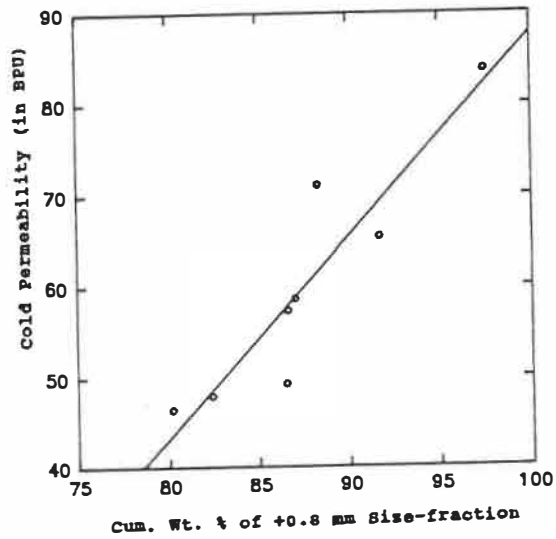


Fig. 6.5 Effect of the Amount of 0.8 mm Size-fraction in the Green Feed on Cold Permeability of the Sinter Bed.

Table 6.2 Degree of Micro-pelletization of the Green Feed Vs. Cold Permeability of the Sinter Bed ($y = ax + b$)

x	Size Fractions	
	%, +1.7 mm	%, 0.8 mm
y		
<u>Cold Permeability</u>		
a	1.13	2.23
b	-15.8	-134.86
r	0.82	0.84

r : Coefficient of the linear regression

From the present work, we have seen that the best condition to obtain the maximum degree of micro-pelletization is achieved by mixing the raw materials in a turbulator for 30 seconds and then in a disc pelletizer for $2\frac{1}{2}$ min. This method is found to be efficient, especially when the amount of fines or concentrates in the sinter mix is increased and a binder is used. Proper mixing in the turbulator enhances the micro-pelletization process during the subsequent mixing in a disc pelletizer.

Roll compactor is not quite useful for the sinter mix with high amount (>25%) of specularite concentrate. Unlike the materials used in the agro-industries (where roll compactor is used), specularite concentrate is difficult to wet and it does not form strong pellets on compaction.

We have seen that although using the combination of turbulator and disc for mixing the raw materials leads to higher amount of micro-pelletization than using only a disc, no such effect is noted in the final production rate values. Sinter production is largely controlled by sintering time which is not only affected by the initial conditions, but also (to a large extent) controlled by the changes in different factors (such as heating characteristics of the fuel and the nature and amount of the melt formed) taking place during sintering. From the production rates obtained for different sintering

conditions, it is seen that up to 40% specularite concentrate in the sinter mix, disc pelletizer is quite effective in micro-pelletizing the sinter mix and in attaining high production rate (>40 tpd/m²).

Quick-lime and to some extent bentonite act as binder in the sinter mix. They help the formation of strong micro-pellets during mixing and improve the size-distribution of the green mix. This leads to high bed permeability and low sintering time. Besides, increase in the sinter strength due to lime addition is also noted. These factors contribute to the increase in the production rate of the sinter. By using 5% lime in a sinter mix containing 40% specularite concentrate, production rate can reach 49 tpd/m².

Although the production rate (in terms of sinter output) decreases with the increase in the specularite content of the mix, (because of high iron content of the specularite concentrate) no marked difference in the net iron output of the sinter is noted.

The production rate obtained with modified fuel addition (i.e. adding fuel in two stages) is quite interesting. For any particular sinter mix, in this method, up to 20% increase in the production rate is noted. This is mainly due to the improvement in the state of fuel present in the sinter mix

(which improves the heating characteristics and decreases sintering time) by adding fuel in two stages.

1.2 Characterization of Sinters

Although no clear relationship has been established sinter properties and size distribution of the green feed, we have noted that, to some extent, improvement in the latter has beneficial effects on sinter properties. This is again due to improvement in bed permeability leading to more efficient burning of fuel and uniform movement of the combustion front.

We know that (see Chapter II) the major mineral phase in the super fluxed sinters ($B > 1.5$) is calcium ferrite. However, the sinters, in this work ($B \approx 2.5$) contains low amount of calcium ferrite (as low as about 15% when no specularite concentrate is present in the sinter mix). Instead, a high amount of magnetite phase (up to about 50%) is noted from the mineralogical observation.

It is known that the properties of the sinter depend on its mineralogical phases and the change in the microstructure of the sinter has a profound effect on its properties. We have noticed a fair correlation between the mineral phases and structure of the sinter and its properties. As the specularite content in the sinter increases, the amounts of calcium ferrite

and hematite increase, the magnetite phase and slag phase decrease and the structure becomes more porous. All these factors have favorable effect on sinter reducibility. However, increase in hematite content and the porosity decrease the RDI of the sinter. The sinter strength is also deteriorated by the porous structure.

Quick-lime increases the strength of the sinter by increasing its calcium ferrite content (which provides a good bonding medium in the sinter) and decreasing its porosity. Other properties are not significantly affected by it.

In this work, we have produced acceptable quality sinter using up to 40% specularite concentrate in the sinter mix, while maintaining a production rate higher than 40 tpd/m². The quality of the laboratory sinters are comparable to that of sinters produced on the industrial strands, although in the latter case, the sintering parameters are quite non-uniform.

1.3 Effect of Fritmag Addition

Fritmag can be used in the sinter mix as a source of MgO. We have seen that the quality of the Fritmag-added sinters are almost similar to that of the dolomite-added or olivine-added sinters.

From the mineralogical observations, a marginal difference in the nature and amount of the mineral phases of these sinters is noticed. This difference is believed to be due to the difference in the degree of assimilation of different MgO-sources into the sinter structure during sintering. All these sinters contain high amount of calcium ferrite and magnetite (about 35% each) and about 20% slag phase; the rest being mainly hematite and/or eutectic of slag with magnetite or calcium ferrite.

2. Summary and Conclusions

2.1 Summary

The present work was undertaken with the following objectives:

- To use more than 15% specular hematite concentrate in the sinter mix without dropping the production rate below 40 tpd/m².
- To produce sinters of "acceptable quality" i.e. reducibility ≥ 1.20 , tumbler index ≥ 60 and RDI ≥ 80 .
- To explore the possibility of using Fritmag as a source of MgO in the sinter mix and to compare the quality of these sinters with that of commonly used dolomite- and olivine-added sinters.

We have succeeded in achieving these objectives. Our results have shown that up to 40% of specular hematite concentrate can be used in a sinter mix. The production rate can be obtained as high as 49 tpd/m² by using quick-lime (as a binder) and a disc pelletizer (as the mixing device). The properties of these sinters are better than those required for the acceptable quality sinter (as per the criteria set in the objectives).

We have also shown that a new MgO containing material, Fritmag can be used as a source of MgO in the sinter mix without any difficulty. The quality of these sinters are similar to that of the commonly used dolomite- or olivine-added sinters.

2.2 Conclusions

■ Conclusions on the Production Rate of the Sinter

- Sintors with acceptable production rate (i.e. higher than 40 tpd/m² can be produced using up to 40% specular hematite concentrate in the sinter mix.
- The production rate decreases with the increase in the specularite content of the sinter.
- For any level of specularite in the sinter mix, the production is significantly improved with quick-lime addition.
- There is a significant increase in the production rate by adding the fuel in two stages.
- Although the sinter production rate decreases significantly with the addition of specularite, the change in the net iron content of the sinter is not so remarkable.
- Turbulator does not have much effect on the production rate.

■ Conclusions on the Quality of the Sinter

- Sinters of acceptable quality (i.e. reducibility ≥ 1.20 , tumbler index ≥ 60 and RDI ≥ 80) can be produced using up to 40% specular hematite concentrate in the sinter mix.
- The reducibility of the sinter increases with the increase in the specularite content of the sinter.
- The strength and RDI of the sinter decreases with the amount specularite in the mix.
- The strength of the sinter is improved by adding quick-lime in the sinter mix.
- The turbulator or bentonite does not have any marked effect on the quality of the sinter.

■ Conclusions on the Effect of Fritmag Addition

- Fritmag can be used as a source of MgO in the sinter mix without any difficulty.
- The quality of the Fritmag-added sinters is similar to that of the dolomite- or olivine-added sinters.

3. Recommendations

The present investigation has been conducted mainly on a laboratory scale. Although some tests have been carried out on the industrial strand, their numbers are quite limited. The test conditions were chosen conforming to the practice at Algoma Steel Corporation. The results may vary with the change in these conditions. It is clear that the process is very crude and the sintering conditions vary significantly in different practices. Hence, in order to use the laboratory results directly in the plants, the sintering parameters should be standardized. More sintering tests should be carried out on the industrial strand and the results obtained from these tests should be correlated with those of the laboratory tests. However, based on our results, we can make the following recommendations:

- i. In order to use higher amount (>15%) of specularite concentrate, use of a disc pelletizer for mixing the raw materials is recommended.
- ii. Addition of quick-lime in the sinter mix is necessary to increase the production rate and to improve the quality of the sinter.

iii. On the laboratory tests, we have seen that production of the sinter increased up to 20% by adding fuel in two stages. Hence, the effect of this method on the industrial strand should be studied.

iv. Since, Fritmag has a tendency to cluster together because of its fibrous nature, proper care should be taken while mixing the raw materials containing Fritmag.

It is to be noted that in order to consider the above recommendations, a techno-economic study should be initially conducted for each case to be considered.

REFERENCES

1. Ishikawa, Y., Sugawara, K. and Umezu, Y., "Latest Development of Sintering Technology", Agglomeration 77, (ed. K. V. S. Sastry), New York, 503-525 (1977).
2. Furui, T., Kawazu, M., Sugawara, K., Fujiwara, T., Kagawa, M., Sawamura, A. and Uno, S., "Technology for Preparation of Raw Materials to be Sintered", Nippon Steel Technical Report, No. 10, Nov., 36-46, (1977).
3. Dennis, D. H., "Foundation of Iron and Steel Metallurgy", Elsevier, p. 111, (1962).
4. Ball, D. F., Datrnell, J., Davison, J., Grieve, A. and Wild, R., "Agglomeration of iron ores", Elsevier Publishing Co. Inc., New York, p. 142, (1973).
5. Ref. 4, p. 97.
6. Bates, H., JISI, 187, 310-314, (1957).
7. Bell, W. C., 2nd International Symp. on Agglomeration, Paris, IRSD, 2, 401-410, (1957).
8. Ball, D. F., JISI, 194, 479-84, (1960).
9. Ref. 4, p. 95.
10. Carmen, P. C., Inst. Chem. Eng., 15, 150-166, (1937).
11. Mitchell, D. F., JISI, 198, 358-63, (1961).
12. Voice, E. W., Brooks, S. H. and Gledhill, P. K., JISI, 174, 136-139, (1953).
13. Wild, R. and Dixon, K.G., Agglomeration (ed. W. A. Knepper), Interscience Publication, New York, 565-583, (1962).

14. Kasa, E., Rankin, W. J. and Ganon, J. F., "The effect of Raw Mixture Properties on Bed Permeability during Sintering", Trans. ISIJ International, 29, 1, 33-42, (1989).
15. Kurosawa, S., Fukuyo, H, Komatsu, O. Sakamoto, N. and Yamaoka, Y., "Recent Advances in Sintering Technologies by NKK", Proceedings of the Ironmaking Conf., ISS-AIME, 451-457, (1989).
16. Ball, D. F., Datrnell, J., Davison, J., Grieve, A. and Wild, R., "Agglomeration of iron ores", Elsevier Publishing Co. Inc., New York, (1973).
17. Meyer, K., "Pelletizing of Iron Ores", Spring Verlag, New York, (1980).
18. Rumpf, H., "Strength of Granules and Agglomerates", Agglomeration, (ed. W. A. Knapper), Inter Science Publishers, 379-418, (1962).
19. Hardesty, J. O., "Principles of Fertiliser Agglomeration", Chem. Engg. Progr. Symp., 60(48), 46-52, (1964).
20. Newitt, D. M. and Conway-Jones, J. M., " A Contribution to the Theory and Practice of Granulation", Trans, Inst. Chem. Eng., 36, 422-442, (1958).
21. Rooda, H. J., Burghardt, O., Kortmann, H. A., Jipping, M. J. and Kater, T., "Organic Binders for Iron Ore Agglomeration", Proc. of the Eleventh Int. Mineral Processing Congress, Calgary, 139-180, (1975).

22. Desouza, R. P., de Mendonca, C. F. and Kater, T., "Production of Acid Iron Ore Pellet for Direct Reduction Using an Organic Binder", Mining Engg., 1437-1441, (1984).
23. Wild, R., "Chemical Constitution of Sinters", JISI, 174, 131-135, (1953).
24. Knepper, W. A., Snow, R. B. and Johnson, R. T., "Properties of Self-fluxing Sinters", Agglomeration, (ed. W. A. Knepper), Interscience Pub., N.Y., 787-807, (1962).
25. Mazanek, E., and Jasienska, S., "Mineralogy and Reducibility of Self-fluxing Sinters", JISI, 201, 60-67, (1963).
26. Kissen, D. A. and Litvinava, T. I., "Mechanism of Mineral Formation in Sintering Fluxed Sinter", Stal in English, No. 5, 318-323, (1960).
27. Mazanek, E., and Jasienska, S., "Properties of Self-fluxing Sinters of Basicity 1.0-3.5", JISI, 206, 1104-1109, (1968).
28. Larson, H. and Chipman, J., Journal of Metals, 5, 9, (1953).
29. Weyl, W. A., Glass Ind., 37, 264, (1956).
30. Nyquist, O., Agglomeration, (ed. W. A. Knepper), Interscience Pub., N.Y., 809-864, (1962).
31. Hass, K. P., Bitsianes, G. and Joseph, T. L., "Calcium Ferrite in Relation to Sintering of Iron Ore", Blast Furnace Cokeoven and Raw Materials Conference, (1960).
32. Edstrom, J. O., Jernkont Ann., 10, 2, 101-115, (1956).

33. Karner, H. M., Trans. AIME, 196, 1114-1117, (1953).
34. Mazanek, E., and Jasienska, S., "Effect of Al_2O_3 on the Mineral Constitution of Self-fluxing Sinters, JISI, 202, 319-324, (1964).
35. Ahsan, S. N., Mukherjee, T. and Whiteman, J. A., "Structure of Fluxed Sinter", Ironmaking and Steelmaking, Vol. 10, No. 2, 54-64, (1983).
36. Hancart, J., Leroy, V. and Braggard, A., "Investigation of the Phases Present in the Blast Furnace Sinters - Consideration on their Mechanism of Formation", CNRM Metallurgical Report, no.11, June, 3-7, (1967).
37. Inoue, K. and Ikeda, T., "The solid Solution State and Crystal Structure of Calcium Ferrite Formed in Lime-Fluxed Iron Ore Sinters", Tetsu-to-Hagane, 68, 15, 2190-2199, (1982).
38. Dawson, P. R., Oswald, I. and Hayes, K. M., "Influence of Alumina on Development of Complex Ferrites in Iron Ore Sinters", Trans. Inst. Min. Metall. Sec. C, 94, June, 608-611, (1985).
39. Rait, J. R., "Basic Refractories, their Chemistry, and Performance", London, (1950).
40. Deer, W. A. et al., "An Introduction to the Rock-Forming Minerals", Longman Publishers, London, (1963).
41. Zudin, V. M. et al., "Effect of Sintering Temperature on the Mineralogical Composition of Sinter and on Its Properties", Stal in English, 417-420, (1963).

42. Panigrahy, S. C., D. Sc. Thesis, Ghent, Belgium, (1982).
43. Hegde, V., "The Role of Basic Additives MgO and CaO during Induration and Reduction of Iron Ore Pellets", Ph.D. Thesis, McMaster Univ., Hamilton, Ontario, (1986).
44. Bragnall, E. J., "Influence of Feed Size Distribution on Sinter Microstructure and Properties", BHP Technical Bulletin, Vol. 17, No. 1, (1973).
45. Thanning, G., "Reduction Strength of Super Fluxed Pellets made from Rich Magnetite Concentrate", Vol. 3, No. 2, 57-63, (1976).
46. Bentell, L. and Mathison, G., "Oxidation and Slag Forming Process in Dolomite Fluxed Pellets Based on Magnetite Concentrates", Scand. Journal of Metallurgy, Vol. 7, 230-236, (1978).
47. Friel, J. J. and Erickson, E. S., "Reduction Characteristics of Dolomite Fluxed Magnetite Pellets", Met. Trans. (B), Vol. 11B, 233-243, (1980).
48. Bleifuss, R. L., Proceedings of ICSTIS, Suppul. Trans. ISIJ, Vol. 11, 51, (1971).
49. Nikerasov, Z. I. et al., "Special Features of the Mineralogical Composition and Structure of Sinter", Stal in English, 951-956, (1966).
50. Cho, Y., and Bae, S., "Effects of Fine Size Distribution of MgO-Bearing Materials on Sintering Properties", Proc. Ironmaking Conf. vol. 45, 355-363, (1986).

51. Currier, J. W. and Green, R. J., "The Function of Magnesia on Iron Ore Burden Materials", Proc. Ironmaking Conf., vol. 45, 23-30, (1986)
52. Currier, J. W., "The Function of Olivine in Blast Furnace Applications", Proc. Ironmaking Conf., vol. 47, (1988).
53. Lyons, R. G. and Davis, W. J., "Evaluation of Sinters with Olivine", ISS-AIME Ironmaking Conf. Proceedings, 647-655, (1988).
54. Ishikawa, Y., Shimomura, Y., Sasaki, M., Hida, Y. and Toda, H., "Improvement of Sinter Quality Based on the Mineralogical Properties of Ore", ISS-AIME Ironmaking Proceedings, 42, 17-29, (1983).
55. Panigrahy, S. C., Jallouli, M. and Rigaud, M., "Porosity of Sinters and Pellets and Its Relationship with Some of Their Properties", ISS-AIME Ironmaking Proceedings, 43, 233-240, (1984).
56. Goldring, D. C. and Fray, T. A., "Characterization of Iron Ore for Production of High Quality Sinter", Ironmaking and Steelmaking, Vol. 16, no. 2, 83-89, (1989).
57. Dartnell, J., "Effect of Burden Quality on Furnace Performance", JISI, 207, 282-292, (1969).
58. Watnabe, S., "Fundamental Studies of Self-fluxing sinter Agglomeration", Agglomeration, (ed. W. A. Knepper), Interscience, New York, 865-894, (1962).

59. Barrie, D. J., Carmichael, I. F. and Kinloch, E. D., "Change in the Strength of Sinter in the Course of Reduction", JISI, 207, 563-569, (1969).
60. Bogan, L. C. and Worner, H. K., "Structure and Bonding Mechanisms in Sinters Made from Fine-Grained Australian Hematites", Agglomeration, (ed. W. A. Knepper), Interscience, New York, 901-925, (1962).
61. Price, C. and Wasse, D., "Relationship Between Sinter Chemistry, Mineralogy, and Quality; and Its Importance in Burden Optimization", Developments in Ironmaking Practice, Iron and Steel Institute, London, 32-52, (1972).
62. Biswas, A. K., "Principles of Blast Furnace Ironmaking", Cootha Publishing House, Brisbane, Australia, (1981).
63. Edstrom, J. O., "The Mechanism of Reduction of Iron Oxides", JISI, Nov., 289-304, (1953).
64. Goldschmidt, H. J., JISI, No. 2, 157-180, (1942).
65. Brill-Edwards, H., Daniel, B. L. and Samuel, R. L., "Structural Changes Accompanying the Reduction of Polycrystalline Hematite", JISI, April, 361-368, (1965).
66. Grebe, C., Stal und Eisen, 88, 1098-1104, (1968).
67. Meyer, K. Rausch, H. and Ottow, M., Stahl und Eisen, 87, 11, 654-660, (1960).
68. Inazumi, T., Nagano, K. and Kojima, K., Proceedings of Int. Conf. on Science and Technology of Iron and Steel, I, ISIJ, 56, (1970).

69. Sasaki M., Enokido, T., Kondo, S. and Nakazawa, T., Tetsu-to-Hagane, 59, 1209, (1973).
70. Toda, H., Senzaki, T., Isozaki, S. and Kato, K., "Relationship between Heat Pattern in Sintering Bed and Sinter Properties", Trans. ISIJ, vol.24, 187-196, (1984).
71. Bragnall, E. J., "Influence of Feed Material Properties on the Sinter for Blast Furnace", Agglomeration 77, 2, 587-603, (1977).
72. Edstrom, J. O., Jernkontoret Ann., 142, 401, (1958).
73. Sugawara, K. and Satoh, K., "On the Degradation of Sintered Ore during Chemical Reduction", Tetsu - to - Hagane, 55, 1107, (1969).
74. Khokhlov, D. G. "Fluxed Sinter with Increased Magnesia Content", Metallurgists, 6-7, (1961).
75. Bonnecamp, H. et al., "Plant Trials on factors Determining Sinter Quality and Resulting Blast Furnace Performance, Iron and Steel Maker, June, 17-24, (1980).
76. Zimmermann, K. et al., "Development of Sintering Technique in the Sinter Plant Schwelgern of Thyssen A. G.", Stahl und Eisen, Vol. 100, No. 1, 12-18, (1980).
77. Oswald, J., "Mineralogy and Microtexture of Australian Iron Ore Sinters", BHP Technical Bull., vol. 25, no.1, 13-20, (1981).
78. Bogdandy, L. v. and Engell H-J., "The Reduction of Iron Ores", Springer - Stahleisen, (1971).

79. Bjorkavall, B. and Ilmoni, P. A., ISS-AIME Ironmaking Conf. Proceedings, Vol. 36, 366-383, (1977).
80. Dawson, P. R., "The Reduction Properties of Complex Calcium Ferrites", 4th International Symposium on Agglomeration, (ed. C. E. Capes), ISS, U.S.A., 243-250, (1985).
81. Taylor, J., JISI, Feb., 129-136, (1950).
82. Taylor, J., JISI, Sept, 701-703, (1962).
83. Sastry, K. V. S., Negm, A. and Kater, T., "Influence of a cellulose Derived Binder on the Growth and Strength Behavior of Taconite Pellets, SME Fall Meeting, Salt Lake City, Utah, (1983).
84. Rigaud, M., Jena, B. C., Panigrahy, S. C. and Paquet, G., "A Method for Production of the Highly Porous Fluxed Pellets Using Peat Moss as a Binder", ISS Trans., vol. 9, 131-138, (1988).
85. Tremblay, R., "Use of Peat Moss as a Binding Agent in the Balling of Iron Oxide Concentrates", 23rd Annual Conf. of the Metallurgists, CIM, Quebec City, (1984).
86. Kozakevitch, P., Rev. Mét., 46, 572, (1949).
87. Matsuno, F., Trans. ISIJ, vol. 19, 595-604, (1979).
88. Panigrahy, S. C., Verstraeten, P. and Dilewijns, J., "Influence of MgO addition on Mineralogy of Iron Ore Sinter", Met. Trans. B, vol. 15B, 23-33, (1984).
89. Davison, J., "Burden Testing and Its Application to Blast-Furnace Operation", JISI, 211, 107-114, (1973).

90. Kortman, H. A. and Burghardt, O. P., "Test Methods for Evaluating Iron Ores, Pellets and Sinters", Agglomeration 77, (ed. K. V. Sastry), A.I.M.E., 219 - 242, (1977).
91. ASTM Designation E 279-69, "Standard Method of Test for Tumbler Test for Iron Ores".
92. I.S.O. 4696, "Iron Ores - Low-temperature Desintegration Test - Method Using Cold Tumbling After Static Reduction", International Organization for Standardization, (1984).
93. Oliver, R. A., "A Survey of Current Reducibility Methods", JISI, Nov., 1131 - 1135, (1967).
94. Davison, J., "Recent Developments in Met. Sci. and Tech. Iron and Steel", Silver Jub. Sym., Ind. Inst. of Metals, New Delhi, 1-36, (1972).
95. I.S.O. 4695, "Iron Ores - Determination of Reducibility", International Organization for Standardization, (1984).
96. Mazanek, E., and Jasienska, S., "Mineralogy and Reducibility of Self-Fluxing Sinter", JISI, 201, 60-67, (1963).
97. Sasaki, M., et al., Trans. ISIJ, vol. 17, 391-400, (1977).
98. Mukherjee, T. and Whiteman, J. A., "Structure of Fluxed Sinter", Ironmaking and Steelmaking, vol. 12, no. 4, 151-156, (1985).
99. Levin, E. M., Robbins, C. R. and McMurdic, H. F., "Phase Diagrams for Ceramists", American Ceramic Society Inc., Columbus, Ohio, (1964), Supplements (1969), (1975), (1981), (1983).

100. Gray, N. B. and Henderson, J., "Hydrogen Reduction of Dense Hematites", Trans. Met. Soc., AIME, 236, 1213-17, (1966).
101. Edstrom, J. O. and Bitsianes, G., Trans. Met. Soc., AIME, 203, p. 760, (1955).
102. McKewan, W. M., "Kinetics of Iron Ore Reduction", Trans. Met. Soc. AIME, 212, 791-93, (1958).
103. McKewan, W. M., "Kinetics of Iron Oxide Reduction", Trans. Met. Soc. of AIME, 218, 2-6, (1960).
104. McKewan, W. M., "Kinetics of Reduction of Iron Ore", Trans. Steelmaking - The Chipman Conf., 141-155, (1965).
105. Hayes, P. C., Metall. Trans. B, 10B, 211-17, (1979).
106. St. John, D. H. and Hayes, P. C., Op. Cit., 13B, 117-124, (1982).
107. St. John, D. H., Mathew, S. P. and Hayes, P. C., Op. Cit., 15B, 701-708, (1984).
108. *ibid.*, 709-717.
109. Jost, W., "On a Problem of diffusion and Simultaneous Gas Flow", Chem. Engng. Sci., 2, 199-202, (1953).
110. Szekely, J. and Themelis, N. J., "Rate Phenomena in Process Metallurgy",
111. Spitzer, R. H., Manning, F. S. and Philbrook, W. O., "Mixed Control Reaction Kinetics in the gaseous Reduction of Hematite", Trans. Met. Soc., AIME, 236, 726-742, (1966).
112. Fihey, J-L., D.Sc.A. Thesis, Ecole Polytechnique, Montreal, (1978).

113. Fihey, J-L. and Ajersch, F., "Etude Theorique de la Reaction Gazeuse d'une Boulette Spherique Poreuse d'Oxyde", Int. J. Heat Mass Transfer, vol. 21, 1491-98, (1982).
114. Szekely, J., Evans, J. W. and Sohn, H. Y., "Gas-Solid Reaction", Academic Press, 108-175, (1976).
115. King, R. P. and Brown, C.P., "The Rate of Movement of the Topochemical Interface During Gas-Solid Reaction", Metall. Trans. B, vol. 11B, 585-592, (1980).
116. Shigematsu, N. and Iwai, H., "Effect of SiO_2 and/or Al_2O_3 Addition on Reduction of Dense Wustite by Hydrogen", Trans. ISIJ, vol.28, 206-213, (1988).
117. Turkdogan, E.T., Met. Trans., 9B, 163-179, (1978).
118. Turkdogan, E.T., Met. Trans., 2, 3175-88, (1971).
119. ibid. 3, (1971).
120. Wiberg, M., Jernkont Ann., 124, 172-212, (1940).

ANNEX 1

IMPORTANT PHASE DIAGRAMS

All the equilibrium phase diagrams presented here are taken from "Phase Diagrams for Ceramists" by Levin et al.⁽⁹⁹⁾.

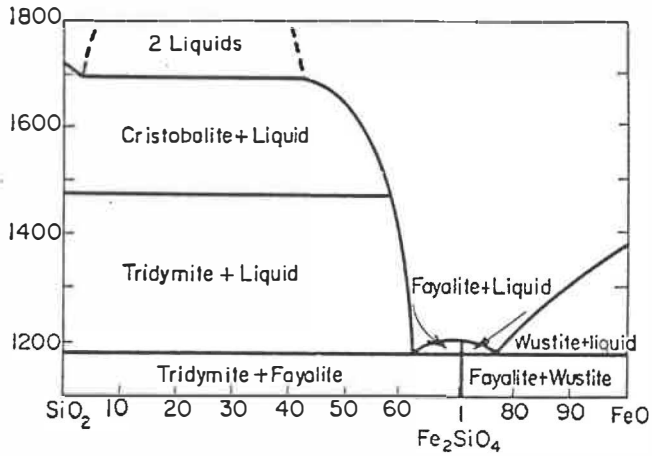


Fig. A1.1 System FeO-SiO₂

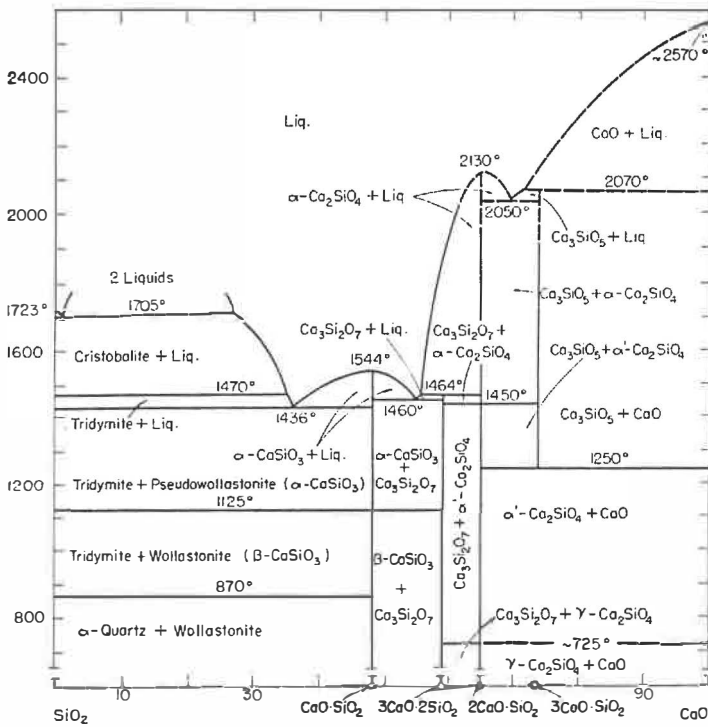


Fig. A1.2 System CaO-SiO₂

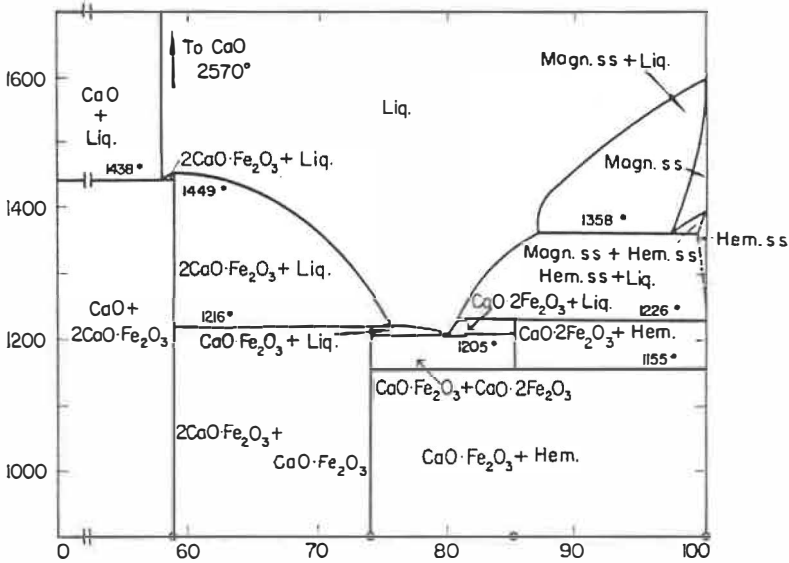


Fig. A1.3 System CaO-Fe₂O₃

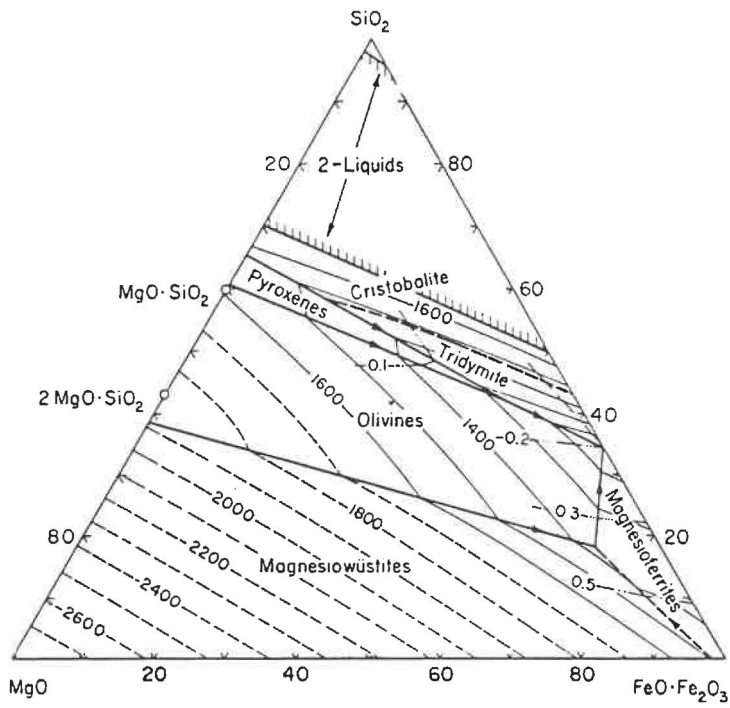


Fig. A1.4 System $\text{FeO}\cdot\text{Fe}_2\text{O}_3\text{-MgO-SiO}_2$

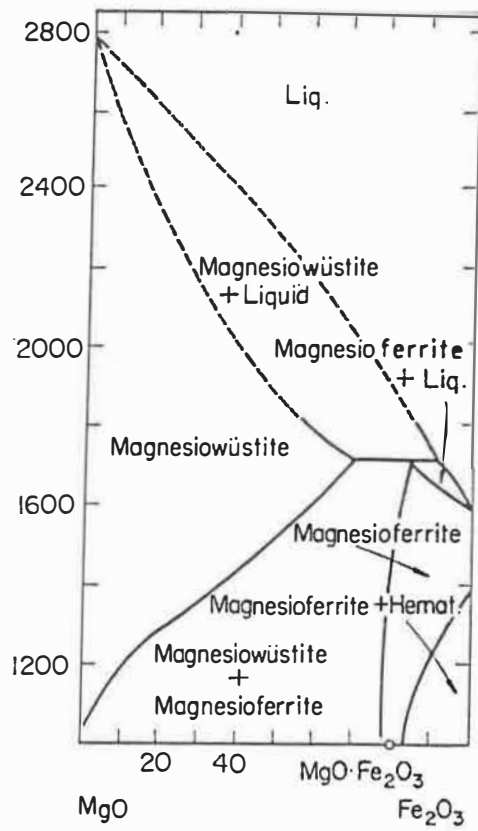


Fig. A1.5 System MgO-Fe₂O₃

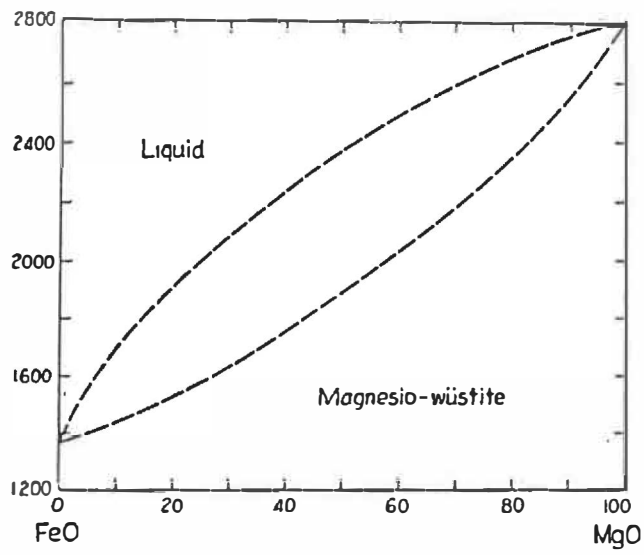


Fig. A1.6 System FeO-MgO

ANNEX 2

KINETICS OF IRON ORE REDUCTION

In recent years, a large number of articles has been published on reduction of iron oxides, iron ores and iron ore-agglomerates. The investigations involve the evaluation of the ores (both hematite and magnetite), different mineral phases present in the ore agglomerates with regard to their reducibilities. Attempts have been made to study the possible mechanisms for the reduction process and effects of different parameters such as temperature, pressure and gas composition on the kinetics of reduction. Few models have also been proposed to analyze the reduction kinetics.

The reduction of iron oxides is a very complex process and it takes place through a series $\text{Fe}_2\text{O}_3/\text{Fe}_3\text{O}_4/\text{FeO}/\text{Fe}$ above 560°C . The reduction of a mass of hematite to iron is schematically shown in Fig. A2.1⁽¹⁰⁰⁾. Wustite is stable only above 575°C . Hence, if the reduction occurs below this temperature the FeO field is absent i.e. the reduction takes place through the series $\text{Fe}_2\text{O}_3/\text{Fe}_3\text{O}_4/\text{Fe}$. It has been reported by Edstrom and Bitsianes⁽¹⁰¹⁾ that the gas-solid type of reaction occurs only at FeO/Fe interface and that the internal reduction proceeds by

diffusion of iron. During the reduction oxygen is transferred to the gaseous phase only at the FeO/Fe interface.

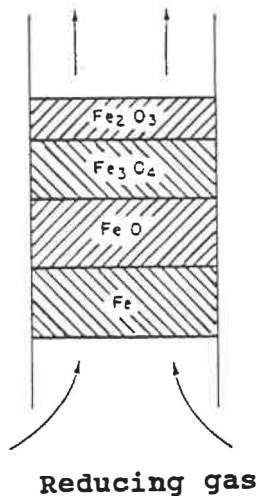


Fig. A2.1 Schematic representation of gaseous reduction of iron oxide (above 575°C)⁽¹⁰⁰⁾.

McKewan⁽¹⁰²⁻¹⁰⁴⁾ has extensively studied the reduction of iron oxides. According to him, during the reduction of a hematite particle, the loss of oxygen takes place only from an oxide-iron interface which in such a way that the original shape of the hematite particle is retained. This shows that the reduction is topochemical. The intermediate oxides, in the transition from hematite to iron form thin layers so that oxygen can be lost from the particle without movement of the oxide-iron interface.

Further, the rate of oxygen loss from the particle is said to be proportional to the area of the receding surface so that the iron layer grows linearly with time and the overall reduction process can be described by the equation;

$$r^0 d^0 [1 - (1 - F)^{1/3}] = Kt \quad (\text{A2.1})$$

where r^0 and d^0 are the initial particle radius and density respectively, F is the fractional reduction at time t and K is the rate constant.

This theory has got a wide support from many scientists. As reported by Edstorm⁽⁶³⁾ and subsequently confirmed by Gray and Henderson⁽¹⁰⁰⁾, below about 575°C (where wustite phase is unstable) the reduction reaction proceeds topochemically and partially reduced particle consists of a core of hematite surrounded by a thin concentric layer of magnetite which in turn surrounded by a layer of porous iron. Above about 575°C, a partially reduced hematite particle shows a hematite core surrounded by a concentric layer of dense magnetite followed by a layer of dense wustite, then porous wustite with dense iron around the pores. As the reduction advances, the magnetite-wustite interface recedes topochemically until the oxide core completely disappears and the only phases remain at this point are wustite and iron.

In the proposed two-stage reduction, the weight loss during the first stage is due to the reduction of the oxide core and the reduction of wustite retained in the outer wustite iron shell. During the second stage, the reduction rate drops significantly and the observed weight loss is from the reaction of numerous islets of wustite. In support of their arguments for "two-stage" nature of reduction, Gray and Henderson⁽¹⁰⁰⁾ have plotted the F-t data for a single crystal of hematite (Fig. A2.2) according to the equation (A2.1) developed by McKewan⁽¹⁰²⁾. In this figure the linear portion of the curve corresponds to the first of reduction when the oxide core still exists. The second stage is represented by the non-linear part. During this period only the retained wustite reacts. The break-away point (from first stage to second stage) is a function of the physical and chemical nature of the hematite particle. The topochemical reaction was only observed in prepared hematite and not in natural single crystal of hematite above 575°C which was suspected to be due to some factors caused during the preparation.

After thoroughly studying the reduction rate and the microstructure of partially reduced hematite, magnetite and magnetite partly or completely oxidized to hematite, Edstorm⁽⁶³⁾ has concluded that below 600°C the reduction of both hematite and magnetite are essentially identical as the rate is controlled by the surface reaction at the magnetite-gas

interface. At a higher temperature there is a large difference in the reduction kinetics of hematite and magnetite. The differences in the rate of reduction of hematite, magnetite and partly oxidised magnetite at 1000°C can be seen in Fig. A2.3. After observing the partly reduced samples, he attributed the difference in their reduction rate mainly to the nature of wustite layer formed. The wustite formed from the reduction of hematite or oxidized magnetite is coarsely porous. On the contrary, wustite formed from magnetite is quite dense.

Moreover, there is an extensive formation of pores during the early stage of reduction of hematite. The structure often disintegrates providing more surface for the gas-attack and reducing the diffusion distances in the solid phase. This contributes to the higher reducibility of hematite to a large extent.

The rate of reduction of wustite (Fe_xO) to iron being the slowest of all the iron oxide reductions, this stage becomes the rate controlling step during the iron oxide reduction. It is, hence, important to discuss this step in details.

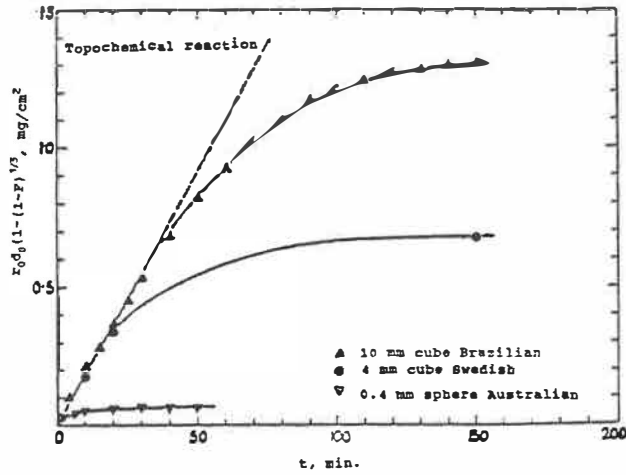


Fig. A2.2 Plot of $r_0 d_0 [1 - (1-F)^{1/3}]$ against t for natural single crystals of hematite reduced at 700°C to $F=0.9$, showing typical breakaway behavior in support of two-stage reaction mechanism⁽¹⁰⁰⁾.

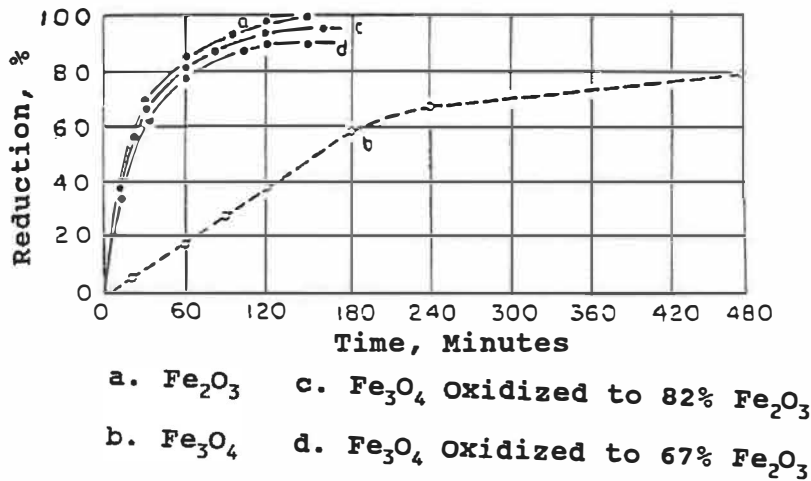


Fig. A2.3 Reduction with CO at 1000°C ⁽⁶³⁾.

As we can see from the Table A2.1, wustite has the lowest oxygen dissociation pressure. Above 575°C the final stage reduction of the iron oxide is wustite to metallic iron. It has been observed that the morphology of the wustite formed from the parent oxides and the product during the initial stages of the wustite reduction has a profound effect on the rate of reduction from wustite to iron.

Table A2.1 : Oxygen dissociation pressure (P_{O_2}) in atmosphere, of iron oxides

Oxide phases	Temperature, °C			
	1000	1200	1300	1400
Fe_2O_3/FeO	5.2×10^{-5}	1.6×10^{-2}	1.4×10^{-2}	1.3×10^{-1}
Fe_3O_4/FeO	2.0×10^{-11}	8.4×10^{-10}	2.2×10^{-5}	3.7×10^{-7}
FeO/Fe	6.0×10^{-14}	1.3×10^{-12}	2.0×10^{-11}	2.1×10^{-10}

It has been mentioned earlier about the difference in the reduction rate of hematite and magnetite. The dense wustite formed during the reduction of magnetite has a lower reduction rate and it eventually reduces the overall reduction rate of magnetite. On the contrary, the wustite formed during hematite reduction is porous and has a higher reduction rate. Besides, the cracks produced due to the structural changes during reduction from hematite to magnetite also helps to increase the reducibility of hematite.

The reduction of wustite starts with the chemical reaction between wustite and the reducing gas mixture. Oxygen is removed from the surface of wustite causing a local increase in iron ion concentration. Due to the resulting difference in concentration, iron ions diffuse from the surface into the bulk wustite and a concentration gradient of iron ions occurs between the surface and the bulk wustite. The actual composition of wustite at the gas oxide interface at any instant is determined by the rates of the chemical reaction and the diffusion of iron into the bulk.

It has been observed during the reduction of wustite that there is a significant change in porosity (both size and distribution). As the metal has a smaller molar volume than the oxide, there is an obvious expansion of the pores. However, formation of a porous sponge iron on the surface the oxide or on the walls of the pores may decrease the size of the original pores, but, there will be a new set of pores in the sponge iron produced. As the reduction proceeds, continuous formation of pores prior to and during the nucleation and growth of iron. Due to this, more FeO-surfaces are exposed to the reducing gas leading to a higher reduction rate. Formation of dense iron can strongly inhibit the reaction. The product morphology during the wustite reduction, thus, plays an important role in its reduction rate.

Hayes and others (105-108) have studied the microstructural changes during the initial stages of reduction of pure dense wustite by H_2/H_2O and CO/CO_2 gas mixtures. They have observed that the iron nucleus formed on the wustite surface depends on the following factors;

- (a) the initial stoichiometry of the wustite and the oxygen potential of the reducing gas,
- (b) the relative rates of the chemical reaction and mass transport of iron on the wustite surface and in bulk wustite, and
- (c) the surface topography of the wustite - as instabilities are favoured by the defects on the surface since they act as preferential sites for chemical reaction.

They have identified mainly three types of product morphologies formed under different reducing conditions;

- dense iron on dense wustite;

when the chemical reaction rate is slower than the mass transport there is a small difference in the iron ion concentration between the surface and the bulk wustite and the product morphology in this case is dense wustite covered with dense iron,

- dense iron on porous wustite;

condition where there is greater difference in surface and bulk iron concentration, consistent with higher reduction

potentials and higher chemical rate, the morphology obtained is porous wustite covered with dense iron, and

- porous iron on dense iron or wustite;

the initial dense iron layer is often breaks down at a later stage leading to a final product structure of porous iron.

Topochemical Model

The reduction of iron oxides by CO or H₂ is a heterogeneous reaction. The mechanism suggested by Edstorm⁽⁶³⁾ is generally accepted for the reduction of dense hematite to metallic iron above 570°C (the temperature at which wustite is stable as an intermediate product). This involves formation of successive product layers of metallic iron, Fe_xO and Fe₃O₄. The gas-solid type of reaction takes place only at Fe_xO/Fe interface and the internal reduction: Fe₂O₃ - Fe₃O₄ - Fe_xO proceeds by solid state diffusion.

Topochemical model developed by Jost⁽¹⁰⁹⁾ is largely used by the researchers to study the kinetics of the iron oxide reduction. According to this model, iron oxide pellet is considered initially to be dense spherical particle and as the reduction progresses, two distinct zones are formed:

- 1) the central dense unreduced core and
- 2) the outer porous reduced shell as shown in Fig. A2.4⁽¹¹⁰⁾.

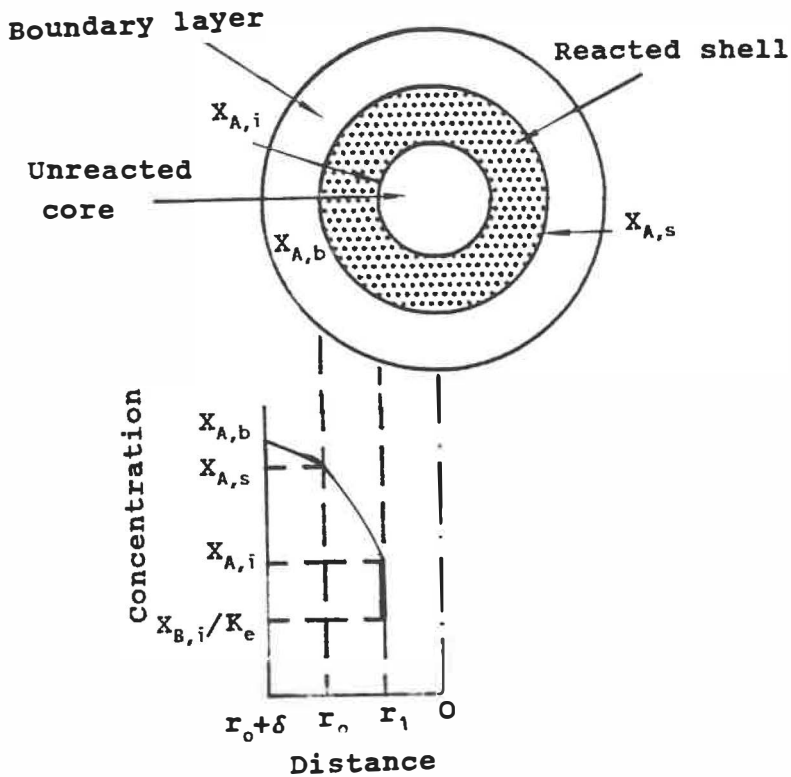


Fig A2.4 Concentration profile of reacting gaseous species along a sectioned spherical particle⁽¹¹⁰⁾.

The removal of oxygen at the iron-wustite interface of a dense oxide particle proceeds through the following five basic steps:

- 1) transport of the reducing gas from the bulk gas phase to the surface of the particle;
- 2) diffusion of the reducing gas through the porous iron layer to the chemical reaction interface;
- 3) chemical reaction between the gas and the oxide at the interface to produce gaseous product;

- 4) outward diffusion of the product gas through the reacted shell;
- 5) transfer of the product gas from the surface of the reacted shell to the bulk gas phase.

These steps offer resistance to the overall reduction rate. Step 1 and 5 are known as gas film resistances, step 2 and 4 are shell layer resistances and step 3 is interface resistance. These five steps may be re-grouped into three basic processes, namely;

- 1) mass transfer through the gaseous boundary layer;
- 2) mass transfer through the reacted shell;
- 3) chemical reaction at the oxide-gas interface.

The slowest of these process effectively control the overall rate of the system.

Szekely and Themelis⁽¹¹⁰⁾ and Spitzer and co-workers⁽¹¹¹⁾ have derived the overall rate equation for isothermal reduction of iron oxides from the individual rate equations for each of the basic processes. This equation has been further simplified by Fihey⁽¹¹²⁾ with the help of two important dimensionless parameters e.g. mass transfer parameter (K_f) and Theile modulus (m^r).

Reduction of Mixed Oxides, Oxide Compounds and Sinters

A number of studies have been made on the reduction kinetics of iron oxides. But, majority of them is for the case of pure dense iron oxides. Several models have been proposed in the literature⁽¹¹³⁻¹¹⁵⁾ to analyze the kinetic parameters of iron oxide reduction. These models provide valuable information about different factors which should be considered in order to determine the kinetic parameters and hence, they are quite important for theoretical studies. However, they have limited use for the industries, particularly, for those who use sinters in their blast furnace burden.

In this section, the effects of formation of various mixed oxides, oxide compounds in the reduction of iron oxides and sinters are discussed.

Reduction of Mixed Oxides and Oxide Compounds

Bogdandy and Engell⁽⁷⁸⁾ have discussed the reduction kinetics of mixed oxides and oxide compounds. According to them, during the reduction, the solid-oxide is resolved into three components:

- a) into oxygen - which in some combined form goes over to the gaseous phase;

- b) into metallic phase - which differs in composition from the molar ratio of the metals in the oxide phase and
- c) into an oxide phase - with a corresponding changed composition.

Different mixed crystals and compounds of iron oxides are formed with MnO , CaO , SiO_2 , MgO , Al_2O_3 etc. present in the gangue of the ore or in the additives. These oxides, when in equilibrium with their metal phase or with a lower oxide, have so small oxygen pressure and hence they cannot be reduced appreciably or only at high temperatures. At lower temperature, the complex oxide splits up into a metallic phase rich in iron, an oxide phase impoverished in iron and oxygen. With limited formation of mixed crystals and with compounds which have only a limited width of phase domain, progress of reduction requires the separation of a second oxide phase from the oxides; e.g. the separation of calcium oxide in the reduction of dicalcium ferrite:

$$2CaO.Fe_2O_3 + 3H_2 = 2Fe + 2CaO + 3H_2O$$

Kinetics of the reduction of mixed oxides and oxide compounds is mainly influenced by two basic phenomena:

- a) The activity of iron oxides is reduced by the formation of the compound and/or mixed oxide and CO_2/CO or H_2O/H_2 ratio required for the reduction to the next lower oxidation stage is decreased. If the reduction is to occur, the gas composition must be less than this ratio. This

shift of equilibrium will affect the rate of gas diffusion in the boundary layer and in the reacted shell and also the chemical reaction (as they depend on the difference between the composition of the gas and the gas composition for equilibrium) and thus it will affect the reduction kinetics. The change in equilibrium condition also worsens the best possible utilization of the reducing gas.

- b) Since in the mixed crystals and oxide compounds, iron oxide is usually the more noble component, when oxygen is removed during reduction, iron or lower oxide of iron separates out leaving behind a crystal with enriched in or pure second component depending on the stage of reduction. This decomposition necessitates diffusion in the solid state.

Both these phenomena adversely affect the reduction rate of mixed oxides and oxide compounds. However, due to the fact that certain mixed oxides have higher rate constants for the chemical reaction at the phase boundary, they are found to have a higher overall reduction rate. Moreover, the effect of formation and decomposition of the compounds or mixed oxides on the porosity may also influence the reduction rate favourably.

Shigematsu and Iwai⁽¹¹⁶⁾ have carried out reduction tests of dense wustite containing SiO_2 and/or Al_2O_3 . They have observed that when $\text{SiO}_2/\text{Al}_2\text{O}_3$ is added to FeO , a part of it dissolves in FeO while the rest forms fayalite/hercynite. At

temperatures below 730°C, the reduction reaction proceeds preferentially along the interface of fayalite/hercynite. It is indicated that the rate constant for the chemical reaction increases with the increase in the amount of hercynite. The acceleration effect of reduction is observed when the reduction rate is slow.

We have already seen in Chapter II that different mineral phases present in the sinter have different reducibilities. Their order of reducibilities has also been discussed.

Reduction of Sinters

As mentioned earlier, iron oxides can form a large number of mixed oxides and oxide compounds with other oxides which are either present in the ore gangue or added to the raw mix during sintering. The simultaneous occurring of the iron-bearing silicates and calcium ferrites in the industrial sinters shows that genuine equilibrium is not attained during sintering. In fact, during sintering, the rise and fall of temperature at any particular layer of sinter mix on the sinter strand is so fast that the chemical reactions taking place hardly get sufficient time to attain equilibrium. The thermodynamic data for the phases formed during the sintering process are not well known. It is, therefore, difficult to follow the course of the reaction.

Besides the mineral phases present, the reduction rate of sinter is also influenced by its the nature and amount of pores, sinter-size and temperature of reaction. The structural changes such as crack formation and change or formation of new pores during reduction also play an important role on the reduction rate of the sinter.

Application of the Models to Study the Reduction of the Sinters

Effort has been made to discuss the Reduction - Time curves of the sinters with respect to the model discussed in the previous section. Some typical reduction - time curves are shown in Fig. A2.5 through Fig. A2.8. It should be noted that unlike in the model where a single spherical pellet has been considered and the fractional reduction is calculated from the change in the dimension of different layers, in this case, the fractional reduction has been calculated from the weight loss of the sinters during reduction of several peices of sinter (10-15 mm, weighing about 100 g). It has been assumed that reduction proceeds uniformly in all the sinter pieces.

As we can see, the reduction - time curve consists of two parts e.g. linear in the beginning which gradually changes into a curve in the later stage of reduction. This nature of the curve indicates that reduction takes place in two stages. End of the first stage is marked by the end of the linear portion. This portion represents the extent of reduction taking place during the first stage of reduction.

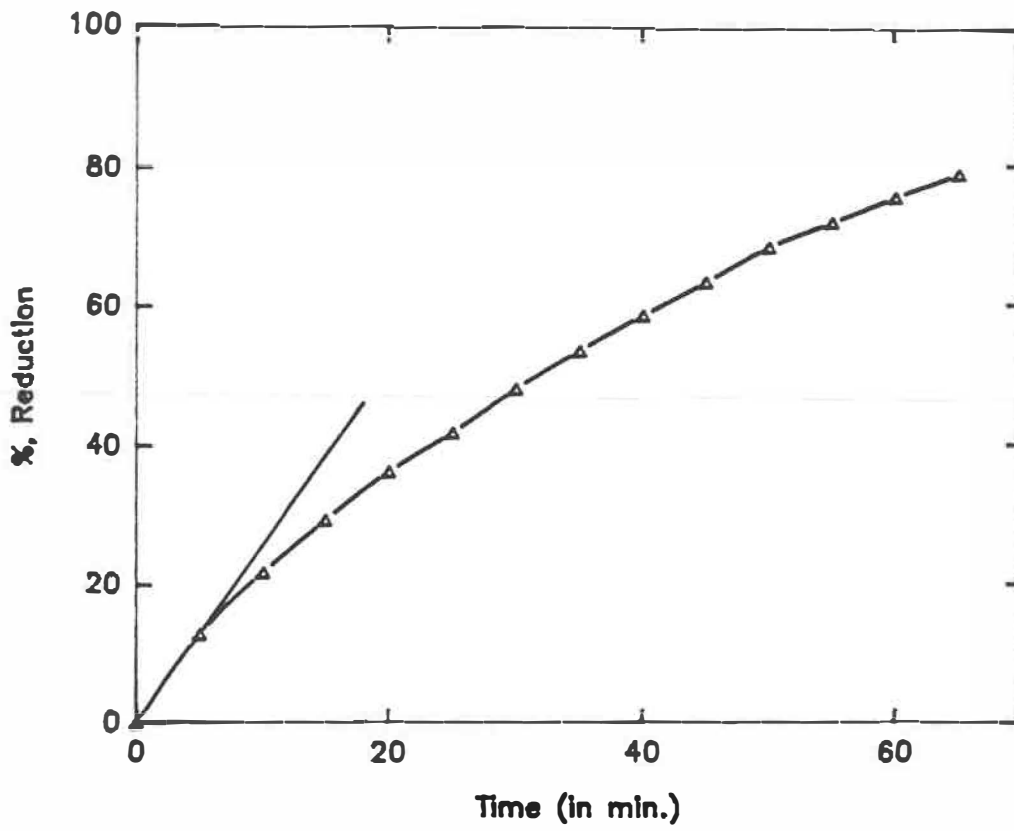


Fig. A2.5 Reducibility curve for the sinter without any specularite concentrate.

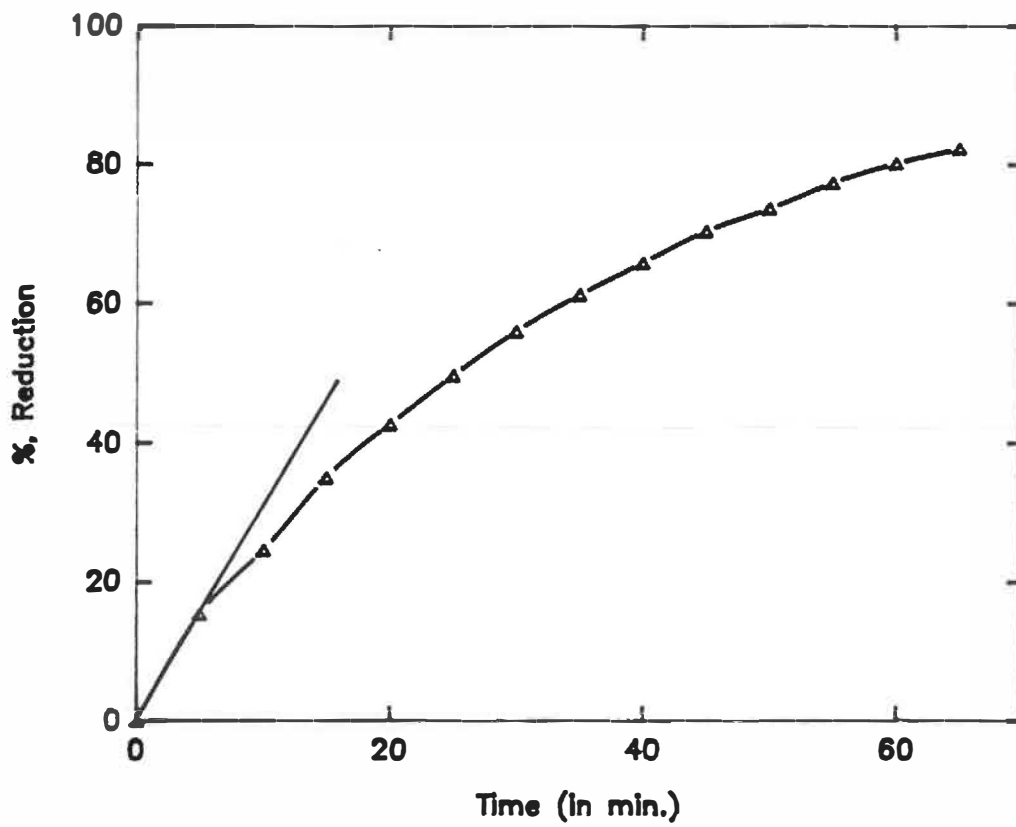


Fig. A2.6 Reducibility curve for the sinter with 25% specularite concentrate.

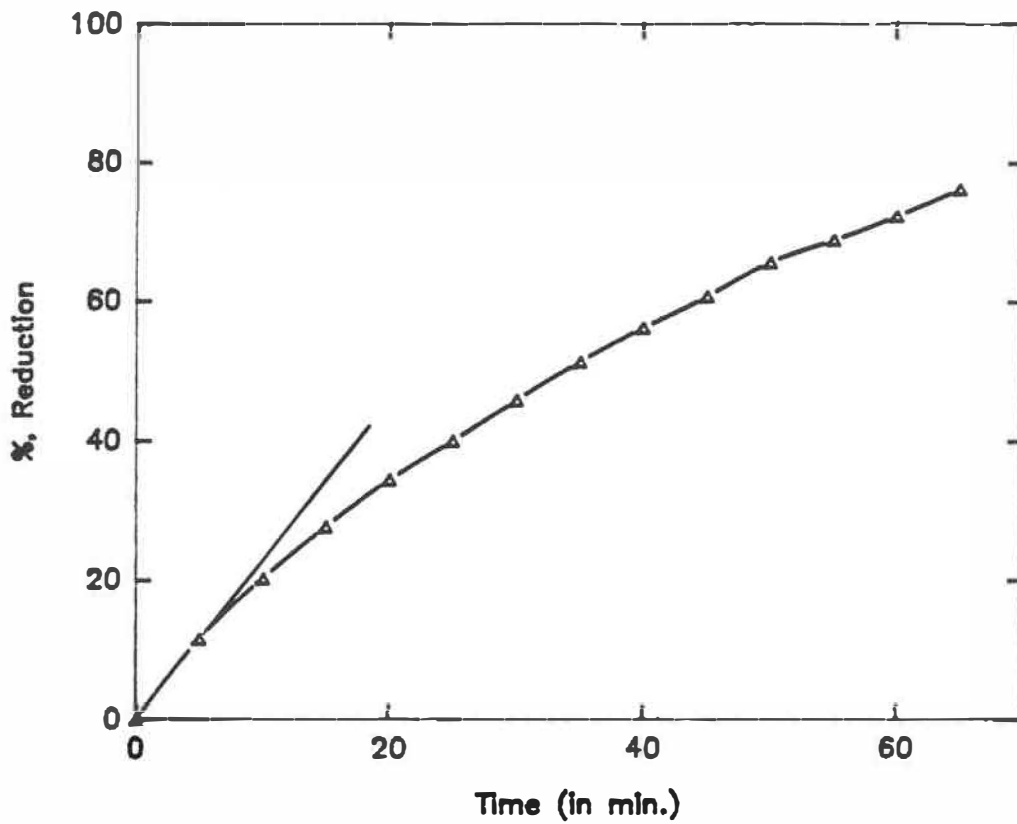


Fig. A2.7 Reducibility curve for the sinter with 40% specularite concentrate.

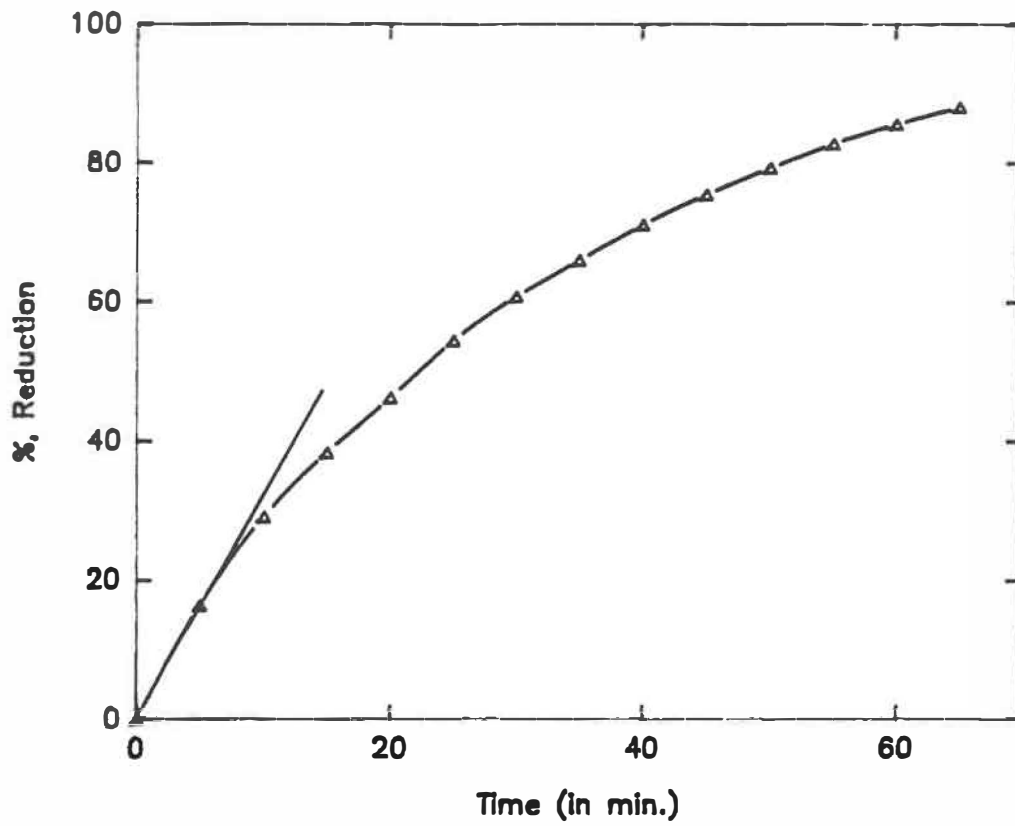


Fig. A2.8 Reducibility curve for the sinter with 100% specularite concentrate.

The phenomena occurring during the first stage of reduction may be discussed in the following way. The porosity of the sinters are quite significant, accounting for about 20% of its volume (or more). Because of this, when the reduction starts, the mass transfer process is fast and it does not control the overall reduction rate. On the contrary, it is controlled by the chemical reaction at the oxide-gas interface. Reduction proceeds linearly with time towards the center of the core (Ref. 110). As the reduction proceeds, the resistances for the mass transfer through the boundary layer and the reacted shell progressively becomes more and more prevelant. The linear nature of the reduction - time curve changes into a curve and this marks the end of the first stage of reduction.

As we see from the Fig. A2.5 through Fig. A2.8, the extent of linear portion of the reduction - time curve increases as the amount of specularite concentrate in the sinter increases. We know that the porosity of the sinters increases with the increase in the specularite content of the sinter. The effective diffusivity increases (D_{eff}) with the porosity⁽¹¹¹⁾ and the Theile modulus varies inversely with the square root of the effective diffusivity⁽¹¹²⁾. In other words, the Theile modulus decreases with the increase in the sinter porosity, and hence the chemical reaction control becomes more predominant and the linear portion of the reduction - time curve increases.

In physical terms it means that more gas can penetrate into the sinter and the degree of reduction will be more.

From the above discussion, it may be said that the reduction of the sinter is characterized by mixed control reaction i.e homogeneous and topochemical. The extent of homogeneous or topochemical type of reaction depends mainly on the porosity of the sinter. As the porosity increases, the homogeneous reaction is more predominant and vice versa.

The models are theoretical and are valid only to limited extent for all practical purposes. Their use is further restricted in case of sinters because of their heterogeneous nature. Unlike the pellets, the final product in sintering consists of a partly molten, spongy sinter cake, which is crushed and screened to obtain the sinters of required size. Hence, their structural parameters such as shape size, size, porosity are not at all uniform.

The problems encountered while using the models to study the reduction kinetics of the iron ore sinters will be discussed in the following paragraphs.

The first one is the shape factor. Because of the fact that sinters are very irregularly shaped, the models developed specifically for spherical pellets can not be effectively used.

In order to calculate the surface area, Szekely et al⁽¹¹⁴⁾ have assumed an uniform distribution of ideally shaped grains inside a spherical pellet. Fihey and Ajersch⁽¹¹³⁾ have also considered a spherical pellet.

As the effective diffusivity of the reduction gas very much depends on the pore surface, the wide variation of the pore size and distribution in the sinter further complicates the reduction process.

Another important factor to be considered is the structural changes taking place during reduction. Szekely et al⁽¹¹⁴⁾ have found their model consistent with the experimental measurement of the rate of reduction of nickel oxide by hydrogen at a temperature at which no serious structural changes occur. Similarly, Fihey and Ajersch⁽¹¹³⁾ have compared their model with iron-titanium oxide reduction (where no structural change takes place) and found a good agreement. In iron ore sinters, however, structural changes occur due to phase transformations. It is sometimes so severe that microcracks are formed which may lead to the breakage of the sinters. It has a significant effect on the reduction rate.

Chemical composition of the mineralogical phases, their morphology and the oxidation degree of iron in the sinters are the factors which can affect their reduction rate.

Besides the above factors the reduction rate is also influenced by the reduction potential, volume, pressure, velocity and the temperature of the reducing gas.

In general, the reduction rate of the sinters in the blast furnace can be increased by maintaining a large surface area to volume ratio and close size distribution of the sinters.

After considering all the facts discussed in the previous chapters, we can see that the reduction of iron ore is a very complicated process. A number of theoretical models have been developed to analyze the kinetics parameters of the reaction taking place during the reduction of iron oxides. The analysis of kinetic parameters of the gas-solid reactions involving the formation of a solid product is not only useful for the reduction of iron oxide but also of considerable technological importance in material process operation such as reduction of oxide ores, roasting of sulfides and the like. These models are often found to be inconsistent with the experimental results. This is mainly because some of the structural factors have not been taken into account while developing these models. In some case, the model is unrealistically idealized in order to keep it simple for analytical purposes. However, they (the models) do provide the insight into the roles played by different structural parameters.

ANNEX 3

CALCULATIONS FOR THE REDUCIBILITY INDEX

The percentage degree of reduction is given by

$$\% \text{ degree of reduction} = \frac{\text{oxygen removed from the iron oxide}}{\text{oxygen originally combined with iron}}$$

The total amount of reducible oxygen in the sinter is calculated from the chemical analysis (by knowing the % of Fe_{total} and FeO). The % reduction is then calculated and plotted against time (in min), the slope of the curve giving the velocity of reduction at any time or at any particular degree of reduction. The reduction rate is critical after a layer of metallic iron is formed from wustite. Hence, the reducibilities are generally compared at 40% degree of reduction. However, this process does not properly compare hematite (which contains more oxygen than magnetite) with magnetite. Hence, a fair comparison is obtained when all the materials are oxidized to 60%, i.e. when the atomic ratio O/Fe = 0.9. These two procedures are illustrated in Fig. A3.1⁽⁸⁹⁾.

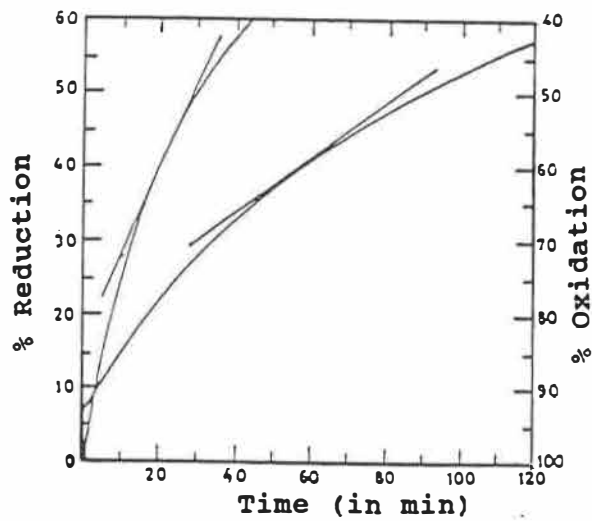


Fig. A3.1A schematic representation of relationship between reduction at 40% degree of reduction and 60% degree of oxidation levels⁽⁸⁹⁾.

The reducibility index is calculated by

$$(dR/dt)_{O/Fe=0.9} = \frac{33.6}{t_{60} - t_{30}} \quad (A3.1)$$

The above formula can be derived by the following method. Assuming the removal of the oxygen from the iron ore is a first order reaction compared to the original oxygen present, we have;

$$-\frac{dO}{dt} = kO_v \quad (\text{A3.2})$$

$$dO = -dR \times \frac{O_{\text{total}}}{100} \quad (\text{A3.3})$$

$$\frac{O_v}{O_{\text{total}}} = 1 - \frac{R}{100} \quad (\text{A3.4})$$

where

O_v : is the original oxygen content;

O_{total} : is the total oxygen combined with the iron ore
(in the form of Fe_2O_3 ;

R : is the degree of reduction;

From the equations (A3.2), (A3.3) and (A3.4), the speed of the reduction:

$$\frac{dR}{dt} = k \left(1 - \frac{R}{100} \right) \times 100 \quad (\text{A3.5})$$

Integrating equation (A3.5) we have,

$$\log_{10} (1 - R/100) = 0.434 kt + C \quad (\text{A3.6})$$

$$k = \frac{-\log_{10} (1 - 60/100) + \log_{10} (1 - 30/100)}{0.434 (t_{60} - t_{30})} = \frac{0.56}{t_{60} - t_{30}} \quad (\text{A3.7})$$

In case of hematite, the ratio of O/Fe of 0.9 has the same significance as $R = 40 \%$. Putting $R = 40 \%$ and the value of k from equation (A3.7) in equation (A3.5) we have;

$$\frac{dR}{dt}(\text{O/Fe} = 0.9) = \frac{33.6}{t_{60} - t_{30}} \quad (\text{A3.8})$$

Controlling Parameters

As discussed earlier in this chapter, it is quite difficult to develop a test method precisely simulating the blast furnace reduction conditions. In practice, a simplified test method is followed. Even though the chemical composition, the mineral phases and the porosity of the sinters are assumed to remain almost the same in both, the industrial practice and the laboratory test, the difference in other kinetic parameters such as the size grading of the sinters, gas composition, flow rate, the reduction temperature and the temperature gradient (for non-isothermal tests) could produce a significant difference in their reducibility values. However, a correlation can be made between the test results and the actual practice by carrying out some blast furnace trials with sinters produced under the same conditions. In fact, the reducibility values obtained in the laboratory are valid for the test conditions and give an indication about the reduction behavior of the sinters inside the blast furnace.

Reduction of the iron ore sinter by CO and/or H₂ gas is a very complicated process. In order that the reaction proceeds, the reducing gas has to diffuse into the sinter. Both, the chemical control and diffusional control play a major role in the mechanism of the reduction reaction and the overall rate of the reaction depends on the relative contribution of these controls. The experimental parameters for the reducibility test, hence, can be discussed with regard to the above control mechanisms.

Sinter Size

The reduction rate of the sinter is a function of its size. As the size of the sinter is reduced, its reducibility increases. Smaller size sinters have a larger surface to volume ratio i.e. more surface area is exposed to the reducing gas - leading to a higher reduction rate. However, it should not be reduced below a certain size. It must not impair the furnace permeability. In practice, usually, the size of the sinter charged into the furnace is + 10 mm. To ensure uniform gas flow the size distribution of the sinters should be kept as narrow as possible.

The variation of the reducibility with the size of the iron ore is shown in Fig. A3.2⁽⁹⁴⁾

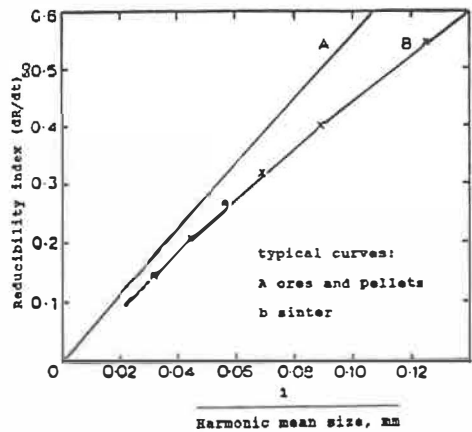


Fig A3.2 Reducibility index dR/dt_{40} vs. $\frac{1}{\text{harmonic mean size, mm}}$

The harmonic mean size d , here, is defined as:

$$1/d = [f_1/d_1 + f_2/d_2 + \dots + f_n/d_n]$$

where f_n is the fraction of the particles between two sieve sizes with a mean size d_n mm.

As we know, sinter is a very heterogeneous both, chemically and physically. Because of the inconsistency of the raw mix and rapid sintering process, the type and the amount of mineral phases vary to a large extent. The physical properties such as porosity is also not uniform in all the sinter samples used for testing. In order to overcome this, it is essential to test a minimum amount of sinter sample for reducibility. It is observed (Fig. A3.3) by repeating the test with 40g and 100g of sinter of size 10 - 12.5 mm that in the former case the results are highly irreproducible while in the later case, the results are fairly close.

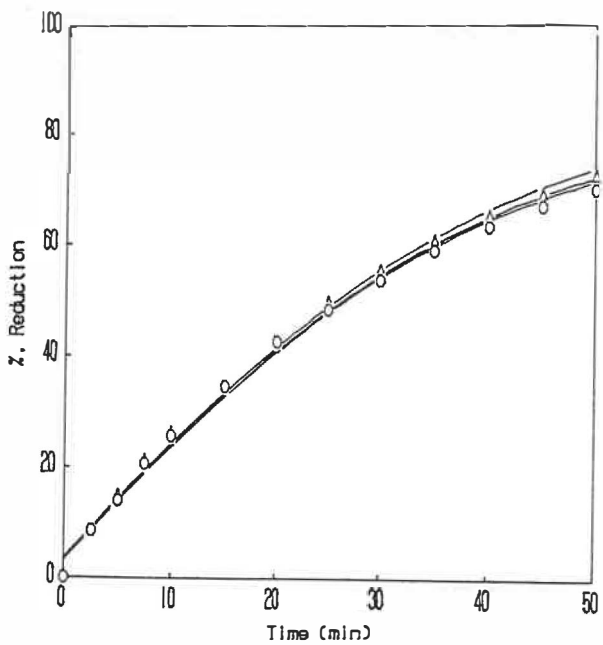
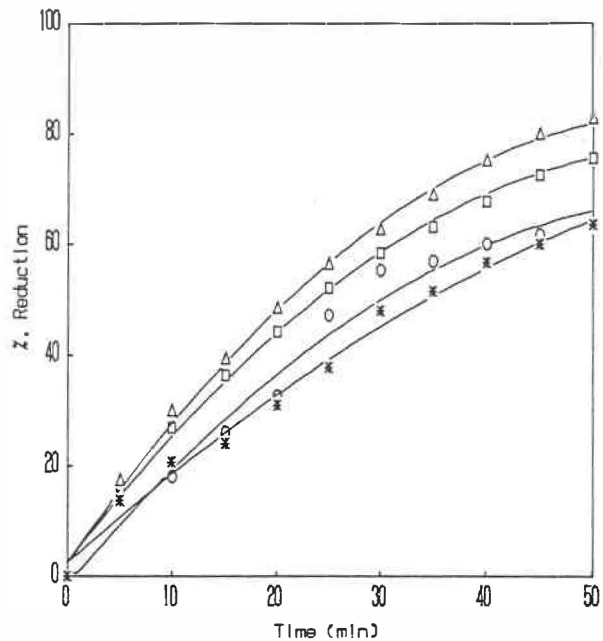


Fig. A3.3 Effect of the amount of sinter sample on the reproducibility of the reducibility test results

a) 40 g; b) 100 g

In the ISO test method for the reducibility of the iron ore sinters 500g of sample of size 10 - 12.5 mm is used.

Temperature

The reduction rate increases with the increase in temperature but the degree depends on the mechanism of the reaction. Depending on the degree of reduction, the chemical control is predominant at lower temperature (about 500-600°C) while at higher temperature (above 600°C) gaseous diffusion becomes the dominant rate controlling mechanism. However, in practice, the temperature zones are not quite well defined and a zone of mixed-control exists. The nature of relation between the reduction reaction of iron oxide and temperature can be seen in Fig. A3.4.

Moreover, the difference in the morphology of the reaction products at different temperature also have large influence on reduction rate⁽¹¹⁷⁻¹¹⁹⁾. At low temperatures, in general the iron layer formed is coarser than that at higher temperature. The structure of the reduced product at higher temperature is porous and permits more gas diffusion in the sinters which increases the reduction rate. Hence, the selection and control of the reduction temperature for the test method is quite important.

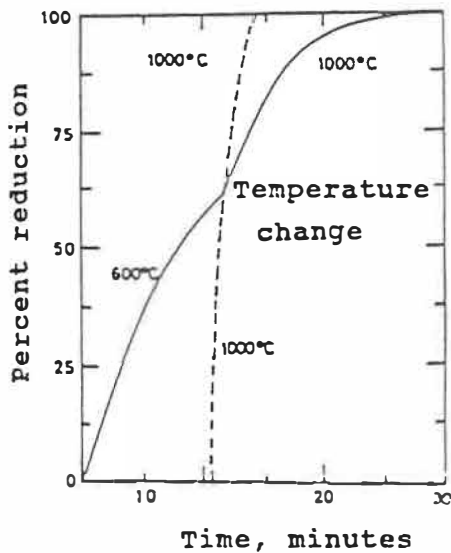


Fig. A3.4 Difference between the reduction rate of a spherical hematite pellet reduced at first to 60% at 600°C and the remainder at 1000°C (solid line) and that of a pellet reduced fully at 1000°C (dotted line)⁽¹¹⁹⁾.

In the ISO static bed reducibility test the sinter sample is reduced isothermally at $950 \pm 10^\circ\text{C}$.

Reducing Gas

The reducing gas inside the blast furnace is mainly CO, although there is some amount of H₂ gas present depending on the moisture content of the blast and other blast additives such as fuel oil or natural gas.

For the reducibility test methods usually CO and/or H₂ gas is used as the reductants. The reduction rate may vary significantly with change in the gas composition and flow rate.

Gas Composition

In general, the overall reduction rate is enhanced as the concentration of the reducing species increases in the gas mixture. The reduction rate of iron oxides by H₂ is faster than that of CO. This is probably due to smaller diffusivity of CO. The pores of the iron layer may also be blocked by the carbon formed by the Boudouard reaction: $2\text{CO} = \text{C} + \text{CO}_2$

The effect of the amount of CO and H₂ in the reducing gas mixture on the reduction rate of iron oxides is shown in Fig. A3.5⁽¹²⁰⁾.

Gas Flow Rate

The reduction rate increases with the increase in the flow rate of the reducing gas. Increase in the linear velocity of the gas reduces the boundary thickness at the bulk-gas/particle interface. However, after reaching a certain velocity, no further increase in the reduction rate is noticed. At this stage, probably, the other processes control the overall

reduction rate. The variation of the reduction rate with the linear velocity of H_2 is shown in Fig. A3.6⁽⁶²⁾.

In the ISO reducibility test method a mixture of 40% CO and 60% N_2 is used. The flow rate is maintained at 50 ± 0.5 l/min.

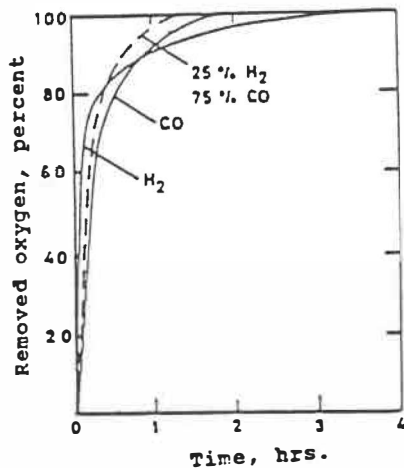


Fig. A3.5 Differences in the reduction rates of iron oxides with pure CO and H_2 and their mixture⁽¹²⁰⁾.

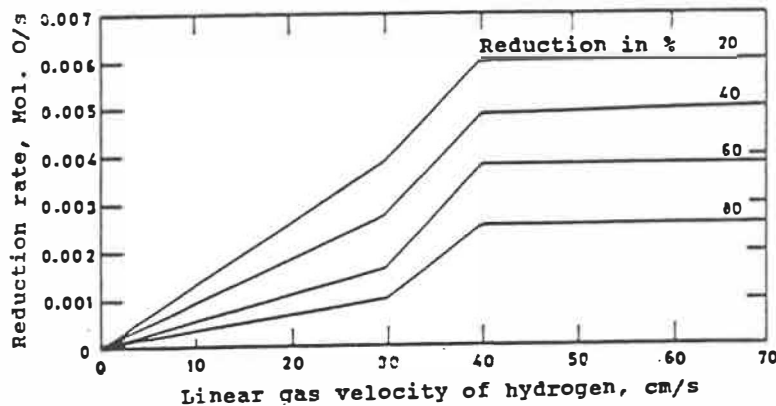


Fig. A3.6 Variations of reduction rate with linear velocity of hydrogen. After a critical velocity, the reduction rate of iron oxide becomes independent of gas velocity for all degrees of reduction⁽⁶²⁾.

ÉCOLE POLYTECHNIQUE DE MONTRÉAL



3 9334 00291721 7

CH